# The role of acetyl-phosphate in the pathogenesis of *Neisseria gonorrhoeae* MS11

by

**Ernesto Félix Díaz Parga**

Submitted in part for the degree of

**Doctor of Philosophy**

in the Department of Infection, Immunity & Cardiovascular

Disease of the University of Sheffield

May, 2021

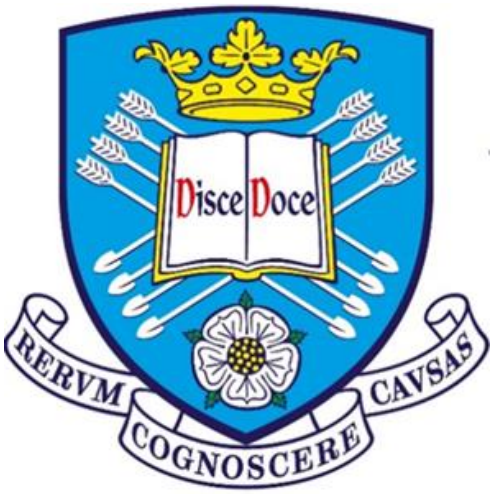

“It is not the strongest of the species that survives, nor the most intelligent that survives. It is the one that is the most adaptable to change.”

**-Charles Robert Darwin**

# Acknowledgements

The conclusion of my doctoral thesis has been a journey that not only lasted almost 4 years. This journey started when I discovered science, the fascinating world that is hidden to our eyes yet present everywhere. To have completed this work has been a challenge that has tested my character and my perseverance to achieve what I always wanted to be, a researcher, doing what I like the most, being at the lab and make crazy experiments. I have learned a vast of techniques and several ways to analyse and interpret data, but this has not been only self-taught, during this journey a lot of people have followed me and had made this journey more pleasant and enjoyable.

I would like to thank the help my supervisor Jonathan Shaw has given during these years, for accepting me to work on his lab and guided me for the almost 5 years of knowing him. His knowledge in the field and kindness were key to achieve my goal.

Thank you to CONACyT for have funding this PhD and given me a scholarship that made possible this, otherwise it would have been really difficult to get the necessary resources to achieve this dream.

To all my previous professors and supervisors that pushed and helped during my academic career.

During this adventure I met so many people that made the journey more exciting and that helped me to be always enthusiastic on what I did, the people that were part are a lot but some of this friends were always there thank you Tania, Lucio, Mau, Baruch, Brian, Charalito, Gio, Bian, Natalia, Sebastiano, Brenda, Ingrid and Dylan.

To all my family, every single of you even at the distance, you were always looking after me, thank you for supporting me.

Finally, but not least to my beloved mother, father and sister, this achievement was completed because of all your help and support. You have always been there and have given me so much love and strong to stay in life, you know all the hard work that this took me and this is simply the way you have showed me to be, to never fail and continue even in adversity. I love you so much.

## Summary

*N. gonorrhoeae* is the aetiological agent of the sexually transmitted disease gonorrhoea. The bacteria has adapted to be an obligate human pathogen and it possesses the ability to survive intracellularly by the expression of virulence factors. Post-translational modifications are found in all organisms, and are involved in the regulation of the metabolism and gene transcription. In this study we investigated the acetylation by acetyl-phosphate in *N. gonorrhoeae* by deleting genes from the phosphotransacetylase-acetate kinase pathway to control acetyl-phosphate production. We found that the metabolism and virulence was altered by the change of acetyl-phosphate concentration, molecule responsible for the acetylation of proteins. Furthermore, we proposed a regulatory pathway for the PTA-AK pathway which involved the histone-like family deacetylase (HDAC). Finally, the data obtained suggests that the enzyme Pta is essential for the pathogenesis of *N. gonorrhoeae*.

# Contents

**1 Introduction ..... 2**

1.1 Acetate metabolism ..... 4

1.2 Phosphotransacetylase-acetate kinase pathway ..... 6

1.2.1 Phosphotransacetylase ..... 7

1.2.2 Acetate kinase ..... 8

1.3 Lysine acetylation ..... 9

1.3.1 Enzymatic lysine acetylation ..... 10

1.3.2 Non-enzymatic lysine acetylation ..... 11

1.3.3 Acetyl-phosphate: the novel regulatory molecule in bacteria ..... 12

1.4 *Neisseria gonorrhoeae* ..... 13

1.4.1 Pathogenesis ..... 15

1.4.2 Internalisation into epithelial cells enhances innate immune system ..... 15

1.4.3 Survival of gonococcus inside PMN ..... 19

1.4.4 PMN: the route for gonococcal dispersion ..... 22

1.5 Lactate: The elect carbon source ..... 24

1.6 Aims of the study ..... 29

**2 Materials and methods ..... 31**

2.1 Bacterial strains and plasmid constructs ..... 31

2.2 Media and growth conditions ..... 33

2.2.1 *Neisseria gonorrhoeae* ..... 33

2.2.2 *Escherichia coli* ..... 38

2.3 Competent cells preparation ..... 39

2.4 Cryogenic preservation ..... 41

2.5 Mutant construction ..... 41

2.5.1 *Neisseria gonorrhoeae* MS11 ..... 41

2.5.2 *Neisseria gonorrhoeae* with GFP ..... 47

2.5.3 Construction of *E. coli* BL21 for Pta overexpression ..... 50

2.6 DNA sequencing ..... 54

2.7 Enzymatic assay ..... 54

2.7.1 Cell free extract (CFE) ..... 54

2.7.2 Acetate kinase (AckA) activity assay ..... 55

2.7.3 Phosphotransacetylase (Pta) activity assay ..... 57

2.8 Acetyl-phosphate (AcP) quantification ..... 59

2.9 Carbon source utilisation ..... 61

2.9.1 Growth conditions ..... 61

2.10 Detection of lysine acetylated proteins ..... 62

2.10.1 Sample preparation ..... 62

2.10.2 Sodium Dodecyl Sulphate-Polyacrylamide Gel Electrophoresis (SDS-PAGE)... ..... 62

2.10.3 Western immunoblot ..... 63

2.11 Acetylome ..... 64

2.11.1 Cell free extract (CFE) ..... 64

2.11.2 Sample preparation for LC-MS/MS ..... 65

2.12 LC-MS/MS ..... 68
2.12.1 Data analysis of MS ..... 69
2.13 Killing larvae assay ..... 69
2.14 Macrophage killing assay ..... 71
2.14.1 Blood samples ..... 71
2.14.2 Monocyte-derived macrophage (MDM) differentiation ..... 71
2.14.3 Killing assay ..... 72
2.15 Microscopy for *in vitro* killing assay ..... 73
2.15.1 Cell and bacteria staining ..... 73
2.15.2 Image analysis ..... 74
2.16 Gene expression quantification by RT-qPCR ..... 75
2.16.1 RNA extraction ..... 75
2.16.2 Genes and primers ..... 76
2.16.3 RT-qPCR ..... 77
2.17 Protein overexpression, purification and crystallisation ..... 78
2.17.1 Growth and CFE ..... 78
2.17.2 His-Trap column ..... 79
2.17.3 Buffer exchange for gel filtration ..... 80
2.17.4 Gel filtration ..... 80
2.17.5 Crystallisation ..... 80
**3 Acetylome of *Neisseria gonorrhoeae* MS11 ..... 85**
3.1 Introduction ..... 85

3.2 Results ..... 87

3.2.1 Characterisation of *N. gonorrhoeae* MS11 Δ*pta* and Δ*ackA* ..... 87

3.2.2 Construction of *Neisseria gonorrhoeae* MS11 Δ*hdac*::*kan*$^{r}$ ..... 90

3.2.3 Acetylome of *Neisseria gonorrhoeae* MS11 ..... 92

3.2.4 Acetylome of isogenic mutants of *N. gonorrhoeae* MS11 ..... 102

3.2.5 Acetyl-phosphate dependent acetylation in *N. gonorrhoeae* MS11 ..... 109

3.3 Discussion ..... 121

3.3.1 Acetylation affects chemical properties of proteins ..... 125

3.3.2 Neisserial histone- deacetylase like protein ..... 127

**4 Role of acetyl phosphate in the metabolism of *N. gonorrhoeae* MS11 ..... 130**

4.1 Introduction ..... 130

4.2 Results ..... 134

4.2.1 Acetyl-phosphate dependent acetylation is enriched in central metabolic pathways ..... 134

4.2.2 PTA-AK pathway is a metabolic flux escape for carbon overflow ..... 143

4.3 Discussion ..... 183

4.3.1 Carbon overflow is possibly regulated by acetylation of Pta ..... 188

4.3.2 Future work ..... 196

**5 Role of acetyl phosphate in the virulence of *N. gonorrhoeae* MS11 ..... 199**

5.1 Introduction ..... 199

5.2 Results ..... 200

5.2.1 Acetylation alters the intracellular survival of *N. gonorrhoeae* ..... 200

5.2.2 Acetylation in *N. gonorrhoeae* affects immune system evasion ..... 202

5.2.3 Pili biosynthesis and a two-component system is possibly altered by acetylation ..... 209

5.2.4 Phosphotransacetylase crystallisation ..... 221

5.3 Discussion ..... 225

**6 Overall conclusions ..... 234**

**7 References ..... 241**

**8 Supplements ..... 281**

# List of figures

Figure 1.1. PTA-AK pathway..... 6

Figure 1.2 Diagnostic rate of gonorrhoea in England from 2012 to 2019..... 14

Figure 1.3 Mechanism of adhesion and internalisation of *Neisseria gonorrhoeae* in epithelial cells..... 17

Figure 1.4. Warburg effect stimulates gonococcal metabolism.. ..... 27

Figure 2.1. Couple reactions for the determination of AckA activity.. ..... 56

Figure 2.2. Coupled reactions for the determination of Pta activity..... 58

Figure 2.3. Inoculation of *G. mellonella* with *N. gonorrhoeae*..... 71

Figure 2.4 Image analysis process in ImageJ.. ..... 75

Figure 2.5 Preparation of the buffers for the crystallisation of Pta.. ..... 82

Figure 2.6 Diagram of sitting drop crystallisation plate..... 83

Figure 3.1 PTA-AK pathway controls the concentration of acetyl-phosphate..... 88

Figure 3.2 Immunoblot for acetylated proteins using an anti-acetyllysine antibody. .... 89

Figure 3.3 Design and construction of *N. gonorrhoeae MS11* Δ*hdac::kan*$^{r}$..... 91

Figure 3.4 Number of identified proteins of *N. gonorrhoeae* MS11 by mass spectrometry. ..... 92

Figure 3.5 Distribution of acetylated proteins. ..... 93

Figure 3.6 Correlation of acetylation sites and protein length. ..... 94

Figure 3.7 Relative location of acetylation sites..... 95

Figure 3.8 Flanking amino acids of the acetylation site. ..... 96

Figure 3.9 Enrichment of gene ontology annotations of *N. gonorrhoeae* MS11 acetylome. ..... 98

Figure 3.10 KEGG pathways network of the *N. gonorrhoeae* MS11 acetylome..... 99

Figure 3.11 Correlation between proteins with high acetylation sites number and pathways in *N. gonorrhoeae* MS11. ..... 101
Figure 3.12 Correlation of CFE for sample validation. ..... 103
Figure 3.13 Volcano plot for acetylation sites in *N. gonorrhoeae* MS11.. ..... 104
Figure 3.14 Distribution and median of acetylation sites in the isogenic mutant strains of *N. gonorrhoeae* MS11. ..... 106
Figure 3.15 Analysis of the sequence motifs for the acetylation sites in the three isogenic strains of *N. gonorrhoeae* MS11. ..... 108
Figure 3.16 Identification of unique acetyl-phosphate-dependent acetylation sites in *N. gonorrhoeae* MS11. ..... 110
Figure 3.17 Sequence motif of acetyl-phosphate dependent acetylation sites. ..... 111
Figure 3.18 Acetyl-phosphate dependent sites. ..... 113
Figure 3.19 Enrichment analysis of the gene ontologies for the proteins with acetyl-phosphate- dependent sites. ..... 114
Figure 3.20 Identification of the possible targets of HDAC. ..... 116
Figure 3.21 Sequence motif and probability for the HDAC targets.. ..... 117
Figure 3.22 Protein targets of HDAC and network analysis. ..... 119
Figure 3.23 Enrichment analysis of the gene ontologies for the HDAC targets. ..... 120
Figure 3.24 Comparison of identified proteins and acetylation sites.. ..... 121
Figure 3.25 Acetylation decreases the charge of a protein by neutralising positive residues. ..... 126
Figure 4.1 Number of publications related to bacterial lysine acetylation. ..... 130
Figure 4.2 Reactions in the PTA-AK pathway. ..... 131
Figure 4.3 Types of lysine acetylation. ..... 132

Figure 4.4 Enrichment analysis of KEGG pathways for the acetylated enzymes in *N. gonorrhoeae* MS11. ..... 135

Figure 4.5 Growth curves of *N. gonorrhoeae* MS11 in glucose, lactate, and pyruvate. ..... 136

Figure 4.6 Doubling time of *N. gonorrhoeae* MS11 and the isogenic strains in three carbon sources. ..... 138

Figure 4.7 Acetylation of proteins in *N. gonorrhoeae* MS11 in different carbon sources.. ..... 140

Figure 4.8 Acetylation of the gluconeogenesis enzymes. ..... 146

Figure 4.9 K202 acetylation of fructose-1, 6-bisphosphate aldolase changes the surface area and hydrogen bonds of catalytic sites. ..... 148

Figure 4.10 Acetylation of K97 is acetyl-phosphate regulated in GPMA. ..... 150

Figure 4.11 Acetylation of K97 changes the electrostatic potential surface of GPMA. ..... 151

Figure 4.12 Electrostatic potential surface (EPS) of enzymes from the gluconeogenesis pathway in *N. gonorrhoeae*. ..... 154

Figure 4.13 Acetylation of the pentose phosphate pathway enzymes. ..... 157

Figure 4.14 Electrostatic potential surface (EPS) of enzymes from the pentose phosphate pathway in *N. gonorrhoeae*.. ..... 160

Figure 4.15 Acetylation of K65 and K337 are outside the active site of the enzyme transaldolase in *N. gonorrhoeae*. ..... 161

Figure 4.16 Acetylation of the residue K197 in 6-phosphogluconolactonase in *N. gonorrhoeae* modifies the interaction and conformation of the active site. ..... 163

Figure 4.17 Acetylation of the pyruvate metabolism enzymes. ..... 167

Figure 4.18 Electrostatic potential surface (EPS) of enzymes from the pyruvate metabolism in *N. gonorrhoeae*. ..... 170

Figure 4.19 Acetylation of K154 interacts with the substrate of LDHA in *N. gonorrhoeae*. ..... 172

Figure 4.20 Alignment of PTA with different bacterial species..... 173

Figure 4.21 Acetylation of K450 residue of phosphate transacetylase is predicted to alter the interaction with the substrate and the conformation of the active site. ..... 175

Figure 4.22Acetate kinase model of *N. gonorrhoeae*..... 176

Figure 4.23 Acetylation of the TCA cycle enzymes. ..... 179

Figure 4.24 Electrostatic potential surface (EPS) of enzymes from the TCA cycle in *N. gonorrhoeae*..... 182

Figure 4.25 *aceEF-lpd* operon..... 187

Figure 4.26 Alignment of phosphoglycerate mutase sequences..... 190

Figure 4.27 Proposal of the regulation of the central metabolic pathway by acetylation.. ..... 191

Figure 5.1 Growth curve of isogenic strains of *N. gonorrhoeae* in BHI. ..... 201

Figure 5.2 Intracellular survival of *N. gonorrhoeae* in MDM..... 202

Figure 5.3 Phagocytosis of *N. gonorrhoeae* labelled with pHrodo. ..... 203

Figure 5.4 Fluorescence microscopy for *in vitro* phagocytosis of *N. gonorrhoeae* MS11 by MDM. *In vitro* microscopy of MDM phagocytising *N. gonorrhoeae*..... 205

Figure 5.5 Analysis of fluorescence microscopy..... 208

Figure 5.6 Volcano plot of the proteome of *N. gonorrhoeae*. ..... 211

Figure 5.7 Killing assay of *Galleria mellonella* infected with *N. gonorrhoeae*..... 213

Figure 5.8 Quality control of primers for RT-qPCR of genes involved in virulence of *N. gonorrhoeae*..... 215

Figure 5.9 Acetylation sites of pili-related proteins.. ..... 219

Figure 5.10 Antibiotic resistance of *N. gonorrhoeae* MS11. ..... 220

Figure 5.11 Domains of neisserial Pta. ..... 221

Figure 5.12 Optimisation of expression, purification and crystallisation of *N. gonorrhoeae* Pta. ..... 223

Figure 5.13 Predicted structure of the crystal of the *N. gonorrhoeae* Pta (NGFG0350). ..... 224

Figure 6.1 Role of acetyl-phosphate in *N. gonorrhoeae*.. ..... 235

Figure 6.2 Proposal of a regulatory mechanism of the PTA-AK pathway in *N. gonorrhoeae*..... 236

Figure 6.3Acetylation of pili-biosynthesis proteins and electrostatic interactions..... 237

Figure 6.4 Effect of acetylation in the two-component system MisRS in *N. gonorrhoeae*. ..... 238

Figure 8.1 Ontologies of the possible target of HDAC. ..... 311

Figure 8.2 Construction of pLES2-GFP. ..... 313

Figure 8.3 Relative mRNA expression of genes involved in the virulence and metabolism of *N. gonorrhoeae* MS11. ..... 314

Figure 8.4 Acetylation sites of two-component system proteins and virulence factors. ..... 315

Figure 8.5 Acetylation sites of transcriptional regulators. ..... 316

Figure 8.6 Construction of *E. coli* BL21 pET28a-pta-His6 for the overexpression of the phosphotransacetylase of *N. gonorrhoeae*..... 317

# List of tables

Table 1.1 Carbon source for the pathogenesis of intracellular bacteria ..... 3

Table 2.1 Strains of bacteria used and plasmid constructs in this study ..... 31

Table 2.2 Composition and preparation of the chemically defined medium (CDM-GC) for the growth of *N. gonorrhoeae*..... 34

Table 2.3. Composition and preparation of 100 mL RF1 solution..... 40

Table 2.4. Composition and preparation of 100 mL RF2 solution..... 40

Table 2.5. Primers for the construction of *N. gonorrhoeae* MS11 Δ*hdac::kan*$^r$ ..... 43

Table 2.6. Reagents and volumes for PCR mix..... 44

Table 2.7. PCR conditions for the amplification of the flanking sequences of *hdac* and the kanamycin resistant gene..... 44

Table 2.8. PCR mix for the construction of *hdac::kan* ..... 45

Table 2.9. Thermal cycler settings for the construction of *hdac::kan*..... 45

Table 2.10. Primers for the amplification of the *gfp* gene from pBHR1-GFP ..... 48

Table 2.11 PCR mix for amplification of *gfp*..... 48

Table 2.12. Thermal cycler settings for *gfp* amplification ..... 48

Table 2.13 Primers for the PCR of *pta*-his ..... 51

Table 2.14 Thermal cycler settings for *pta*-his amplification ..... 51

Table 2.15 Primer for insert validation of the vector pET28..... 53

Table 2.16 Thermal cycler settings for T7 polymerase amplification with pta-his insert ..... 53

Table 2.17 Reaction mix for the AckA activity..... 56

Table 2.18. Reaction mix for the Pta activity ..... 57

Table 2.19. Preparation of 12% SDS-PAGE..... 63

Table 2.20 Genes and primer used for RT-qPCR..... 76

Table 2.21 Reaction mix for RT-qPCR ..... 78

Table 2.22 Settings for RT-qPCR..... 78

Table 2.23 Conditions for sitting drop crystallisation of Pta..... 81

Table 3.1 Pta and AckA activity of the three strains of *N. gonorrhoeae* MS11..... 87

Table 3.2 Number of significant proteins and acetylation sites in the isogenic mutant strains of *N. gonorrhoeae* MS11. ..... 105

Table 3.3 Comparison of studies with bacterial acetylomes. ..... 122

Table 4.1 Comparison in the acetylation of isogenic strains of *N. gonorrhoeae* MS11 growing in different carbon sources.. ..... 141

Table 5.1 Gene expression in isogenic strains of *N. gonorrhoeae* MS11. ..... 217

Table 8.1 Genes of proteins with five or more acetylation sites identified in the KEGG pathway sin *N. gonorrhoeae* MS11 ..... 281

Table 8.2 Acetylome of isogenic mutant strains.. ..... 284

Table 8.3 Proteins with acetyl-phosphate-dependent acetylation sites. ..... 299

Table 8.4 Acetylation sites of tRNA proteins in the three isogenic mutants of *N. gonorrhoeae* MS11..... 309

Table 8.5 T-test analysis of growth in different carbon sources. ..... 312

# Abbreviations table

| | | |
|---|---|---|
| **AckA** | - | Acetate kinase |
| **AcP** | - | Acetyl-phosphate |
| **CDM** | - | Chemically defined medium |
| **CFE** | - | Cell free extract |
| **CFU** | - | Colony formation unit |
| **CMP** | - | Central metabolic pathways |
| **DNA** | - | Deoxyribonucleic acid |
| **DUS** | - | DNA uptake sequence |
| **ED** | - | Entner-Doudoroff pathway |
| **EPS** | - | Electrostatic potential surface |
| **GPA** | - | Gentamicin protection assay |
| **HDAC** | - | Histone deacetylase-like protein |
| **kb** | - | Kilobase |
| **kDa** | - | Kilodalton |
| **LDH** | - | Lactate dehydrogenase |
| **MDM** | - | Monocyte-derived macrophage |
| **mRNA** | - | messenger ribonucleic acid |
| **МΦ** | - | Macrophage |
| **OD** | - | Optical density |
| **PCR** | - | Polymerase chain reaction |
| **PDC** | - | Pyruvate dehydrogenase complex |
| **PPP** | - | Pentose phosphate pathway |
| **PTA** | - | Phosphotransacetylase |
| **PTM** | - | Post-translational modifications |
| **RNA** | - | Ribonucleic acid |
| **RT-qPCR** | - | Real time-quantitative polymerase chain reaction |
| **STI** | - | Sexually transmitted infection |
| **TCA** | - | Tricarboxylic acid cycle |
| **TCS** | - | Two-component system |

# Chapter 1

# Introduction

# 1 Introduction

Bacteria have existed on Earth for billions of years leading them to evolve and adapt to their environment for the inheritance of their genome. It is considered that approximately one billion bacterial species exist worldwide and that the environment is a crucial factor for the bacterial diversity (Dykhuizen, 2005). Microorganisms have been able to adapt and survive in different niches depending on the nutrients available, however, only a small number of bacteria are able to survive within the human body. Due to the existence of different microenvironments across the body, bacteria colonise specific niches that provide for their metabolic requirements. More than a hundred molecules are accessible as carbon sources for commensals and symbiotic bacteria for the generation of energy and growth (Brown, Palmer and Whiteley, 2008; Eisenreich *et al.*, 2010).

Around 1,000 species of bacteria are living in our body contributing to the appropriate functioning of our metabolism (Munoz-Elias and McKinney, 2006). However, evolution determined that some species of bacteria possess genes that encode factors that can harm human cells. Moreover, only a select group of prokaryotes have adapted to survive intracellularly (de Barsy and Greub, 2013). These bacteria have developed different virulence factors to invade and colonise different cells (i.e. epithelial cells, macrophages) but specifically, they have adapted to exploit the metabolites found in these niches. It has been shown that intracellular bacteria only metabolise a few carbon sources, found within host cells, necessary for the biosynthesis of different metabolites required for replication (table 1.1) (Brown, Palmer and Whiteley, 2008; Ray *et al.*, 2009; Shibutani and Yoshimori, 2014)

**Table 1.1 Carbon source for the pathogenesis of intracellular bacteria**

| Bacteria | Location | Intracellular niche | Carbon substrate | Virulence impact |
|---|---|---|---|---|
| *Listeria monocytogenes*[1] | Bloodstream | Cytosol of macrophages | Hexose phosphates, lipoate | Persistence and growth |
| *Shigella flexneri* [1, 2] | Colon | Cytosol of epithelial cells | Pyruvate | Growth and intracellular invasion |
| *Neisseria meningitidis* [3] | Nasopharynx, bloodstream, cerebrospinal fluid | Phagosome | Lactate | Molecular mimicry and growth |
| *Mycobacterium tuberculosis* [3] | Lung | Phagosome | Cholesterol | Virulent lipids |
| *Neisseria gonorrhoeae* [4,5,6] | Urogenital epithelium, macrophages | Endosome, phagosome | Lactate | Molecular mimicry and growth |

[1] Ray *et al.*, 2009; [2] Waligora *et al.*, 2014; [3] Brown, Palmer and Whiteley, 2008; [4] Parsons *et al.*, 1996; [5] Château and Seifert, 2016; [6] Harvey *et al.*, 2001.

One of the facultative intracellular bacteria able to survive and reproduce within phagosomes is *Neisseria gonorrhoeae* (gonococcus), a Gram-negative gonococcus and the etiological agent of the sexually transmitted infection gonorrhoea. It was first thought that *N. gonorrhoeae* solely grew in glucose, pyruvate, and lactate (Stephen A Morse, Stein and Hines, 1974). However, genomic sequencing and enzymatic assays revealed that gonococcus possesses enzymes capable to utilise amino acids as carbon source (Baart *et al.*, 2007, 2010; Catenazzi *et al.*, 2014). Lactate is one of the molecules that is present in

the human body at high concentrations, especially in the niches where *Neisseria gonorrhoeae* colonises (i.e. human serum, leukocytes, female genital tract, ejaculate) (Gao *et al.*, 1998; Atack *et al.*, 2014). This three-carbon molecule has been shown to be relevant for the pathogenesis of the gonococcus; it contributes to molecular mimicry; decreases reactive oxygen intermediates; enhances general metabolism; and it appears to be metabolised by the phosphotransacetylase-acetate kinase (PTA-AK) pathway (Britigan *et al.*, 1988; Mcgee and Rest, 1996; Parsons *et al.*, 1996; Gao *et al.*, 1998).

However, in recent years, a process thought to be only present in eukaryotic cells, has been found in several microorganisms, possessing a role in the post-translational modification of proteins involved in the pathogenesis of bacterial infections (Wagner and Payne, 2013; Kuhn *et al.*, 2014). Acetyl-phosphate (AcP) is a high energy molecule found as an intermediate metabolite in different pathways, being produced by gonococcus in the PTA-AK pathway. The main role of this molecules is to acetylate enzymatically or nonenzymatically the ε-amino group of lysine residues ($N^{\varepsilon}$-lysine), this post-translational modification has shown to be relevant for the activation of some virulence genes in bacteria (Barak and Eisenbach, 2001; Starai and Escalante-Semerena, 2004; Verdin and Ott, 2013). Moreover, a recent study demonstrated the presence of $N^{\varepsilon}$-lysine acetylation in *Neisseria gonorrhoeae* and the relation it has with virulent factors (Post *et al.*, 2017). The study of the role of intracellular metabolites in gonococci, specifically AcP, is an attractive field of research for the better understanding of its pathogenesis.

## 1.1 Acetate metabolism

The central metabolic pathway (CMP) includes the pathways, glycolysis, pentose phosphate, pyruvate metabolism, and tricarboxylic acid cycle (TCA). Glucose is the molecule that is consumed by glycolysis or Entner-Doudoroff (ED), depending on the

encoded enzymes in the bacteria. *N. gonorrhoeae* metabolises glucose through the ED pathway since it does not encode the gene phosphofructokinase, key enzyme for glycolysis that phosphorylates fructose-6-phosphate to fructose-1, 6-bisphosphate. The final product of both glycolysis and ED is pyruvate (Wolfe, 2005; Baart *et al.*, 2007, 2010).

Pyruvate is metabolised by the pyruvate dehydrogenase complex (PDC). This complex is formed by pyruvate dehydrogenase E1, dihydrolipoamide acetyltransferase E2, and dihydrolipoamide dehydrogenase. A series of reactions catalyses the conversion of pyruvate to acetyl-coenzyme A (acetyl-CoA). The latter molecule is the final product of different metabolic pathways including, amino acids and fatty acids metabolism (Sauer and Eikmanns, 2005; Patel *et al.*, 2014).

Acetyl-CoA has two paths two follow, enter either the TCA or the phosphotransacetylase-acetate kinase pathway (PTA-AK). When acetyl-CoA is metabolised through TCA energy is synthesised for the growth of the bacteria. In the PTA-AK pathway the acetyl-CoA is transformed first to acetyl-phosphate (AcP) by the enzyme phosphotransacetylase (Pta) and then AcP is converted to acetate.

During bacterial growth in medium where glucose is the sole carbon source acetate is excreted extracellularly at high concentrations due to saturation of the CMP. This phenomenon is known as carbon overflow. The saturation of the TCA promotes the path of acetyl-CoA to the PTA-AK pathway which it is used as an escape valve of carbon overflow. An interesting effect was described in *E. coli* as acetate switch where acetate is now used as carbon source (Schilling *et al.*, 2015; Bernal, Castaño-Cerezo and Cánovas, 2016). As consequence of this switch, the biomass production is decreased and the bacterial growth is abolished.

Acetate is metabolised by two enzymes to convert is to acetyl-CoA, acetate kinase (AckA) and acetyl-coenzyme A synthetase (Acs). At low and high concentration, acetate is mainly metabolised by Acs and AckA, respectively (Brinsmade and Escalante-Semerena, 2007; Campos-Bermudez *et al.*, 2010). However, a recent study in *E. coli* demonstrated that acetate metabolism was significantly reduced in a Δ*ackA* than in a Δ*acs* isogenic strain. Proving that ackA is the responsible enzyme to metabolise acetate during acetate overflow (Enjalbert *et al.*, 2017). This study provided evidence of the importance of the PTA-AK pathway for the acetate metabolism. Moreover, the intermediate acetyl-phosphate produced in this pathway has given attention to researchers due to the role it possesses in post-translational modifications of proteins.

## 1.2 Phosphotransacetylase-acetate kinase pathway

Acetyl-coenzyme A (acetyl-CoA) is final product of several pathways and this molecule is then metabolised via TCA. However, when the cycle is limited due to carbon overflow, acetyl-CoA is metabolised through the PTA-AK pathway, releasing acetate as a final product and obtaining a molecule of ATP. This pathway is composed by the two enzymes named after this metabolic route (fig. 1.1) (Wolfe, 2005; Sadykov *et al.*, 2013).

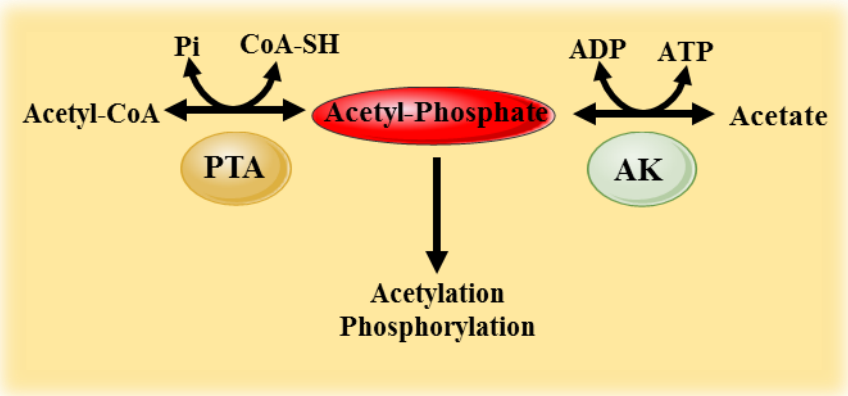


**Figure 1.1. PTA-AK pathway.** Acetyl-CoA is converted to acetyl-phosphate by the enzyme phosphotransacetylase (PTA) and the enzyme acetate kinase (AK) converts AcP to acetate, both

reactions are reversible. AcP is the responsible molecule for the non-enzymatically acetylation and it is also a substrate for the phosphorylation of proteins. Pi, orthophosphate; CoA-SH, coenzyme A; ADP, adenosine diphosphate; ATP, adenosine triphosphate (Verdin and Ott, 2013).

Several studies have highlighted the importance of PTA-AK in bacterial metabolism during carbon overflow. The depletion of this pathway has shown decrease in biomass yield, reduce in bacterial fitness to survive, and lack to growth in medium with acetate. Moreover, the deletion of this pathway in bacteria such as *Staphylococcus aureus* has caused cell death (Chang *et al.*, 1999; Somerville *et al.*, 2003; Ramos-Montañez *et al.*, 2010; Sadykov *et al.*, 2013; Won *et al.*, 2021).

Moreover the intermediate acetyl-phosphate has gained recent interest in bacteria due to its dual role to donate acetyl and phosphoryl groups to enzymes, causing enzymatic regulation and altering the metabolism of organism.

### 1.2.1 Phosphotransacetylase

Phosphotransacetylase (Pta) is a dimeric enzyme which converts acetyl-CoA to acetyl-phosphate (AcP) through a transferase reaction between the acetyl group of acetyl-CoA and an inorganic phosphate (Brinsmade and Escalante-Semerena, 2007).

Two different classes of Pta have been discovered possessing each other almost twice length of amino acids. The Pta class I (Pta I) has a length of approximately 350 aa while the Pta class II (Pta II) is ~700 aa length. The homology of sequences between from both classes is the same from the C-terminus side. Different studies have crystallised Pta I and determined that the active site is located in the homologous sequences between Pta I and Pta II, however, different attempts to crystallised complete Pta II have not been successful. Different studies have suggested that the BioD-like N-terminal domain located in the N-terminus of Pta II is used as an allosteric place for the regulation of the

enzymatic activity of Pta. The molecules that found a decrease in the activity were ATP, ADP and NADH. Interestingly, *N. gonorrhoeae* possesses a Pta II (NGO0214) and neither its structure or function of the BioD-like N-terminal domain have been studied (Chittori, Savithri and Murthy, 2012; Yoshida *et al.*, 2019).

The reaction between acetyl-CoA to AcP is reversible. Pta is eight-fold more active in the synthesis of acetyl-CoA, however, pyruvate and phosphoenolpyruvate inhibit this reaction and favours the conversion of acetyl-CoA to AcP. Hence, the reaction towards synthesis to AcP is favoured at normal physiological concentration of pyruvate (Campos-Bermudez *et al.*, 2010). In fact, it was observed in a study in *E. coli* that the intracellular concentration of acetyl-CoA was increased during carbon overflow compared to growth in glucose (Bennett *et al.*, 2009). This effect is not only due to the reversible enzymatic activity of Pta towards acetyl-CoA during carbon overflow but also due to the action of the second enzyme of the PTA-AK pathway.

### 1.2.2 Acetate kinase

The last reaction of the PTA-AK pathway is responsible for the conversion of acetyl-phosphate (AcP) to acetate. As mention previously, acetate kinase (AckA) is important during carbon overflow. This enzyme is responsible to metabolise acetate during carbon overflow to compensate the carbon flux. Enjalbert *et al.*, 2017, found in *E. coli* that AckA is responsible for acetate consumption instead of the previous thought enzyme acetate synthetase Acs. This was concluded after measuring the flux of carbon molecules extracellularly. Interestingly, it was firstly thought that the PTA-AK pathway was exclusive of bacteria, however, blast analysis of different organism genomes have revealed the genomic presence of the gene that encodes for AckA. These unicellular

eukaryotic organisms have incorporated the enzyme as part as other pathways (Ingram-Smith, Martin and Smith, 2006)

Structural analysis of AckA crystals from *S. enterica* serovar Typhimurium and *Porphyromonas gingivalis* showed that AckA showed a dimer conformation of the enzyme during native state. Studies have also shown that AckA requires $Mg^{2+}$ or $Mn^{2+}$ for catalytic activity, and molecules of sulphate and ADP in the active site (Gorrell, Lawrence and Ferry, 2005; Chittori, Savithri and Murthy, 2012; Yoshida *et al.*, 2019).

Several bacteria have shown several copies of AckA in their genomes (Ingram-Smith, Martin and Smith, 2006; Chan *et al.*, 2014). *N. gonorrhoeae* possesses two different acetate kinase NGO1521 and NGO0977. Although these two enzymes have not been studied, a study in *Lactobacillus lactis* and *Neisseria meningitidis* agree that AckAI is synthesised at higher concentration than AckAII, and its catalytic activity is favoured to produce acetate. While AckAII has a higher affinity to acetate, and in *N. meningitidis* was shown to be more affined to propionate (Catenazzi *et al.*, 2014; Chan *et al.*, 2014).

## 1.3 Lysine acetylation

Lysine acetylation is a post-translational modification (PTM) that involves the acetylation of the $N^{\varepsilon}$-lysine residue in proteins. This PTM was firstly observed uniquely in eukaryotic cells involved in the regulation of gene expression by the acetylation and deacetylation of histones, the reaction mediated by the enzyme lysine acetyltransferase (KAT) and deacetylases (KDAC) respectively (Yang and Seto, 2008). Then it was observed that acetyl-CoA present in mitochondria at high concentrations could acetylate proteins non-enzymatically (Wagner and Payne, 2013). Initially thought that lysine acetylation was exclusive of eukaryotic cells, it was then discovered that bacteria possessed acetylated proteins. In the same way as eukaryotic cells, acetyltransferases were found in *S. enterica*

and *E. coli*. Later it was shown that lysine acetylation was also performed non-enzymatically, concluding that acetylation occurs enzymatically and non-enzymatically.

### 1.3.1 Enzymatic lysine acetylation

Three families of acetyltransferases have been described. The Gcn5-related N-acetyltransferases (GNAT) family, MYST family, and the p300/CBP family. However, only the GNAT are only found in bacteria. There are around 300,000 different acetyltransferases and they are not homologous between each other, hence, the way to classify and identify them is by comparing the core GNAT domain. The role of GNAT in bacteria has been related to antibiotic resistance, regulation of metabolism and gene expression (Thao and Escalante-Semerena, 2011; David G Christensen *et al.*, 2019; Burckhardt and Escalante-Semerena, 2020).

GNATs are formed from the N-terminus by two antiparallel β-strands, two α-helices, three antiparallel β-strands, followed by a highly variant central α-helix, a fifth β-strand, a fourth α-helix, and a final sixth β-strand. The acetyl-CoA binds between β4 and β5 strand where the pantothenate interacts with the C-terminal of β4. The enzyme transfer the acetyl group by an acid/base mechanism, where a glutamate or aspartate are the base to subtract the proton from the amine group (Vetting *et al.*, 2005; Thao and Escalante-Semerena, 2011; David G Christensen *et al.*, 2019; Burckhardt and Escalante-Semerena, 2020)

First discovered in *Salmonella enterica*, the acetyltransferase (PTA) enzyme showed to deactivate the function of the acetyl-CoA synthetase (Acs), an enzyme that catalyses the conversion of acetate to acetyl-CoA (CoA), by acetylating the ATP binding region. *Escherichia coli* synthesises more than 20 lysine acetyltransferases, however, only one

has been assigned to have acetyltransferase activity (Starai *et al.*, 2002; Starai and Escalante-Semerena, 2004).

### 1.3.2 Non-enzymatic lysine acetylation

Interestingly, in 2013, Wagner and Payne found the novelty that lysine acetylation occurs non-enzymatically in mitochondria. Isolated liver mitochondria were heated for protein denaturation to inhibit the activity of any acetyltransferase. Later incubation with CoA at physiological concentration (0.1 to 1.5 mM), which is 3-50 times higher than other compartments, showed acetylation of proteins. This proved that at high concentrations of CoA, the PTM lysine acetylation occurs non-enzymatically. Although it was thought that the process was exclusive of eukaryotic cells, Kuhn *et al.*, (2014), demonstrated that a similar process occurs in bacteria.

In a previous study, it was observed that the acetylation of a RNA transcriptional factor in *E. coli* was altered when the acetate kinase gene was mutated (Δ*ackA*). The enzyme AckA catalyses the reaction to convert acetyl-phosphate (AcP) to acetate in the PTA-AK pathway. Therefore, the mutation of the enzyme results in an accumulation of AcP. Nevertheless, in this study, they created two mutants that possess a contrasting concentration of AcP by mutating the two enzymes, Pta and AckA. The analysis of cell extract of both mutants by mass spectrometry to identify lysine acetylation, as expected, showed an increase of acetylated proteins in Δ*ackA* compared to the wild type (WT). This work concluded that the molecule responsible for non-enzymatically lysine acetylation in bacteria is AcP. Indeed, further studies have proved that this evolutionary conserved PTM is present in several bacteria including *Neisseria gonorrhoeae* (Kim *et al.*, 2013; Kuhn *et al.*, 2014; Kosono *et al.*, 2015; Mizuno *et al.*, 2016; Post *et al.*, 2017).

### 1.3.3 Acetyl-phosphate: the novel regulatory molecule in bacteria

Acetyl-phosphate (AcP) is the intermediate metabolite of the PTA-AK pathway (fig. 1.3). Although, it was recently discovered to be involved in lysine acetylation, several studies have shown the dual role it possesses in both acetylation and phosphorylation of proteins, for the regulation of metabolism, synthesis of virulence factors, and regulation of transcription factors (Barak and Eisenbach, 2001; Gueriri *et al.*, 2008; Lima *et al.*, 2011; Verdin and Ott, 2013; Castaño-Cerezo *et al.*, 2014; Liu *et al.*, 2016).

A study conducted in *E.coli* showed that the acetylation of the transcriptional factor RcsB blocked the transcription of the proteins required for flagella biosynthesis, resulting in an effect on motility. Although, the author mutated the acetyltransferase enzyme instead of the PTA-AK enzymes and non-enzymatically acetylation is not discussed. The results showed that acetylation, which nowadays is well known to be modulated by AcP, regulated the transcription of virulence factors (Castaño-Cerezo *et al.*, 2014). Moreover, AcP has also shown to regulate motility in *Listeria monocytogenes*, and in *Bacillus amyloliquefaciens* regulates the synthesis of antibiotics (Gueriri *et al.*, 2008; Liu *et al.*, 2016). Recently, it was demonstrated that lysine acetylation is present in *Neisseria gonorrhoeae*. The results obtained by mass spectrometry from a Δ*ackA*, indicate that the biosynthesis of the pilus, proteins involved in iron acquisition and several regulatory proteins possess regulated sites for acetylation. Furthermore, the gonococcus was unable to generate a biofilm and general metabolism was altered (Post *et al.*, 2017).

Lysine acetylation is increased in carbon overflow. Cells in presence of an augmentation of carbon flux are exceeded in the obtainment of energy through the tricarboxylic cycle (TCA), therefore, acetyl-CoA is accumulated and it is metabolised by the PTA-AK pathway. Acetylation was observed to be induced in the presence of glucose or lactate in

*E. coli* and the enzymes of the central metabolic pathways show to be regulated by the PTM (Schilling *et al.*, 2015).

AcP has shown to participate in the phosphorylation of proteins. Before the discovery of acetylation, it was already described that the pool of AcP was involved in the phosphorylation of transcription factors in *E. coli* (McCleary and Stock, 1994). It was later found that, indeed, the concentration present of acetyl phosphate is sufficient for the direct phosphorylation of the transcription factor RcsB (Klein *et al.*, 2007). Recently, the dual role of AcP was shown in a study in the enterobacteria *E. coli*. By using site-directed mutagenesis, the transcription factor *cpxR* was mutated in the amino acid that is phosphorylated. It was observed that AcP was required for the activation of CpxR. Moreover, it was also found that RNA polymerase acetylation is also modulated by the intermediate metabolite of the PTA-AK pathway (Lima *et al.*, 2016).

## 1.4 *Neisseria gonorrhoeae*

In the last decade, gonorrhoea has gained more relevance worldwide because it has positioned as the second most common bacterial sexually transmitted infection (STI). In 2019, the World Health Organisation (WHO) estimated approximately 376 million new cases of bacterial STI. In 2016, 86.9 million resided with the disease caused by *Neisseria gonorrhoeae* (Rowley *et al.*, 2019; WHO, 2019b). In England, the number of new cases has increased yearly (fig. 1.2). The number increased from 56,232 in 2018 to 70,936 in 2019, this meant an increase of 26% (Wise, 2020). The isolation of gonococcus strains resistant to the current dual treatment, extended-spectrum cephalosporin (ESC) ceftriaxone and azithromycin, has arisen and different international organisations classify *Neisseria gonorrhoeae* as a global threat (Fifer, Natarajan and Unemo, 2016). Therefore the WHO has designated as high priority, within the classification of the emergent

resistant pathogens, the creation of new antibiotics against the gonococcus (Tacconelli and Magrini, 2017). The aim of this strategy is to decrease 90% the global incidence of gonorrhoea by 2030 (WHO, 2016).

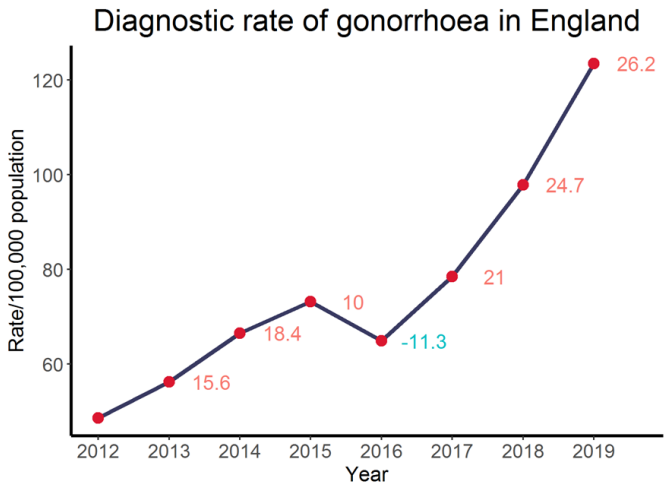


**Figure 1.2 Diagnostic rate of gonorrhoea in England from 2012 to 2019.** The line shows the diagnostic rate of gonorrhoea per 100,000 population. The number next to each point is the percentage difference compared to the previous year (Public Health England, 2021).

*Neisseria gonorrhoeae* is a pathogen that only infects humans. It colonises the urogenital tract causing urethritis in male and cervicitis in the female, although the presence in pharynx, conjunctiva and rectal mucosa are also observed. Generally, the STI is asymptomatic in women (50-80%) whilst in men, 90% of the cases present the characteristic purulent discharge (Unemo and Jensen, 2017). Occasionally, the gonococcus disseminates causing septic arthritis, bacteraemia or pustular skin lesion, however, the percentage of disseminated gonococcal infection (DGI) from the total cases is lower than 3% (Morgan and Decker, 2016). In order to infect such a specific microenvironment, the gonococcus possesses distinct mechanisms for the colonisation and internalisation within cells and evasion of the immune system.

### 1.4.1 Pathogenesis

The microenvironment of *Neisseria gonorrhoeae* for the development of the infection is the urogenital tract. Although the primary site of infection is the urogenital mucosae, the gonococcus possesses several proteins for the internalisation within the urethral and cervical epithelial cells, and polymorphonuclear cells (PMN) which lead to a systemic infection (Edwards and Apicella, 2004).

### 1.4.2 Internalisation into epithelial cells enhances innate immune system

Bacterial colonisation commences by the attachment of the type IV pili to the urogenital epithelial cells, where it acts a retractile motor for the motility of the bacteria and as a transporter of extracellular DNA (Winther-Larsen *et al.*, 2001; Ramsey, Woodhams and Dillard, 2011). This tight gonococcus-cell contact permits the recognition of membrane molecules (fig. 1.3). For instance, the gonococcus lipooligosaccharide (LOS), and porins, an immunogenic protein that transport water, are recognised by the toll-like receptor 2 (TLR-2), which lead the release of chemokines and cytokines, necessary for the recruitment of PMN. Interestingly, it has been shown that the expression of this stimulatory molecules is higher in males than females, explaining the higher rate of symptomatic gonorrhoea in men (Massari *et al.*, 2002; Fisette *et al.*, 2003; Edwards and Apicella, 2004).

Once the epithelial cells have triggered the inflammatory response, *Neisseria gonorrhoeae*, in order to survive, internalises into the epithelial cells and PMN. The recognition of LOS leads to the endocytosis of gonococci. However, the receptor is different depending on the colonised epithelial cell. An asialoglycoprotein receptor (ASGP-R) binds to LOS in urethral cells, and in cervical epithelial cells, the complement

receptor 3 receptor (CR3) binds to three bacterial proteins: type IV pili, porin and the inactivated complement 3 protein (iC3b) which is bound to the lipid A a portion of LOS. The binding causes the re-arrangement and ruffling of the plasmatic membrane, and as a consequence, bacteria are engulfed by the epithelial cell and internalised within the cytosol, this process is named macropinocytosis (Harvey *et al.*, 2001; Edwards and Apicella, 2002; Lim and Gleeson, 2011).

*Neisseria gonorrhoeae* within the epithelial cells stimulates the innate immune system. The microorganism produces phospholipase D within the macropinosome in cervical cells. This enzyme causes the displacement of the CR3 in the apical epithelial cells which lead to the internalisation of more gonococci, increasing invasion (Edwards, Entz and Apicella, 2003). Moreover, gonococci begin to grow releasing fragments of peptidoglycan, the main component of bacterial wall. This sugar-peptide polymer is recognised by NOD-like receptors (NLR), a family of cytoplasmic receptors that detect conserved molecules of bacteria and once stimulated, the receptor triggers a signalling cascade for the expression of proinflammatory mediators (Kanneganti, Lamkanfi and Núñez, 2007; Mavrogiorgos *et al.*, 2014). The chemokines and cytokines released activate neutrophils which then phagocytose the gonococcus.

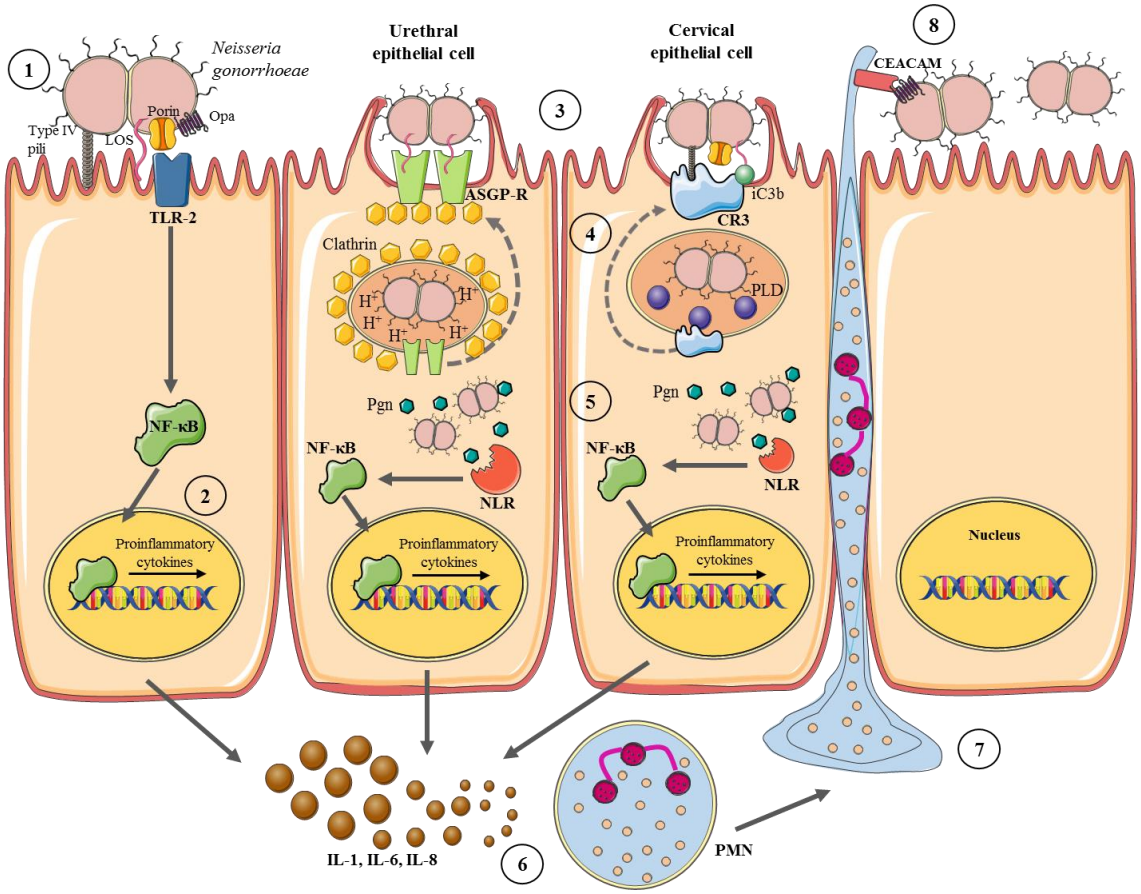


**Figure 1.3 Mechanism of adhesion and internalisation of *Neisseria gonorrhoeae* in epithelial cells. 1)** The invasion commences with the attachment of type IV pili to the urogenital epithelium, causing the binding between lipooligosaccharide (LOS), porin and opacity-associated protein (Opa), to toll-like receptor 2 (TLR-2). **2)** The binding triggers a molecular cascade that activates the transcription factor NF-κB for the synthesis of cytokines. **3)** The endocytosis of gonococcus is mediated by the recognition of an asialoglycoprotein receptor (ASPG-R) to LOS in urethral epithelial cells and in cervical epithelial cells, by the binding between type IV pili, porin, and inactivated complement 3 (iC3b), to complement receptor 3 (CR3). **4)** In urethral epithelial cells, *Neisseria gonorrhoeae* is internalised and surrounded by clathrin molecules, a protein that is involved in the formation of coated vesicles, coupled to ASPG-R. The disruption of the clathrin-coated vesicle is led by the decreased of pH, triggering the recycling of clathrin and ASPG-R to the apical membrane of the cell. In cervical epithelial cells, the endocytosis is clathrin-independent. The gonococcus releases phospholipase D (PLD) mediating the

mobilisation of CR3 to the membrane. In both cases, the recycling of receptors promotes the internalisation of more bacteria. **5)** *Neisseria gonorrhoeae*, start growing within the cytoplasm causing the release of peptidoglycan (Pgn) which is recognised by NOD-like receptors (NLR). The receptor activates NF-κB and proinflammatory cytokines are synthesised (i.e. IL-1, IL-6, IL-8). 6-8) Cytokines recruit polymorphonuclear cells (PMN) migrating from the vascular system to the lumen of the urethra or cervix recognising the opacity-associated protein (Opa) of gonococci by carcinoembryonic antigen cellular adhesion molecules (CEACAM).

PMN are the first line cells of the innate immune response. The recognition of the cells is via opsonisation or non-opsonisation. *Neisseria gonorrhoeae* is opsonised by either immunoglobulins G (IgG) and IgA1, or complement proteins. However, higher rates of antigenic variation have been observed in the surface molecules of gonococci (i.e. type IV pili, LOS and opacity-associated (Opa) proteins) resulting in a low response of the adaptive immune system (Haas and Meyer, 1986; Stern *et al.*, 1986; Hedges *et al.*, 1999). Therefore, the phagocytosis of gonococci is mainly mediated by non-opsonised molecules.

Gonococcal Opa, is a transmembrane protein of eight β-barrels, and is responsible for the internalisation into PMN. This highly genetically variable protein is recognised by carcinoembryonic antigen-related cell adhesion molecule (CEACAM) receptors. Recently, it was shown that the role of this receptor not only causes the clearance of the bacteria but that it also contributes to the pathogenesis of gonorrhoea. The activation of CEACAM3, a receptor that characterises from the others by the presence of the cytoplasmic immunoreceptor tyrosine-based activation motif (ITAM), leads to the activation of signalling pathways involved in the synthesis of pro-inflammatory cytokines

which are fundamental for the recruitment of PMN, causing an exacerbation of the inflammatory response (Sintsova *et al.*, 2014).

Although Opa is the most efficient molecule for non-opsonised phagocytosis, PMN possess other ways to engulf the gonococcus. As was previously described, in the attachment to epithelial cells, the complex of type IV pili, iC3b, and porin, bind to CR3 located on the PMN membrane. Even though LOS has been observed to promote phagocytosis, the binding receptor has not been identified (Virji, 2009; Johnson and Criss, 2011; Criss and Seifert, 2012; Sintsova *et al.*, 2015). These series of molecular recognitions lead to the phagocytosis of the gonococcal bacteria.

### 1.4.3 Survival of gonococcus inside PMN

The internalisation of bacteria through phagosomes is a process that generally causes the death of bacteria. However, *Neisseria gonorrhoeae* has elucidated the way to escape from the two phagocytic mechanisms that exist in PMN to kill bacteria, which are oxygen-dependent and independent, in order to survive and grow within the cells. Moreover, it has been recently shown in gonococci a mechanism that extends the lifespan of PMN (Johnson and Criss, 2011).

The oxygen-dependent mechanism involves the generation of ROS (reactive oxygen species) by the NOX2 NADPH-oxidase (nicotinamide adenine dinucleotide phosphate-oxidase). The enzyme transports electrons from the cytoplasm of the PMN into the phagosome causing the production of ROS, such as hydroxyl radical ($^{\bullet}OH$), hydrogen peroxide ($H_2O_2$), and superoxide anion ($O_2^-$) (Flannagan, Cosío and Grinstein, 2009; Johnson and Criss, 2011). The production of these toxic molecules for bacteria causes an augmentation in oxygen consumption by the neutrophil in a process known as oxidative burst (El-Benna *et al.*, 2016). Interestingly, it was found that species of *Lactobacillus*

isolated from the vagina, produce high concentrations of hydrogen peroxide, giving a protection to women against vaginosis (Eschenbach *et al.*, 1989). However, O'Hanlon *et al.* (2010), observed that cervicovaginal fluid and semen inhibit the activity of hydrogen peroxide. Although this study proved the ROS produced by lactobacilli bacteria is not critical for the control of vaginal infections, a recent study shows that, indeed, *Lactobacillus* inhibits the growth of pathogenic bacteria, such as *Neisseria gonorrhoeae*, but by decreasing pH through the production of lactic acid (Foschi *et al.*, 2017).

*Neisseria gonorrhoeae* averts the oxidative burst by two mechanisms; converting ROS into molecules of oxygen and water; and consuming oxygen in presence of lactate. The conversion to non-toxic molecules is mediated by peroxidases, such as superoxide dismutase (SodB) and cytochrome *c* peroxidase, and a single cytoplasmic catalase (KatA) which also possesses peroxidase activity. Its activity was discovered from a gonococcus $KatA^-$ strain isolated from a patient treated with penicillin which in the presence of hydrogen peroxide the bacteria died (Johnson *et al.*, 1993; Johnson and Criss, 2011). Another mechanism to survive from the oxidative burst is the increase of respiration. *Neisseria gonorrhoeae* only metabolises glucose, pyruvate and lactate, the latter the carbon source that increases the metabolism of the bacteria. Macrophages in a stress condition demonstrate a higher level of lactate which is used by gonococci for respiration. Therefore, the level of oxygen which originally is used for the production of ROS is decreased by *Neisseria gonorrhoeae* (Britigan *et al.*, 1988; Smith, Tang and Exley, 2007; Johnson and Criss, 2011). Although the oxidative burst is essential in the response against microorganisms in macrophages, Criss, Katz and Seifert (2009), showed that the main mechanism of gonococcal survival is resistance against non-oxidative killing. By testing mutants deficient in enzymes previously detected to participate in the protection against hydrogen peroxide, fluorescent microscopy showed a similar percentage of intracellular

survival in PMN of *Neisseria gonorrhoeae* between wild type and mutants. This finding showed that resistance against ROS is non-essential for the survival of gonococcus within PMN.

The non-oxidative killing in PMN is mediated by three types of granules: primary or azurophilic, secondary or specific, and tertiary, each one possesses molecules that are involved in the disruption of the plasma membrane of bacteria. The two main molecules involved in the defence against *N. gonorrhoeae* are cathepsin G protease and permeability-increasing protein (hCAP57) contained in the azurophilic and secondary granules, respectively (Johnson and Criss, 2011). The action mechanism of cathepsin G was firstly thought to be proteolytic by cleaving proteins from the outer membrane. However, its main function is to disrupt the biosynthesis of peptidoglycan (Shafer *et al.*, 1990). In contrast, hCAP57 is converted by a protein present in azurophilic granules into the active form, LL-37. The 37 amino acid residues antimicrobial peptide, is the only cathelicidin presents in humans and its role is to disrupt the membrane by forming pores, it also functions as a regulator of the immune response (Bucki *et al.*, 2010). It is found in PMN and epithelial cells. Interestingly, it was observed a reduction of LL-37 expression in cervical cells using immunostaining when infected with *N. gonorrhoeae* (Bergman *et al.*, 2005).

*Neisseria gonorrhoeae* counteract the effect of non-oxidative killing using distinct mechanisms. The outer membrane proteins type IV pili and porins halt degranulation of primary and secondary granules (Bjerknes *et al.*, 1995; Lorenzen *et al.*, 2000). Furthermore, enhanced by the presence of lactate, the modification of LOS, by the sialylation or substitution of the oligosaccharide, inhibits the binding of cathepsin G (Johnson and Criss, 2011; Matthias and Rest, 2014). Another mechanism that the gonococcus possesses is the presence of efflux pumps embedded in the inner membrane.

This efflux mechanism is composed by trimeric proteins which transport antibiotic and host antimicrobials from the cytoplasm to the environment. The pump is composed by three genes located within the *mtrCDE* operon, and it is regulated by a transcriptional activator and repressor, MtrA and MtrR, respectively (Zalucki, Dhulipala and Shafer, 2012; Rouquette-Loughlin *et al.*, 2017a). Although *N. gonorrhoeae* has elucidated a variety of mechanism to resist the immune response, it has been recently proved that the gonococcus has evolved not only to survive but to regulate the immune response.

### 1.4.4 PMN: the route for gonococcal dispersion

The ability of *N. gonorrhoeae* to survive within PMN has been well documented. However, recent studies showed that the adaptation of the bacteria to the host cells is more complex. Once bacteria have been engulfed, a series of mechanisms not only for escaping from the antimicrobial action but for the regulation and controlling of immune system commence. The induction of immunosuppressive molecules and the regulation of apoptosis lead to the increase of the bacterial lifespan within the PMN (Chen and Seifert, 2011; Zhu *et al.*, 2012; Château and Seifert, 2016). Therefore, gonococci are transported through the vessels allowing the dissemination of the infection through the body.

Apoptosis, programmed cell death mechanism, is a highly regulated process present in every single cell. The aim of this genetically encoded process is to maintain an equilibrium in tissues and as an immune response to executing cells when an infection or damage occur (Buchakjian and Kornbluth, 2010; Tait and Green, 2010; Hongmei, 2012). *Neisseria gonorrhoeae* has shown to be involved in the inhibition of apoptosis, although the regulation of apoptosis has also been observed in *Mycobacterium tuberculosis*, the mechanism explained subsequently is exclusively from gonococci (Velmurugan *et al.*, 2007; Chen and Seifert, 2011; Château and Seifert, 2016).

Neisserial porin (PorB) prevents apoptosis of PMN and epithelial cells. It was demonstrated that purified PorB from *Neisseria meningitidis* prevented apoptosis in HeLa cells (Faherty and Maurelli, 2008). Although a discrepancy was found when *N. gonorrhoeae* was used (Müller *et al.*, 2000). The team that initially reported the anti-apoptotic mechanism repeated the experiments made by Müller *et al*. but using their protocol and the results found in meningococcus were found in *N. gonorrhoeae*, confirming the inhibition of apoptosis. PorB migrates to the mitochondrial membrane preventing the release of cytochrome *c*, and it also halts caspase-3 activation, both required factors for the initiation of apoptosis. Interestingly, this mechanism works even if the bacteria is dead (Massari *et al.*, 2003). Chen and Seifert, (2011), studied the apoptosis in HL-60 cells, a myeloid leukaemia cell line, and apoptosis in primary PMN. Cells were pre-incubated with *N. gonorrhoeae* and then apoptosis was stimulated using staurosporine (STS). The infected PMN incubated with STS showed a decrease of DNA fragmentation which corresponds to the last step of apoptosis. This study showed for the first time that *Neisseria gonorrhoeae* inhibits apoptosis in primary cell culture.

Indeed, the results were confirmed in another work conducted in primary macrophages and a differentiated THP-1 cell line. The findings proved that the gonococcal infection prevents cells to die by measuring DNA fragmentation. Moreover, infection of primary macrophages caused the release of not only pro-inflammatory cytokines (IL-6, IL-8) but immunosuppressive (IL-10). Furthermore, PD-L1 (Programmed Death Ligand 1), a molecule which acts in the suppression of the immune system, was found upregulated in macrophages infected with *Neisseria gonorrhoeae*. However, the role that these immunosuppressive molecules play during infection needs further studies. In both studies, IL-10 was quantified at 10 h and 24 h respectively, and PD-L1 at 24 h. The

expression of the molecules at earlier times will indicate the function of the upregulation in the macrophages (Ortiz *et al.*, 2015; Château and Seifert, 2016).

These findings prove the high adaptation that gonococci have developed to survive and regulate the immune response mechanism. The regulation of apoptosis leads to the possession of a niche which lifespan is expanded by inhibiting cellular death, moreover, the upregulation of immunosuppressive cytokines derive in the mobilisation of *Neisseria gonorrhoeae* through the vessels to colonise new tissues. However, all these events could not be possible without the requirement of energy. The gonococcus has evolved to benefit from metabolites present when the body is under stress.

## 1.5 Lactate: The elect carbon source

Lactate is one of the metabolites that is found at high concentrations in the body and one of the carbon sources that *Neisseria gonorrhoeae* metabolises. Lactate is found in all the body, but especially muscles cells and astrocytes possess the ability to synthesise lactate at higher levels. In women, lactobacilli are present in the vagina producing high concentrations of lactate. The production of lactate is inversely correlated to the concentration of oxygen in the body, and glycolysis is the pathway that from one molecule of glucose synthesises two molecules of lactate as a last metabolite. It is converted from pyruvate by the enzyme lactate dehydrogenase (LDH) whose reaction leads the oxidation of $NADH+H^+$ (nicotinamide adenine dinucleotide reduced) to $NAD^+$ and in a high concentration of lactate, the reaction is reversible. In normal conditions, lactate is found in blood at 2.0 to 2.5 mmol/L and the concentration is increased in stress conditions (i.e. exercise, bacterial infection, after surgery) (Andersen *et al.*, 2013; Bakker, Nijsten and Jansen, 2013; Todd, 2014).

As it was mentioned previously, *Neisseria gonorrhoeae* utilises glucose, pyruvate, and lactate, to obtain energy (Stephen A Morse, Stein and Hines, 1974). However, a variety of studies have postulated the effects of lactate, in the metabolism of gonococcus and the role it has in pathogenesis (Yates *et al.*, 2000; Smith *et al.*, 2001; Exley *et al.*, 2007; Atack *et al.*, 2014). The gonococcus metabolises the L-lactate isoform, which is the most abundant in the body, by translocating lactate through a lactate permease (LctP). L-lactate is then converted to pyruvate by LldD (respiratory L-LDH), thus, the cytosolic LdhA ($NAD^+$-linked D-LDH) converts pyruvate into D-lactate and it is converted back to pyruvate by LdhD (respiratory D-LDH). The activity of the three LDH results in an accumulation of pyruvate (Atack *et al.*, 2014).

The gonococcus is well known for possessing molecular mimicry, this means that the molecules present on the surface of the bacteria imitate the ones found in host cells. Sialylation of LOS is the mechanism by which the gonococcus avert phagocytosis. It was found that the bacteria presented resistance to complement-mediated killing when exposed to serum. The molecule that was found to be involved in the protection of the bacteria against the innate immune response was cytidine 5′-monophosphate-N-acetylneuraminic acid (CMP-NANA). Sialylation is catalysed by the enzyme sialyltransferase (Lst) which incorporates the sialyl group on the terminal Galβ1-4GlcNAc of LOS. The incorporation of the host cell molecule results in a molecular mimicry which includes the inhibition of complement deposition on the surface of the gonococcus, the avoidance of phagocytosis but also it halts the internalisation into the epithelial cells (Gill *et al.*, 1996; Mcgee and Rest, 1996; Parsons *et al.*, 1996; Regan *et al.*, 1999). The synthesis of Lst was thought to be mediated in the presence of lactate (Mcgee and Rest, 1996). Nevertheless, later studies, by comparing growth between the three different carbon sources, showed that lactate is not the responsible for an increase

sialylation but the molecule that enhances gonococcus metabolism. Therefore, in presence of lactate LOS is synthesised at higher rates resulting in a higher sialylation (Parsons *et al.*, 1996; Regan *et al.*, 1999).

Interestingly, it was recently reported that desialylation of gonococcus in infected women contributes to the dispersal of the STI in men. In order to internalise to urethral cells, *Neisseria gonorrhoeae* binds to the surface of the epithelial cells, however, sialylation inhibits it. Sialidase is the enzyme that catalyses the desialylation of LOS and cervicovaginal microbiome, especially conformed of *Lactobacillus* sp., produce high concentrations of this enzyme (Edwards and Apicella, 2004; Ketterer *et al.*, 2016).

The concentration of lactate in normal conditions is lower than glucose, however, sites of gonococcus colonisation present 2-10 times higher threshold of lactate concentration. In stress conditions, the body metabolises high concentrations of oxygen generating a hypoxic environment which promotes the anaerobic pathway. Pyruvate which normally enters the tricarboxylic cycle (TCA) is converted instead to lactate because the oxidative phosphorylation is decreased by the depletion of oxygen (Gao *et al.*, 1998; Bakker, Nijsten and Jansen, 2013; Atack *et al.*, 2014). In PMN this phenomenon is observed during infection and it is activated during bacterial infection. The recognition of LOS by PMN lead to the activation of oxidative burst which requires high concentrations of oxygen and ATP, by switching the metabolism from oxidative phosphorylation to anaerobic glycolysis, the cell obtains ATP faster by producing lactate, this process is known as Warburg effect (fig. 1.4) (Kelly and O'Neill, 2015).

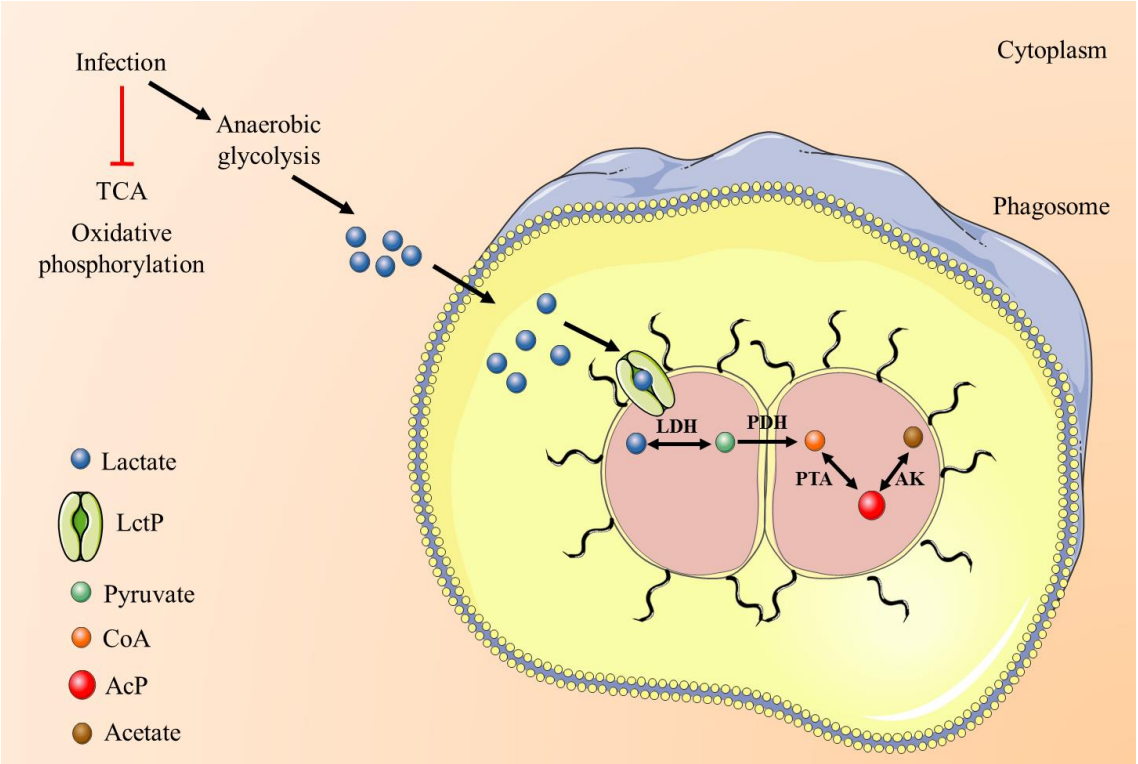


**Figure 1.4. Warburg effect stimulates gonococcal metabolism.** PMN in stress conditions such as bacterial infection, the cell switches the metabolism to anaerobic respiration, and the tricarboxylic cycle (TCA) and oxidative phosphorylation are inhibited. As consequence, the concentration of lactate is increased and it is metabolised by *Neisseria gonorrhoeae*. Lactate is transported through a lactate permease (LctP) and it is metabolised by the phosphotransacetylase-acetate kinase (PTA-AK) pathway. The high concentration of lactate enhances bacterial growth, thus, oxygen used by the PMN for the oxidative burst is depleted. CoA, acetyl-coenzyme A; AcP, acetyl-phosphate; LDH, lactate dehydrogenase; PDH, pyruvate dehydrogenase.

Although this effect has not been described in gonococcal infection, it is known that bacteria that survive within PMN promotes the production of lactate (i.e. *Listeria monocytogenes*, *Mycobacterium tuberculosis*) (Kelly and O'Neill, 2015; Shi *et al.*, 2015). However, it is likely that gonococcus stimulates the Warburg effect. Britigan *et al.*, (1988), observed that the concentration of oxygen was depleted in HL-60 cells when infected with *Neisseria gonorrhoeae* and it was a consequence of lactate metabolism.

The possession of three LDHs in *Neisseria gonorrhoeae* lead to an accumulation of pyruvate which is then converted to acetyl-coenzyme A. The conversion of acetyl-CoA to acetate through the phosphotransacetylase-acetate kinase (PTA-AK) pathway has shown to be a promising route, relevant for the global metabolism of the gonococcus due to the versatile intermediate metabolite, acetyl-phosphate.

## 1.6 Aims of the study

The initial aims of this study was to disrupt the PTA-AK pathway of *N. gonorrhoeae* to observe an alteration in the levels of acetyl-phosphate. This was achieved by constructing two isogenic mutants Δ*ackA* and Δ*pta*. However, it was then decided that a strain lacking the histone deacetylase-like protein would be interesting to observe possible targets of this enzyme, since no studies have been performed to analyse this study. In fact, two of the created isogenic mutants are novel Δ*pta* and Δ*hdac* for *N. gonorrhoeae*.

These strains were analysed to characterise them phenotypically by growing hem in different carbon sources to determine how PTA-AK is involved in the metabolism. Thus, the proteome and acetylome of the four strains was analyse to analyse the proteins that suffer lysine acetylation.

The acetylome gave us important information of how this is involved in the metabolism and virulence of the bacteria. Interestingly, the isogenic strain Δ*pta* showed less virulence than the WT and therefore, it was decided to crystallise the enzyme phosphotransacetylase since it is a Pta class II and no structure of this enzyme has been obtained.

# Chapter 2

# Materials & Methods

# 2 Materials and methods

## 2.1 Bacterial strains and plasmid constructs

In this study, twelve strains were used (table 2.1). *N. gonorrhoeae* MS11 was used to create strains with a kanamycin insertion in three different enzymes involved in either acetylation or deacetylation. *Escherichia coli* DH5α, *E.coli* XL-1 blue and *E. coli* BL21-DE3 were used to construct an *E. coli* strain that overexpresses the protein Pta.

**Table 2.1 Strains of bacteria used and plasmid constructs in this study**

| Strain | Description and genotype | Source |
|---|---|---|
| *N. gonorrhoeae* MS11 | Wild type, isolated from uncomplicated gonorrhoeae, contains gonococcal genetic island and it possesses a higher rate transformation than *N. gonorrhoeae* FA1090 (Jordan, Snyder and Saunders, 2005; Duffin and Seifert, 2010). | J. Sayers |
| *N. gonorrhoeae* MS11 Δ*ackA*::*kan*$^r$ | MS11 with disrupted genomic copy of *ackA* by insertion of kanamycin resistance gene. | Felix-Diaz Parga, 2017 |
| *N. gonorrhoeae* MS11 Δ*pta*::*kan*$^r$ | MS11 with disrupted genomic copy of *pta* by insertion of kanamycin resistance gene. | Felix Diaz Parga, 2017 |
| *N. gonorrhoeae* MS11 Δ*hdac*::*kan*$^r$ | MS11 with disrupted genomic copy of *hdac* by insertion of kanamycin resistance gene. | This study |
| *Escherichia coli* DH5α | F$^-$ *endA1 gln*V44 *thi-1 recA1 relA1 gyr*A96 *deoR nupG purB20* φ80d*lac*ZΔM15 Δ(*lacZYA-argF*)U169, hsdR17($r_k^-m_k^+$), λ$^-$<br>Competent bacterium with high transformation rate. Deletion of *lacZ*α gene. | Hanahan, 1983 |

| | | |
|---|---|---|
| *Escherichia coli* DH5α pBHR1-GFP | *E. coli* DH5α transformed with a PBHR1 plasmid, which possesses kanamycin resistance and the insert of *gfp* that encodes the green fluorescent protein. | This work |
| *Escherichia coli* DH5α pLES2 | *E. coli* DH5α transformed with the pLES2 plasmid, which contains the *lacZα* gene, and ampicillin resistance (*amp*$^{r}$) gene. | This work |
| *Escherichia coli* DH5α pLES2-GFP | *E. coli* DH5α transformed with the pLES2 plasmid containing the *gfp* gene. | This work |
| *Escherichia coli* XL1-blue | *recA1 endA1 gyrA96 thi-1 hsdR17 supE44 relA1 lac [F' proAB lacI*$^{q}$*ZΔM15 Tn10 (Tet*$^{r}$*)]*<br>High transformation rate and tetracycline resistant. | Bullock, Fernandez and Short, 1987 |
| *Escherichia coli* XL1-blue pET28a-pta-his | *E. coli* XL1-blue transformed with the expression vector pET28a containing the insert to express, pta-his. | This work |
| *Escherichia coli* BL21-DE3 | F$^{-}$ *ompT gal dcm lon hsdS*$_{B}$($r_{B}^{-}m_{B}^{-}$) λ(DE3 [*lacI lacUV5-T7p07 ind1 sam7 nin5*]) [*malB*$^{+}$]$_{K\text{-}12}$(λ$^{S}$)<br>Also known as *E. coli* str. B, contains a λ prophage carrying the T7 RNA polymerase and the lactose operon repressor *lacI*$^{q}$. | Studier and Moffatt, 1986 |
| *Escherichia coli* BL21-DE3 pET28a-pta-his | *E. coli* str. B transformed with the expression vector pET28a containing the insert pta-his. | This study |

## 2.2 Media and growth conditions

### 2.2.1 *Neisseria gonorrhoeae*

Gonococcus is a fastidious bacterium that requires special nutrients for growing. Therefore, four different media were used and each medium was employed for a specific aim.

#### 2.2.1.1 Solid medium

Stocks of *N. gonorrhoeae* stored at -80 °C were routinely grown on chocolate agar (CHO) (E & O Laboratories Limited, Scotland) or Gonococcus agar (GC) (Oxoid, UK) with 1% Kellogg's supplement (glucose, 40.0 g; glutamine, 0.5 g; ferric nitrate, 0.05 g; cocarboxylase, 2.0 mg; dissolved in 100 mL distilled water) (Kellogg et al., 1963) at 37 °C and 5% CO2 atmosphere in a $CO_2$ incubator model MCO-15AC (Sanyo, Osaka, Japan). The isogenic mutant strains of the gonococcus were growth on a GC agar supplemented with 80 µg/mL kanamycin at the same growing conditions mentioned previously.

#### 2.2.1.2 Liquid medium

For growth in liquid culture, it was utilised brain heart infusion broth (Oxoid, UK) supplemented with 0.5% yeast extract (Oxoid, UK) (BHI-Y). The cultured was incubated at 37 °C and with shaking, at 180 rpm for 25 mL tubes in a C25KC incubator shaker (New Brunswick Scientific, NJ, USA) and 120 rpm for 500 mL flasks in an Excella E25 incubator shaker (New Brunswick Scientific, NJ, USA), 10 mM $NaHCO_3$ was added to create a $CO_2$ atmosphere.

A chemically defined medium for *N. gonorrhoeae* (CDM-GC) was used to observe the utilisation of three different carbon sources, glucose, lactate and pyruvate. This medium contains all the necessary nutrients for the gonococcus growth (table 2.2).

**Table 2.2 Composition and preparation of the chemically defined medium (CDM-GC) for the growth of *N. gonorrhoeae***

| Solutions and reagents | Amount (weight or volume) |
|---|---|
| **Solution I** | |
| Sodium chloride | 58.45 g |
| Potassium sulphate ($K_2SO_4$) | 10.00 g |
| Magnesium chloride (MgCl2) | 2.18 g |
| Ammonium chloride | 2.20 g |
| EDTA | 0.03 g |
| $H_2O$ | 250 mL |
| **Solution II** | |
| Potassium phosphate dibasic ($K_2HPO_4$) | 17.42 g |
| Potassium phosphate monobasic ($KH_2PO_4$) | 13.61 g |
| $H_2O$ (Total volume) | 100 mL |
| **Solution III** | |
| L-aspartic acid | 2.00 g |
| L-glutamic acid | 5.20 g |

| | |
|---|---|
| L-arginine HCl | 0.60 g |
| Glycine | 0.10 g |
| L-Serine | 0.20 g |
| L-leucine | 0.364 g |
| L-isoleucine | 0.12 g |
| L-valine | 0.24 g |
| L-tyrosine | 0.284 g |
| L-cysteine | 0.22 g |
| L-cysteine (dissolved in 1M HCl) | 0.144 g |
| L-alanine | 0.40 g |
| L-lysine | 0.197 g |
| L-proline | 0.198 g |
| L-tryptophan | 0.32 g |
| L-threonine | 0.20 g |
| L-phenylalanine | 0.10 g |
| L-asparagine H2O | 0.104 g |
| L-glutamine | 0.20 g |
| L-histidine | 0.096 g |
| L-methionine | 0.06 g |
| Glutathione (reduced form) | 0.184 g |
| $H_2O$ | 1000 mL |

**Solution IV**

| | |
|---|---|
| Thiamine HCl | 0.02 g |
| Calcium pantothenate | 0.019 g |
| Cocarboxilase (Thiamine pyrophosphate chloride) | 0.0048 g |
| $H_2O$ | 100 mL |

**Solution V**

| | |
|---|---|
| Biotin | 0.015 g |
| 50% ethanol | 50 mL |

**Solution VI**

| | |
|---|---|
| Calcium chloride dihydrate | 0.37 g |
| Ferric nitrate | 0.04 g |
| $H_2O$ | 10 mL |

**Other solutions**

**Hypoxanthine**

| | |
|---|---|
| Hypoxanthine | 0.25 g |
| 0.1 M NaOH | 50 mL |

**Phenol red 0.001%**

| | |
|---|---|
| Phenol red | 0.001 g |
| $H_2O$ | 100 mL |

**Sodium hydrogen carbonate ($NaHCO_3$) 1 M**

| | |
|---|---|
| $NaHCO_3$ | 8.4 g |
| $H_2O$ | 100 mL |

**Glucose 1 M**

| | |
|---|---|
| Glucose | 18.00 g |
| $H_2O$ | 100 mL |

**Lactate 1 M**

| | |
|---|---|
| Lactate | 9.00 g |
| $H_2O$ | 100 mL |

**Pyruvate 1 M**

| | |
|---|---|
| Pyruvate | 8.80 g |
| $H_2O$ | 100 mL |

**Preparation of 100 mL CDM-GC**

| **Solution** | **Volume (mL)** |
|---|---|
| Solution I | 2.50 |
| Solution II | 2.00 |
| Solution III | 25.00 |
| Solution IV | 1.00 |
| Solution V | 1.00 |

| | |
|---|---|
| Solution VI | 0.10 |
| Hypoxanthine | 1.00 |
| Phenol red 0.001% | 1.00 |
| Glucose 1 M | 1.00 |
| $H_2O$ | 64.40 |
| or | |
| Lactate or pyruvate 1 M | 2.00 |
| $H_2O$ | 63.40 |
| $NaHCO_3$ 1 M (Freshly made and added before bacteria inoculation) | 1.00 |
| Adjust to a pH of 7.0 with 5 M NaOH | |

Media were autoclaved at 121 °C and 15 PSI for 20 min, except for the CDM, which all solutions were filter sterilised with a sterile and endotoxin free 0.2 µm PES filter Puradisc$^{TM}$ (GE Healthcare, UK).

## 2.2.2 *Escherichia coli*

### 2.2.2.1 Solid medium

*E. coli* DH5α was grown in Luria-Bertani (LB) agar (tryptone, 10.0 g; yeast extract, 5.0 g; NaCl, 10.0 g; bacteriological agar, 15 g; $H_2O$, 1000 mL). Several types of LB agar were prepared by adding antibiotics depending on the strain to select in the transformation experiments, which will be explained in the next sections.

### 2.2.2.2 Liquid medium

LB broth (same composition but without agar) broth was used to grow the different strains of *E.coli* at 37 °C with rotation using incubator shakers mentioned in section (section

2.2.1.2) depending on the volume to employ. This liquid medium was used as a base for other experiments that required specific growing conditions for either selection or protein expression.

## 2.3 Competent cells preparation

The transformation of the different *E. coli* strains (*E. coli* DH5α, *E. coli* XL1-blue and *E. coli* str. B) required that the bacteria were competent, this means that they were able to uptake extracellular DNA. In order to obtain competent cells, the Hanahan method was employed (Hanahan, 1983).

*E. coli* strains were grown overnight on LB agar plates. Colonies were taken to inoculate 50 mL LB broth and incubated for 6 h at 37 °C and 180 rpm in a C25KC incubator shaker (New Brunswick Scientific, NJ, USA) until the culture reached an optical density ($OD_{600}$) of 0.3. The growth was chilled on ice for 15 min and centrifuged at 3,500 x *g* for 20 min at 4 °C in an Allegra™ X-22R centrifuge (Beckman-Coulter, Krefeld, Germany). The bacterial pellet was re-suspended in 16.65 mL RF1 solution (table 2.3), a 1/3 of the original volume, and incubated on ice for 15 min. The bacterium was centrifuged again at the same conditions and the pellet was re-suspended with 4 mL RF2 solution (table 2.4), a 1/12.5 of the original volume, and incubated on ice for 15 min. 200 µL aliquots were added into 1.5 mL microcentrifuge tubes and stored at -80 °C until use.

**Table 2.3. Composition and preparation of 100 mL RF1 solution**

| Component | Final concentration | Amount |
|---|---|---|
| Potassium chloride (KCl) | 100 mM | 0.75 g |
| Manganese (II) chloride ($MnCl_2$ ) | 50 mM | 0.99 g |
| Potassium acetate ($CH_3CO_2K$) | 30 mM | 0.29 g |
| Calcium chloride dehydrate ($CaCl_2$-$2H_2O$) | 10 mM | 0.15 g |
| Glycerol | 15% (v/v) | 15.00 mL |
| $H_2O$ | | 85.00 mL |
| Adjust to a pH of 5.8 with 10% glacial acetic acid, and filter sterilise through a pre-rinsed 0.22 micron membrane. | | |

**Table 2.4. Composition and preparation of 100 mL RF2 solution**

| Component | Final concentration | Amount |
|---|---|---|
| MOPS (3-(N-morpholino) propanesulfonic acid) pH 6.8 | 10 mM | 0.21 g |
| Potassium chloride (KCl) | 10 mM | 0.074 g |
| Calcium chloride dehydrate ($CaCl_2$-$2H_2O$) | 75 mM | 1.1 g |
| Glycerol | 15 % (v/v) | 15.00 mL |
| $H_2O$ | | 85.00 mL |
| Adjust to a pH of 6.8 with 1 M NaOH and filter sterilise as with RF1. | | |

## 2.4 Cryogenic preservation

Liquid cultures of BHI-Y and LB for *N. gonorrhoeae* and *E. coli*, respectively, were grown overnight at 37 °C on a rotary shaker at 180 rpm overnight.

In a 1.0 mL cryogenic tube (Thermo Scientific™ Nalgene™, Waltham, MA, USA) 500 µL of culture was mixed with the same volume of 20% glycerol (v/v) and stored in an ultra-low-temperature freezer at -80 °C.

## 2.5 Mutant construction

### 2.5.1 *Neisseria gonorrhoeae* MS11

#### 2.5.1.1 Genomic DNA (gDNA) extraction

*N. gonorrhoeae* MS11 was grown overnight on chocolate agar plate as described in section 2.2.1.1 and then in 10 mL liquid medium as described in section 2.2.1.2. 1.5 mL of culture was centrifuged at 12,000 x *g* for 2 min and re-suspended in 1 mL PBS. The extraction was performed following the protocol of GenElute™ Bacterial genomic DNA kit (Sigma® Life Science, St. Louis, MO, USA). The steps include cell lysis, DNA binding to a column, column washing and gDNA elution. The gDNA was eluted in a final volume of 80 µL. The quality and concentration of the gDNA were quantified using a NanoDrop® ND-1000 spectrophotometer (Thermo Fisher Scientific™, Waltham, MA, USA). The extraction was validated with a 260/280 ratio value of ~1.8.

#### 2.5.1.2 Annealing PCR

Annealing PCR is a technique to construct DNA fragments by designing primers with a complementary sequence of the adjacent fragment of DNA. With this technique, a set of 3 to 4 DNA fragments are able to form a unique DNA sequence.

For the construction of the *N. gonorrhoeae* MS11 Δ*hdac*::*kan*$^{r}$ two fragments of the *hdac* gene (NGFG_00325) and the kanamycin resistant gene (*kan*) were amplified by PCR. The primers were designed to possess the complementary sequence of the adjacent fragments, in order to obtain the sequence of the gene *hdac* with the insertion of the kanamycin resistant gene (table 2.5).

**Table 2.5. Primers for the construction of *N. gonorrhoeae* MS11 Δ*hdac::kan*$^r$**

| Strain constructed | Gene | Fragment | Length | Name | Primer sequence (5' → 3') | Nucleotide position |
|---|---|---|---|---|---|---|
| *N. gonorrhoeae* MS11 Δ*hdac::kan*$^r$ | *hdac** | 1 | 467 bp | *hdac*1-F | TGAAACTCTACGCCCTGTTG | 23-42 |
| | | | | *hdac*1-R | *TCATTTTAGCCAT*AACGTTGTTCAGCAG | 453-467 |
| | | 3 | 501 bp | *hdac*2-F | *TGAATTGTTTTAG*TGTTTGAAACCGACCTTTT | 620-638 |
| | | | | *hdac*2-R | TTCAGACGGCATTTATATCG | 1101-1120 |
| | *kan** | 2 | 795 bp | *kan*-F | *CTGAACAACGTT*ATGGCTAAAATGAGAATATCAC | 1-22 |
| | | | | kan-R | *TCGGTTTCAAACA*CTAAAACAATTCATCCAGTAAAA | 773-795 |

*Underlined sequences in italics are complementary to the other fragments for the annealing PCR.

All PCRs were performed using the Q5® High-Fidelity DNA Polymerase ((New England BioLabs®, MA, USA)) and a T100™ thermal cycler (Bio-Rad Laboratories, Hercules, CA, USA). The parameters for the amplification for each of the three fragment are shown in the table 2.6.

**Table 2.6. Reagents and volumes for PCR mix**

| Reagent | Volume (µL) | Final concentration |
|---|---|---|
| 5x Q5® reaction buffer | 10.0 | 1x |
| 10 mM dNTPs | 1.0 | 200 µM |
| 10 µM Forward primer | 2.0 | 0.4 µM |
| 10 µM Reverse primer | 2.0 | 0.4 µM |
| Template DNA | Variable | < 1,000 ng |
| 5x Q5® high GC enhancer | 10 | 1x |
| Q5® High-Fidelity DNA polymerase | 0.5 | 0.02 U/µL |
| Nuclease-free water | To 50 µL | - |

**Table 2.7. PCR conditions for the amplification of the flanking sequences of *hdac* and the kanamycin resistant gene**

| Step | | Temperature | Time |
|---|---|---|---|
| **Initial denaturation** | | 98 °C | 30 s |
| **Denaturation** | 30 cycles | 98 °C | 10 s |
| **Annealing** | | 50.8 °C | 30 s |
| **Extension** | | 72 °C | 1:10 min |
| **Final extension** | | 72 °C | 3:00 min |
| **Hold** | | 4 °C | ∞ |

Finally, the three fragments were used for the PCR (table 2.8) as templates for the final construct (hdac1-kan-hdac2) following the PCR conditions shown in the table 2.9. This fragment was used to transform the strain of *N. gonorrhoeae* MS11.

**Table 2.8. PCR mix for the construction of *hdac::kan***

| Reagent | Volume (µL) | Final concentration |
|---|---|---|
| 5x Q5® reaction buffer | 10.0 | 1x |
| 10 mM dNTPs | 1.0 | 200 µM |
| 10 µM primer (*hdac*1-F) | 2.0 | 0.4 µM |
| 10 µM primer (*hdac*2-R) | 2.0 | 0.4 µM |
| Template DNA *hdac*1 | 1.0 | < 1,000 ng |
| Template DNA *hdac*2 | 1.0 | < 1,000 ng |
| Template DNA *kan* | 1.0 | < 1,000 ng |
| 5x Q5® high GC enhancer | 10 | 1x |
| Q5® High-Fidelity DNA polymerase | 0.5 | 0.02 U/µL |
| Nuclease-free water | 21.5 | - |

**Table 2.9. Thermal cycler settings for the construction of *hdac::kan***

| Step | | Temperature | Time |
|---|---|---|---|
| **Initial denaturation** | | 98 °C | 1:00 min |
| **Denaturation** | 30 cycles | 98 °C | 10 s |
| **1st annealing** | | 60 °C | 30 s |
| **2nd annealing** | | 52 °C | 30 s |
| **Extension** | | 72 °C | 2:30 min |
| **Final extension** | | 72 °C | 6:00 min |
| **Hold** | | 4 °C | ∞ |

### 2.5.1.3 DNA gel extraction

Amplicons from PCR were extracted from agarose gels whenever secondary amplicons were detected by the transilluminator. Samples were run on a 0.6% agarose gel at 110 V for 70 min using a PowerPac™ 300 power supply (Bio-Rad Laboratories, CA, USA). The DNA product was then purified from the electrophoresis gel following the protocol of Monarch® DNA gel extraction kit (New England BioLabs®, MA, USA). The DNA was quantified in a NanoDrop 1000 spectrophotometer (Thermo Scientific™, Waltham, MA, USA). If the concentration of the sample was low (<40 ng/µL), thus was concentrated using a concentrator 5301 (Eppendorf, Hamburg, Germany) and re-suspended in nuclease free water to obtain a minimum DNA concentration of 100 ng/µL and a 260/280 ratio of at least 1.8.

### 2.5.1.4 Agar spot transformation and mutant selection

The spot transformation on agar plates protocol was followed as described previously by Dillard, 2011. On a chocolate agar plate, 12 µL of PCR product (≈ 2 µg DNA) $^{r}$ were added on 2 different locations of the plate were the bacteria growth is medium and thin. Colonies of *N. gonorrhoeae* MS11 grown overnight on chocolate agar were streaked on the DNA spots once they were dried. The plates were incubated as described in section 2.2.1.1 for 48 h.

Colonies that grew were streaked individually on GC agar supplemented with 80 µg/mL kanamycin and grew overnight as described in section 2.2.1.1. After 48 h the grown colonies were inoculated in liquid medium for PCR, sequencing and cryogenic conservation. The colonies that showed the correct sequencing were stored at -80 °C and only one colony was used during the whole project.

### 2.5.2 *Neisseria gonorrhoeae* with GFP

*N. gonorrhoeae* possesses the ability to survive within macrophages (Château and Seifert, 2016). Therefore, the construction of *N. gonorrhoeae* with GFP expression could show us by microscopy if the acetylation affects the mechanisms that help gonococci to remain within immune cells. In order to achieve this, a vector carrying the *gfp* gene of *Aequoria victoria* able to be transformed into *N. gonorrhoeae* was constructed. pLES2 is a plasmid that has shown to transform strains of both *E. coli* and *N. gonorrhoeae* (Stein *et al.*, 1983).

#### 2.5.2.1 Transformation and plasmid pBHR1-GFP purification

A vial with 200 µL of competent *E. coli* DH5α was taken from the -80 °C and thawed on ice. 2 µL of pBHR1-GFP was added and incubated on ice for 1 h. Then the microcentrifuge tube was hot shocked at 48 °C for 90 s and incubated on ice for 5 min. 800 µL LB broth were added and the tube was incubated for 1 h at 37 °C with shaking at 180 rpm. 100 µL of culture were plated on LB agar with 100 µg/mL kanamycin (LB-Kan100) plate and incubated as described above (section 4.2.1). Colonies grown on the agar were streaked on LB-Kan and to verify that the strain was producing GFP the plate was located onto a UV transilluminator to observe fluorescence. The plasmid was extracted following the protocol of the E.Z.N.A.® Plasmid Mini Kit I (Omega Bio-tek, GA, USA) and a 0.6% agarose gel was run at 110 V for 70 min to verified the size of the vector. A set of primers were designed to amplify the *gfp* gene containing a BamHI restriction site sequence for the ligation to the pLES2 plasmid (table 2.10).

**Table 2.10. Primers for the amplification of the *gfp* gene from pBHR1-GFP**

| Strain constructed | Gene | Length | Feature | Orientation | Primer sequence (5' → 3') | Nucleotide position |
|---|---|---|---|---|---|---|
| *Escherichia coli* DH5α pLES2-GFP | *gfp* | 1194 bp | **BamHI**** | F | GGTCAG**GGATCC**CTCCCTTTTGGTGTCC | 1-18 |
| | | | **BamHI**** | R | GGTCAG**GGATCC**ATTACTGAGTATCTATTTGTATAGTTCATCC | 1175-1194 |

** Underlined sequence corresponds to the BamHI restriction site.

**Table 2.11 PCR mix for amplification of *gfp***

| Reagent | Volume (µL) | Final concentration |
|---|---|---|
| 5x Q5® reaction buffer | 10.0 | 1x |
| 10 mM dNTPs | 1.0 | 200 µM |
| 10 µM Forward primer | 2.0 | 0.4 µM |
| 10 µM Reverse primer | 2.0 | 0.4 µM |
| Template DNA | Variable | < 1,000 ng |
| 5x Q5® high GC enhancer | 10 | 1x |
| Q5® High-Fidelity DNA polymerase | 0.5 | 0.02 U/µL |
| Nuclease-free water | To 50 µL | - |

**Table 2.12. Thermal cycler settings for *gfp* amplification**

| Step | | Temperature | Time |
|---|---|---|---|
| **Initial denaturation** | | 98 °C | 30 s |
| **Denaturation** | 30 cycles | 98 °C | 10 s |
| **Annealing** | | 48 °C | 30 s |
| **Extension** | | 72 °C | 1:10 min |
| **Final extension** | | 72 °C | 3:00 min |
| **Hold** | | 4 °C | ∞ |

A PCR for *gfp* amplification was performed with the Q5® High-Fidelity DNA Polymerase (table 2.11) using a T100™ thermal cycler (Bio-Rad Laboratories, Hercules, CA, USA) set with the parameters of the table 2.12.

The PCR sample was run in an agarose gel and the band corresponding to *gfp* (~ 1.2 kb) was extracted from the gel as mentioned previously. The purified product was then ligates to the pLES2 plasmid.

#### 2.5.2.2 pLES2-GFP construction

*E. coli* DH5α was transformed with pLES2 as described above, however, for the selection of the transformed colonies LB agar with IPTG/X-Gal and 100 µg/mL ampicillin (section 4.3.2) was used, selecting the blue colonies. The plasmid was then extracted and a 0.6% agarose gel was run as described above to confirm the plasmid extraction. pLES2 and *gfp* PCR product were digested with BamHI enzyme (New England BioLabs®, MA, USA) using 600-1500 ng of DNA. The digestion was at 37 °C for 1.5 h and the samples were run on an agarose gel to check the restriction digestion.

pLES2 vector and the *gfp* PCR product were then ligated with a T4 ligase (Thermo Scientific™, Waltham, MA, USA) using a DNA to vector ratio of 3:1. The reaction was incubated at 22 °C for 15 min and 10 µL of the suspension were dispersed on a LB agar with IPTG/X-Gal and 100 µg/mL ampicillin. The plates were incubated at 37 °C overnight and white colonies were re-cultured on same agar plates. To prove the construction of pLES2-GFP, plasmid extraction was made as described above and a 0.6% agarose gel was run.

*E. coli* DH5α was then transformed with pLES2-GFP following the protocol mentioned above and the bacteria was cultured on LB agar with IPTG/X-Gal and 100 µg/mL

ampicillin. The plasmid was extracted and it was stored at -20 °C until used for the transformation of *N. gonorrhoeae*.

All steps of the construction of the plasmid were verified by DNA sequencing.

### 2.5.3 Construction of *E. coli* BL21 for Pta overexpression

In this study, as later will be explained, the enzyme phosphotransacetylase (NGFG00350) from *N. gonorrhoeae* MS11 is proposed as a good target for an antimicrobial molecule. However, there is no structure of the enzyme and a crystal was needed. Therefore, the enzyme was overexpressed in *E. coli* BL21.

#### 2.5.3.1 PCR of *pta* with polyhistidine tag (pta-his)

The system his-tag was used to purify the enzyme. This mechanism works through the addition of 6 histidine at the N- terminus or C-terminus of the enzyme, in this study was used the latter since the cleavage of the histidine tag is not necessary.

A PCR was performed using gDNA from *N. gonorrhoeae* MS11 as DNA template. The primers (table 2.13) were designed to contain the his-tag, and two different restriction sites. The first restriction sequence corresponded to NcoI, this restriction enzyme was selected because it codifies for a methionine, amino acid required for the open reading frame. The second restriction enzyme was BamHI. The two restrictions sites are present in the plasmid pET28 where the pta-his was transformed.

The amplification of pta-his was performed following the PCR conditions showed in table 2.14.

**Table 2.13 Primers for the PCR of *pta*-his**

| Strain constructed | Gene | Length | Feature | Orientation | Primer sequence (5' → 3') | Nucleotide position |
|---|---|---|---|---|---|---|
| *Escherichia coli* XL1-blue pET28a-pta-his | *pta* | 1541 bp | **NcoI**** | F | CTGAGT**CCATGG**CAAAAGTACTCGTCGTAC | 1-31 |
| | | | **BamHI**** and 6x his tag | R | CTGACC**GGATCC**TCAGTGGTGGTGGTGGTGGTGCCTTCCATTTGTTTTGCCTG | 1488-1541 |

**Table 2.14 Thermal cycler settings for *pta*-his amplification**

| Step | | Temperature | Time |
|---|---|---|---|
| **Initial denaturation** | | 98 °C | 1:00 min |
| **Denaturation** | 34 cycles | 98 °C | 10 s |
| **Annealing** | | 63 °C | 30 s |
| **Extension** | | 72 °C | 1:00 min |
| **Final extension** | | 72 °C | 2:00 min |
| **Hold** | | 4 °C | ∞ |

### 2.5.3.2 Construction of plasmid pET28-pta-his

The plasmid pET28 is used for the overexpression of proteins due to the presence of the lac promoter that is activated by the addition IPTG in the medium.

#### 1.1.3.2.1. Plasmid extraction

*E. coli* α pET28 was grown overnight on an LB agar supplemented with 50 µg/mL kanamycin (LB-Kan50) at 37 °C and then in a liquid medium of LB-Kan50 overnight with shaking at 37 °C. The plasmid was extracted following the protocol of the E.Z.N.A.® Plasmid Mini Kit I (Omega Bio-tek, GA, USA) and the sample was run in a 0.6% agarose gel to check the size and success of extraction. Then it was quantified using a NanoDrop® ND-1000 spectrophotometer (Thermo Fisher Scientific™, Waltham, MA, USA). The extraction was validated with a 260/280 ratio value of ~1.8 and a concentration higher than 100 ng/µL.

#### 1.1.3.2.2. Restriction enzyme digestion

For the restriction, 2 µg of plasmid pET28 and pta-his amplicon were enzymatically digested with NcoI and BamHI (New England BioLabs®, MA, USA) for 2 h at 37 °C in 50 µL volume. Each sample was run in a 1.4% agarose gel at 100 V for 80 min using a PowerPac™ 300 power supply (Bio-Rad Laboratories, CA, USA) to prove the efficacy of the digestion.

#### 1.1.3.2.3. Ligation and transformation

In order to construct the pET28-pta-his the PCR product was ligated to the pET28 vector using the T4 ligase (Thermo Fisher Scientific™, Waltham, MA, USA). It was used an insert-plasmid ratio of 3:1 and it was followed the protocol. Two different ligation reactions were set a 16 and 22 °C for 15 min and 1 h, respectively. Then the T4 ligase was heat inactivated at 70 °C for 5 min. Then the ligation product was transformed as

described in section 2.2.6.1 in a strain of *E. coli* XL-1 blue and the plasmid was then extracted for the transformation of *E. coli* BL21-D3.

To validate and confirm the correct ligation of the pta-his insert into the pET28 vector, a PCR (table 2.16) was performed using universal T7 polymerase primers (table 2.15).

**Table 2.15 Primer for insert validation of the vector pET28**

| Gene | Orientation | Primer sequence (5' → 3') |
|---|---|---|
| **T7 polymerase** | F | TAATACGACTCACTATAGGG |
| | R | TATGCTAGTTATTGCTCAG |

**Table 2.16 Thermal cycler settings for T7 polymerase amplification with pta-his insert**

| Step | | Temperature | Time |
|---|---|---|---|
| **Initial denaturation** | | 98 °C | 2:00 min |
| **Denaturation** | 34 cycles | 98 °C | 10 s |
| **Annealing** | | 55 °C | 30 s |
| **Extension** | | 72 °C | 1:15 min |
| **Final extension** | | 72 °C | 3:00 min |
| **Hold** | | 4 °C | ∞ |

### 2.5.3.3 Construction of *E. coli* BL21-DE3 pET28a-pta-his

*E. coli* Bl21-D3 is a strain that is widely used in laboratories for the overexpression of proteins due to the presence of T7 RNA polymerase and the lactose operon repressor *lacI*$^{q}$, repressing the expression of the recombinant protein until the addition of IPTG to the medium.

*E. coli* BL21-D3 was transformed with the pET28 *pta*-his vector following the protocol of section 2.2.6.1. The bacteria was grown overnight at 37 °C on LB-Kan50 agar plates for the selection of transformed colonies. A screening PCR, described in section 2.2.7.2.3 was performed to the grown colonies to confirm the successful transformation. The amplicon was cleaned up and sent for sequencing. The selected colony was cryogenic preserved as described in section 2.4.

## 2.6 DNA sequencing

DNA sequencing was used in order to check if the obtained colonies possessed the correct DNA insert. Briefly, PCR products, plasmids, and primers were diluted to 50 ng/µL, 100 ng/µL, and 1 pmol/µL in a final volume of 10 µL distilled water, respectively. All sequencing were performed at the Genomics Core Facility, The Medical School, University of Sheffield, UK.

## 2.7 Enzymatic assay

In order to prove that the mutant strains of *N. gonorrhoeae* MS11 lack of enzymatic activity on the mutated genes *ackA* and *pta*, an enzymatic assay was assessed for each enzyme.

### 2.7.1 Cell free extract (CFE)

CFE was obtained from the three strains of *N. gonorrhoeae*, WT, Δ*ackA* and Δ*pta*. Liquid cultures of each strains were grown in 30 mL BHI-Y at 37 °C overnight at 180 rpm. The culture was transferred to a 500 mL capped flask containing 450 mL BHI-Y and incubated overnight at 37 °C at 120 rpm. The culture was centrifuged at 12,000 x *g* for 15 min in an Avanti J-26XP high-speed centrifuge (Beckman-Coulter, Krefeld, Germany) using a Jla 16.250 Rotor.

The supernatant was discarded and the pellet was re-suspended in 20 mL 10 mM Tris/HCl buffer (pH 8.0) in a 50 mL tube and it was centrifuged at 12,000 x *g* for 15 min using a Jla 25.50 rotor. The pellet was re-suspended in 2 mL 10 mM Tris/HCl buffer (pH 8.0) in a 20 mL capped tube and it was sonicated 7 times during 30 s each at 20 amplitude maintaining the tubes on ice during sonication. The suspension was transferred to a 1.5 mL microcentrifuge tubes and centrifuged at 13,000 x *g* for 25 min at 4 °C in a Mikro 220R centrifuge (Hettich, Tuttlingen, Germany). The supernatant was then transferred into a 1.5 mL microcentrifuge tubes. The protein concentration was quantified at a 280 nm wavelength using a NanoDrop 1000 spectrophotometer (Thermo Scientific™, Waltham, MA, USA) and stored at -20 °C until use.

### 2.7.2 Acetate kinase (AckA) activity assay

The quantification of AckA activity was determined using a modified version of a couple reaction protocol (Allen *et al.*, 1964). The activity was traced by detecting the formation of ADP from ATP and acetate at 340 nm by coupling the reaction with the reduction of $NAD^+$ with the enzymes pyruvate kinase and lactate dehydrogenase (fig 4.1). To the reaction was added P1, P5-Di(adenosine-5')pentaphosphate ($Ap_5A$) to inhibit the activity of adenylate kinase, an enzyme that is involved in the regulation of ATP, ADP and AMP.

A 1 mL final volume of the reaction mix (table 4.5) was added into quartz SUPRASIL® cuvette with a 10 mm light path (Hellma® Analytics, Müllheim, Germany). The cuvette was inserted into the spectrophotometer and the reaction was started by the addition of the CFE. A BioSpectrometer Kinect spectrophotometer (Eppendorf, Hamburg, Germany) was used for the enzymatic assay and it was set to a 340 nm wavelength at 37 °C and interval readings of 15 s during 60 m. All the reactions were standardised with the same amount of protein and a reaction mix containing no CFE was used as blank.

**Table 2.17 Reaction mix for the AckA activity**

| Reagent | Final concentration | Volume (µL) |
|---|---|---|
| 1.5 M Tris/HCl buffer (pH 8.0) | 100 mM | 66.7 |
| 0.1 M $MgCl_2 \cdot H_2O$ | 2 mM | 20 |
| 0.1 M Phosphoenolpyruvate (PEP) | 2 mM | 20 |
| 5 mM NADH | 0.1 mM | 20 |
| 3 U/µL Pyruvate kinase | 9 U | 3 |
| 7 U/µL malate dehydrogenase | 26 U | 3.7 |
| 10 mM $Ap_5A$ | 0.2 mM | 20 |
| 100 mM Acetate | 2 mM | 20 |
| 75 mM ATP | 1.5 mM | 20 |
| CFE | 8-15 mg/mL | Variable |
| $H_2O$ | | to 1 mL |

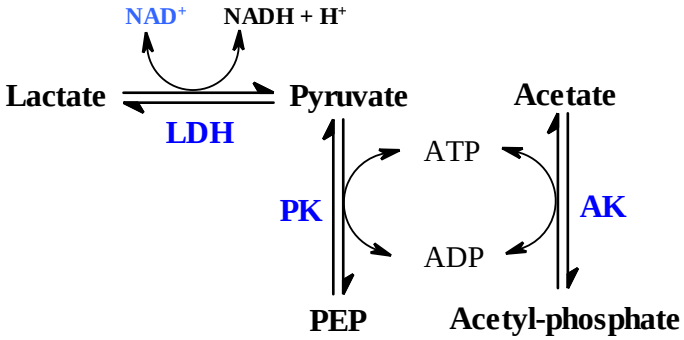


**Figure 2.1. Couple reactions for the determination of AckA activity.** The reaction was linked with the activity of lactate dehydrogenase (LDH) and pyruvate kinase (PK) in order to determine the activity of acetate kinase (AK). PEP, phosphoenolpyruvate. (Adapted from: Allen *et al.*, 1964).

### 2.7.3 Phosphotransacetylase (Pta) activity assay

The determination of Pta activity was performed using a modified couple reaction protocol (Pickett, Williamson and Kelly, 1994). Pta activity was traced by coupling three reactions which are involved in the acetyl-CoA dependent synthesis of citrate. NADH formation was measured at 340 nm whereas its formation by malate dehydrogenase is negligible in the absence of acetyl-CoA (fig. 2.2).

A 1 mL final volume of the reaction mix (table 2.18) was added into quartz SUPRASIL® cuvette with a 10 mm light path (Hellma® Analytics, Müllheim, Germany). The cuvette was inserted into the spectrophotometer and when a baseline was observed, acetyl-phosphate was added to start the reaction. A BioSpectrometer Kinect spectrophotometer (Eppendorf, Hamburg, Germany) was used for the enzymatic assay and it was set to a 340 nm wavelength at 37 °C and interval readings of 15 s during 60 min. All the reactions were standardised with the same amount of protein and a reaction mix containing no CFE was used as blank.

**Table 2.18. Reaction mix for the Pta activity**

| Reagent | Final concentration | Volume (µL) |
|---|---|---|
| 1.5 M Tris/HCl buffer (pH 8.0) | 100 mM | 66.7 |
| 0.1 M $MgCl_2 \cdot H_2O$ | 2 mM | 20 |
| 50 mM $NAD^+$ | 1 mM | 20 |
| 5 mM CoA-SH | 0.2 mM | 40 |
| 250 mM D/L malic acid | 5 mM | 20 |
| 6 U/µL malate dehydrogenase | 12 U | 2 |
| 3 U/µL citrate synthase | 25 U | 8 |
| CFE | 4-5 mg/mL | Variable |

| | | |
|---|---|---|
| $H_2O$ | | to 1 mL |
| 200 mM AcP | 10 mM | 50 |

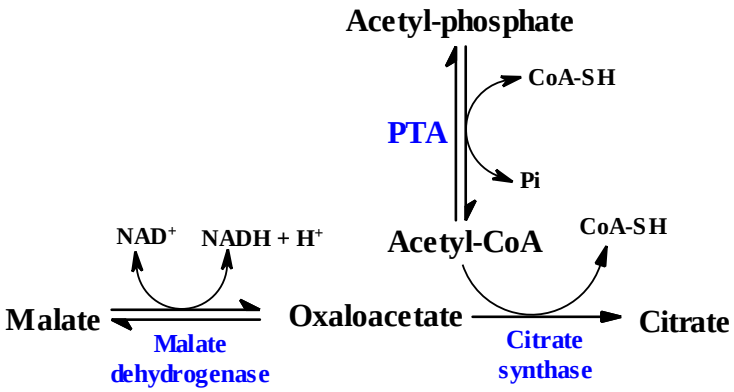


**Figure 2.2. Coupled reactions for the determination of Pta activity.** Pta activity was determined by tracing the formation of acetyl-CoA reaction coupled to citrate synthase and malate dehydrogenase that produces NADH which can be measure at 340 nm (Adapted from: Whiteley and Pelroy, 1972).

The enzymatic activity was calculated using the Beer's formula:

$$\mathbf{\Delta c} = \frac{\Delta A}{(\varepsilon)(d)}$$

Where the enzyme activity (Δc) is derived from the change in absorbance per minute (ΔA), divided by the mM absorptivity of the product (ε) which is NADH (6.22 $mM^{-1}$ $cm^{-1}$) and the path length of light through the sample which was 1 cm.

The activity is expressed in nano moles of product synthesise per minute per mg of protein ($nmol^{-1}$ $min^{-1}$ mg $protein^{-1}$).

## 2.8 Acetyl-phosphate (AcP) quantification

The different strains of *N. gonorrhoeae* MS11 were thought to have varying concentrations of AcP. Therefore, it was used a method that quantifies the amount of AcP by determining the ATP released in the reaction of AcP to acetate performed by acetate kinase. The assay was followed as previously (Ramos-Montañez *et al.*, 2010; Weinert *et al.*, 2013) with the following modifications.

35 mL of BHI-Y cultured were grown for 10 h from an initial $OD_{600}$ 0.5. The culture was centrifuged at 3,500 rpm x *g* for 20 min at 4 °C in an Allegra™ X-22R centrifuge (Beckman-Coulter, Krefeld, Germany). The pellet was washed twice with 500 µL ice-cold assay buffer (10 mM sodium phosphate [$Na_3PO_4$] pH 7.5; 10 mM $MgCl_2$; 1 mM EDTA) and centrifuge at 13,000 x *g* for 2 min in 5415 D centrifuge (Eppendorf, Hamburg, Germany). 20 µL were set aside for protein quantification reading the sample at $OD_{280}$. Protein concentration was used to normalise AcP measurements. Cell suspensions were extracted by addition of 100 µL 3 M $HClO_4$ (perchloric acid) and incubated on ice for 30 min. The suspensions were clarified by centrifugation at 10,000 x *g* for 2 min at 4 °C and the supernatant neutralised with 100 µL saturated $KHCO_3$ (potassium bicarbonate). The samples were then clarified by the same centrifugation conditions and the supernatant was transferred to a new 1.5 mL microcentrifuge tube with 30 mg activated charcoal to remove ATP. Lysates were incubated on ice for 15 min and then filtered to remove the charcoal using a sterile and endotoxin free 0.2 µm PES filter Puradisc™ (GE Healthcare, UK).

The lysates were divided in three groups; ATP conversion assays for AcP measurements; control reactions without acetate kinase and ATP measurement for efficiency of ATP removal. The reaction mix for AcP measurement contained 50 µL lysate, 2 µL 100 mM

$MgCl_2$, 4 µL 300 mM ADP, and 4 µL 0.4 U/µL acetate kinase. The assay was performed in triplicates and the control reaction contained the same reagents except ice-cold buffer was used instead of the enzyme, the control assay was performed in duplicates. The tubes were mixed and incubated at 37 °C for 90 min. ATP was determined by mixing 50 µL of the reaction with 50 µL CellTiter-Glo® reagent (Promega, Madison, WI, USA), which is a luminescent viability assay that quantifies the amount of ATP by the reaction of luciferase that converts luciferin to oxyluciferin with the release of light. ATP measurement was performed to determine the level of ATP contamination of the sample by mixing 50 µL of the filtrated lysate with 50 µL CellTiter-Glo® reagent.

To validate the results, a control for the recovery of AcP was performed. This control was done by adding known samples of AcP (1, 5, 10, 25, and 50 µM) to the reaction mix instead of the sample at the beginning of the procedure. ATP concentrations were determined by comparing the results to an ATP standard curve (1, 5, 10, 25, and 50 µM). A specific concentration of ATP was added into the reaction and the procedure was followed as described above but without the addition of charcoal and the posterior filtering. As with the samples, the control and the ATP standard curve, were mixed 1:1 with the CellTiter-Glo® reagent in triplicates.

The samples were read on a Varioskan™ Flash multimode reader (Thermo Scientific™ Nalgene™, Waltham, MA, USA), instrument that can detect luminescence released by the luciferase. The samples were loaded on a Microfluor® 1 black 96-well microplate with flat bottom (Thermo Scientific™, Waltham, MA, USA). The concentration of AcP and ATP was determined by interpolating the result to the standard curve of both molecules.

## 2.9 Carbon source utilisation

*N. gonorrhoeae* can only metabolise three molecules as carbon and energy sources (Mcgee and Rest, 1996). The four different strains of gonococci were grown on the CDM-GC supplemented with glucose, lactate or pyruvate, in order to determine if the mutations in the *ackA, pta,* and *hdac* genes affected the metabolism of these three carbon sources.

### 2.9.1 Growth conditions

The four strains of *N. gonorrhoeae* MS11, WT, Δ*hdac*, Δ*ackA* and Δ*pta*, were grown on CHO agar for 18 h as described in section 2.2.1.1. Colonies were taken from the agar plates and inoculated each strain in two 25 mL capped tubes (Sarstedt, Nümbrecht, Germany) containing 10 mL CDM-GC supplemented with glucose section 2.2.1.2. The tubes were incubated at 37 °C with shaking at 180 rpm for 16 h. Then they were centrifuged at 4,000 x *g* for 10 min, and the pellets were re-suspended with 10 mL CDM-GC with the carbon source to test, either lactate or pyruvate. The growth was measured using an Ultrospec III spectrophotometer (Pharmacia, Sweden) at 600 nm in disposable 1.5 mL polystyrene cuvettes with a 10 mm light path (Sarstedt, Nümbrecht, Germany). The culture was adjusted to a final 0.05 $OD_{600}$ with the bacterial culture and the CDM-GC with the supplemented carbon source to test. The amount of culture to use for the adjustment of optical density was calculated using the formula:

$$\text{Volume of culture} = \frac{0.75}{\text{OD}_{600} \text{ of stock culture}}$$

An initial $OD_{600}$ was measured and the tubes were incubated at 37 °C with shaking at 180 rpm. $OD_{600}$ measures were read every hour for 10 h.

## 2.10 Detection of lysine acetylated proteins

The constructed mutants are involved in the production of acetyl phosphate and in the deacetylation. In order to compare a difference in the acetylation of proteins between the four strains of *N. gonorrhoeae* MS11, an anti-acetyllysine antibody was used to screen the acetylated proteins.

### 2.10.1 Sample preparation

Samples collected from the growth curves (section 4.8) were thawed and centrifuged at 13,000 x *g* for 3 min in a 5415 D centrifuge (Eppendorf, Hamburg, Germany). Then the pellet was re-suspended in 100 µL modified Laemmli buffer (240 mM Tris-HCl pH 6.8, 10% glycerol (v/v), 2% SDS (w/v)) and heated at 95 °C for 10 min. The concentration of total proteins was quantified in a NanoDrop 1000 spectrophotometer (Thermo Scientific™, Waltham, MA, USA). The samples were stored at -20 °C until use.

### 2.10.2 Sodium Dodecyl Sulphate-Polyacrylamide Gel Electrophoresis (SDS-PAGE)

The SDS-PAGE gel was prepared as described in table 2.19. The samples were loaded at a normalised concentration in two different gels, used for Coomassie staining and western blot. The samples were loaded using 4x Laemmli buffer (1 M Tris-HCl, 8% SDS (w/v), 40% glycerol (v/v), 10% β-mercapto ethanol (v/v), 0.04% bromophenol blue (w/v)). The gels were run in a denaturing buffer (0.25 M Tris, 1.9 M glycine, 0.03 M SDS) at 100 V for 45 min and then at 150 V for 1.5 h using a PowerPac™ 300 power supply (Bio-Rad Laboratories, Hercules, CA, USA).

**Table 2.19. Preparation of 12% SDS-PAGE**

| Reagent | Resolving gel | Stacking gel |
|---|---|---|
| Acrylamide | 3 mL | 0.63 mL |
| $H_2O$ | 4.3 mL | 3.2 mL |
| 10% APS | 100 µL | 50 µL |
| 10% SDS | 100 µL | 50 µL |
| Tris-HCl 1.5 M pH 8.8 | 2.5 mL | - |
| Stacking buffer | - | 0.63 mL |
| TEMED | 10 µL | 4 µL |

For the observation of total proteins, one of the gels was stained during 3 h in Coomassie blue solution (50% methanol (v/v), 10% glacial acetic acid (v/v), 0.25% Coomassie blue (w/v)) and then detained until the protein bands were observed with a destaining solution (40% methanol (v/v), 10% glacial acetic acid (v/v)).

## 2.10.3 Western immunoblot

To detect the lysine acetylated proteins, a western blot was performed using SDS-PAGE gel. The proteins were transferred to an Amersham™ Protran™ nitrocellulose blotting membrane (GE Healthcare Life Science®, Piscataway, NJ, USA) in a transfer buffer (25 mM Tris, 190 mM glycine, 20% (v/v) methanol) at 120 V for 2 h using a PowerPac™ 300 power supply (Bio-Rad Laboratories, Hercules, CA, USA). The blot was then blocked in PBST (PBS with 0.1% Tween® 20 (v/v)) with 5% skimmed milk (w/v) for 1 h. The blot was located into a 50 mL falcon tube (Sarstedt, Nümbrecht, Germany) containing 10 mL PBST with 5% skimmed milk. An anti-acetyllysine monoclonal rabbit antibody (9441 Cell Signaling Technology®, MA, USA) was added (1:1,000) and the tube was incubated at 4 °C on a shaker overnight. The blot was washed three times with PBST with shaking for 5 min each wash and a horseradish peroxidase-conjugated goat anti-rabbit secondary

antibody (Cell Signaling Technology®, Danvers, MA, USA) was used at a 1:5,000 dilution in PBST with 5% (w/v) skimmed milk for 1 h with gentle shaking at room temperature. The membrane was washed as described above. To reveal the blot 4 mL of the chemiluminescence substrate (Amersham™ ECL™ GE Healthcare Life Science®, Piscataway, NJ, USA) were added and a ChemiDoc™ XRS+ System imager (Bio-Rad Laboratories, Hercules, CA, USA) was used to image the bands. The software was set to take images every 3 min during 15 min.

## 2.11 Acetylome

The acetylome is the study of all the protein lysine acetylation sites of an organism. In this study, we used a sensitive immune-affinity purification and high-resolution LC-MS/MS to identify all the acetylation sites of the four different strains of *N. gonorrhoeae* MS11.

### 2.11.1 Cell free extract (CFE)

The four strains of *N. gonorrhoeae* MS11, WT, Δ*hdac*, Δ*ackA* and Δ*pta*, were grown in different steps to amplify the biomass to have a final culture of 1 L. For each strain, four replicates were prepared. The strains were streaked on CHO agar at 37 °C for 18 h. Capped tubes of 25 mL (Sarstedt, Nümbrecht, Germany) containing 15 mL CDM-GC supplemented with glucose each were inoculated with the bacteria and incubated at 37 °C with shaking at 180 rpm in a C25KC incubator shaker (New Brunswick Scientific, NJ, USA) for 18 h. The growth was measured using an Ultrospec 2100 pro spectrophotometer (Biochrom, Cambridge, UK). Falcon tubes of 50 mL (Sarstedt, Nümbrecht, Germany) were inoculated and adjusted to an $OD_{600}$ 0.05 with the growth and CDM-GC with glucose in a final volume of 40 mL. The tubes were then incubated at 37 °C and with shaking at 180 rpm for 16 h. This growth was used to inoculate 1 L CDM-GC

supplemented with glucose divided in 50 mL falcon tubes, adjusting the culture to an $OD_{600}$ 0.1. The tubes were incubated as previously described for 7 h to reach the logarithmic bacterial growth. The culture was transferred into two 1 L bottles (Thermo Scientific™ Fiberlite™, Waltham, MA, USA) and centrifuged at 15,500 x *g* for 40 min at 4 °C in a Sorvall Lynx 6000 ultracentrifuge (Thermo Scientific™, Waltham, MA, USA). The pellet was then re-suspended with 19 mL PBS, previously filtered with an endotoxin free 0.2 µm PES filter Puradisc™ (GE Healthcare, UK) and transferred to a 25 mL capped tube. The tube was centrifuged at 4 °C and 3,900 x *g* for 35 min in an Allegra™ X-22R centrifuge (Beckman-Coulter, Krefeld, Germany). The pellet was then re-suspended with 2.5 mL denaturation buffer (denaturation buffer composition). The sample was then sonicated on ice ten times using a Vibracell sonicator (Sonics & Materials, Danbury, CT, USA) at ~20 A for 30 s. The sample was transferred to 1.5 mL microcentrifuge tubes and centrifuged at 30,000 x *g* for 20 min at 4 °C in a Mikro 220R centrifuge (Hettich, Tuttlingen, Germany). The supernatant was transferred to a new 2.5 mL microcentrifuge tube and stored at – 20 °C. A 50 µL aliquot was taken for protein quantification using the Pierce BCA protein assay kit (Thermo Scientific™, Rockford, IL, USA) and a Varioskan™ Flash multimode reader (Thermo Scientific™ Nalgene™, Waltham, MA, USA) to read the absorbance of the solution at 562 nm. Each sample was expected to contain at least 10 mg of protein for a good resolution in the mass spectrometry.

### 2.11.2Sample preparation for LC-MS/MS

The preparation of the sample comprises reduction, alkylation, peptide digestion, desalting, and immunoaffinity purification. This protocol was performed in the Biological Mass Spectrometry Facility of the University of Sheffield.

#### 2.11.2.1 Reduction and alkylation

The proteins prior to analysis have to be in a denaturalised conformation. Therefore, the disulphide bonds are cleaved using an oxidising reagent, then the reduced sulphur groups are alkylated in order to avoid the oxidation and re bonding of the disulphide bonds (Müller and Winter, 2017).

The samples were reduced using 0.5 M tris-2(-carboxyethyl)-phosphine (TCEP) to a final concentration of 10 mM and incubated at 37 °C for 15 min. Then it was alkylated with 0.5 M iodoacetamide to a final concentration of 20 mM, and incubated at 37 °C for 15 min, covering from light. The sample was then diluted eight folds with 50 mM ammonium bicarbonate in order to dilute the urea from 8 M to 1 M.

#### 2.11.2.2 Trypsin digestion

Trypsin is a serine protease that cleaves the carboxyl side of arginine and lysine residues. This protease is used for acetylome analysis since lysine acetylated residues are not cleaved by the enzyme.

Trypsin-TPCK (Cell Signaling Technology®, MA, USA) was diluted in 0.1% trifluoroacetic acid (TFA) and 300 µg were added to the sample and incubated overnight at 37 °C and shaking at 150 rpm.

#### 2.11.2.3 Desalting

The next step of the sample preparation is the depletion of salts that could affect the electrospray ionisation (ESI). This is achieved by using a column with a hydrophobic material, this leads to the binding of the peptides and the elution of salts, DNA/RNA, and proteins, as well as hydrophilic molecules (Kim, Zhong and Pandey, 2016).

The sample was first acidified, in order to remove fatty acids, with 100% TFA until a pH 3.0 was reached measuring with pH strips. The sample was centrifuged at room temperature at 4,150 x *g* for 5 min, this to remove any precipitation as consequence of the addition of TFA. The supernatant was transferred to a new 50 mL falcon tubes.

Before loading the sample, the column was connected to a 20 mL syringe. Using a Preppy™ 12-Port vacuum manifold (Sigma Aldrick, Oakville, Canada) the column was first conditioned with 10 mL of 100% acetonitrile (ACN) followed by 5 mL of 50% ACN and 0.1% TFA. Then the cartridge was equilibrated with 10 mL of 0.1% TFA. The acidified sample was slowly loaded three times on an empty syringe connected to a 360 mg silica Sep-Pak® $C_{18}$ column (Waters, Ireland). The cartridge was then washed with 10 mL of 0.1% TFA and it was slowly eluted with 4 mL of 50% ACN and collected in two 2 mL microcentrifuge tubes. The sample was dried down in a concentrator 5301 (Eppendorf, Hamburg, Germany), before fully dried the sample was re-suspended with 1.4 mL of 1X immunoaffinity purification buffer (PTMScan® IAP buffer 10X, 9993 Cell Signaling Technology®, MA, USA).

#### 2.11.2.4 Immunoaffinity purification (IAP)

The purification of peptides with the PTM of acetylation requires the enrichment of this type of peptides with an antibody that binds to lysine acetyl residues. A kit from Cell signalling containing beads covered with anti-acetyllysine antibodies was used to purify the acetylated peptides from the solution.

The beads were washed with 1 mL of PBS and centrifuged at 4 °C for 30 s at 2,000 x *g*, this step was repeated four times. Afterwards, the beads were re-suspended in 40 µL of PBS. Before the addition of the samples, the pH was measured and adjusted with 1 M Tris to a neutral pH. The sample was the transferred into the tube with the beads and

incubated at 4 °C for 2 h on a rotor. The tube was then centrifuged at 2,000 *g* for 30 s at 4 °C and the supernatant was transferred to a new tube and saved at -20 °C. The following steps were performed at 4 °C. 1 mL of IAP buffer was added and the tube was inverted five times to mix the beads. Then it was centrifuged at 2,000 x *g* for 30s and the supernatant removed, the wash and centrifugation were repeated one more time. 1 mL of HPLC water was added and mixed by inverting the tube five time. The tube was then centrifuged at 2,000 x *g* for 30s. The last two steps were repeated two more times. The remained water was removed using a gel loading tip. Then 55 µL of 0.15% TFA were added to the beads and incubated at room temperature for 10 min with shaking at 800 rpm. The supernatant was transferred to a microcentrifuge tube and the beads were washed once again with 50 µL of 0.15% TFA and centrifuged as previously described.

#### 2.11.2.5 Concentration and purification of peptides for LC-MS/MS

A last purification was performed using 200 µL $C_{18}$ stage tips (Thermo Scientific™, Waltham, MA, USA). The stage tip was washed with 100 µL of 0.1% TFA/50% ACN followed by 100 µL 0.1% TFA. The sample was passes through the stage tip three times and it was then washed 3 times with 100 µL of 0.1% TFA. The sample as then slowly eluted with 100 µL of 0.1% TFA/50% ACN. The sample was then dry in vacuum concentrator and re-suspended in 20 µL of HPLC water.

## 2.12 LC-MS/MS

The samples were processed by the bIOMICS facility in the University of Sheffield. The samples were loaded in a Orbitrap Elite™ Hybrid Ion Trap-Orbitrap (Thermo Scientific™ , Waltham, MA, USA) coupled to a Dionex Ultimate 3000 HPLC system (Dionex, Sunnyvale, CA, USA) for upstream separation of molecules and utilises an

EASY-Spray™ Ion Source (Thermo Scientific™ , Waltham, MA, USA) for ease of sample delivery and improved sensitivity through nanolitre flow rates.

### 2.12.1 Data analysis of MS

Raw data was analysed using MaxQuant software version 1.6.5.0 (Tyanova, Temu and Cox, 2016). The peptides were analysed against *N. gonorrhoeae* FA1090 proteomic database. Trypsin was set as the enzyme with a maximum of three missed cleavages. The precursor ion tolerance was set to 20 ppm and the fragment ion tolerance was set to 0.5 Da. Carbamidomethylation in cysteine was set as a fixed modification, while oxidation in methionine, acetyl (protein N-term) and acetyl in lysine were used as variable modifications. All peptides were used for quantification studies, but to find significantly acetylated peptides only those found in two or more replicates and with a FDR < 0.05 were used (t-test adjusted for multiple testing using permutation-based FDR). Data filtering was carried out using the following parameters: Peptide false discovery rate (FDR) was set to 1%; minimum peptide length was set to 8; peptides used for protein quantification was set to razor and unique peptides. Further data processing was performed using the Perseus tool (version 1.6.7.0) and R version 3.6.3.

## 2.13 Killing larvae assay

*Galleria mellonella* (greater wax moth) larvae have been used as an *in vivo* model for the study of bacterial virulence (i.e. *Escherichia coli, Pseudomonas aeruginosa, Staphylococcus aureus*) due to the similarities in the innate immune system with mammals and the ability to grow at 37 °C. *G. mellonella* possesses at least 8 different types of hemocytes, the innate immune cells of insects, each playing a specific role in the innate immune system. However, one of the hemocytes has the ability to phagocytose as human neutrophils. These cells recognise bacteria by Toll-like receptors and produce

ROS (i.e. $O2^{-}$, $H_2O_2$, $NO^{-}$) (Jander, Rahme and Frederick, 2000; Peleg *et al.*, 2009; Browne, Heelan and Kavanagh, 2013; Tsai, Loh and Proft, 2016). Therefore, this *in vivo* model was selected to test if larvae could be infected and killed by *N. gonorrhoeae* MS11 and to observe if the acetylation of proteins is involved in the virulence of the bacteria.

In order to determine if the gonococcus infects larvae a modified protocol of killing larvae assay was performed (Wand *et al.*, 2011). *N. gonorrhoeae* MS11 WT was cultured on CHO agar overnight. 15 mL BHI-Y broth were inoculated and incubated overnight as described above (section 2.2.1.2). 5 mL BHI-Y were inoculated with the overnight culture and adjusted to an $OD_{600}$ 0.1. The tube was incubated at 37 °C for 4 h, time to reach mid-exponential phase, on a rotary shaker at 180 rpm. The culture was centrifuged at 3,900 x *g* for 10 min in an Allegra™ X-22R centrifuge (Beckman-Coulter, Krefeld, Germany). The pellet was re-suspended with 2 mL sterile PBS and the suspension was adjusted to an $OD_{600}$ of 0.5 equating to approximately $4x10^8$ CFU/mL. Eight 10-fold serial dilutions were prepared using sterile PBS. Groups of 20 larvae were injected into the haemocoel via the hindmost left proleg of the larva (fig. 2.3) with 10 µL of the dilutions ($10^2$, $10^3$, $10^4$, $10^5$, $10^6$, $10^7$, $10^8$) each using a semi-automatically PB-600-1 repeating dispenser (Hamilton®, NV, USA) affixed to a to a Gastight 500µl Hamilton syringe (Model 1750 RN large hub SYR, with a 22 gauge, large hub RN NDL, 2 inch, point style 2 needle). Control groups were injected with 10 µL sterile PBS, or 10 µL heat killed bacteria boiled for 15 min at 95 °C. Another group was left untreated. The larvae were located in plastic Petri dishes and incubated at 37 °C in a $CO_2$ incubator. Larvae were check at different time points and the number of dead/alive larvae was recorded.


**Figure 2.3. Inoculation of *G. mellonella* with *N. gonorrhoeae*.** The larvae was inoculated with *N. gonorrhoeae* into the haemocoel in the zone indicated with a black arrow.

To calculate the number of inoculated bacteria Miles and Misra method was followed (Miles, Misra and Irwin, 1938), 10 μL of each dilution were spotted by triplicates onto a CHO agar and the plates were incubated as described in section 4.2.1. The colonies grown on the agar were counted and the CFU injected into larvae was calculated.

To compare the virulence between the WT, Δ*ackA* and Δ*pta* strains of *N. gonorrhoeae*, it was followed the protocol as mentioned above with minor alterations. 15 larvae per strain were infected with the dilution $10^5$ to $10^8$. The dead/alive number of larvae were monitored at different time points.

## 2.14 Macrophage killing assay

This assay was performed to observe the capacity of intracellular survival of the four different strains of *N. gonorrhoeae*.

### 2.14.1 Blood samples

The blood samples were obtained from volunteers after informed consent. The study was approved by the South Sheffield Research Ethics Committee with number 07-Q2305/7.

### 2.14.2 Monocyte-derived macrophage (MDM) differentiation

Human monocytes were obtained from normal blood donor buffy coats by two-step gradient centrifugation. The monocytes differentiate after 14 days seeded in a 24 wells cell culture plate, tissue culture treated (Corning® Costar®, Kennebunk, ME, USA) with

1 mL of RPMI 1640 supplemented with 10% of heated inactivated foetal bovine serum (HIFBS) and 2 mM L-glutamine to a final cell number of $2x10^5$ cells/mL. The media culture was changed every 4 days and the cells were incubated at 37 °C in a 5% $CO_2$ atmosphere.

### 2.14.3Killing assay

The four strains of *N. gonorrhoeae* were cultured in 15 mL of BHI-Y for 18 h at 37 °C with shaking at 180 rpm. The OD was read on an Ultrospec 2100 pro spectrophotometer (Biochrom, Cambridge, UK) at 600 nm and 15 mL of BHI-Y were inoculated with bacteria to a final $OD_{600}$ of 0.05 and incubated as previously mentioned for 4 h to reach the exponential phase. The tubes were centrifuged at 3,900 x *g* for 8 min at room temperature. The pellet was re-suspended with 1 mL of filtered PBS and transferred to a 1.7 mL microcentrifuge tube for centrifugation at 12,000 x *g* for 2 min at room temperature the pellet was washed and centrifuged again. The pellet was re-suspended in 2 mL of RPMI 1640 supplemented with 10% of HIFBS and 2 mM L-glutamine and the OD was read at 600 nm. 5 mL of RPMI were inoculated with the bacterial suspension at an OD of 0.01 which equivalents to a MOI of 5 and incubated at 37 °C for 30 min. The Miles-Misra method was performed on GC agar plates and incubated as mentioned in section 2.2.1.

The medium from the plate with the MDM was removed and washed with 1 mL of cold sterile PBS. The PBS was removed and the bacterial suspension was added in triplicates for each strain. Three wells were inoculated only with the medium to be the negative control. The plates were centrifuged at 150 x *g* and 4 °C for 5 min. The two plates were incubated at 37 °C and 5% $CO_2$ for 2 and 3 h. After incubation 100 µL of each well was taken and dilutions 1:10 were made with sterile PBS up to $10^{-4}$. On GC agar plates 10 µL

of the last three dilutions were plated and incubated at 37 °C overnight to determine the bacterial CFU in the medium. The medium from the wells was removed and the wells were washed twice with 2 mL of ice cold sterile PBS. Then 1.5 mL of RPMI medium with 100 µg/mL of gentamicin were added to the wells. This step is too killed all the bacteria that are extracellular. The plates were incubated for 50 min at 37 °C in a $CO_2$ incubator.

The wells were washed twice with 2 mL of ice cold sterile PBS and 250 µL of 1.5% saponin was added and the plates were incubated at 37 °C for 15 min in a $CO_2$ incubator. Using 1 mL tips the wells were scrapped and the wells were washed with 750 µL of sterile PBS and the suspension was mixed with the pipette. Miles-Misra technique was performed as previously mentioned using the $10^0$ and $10^{-1}$ to inoculate 10 µL on GC agar plates. The CFU colonies were counted after 48 h of incubation.

## 2.15 Microscopy for *in vitro* killing assay

The microscopy was performed using a Leica AF6000LX inverted microscope. It is fitted with an environmental chamber maintained at 37°C and equipped with a gas mixer for the supply of $CO_2$. The microscopy was set to take pictures every 5 min during 9 h. The areas were chosen in the centre of the well with 10 pictures taken from three different wells for each strain.

### 2.15.1 Cell and bacteria staining

The MDMs were obtained as mentioned in section 2.15 and dyed each well with 2 drops of NucBlue™ Live ReadyProbes™ Reagent (Thermo Fisher Scientific™, Waltham, MA, USA) 30 minutes before infection with the different isogenic strains of *N. gonorrhoeae*. Meanwhile the gonococcal strain were grown overnight at 37 °C in BHI medium as mention in section 2.2.1.2. The tubes were centrifuged at 3,900 x *g* for 8 min and re-

suspended with 1.6 mL PBS. The suspension was transferred and centrifuged at 12,000 x *g* for 2 min and re-suspended with 500 µL PBS. 200 µL of bacterial suspension were transferred to a microcentrifuge tube and 0.5 µL of pHrodo red succinimidyl ester (Thermo Fisher Scientific) was added. The tube was vortexed and incubated for 30 min and 37 °C on a shaker. The suspension was re-suspended in 1 mL Tris (2.5 mM; pH 8.4) and incubated for 1 min in dark. The tube was centrifuged at 12,000 x *g* and re-suspended with 1mL PBS. The OD was read in a spectrophotometre and the suspension was adjusted to a final $OD_{600}$ of 0.005 in 1 mL RPMI. The MDMs were inoculated with a MOI of 5 with the bacterial suspension.

### 2.15.2Image analysis

The image files were analysed in software ImageJ. The file was loaded in split channels and the channel 1 and 2 were used to quantify the number of bacteria and cells present in the image, respectively. The threshold to identify bacteria and cells was adjusted at a minimum of 22 and 24, respectively and a maximum of 255 for both channels. Then the images were converted to mask and finally, processed for analysis of particles (fig. 2.4). The measurements to analyse were number of bacteria or cells, area, total area and average size. The data was then processed using R.

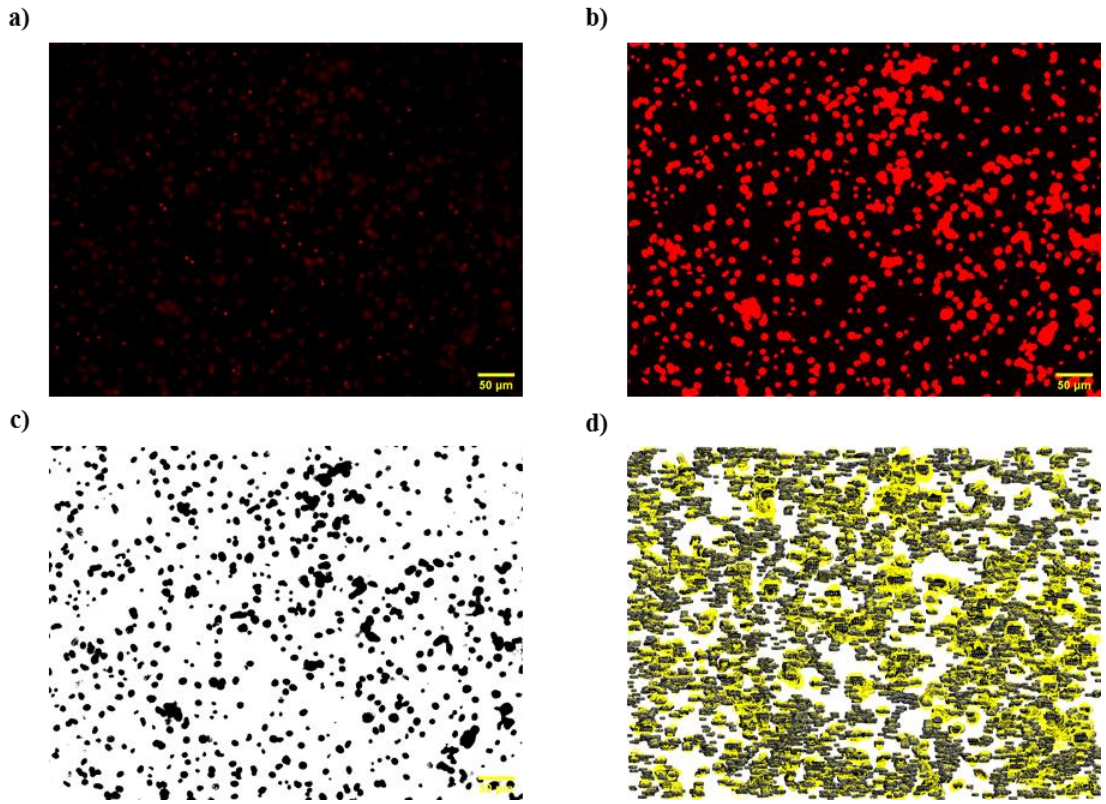


**Figure 2.4 Image analysis process in ImageJ.** Images obtained from fluorescence microscopy were analysed to quantify different parameters. In this figure is shown the process to analyse the file from the channel 2 which corresponds to the nuclei of the MDM. **a)** The image is loaded to the software; **b)** then a threshold is set to determine the best values to identify only the cells; **c)** the image is converted to mask; **d)** to be processed for the analysis of particles that quantifies the number of cells, size, area and total area. At the bottom right is a 50 µm bar scale.

## 2.16 Gene expression quantification by RT-qPCR

Several genes involved in the virulence of *N. gonorrhoeae* were analysed using RT-qPCR. This technique quantifies the mRNA present within bacteria.

### 2.16.1 RNA extraction

The four strain of *N. gonorrhoeae* were grown in 15 mL of BHI-Y medium for 18 h with shaking at 180 rpm. The $OD_{600}$ was measured using a spectrophotometer 15 mL of BHI-Y were inoculated with the bacterial suspension and adjusted to an $OD_{600}$ of 0.1. The tubes were then incubated for 7 h to reach the exponential phase. The tubes were

centrifuged at 3,900 x *g* for 8 min at 4 °C and the pellet was re-suspended with 1 mL of molecular grade water and transferred to a microcentrifuge tube. The tube was centrifuge at 12,000 x *g* for 2 min at room temperature. The RNA was extracted using the Monarch® total RNA miniprep kit (New England BioLabs®, MA, USA) with some modifications the sample two times through the gDNA removal column, incubating the sample 30 min with the DNase; washing thrice and eluting the sample with 80 µL of water. The RNA concentration was quantified with a NanoDrop® ND-1000 spectrophotometer (Thermo Fisher Scientific™, Waltham, MA, USA). The sample required a 280/260 ratio higher than 1.8 and a concentration higher than 50 ng/µL.

## 2.16.2Genes and primers

A total of 24 genes were analysed (table 2.20). Including genes involve in pili biosynthesis, two component system, transcriptional regulator, iron acquisition genes and metabolic genes. The primers were designed with Primer Blast website having as parameters; a product size between 140 and 180 bp; a primer melting temperature ($T_m$) between 60 and 62 °C; and a primer GC content of between 48 and 51%. This parameter were chosen in order to do the qPCR using the same settings for all the genes. Previous RT-qPCR the primers were validated by PCR of the gDNA of *N. gonorrhoeae*.

**Table 2.20 Genes and primer used for RT-qPCR**

| Gene | Primer (5' →3') | Length | Blast $T_M$ | Product size (bp) |
|---|---|---|---|---|
| ***16S rRNA*** | AATTCCGATTAACGCTCGCACC | 22 | 61.87 | 149 |
| | AAGGCCTTCGGGTTGTAAAGGA | 22 | 61.89 | |
| ***ackA*** | GATCTTGGTTTTGAACTGCGGC | 22 | 60.92 | 162 |
| | GCGGACAGATCGACTTTGTGTT | 22 | 61.43 | |
| ***hdac*** | GGTTTGGAGGTGCTGCCAAATA | 22 | 61.41 | 180 |
| | TTCCTGAAACTCTACGCCCTGT | 22 | 61.35 | |
| ***aceE E2*** | GGAGATTTTGTCGCCGACTTTG | 22 | 60.41 | 154 |
| | CGACATCATCGCCGTAGAAGTT | 22 | 60.79 | |
| ***fnr*** | GGATGGCAAAGAGCGAGGTAAA | 22 | 60.94 | 153 |
| | CTTCCTGTTCTTTGCGGGAACT | 22 | 61.07 | |
| ***hemO*** | ATCAACCGCTTTGTGGAACACG | 22 | 62.20 | 160 |
| | CGAAAACCAAGCCCTGACGTTT | 22 | 62.15 | |

| | | | | |
|---|---|---|---|---|
| ***hmbR*** | CACCAAGTCTTTGTTGTCGCGT | 22 | 62.13 | 179 |
| | GCAGTATTTTCGGCAATCCGGT | 22 | 61.83 | |
| ***katA*** | GTTGCCGACAATCAAAACAGCC | 22 | 61.43 | 160 |
| | TTACGGTAAACGTACCGAACGC | 22 | 61.23 | |
| ***lst*** | TCAGCACCACATAAAACCGCTC | 22 | 61.45 | 162 |
| | TAAATCAGGGGGAAAGGAACGC | 22 | 60.62 | |
| ***misR*** | ATCCAAGCCGTTCATTTTGGGC | 22 | 62.31 | 149 |
| | TGACCGAACTGCTGACCGAATA | 22 | 61.72 | |
| ***misS*** | AGACGGGGCTGTTTTTCCATTC | 22 | 61.40 | 156 |
| | CTTTTTGGCTGGTGCAGAACAC | 22 | 61.05 | |
| ***mtrC*** | TTGTTTACTGATGGCATCGGCG | 22 | 61.82 | 148 |
| | GCTGTATCAGATCGACAGTTCCAC | 24 | 61.26 | |
| ***mtrD*** | CAAACCTTCCACGCCGTTCATA | 22 | 61.45 | 165 |
| | GCGGCAGGTATTTTCGGCATTA | 22 | 61.89 | |
| ***mtrE*** | GTGCGATGTCGATCAGCTTTTG | 22 | 60.79 | 178 |
| | GTTGCAGCAGCCTTTGCATT | 20 | 60.60 | |
| ***mtrR*** | TGCCGCCTTGGAAACCTTTT | 20 | 61.05 | 142 |
| | ACGTTGGAACAACGCGTCAA | 20 | 61.36 | |
| ***narL*** | GTCAGCATAATGACTGCCTGCT | 22 | 61.00 | 140 |
| | GGACTCTCGGGCATCAAAATGA | 22 | 60.68 | |
| ***narX*** | GGATGGCATCGCTTTGGGAAAT | 22 | 61.86 | 173 |
| | TTCTTTCCGCCTGGAAAATGCC | 22 | 61.98 | |
| ***ntrX*** | CAGCAGCTTTTGCAGGGAAATC | 22 | 60.93 | 165 |
| | GATTGCGACGGTATCACCCTTT | 22 | 61.00 | |
| ***ntrY*** | GGAAATGCCGAACAGGAACAAG | 22 | 60.35 | 179 |
| | GGATAGTCTCGTTCAGCGCAAT | 22 | 60.80 | |
| ***pilE*** | TCCGCAGAACCATTTTACCGAAC | 23 | 61.66 | 169 |
| | CGTGGCATCCGCTTCAAAAATC | 22 | 61.29 | |
| ***pilQ*** | GGTTTGTTCAAAGTCCAAGGCG | 22 | 60.80 | 151 |
| | GGCATCGGCAGGAAACATTACA | 22 | 61.52 | |
| ***pilS2*** | GTCCGCAGAACCATTTTACCGA | 22 | 61.19 | 160 |
| | CCCACCGACATCAAAGGCAAAT | 22 | 61.73 | |
| ***pta*** | TCGAACCAGTCGTCGCTTTT | 20 | 60.25 | 151 |
| | CAAAAGTACTCGTCGTACCCGT | 22 | 60.35 | |
| ***tbpA*** | AGGGTGTTGAATCGAGCTGGTA | 22 | 61.41 | 156 |
| | ACTTTGCGTATGGACAGCCAAC | 22 | 61.71 | |

## 2.16.3RT-qPCR

The RNA from the four strains of *N. gonorrhoeae* MS11 were analysed for the detection of the genes previously mentioned. Three biological and three to five technical experiments were performed for each gene. Triplicates of each gene were run on plates of 96 wells (Applied Biosystems, Life Technologies Corp., Carlsbad, CA, USA) with a final volume of 10 µL. The Luna® Universal One-Step TR-qPCR Kit (Monarch, New England BioLabs®, MA, USA) was used due to the efficiency in doing the reverse transcription and quantitative PCR in the same reaction (table 2.21).

**Table 2.21 Reaction mix for RT-qPCR**

| Reagent | Volume (µL) | Final concentration |
|---|---|---|
| Luna Universal One-Step Reaction Mix (2X) | 5.0 | 1x |
| Luna WarmStart® RT Enzyme Mix (20X) | 0.5 | 200 µM |
| 10 µM Forward primer | 0.4 | 0.4 µM |
| 10 µM Reverse primer | 0.4 | 0.4 µM |
| Template RNA | Variable | 0.1 ng |
| Nuclease-free water | to 10 µL | - |

The reaction was performed in a QuantStudio 5 Real-Time PCR Systems (Applied Biosystems, Life Technologies Corp., Carlsbad, CA, USA). The settings for the RT-qPCR are shown in table 2.22.

**Table 2.22 Settings for RT-qPCR**

| Step | | Temperature | Time |
|---|---|---|---|
| **RT** | | 55 °C | 10:00 min |
| **Initial denaturation** | | 95 °C | 1:00 min |
| **Denaturation** | 40 cycles | 95 °C | 10 s |
| **Annealing, extension and read** | | 61.5 °C | 1:15 min |
| **Melt curve** | | 95-60 °C | 0.1 °C/s |

The gene expression was calculated by comparing the CT delta of each gene compared to the CT of the 16S rRNA housekeeping gene.

## 2.17 Protein overexpression, purification and crystallisation

### 2.17.1 Growth and CFE

The protein Pta from *N. gonorrhoeae* MS11 was overexpressed using the strain constructed in section 2.5.3. *Escherichia coli* BL21-DE3 pET28a-pta-his was grown overnight on LB agar plates with 50 µg/mL of kanamycin (LB-Kan50) overnight at 37

°C. Six 50 mL falcon tubes with 30 mL of LB-Kan50 were inoculated with the bacteria and incubated at 37 °C with shaking at 180 rpm for 18 h. The $OD_{600}$ was read and five 2.5 L flasks with 600 mL of LB were inoculated with the culture and adjusted to an $OD_{600}$ of 0.03. The flasks were incubated at 37 °C and shaking at 260 rpm for 2:30 h or until an $OD_{600}$ of between 0.8 and 1.0 was reached. 1 M of IPTG (Isopropyl-β-D-thiogalactoside) was added to a final concentration of 250 mM and incubated at 18 °C and shaking at 260 rpm for 20 h. The cultured was transferred to 1 L bottles (Thermo Scientific™ Fiberlite™, Waltham, MA, USA) and centrifuged at 15,000 x *g* and 4 °C for 35 min in a Sorvall Lynx 6000 ultracentrifuge (Thermo Scientific™, Waltham, MA, USA). The pellet was re-suspended with 100 mL sterile PBS and the suspension was centrifuge in a 250 mL bottle (Thermo Scientific™ Fiberlite™, Waltham, MA, USA) at 15,000 x *g* and 4 °C for 20 min. The pellet was re-suspended in 30 mL of binding buffer (50 mM phosphate buffer, 0.5 M NaCl, 30 mM imidazole). The suspension was divided in three tubes of 25 mL and the suspension was sonicated on ice ten times at 20 A for 30 s each time waiting 30 s between each sonication. The suspension from the three tubes was collected in a 50 mL tube and it was centrifuged at 30,000 x *g* and 4 °C for 25 min. The supernatant was collected and stored at 4 °C until purification.

## 2.17.2His-Trap column

Columns of 5 mL with nickel sepharose™ were used as first step for the purification of the protein. The protein binds to the column by immobilised metal ion affinity (IMAC). The column was washed five column volumes (CV) with water and then five CV with binding buffer previously mentioned. The samples was slowly loaded and the column was washed ten CV with the binding buffer. The sample was eluted with four CV of elution buffer (50 mM phosphate buffer, 0.5 M NaCl, 150 mM imidazole).

### 2.17.3 Buffer exchange for gel filtration

The sample was concentrated in a 10,000 MW cut off tube (Amicon®, Millipore, Billerica, MA, USA) by centrifugation at 3,900 x *g* and 4 °C for 20 min. The column was washed two times with gel filtration buffer (25 mM Tris-HCl; 200 mM NaCl; pH 7.6) and centrifuged as described previously. The sample was re-suspended with 1.5 mL of gel filtration buffer.

### 2.17.4 Gel filtration

A final purification step consisted in the separation of the pta protein from the rest by gel filtration. This method allows the separation by size exclusion. Fast-protein liquid chromatography (FPLC) was performed using an ÄKTA-Purifier 10 FPLC (GE Healthcare Life bioscience) and Superdex High-performance column (GE Healthcare Life bioscience) with a bead volume of 120 mL. The column was washed overnight with 70% of ethanol overnight at a flowrate of 0.2 mL/min and it was then loaded with gel filtration buffer until a stable was observed in the plot. The sample was loaded in a 5 mL loop with a flow rate of 0.4 mL/min and fractions of 2 mL were collected in microcentrifuge tubes. The eluted fraction were then run in a SDS-PAGE gel as mentioned in section 2.10.2. The samples was then concentrated using a 10,000 MW cut off tube and centrifuged at 3,900 x *g* and 4 °C for 20 min and the sample was then re-suspended with 40 µL gel filtration.

### 2.17.5 Crystallisation

The crystallisation of protein was performed by testing different conditions. Four different were tested for the crystallisation. Using a buffer, a salt, and a precipitant; using an organic molecule and a precipitant; organic molecule, precipitant, and seeding; and organic molecule, precipitant, seeding, and silver bullet screening portfolio (table 2.23).

**Table 2.23 Conditions for sitting drop crystallisation of Pta**

| Condition | Buffer/Organic molecule | | Salt | | Precipitant | | Silver bullet | Seeding | pH |
|---|---|---|---|---|---|---|---|---|---|
| | [M] | Molecule | [M] | Molecule | [%] | Molecule | | | |
| **1** | 0.1 | Sodium cacodylate | 1-4 | Ammonium sulfate | - | - | No | No | 5.5-8.0 |
| **2** | 0.2 | Ammonium tartrate dibasic | - | - | 12-18 | PEG 3350 | No | No | 5.5-8.0 |
| **3** | 0.1 | HEPES | 0.1-0.4 | Magnesium chloride hexahydrate | 16-22 | PEG 6000 | No | No | 5.5-8.0 |
| **4** | 0.1 | Bis-Tris | 0.1-0.4 | Lithium sulfate | 21-27 | PEG 3350 | No | No | 6.0-8.0 |
| **5** | 0.1 | Bis-Tris | 0.2 | Lithium sulfate | 12-18 | PEG 3350 | No | No | 5.5-8.0 |
| **6** | 0.2 | Ammonium tartrate dibasic | - | - | 12-18 | PEG 3350 | No | No | 5.5-8.0 |
| **7** | 0.1 -0.5 | Malic acid | - | - | 18-22 | PEG 3350 | No | No | 5.5-8.0 |
| **8** | 0.1 -0.5 | Malic acid | - | - | 18-22 | PEG 3350 | Yes | Yes | 5.5-8.0 |

96 deep well plates were used for the preparation of the buffer as shown in the figure 2.5, depending on the utilisation of the number of components of the buffer.

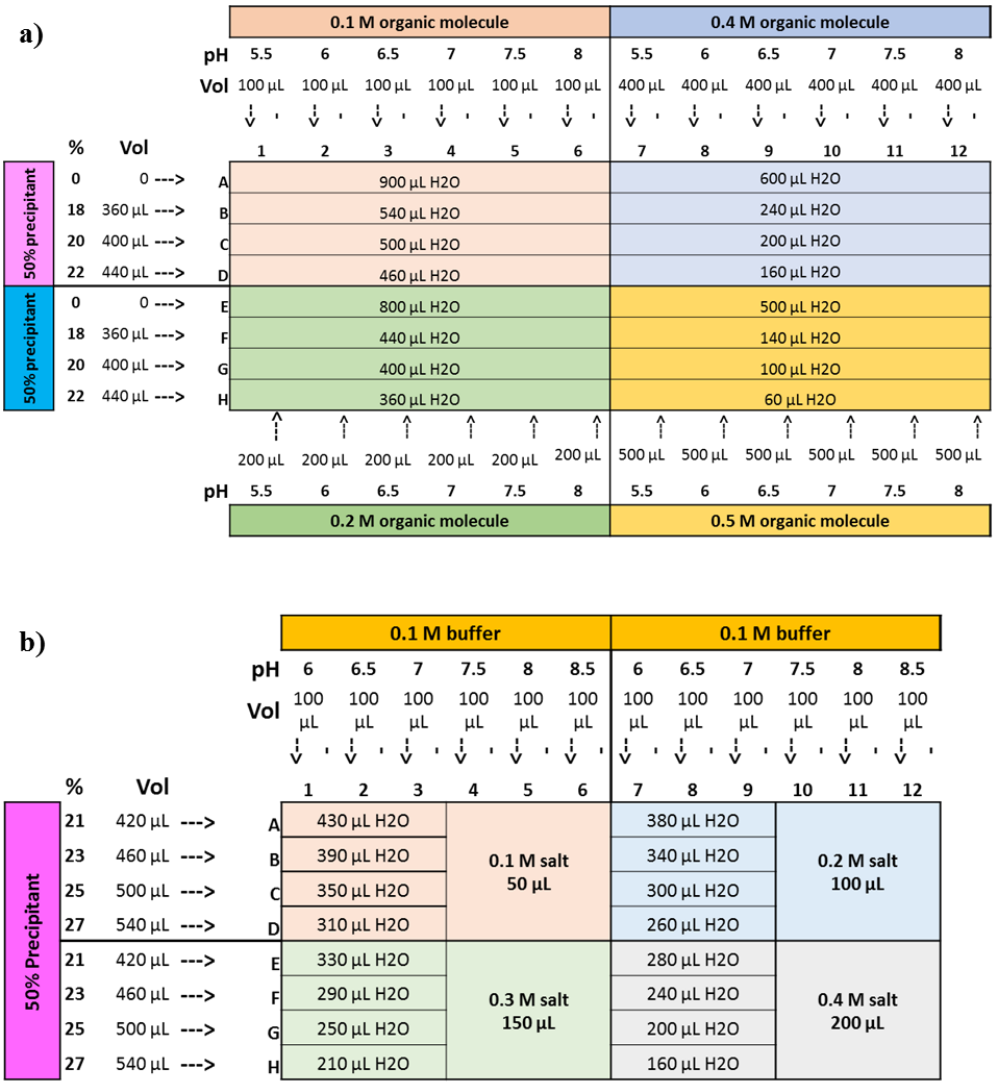


**Figure 2.5 Preparation of the buffers for the crystallisation of Pta.** Volume used of each component for the preparation of buffers in 96 deep well plates. The organic molecule volume are considered for a 1 M stock solution. **a)** Preparation of buffer with organic molecule and precipitant. **b)** Preparation of plate with buffer, salt and precipitant. The buffer volume are considered for a 1 M stock solution.

The buffer was then transfer to 96 wells plate used for sitting drop crystallisation. This type of plates contain three different wells. One well of 150 µL used as the reservoir for

the buffer and two small wells for the addition of the concentrated protein and the buffer (fig 2.6).

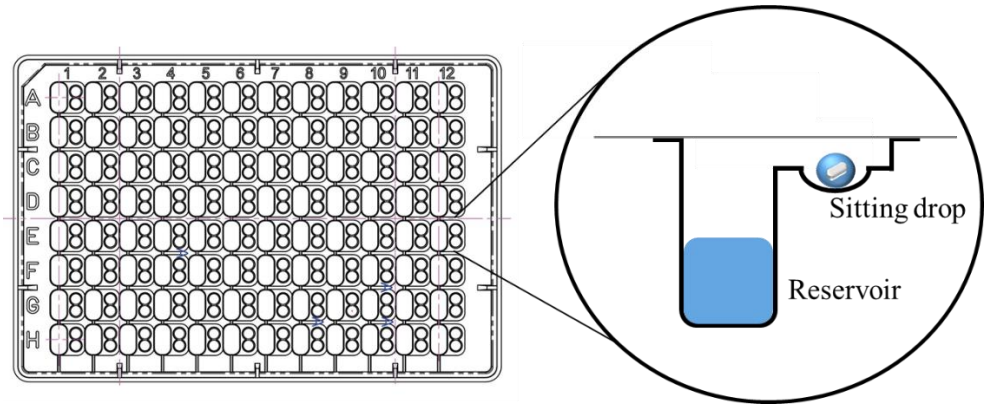


**Figure 2.6 Diagram of sitting drop crystallisation plate.** The 96 well plate contains a reservoir of 150 µL and a sitting drop for 10 nL - 5 µL.

The plates were set with 50 µL of the buffer in the reservoir and using the liquid handler Mosquito® crystal robot (TTP Labtech, Melbourne, UK), 150 nL of buffer and protein were disposed on the sitting drop. For seeded plates 20 nL of the suspension of crystals with buffer was added to the sitting drop. The plates were incubated at 17 °C until the formation of crystals was observed with a microscope.

# Chapter 3

## Acetyl-phosphate-dependent acetylation and histone deacetylase family enzyme in *Neisseria gonorrhoeae* MS11

# 3 Acetylome of *Neisseria gonorrhoeae* MS11

## 3.1 Introduction

*N. gonorrhoeae* MS11 is a clinically isolated strain from an uncomplicated case of gonorrhoea. This strain is used worldwide for its ability to uptake DNA and for the 96.5% similarity to the reference strain *N. gonorrhoeae* FA 1090 genome (Jordan, Snyder and Saunders, 2005).

In order to understand the role of acetyl-phosphate in protein acetylation, the phosphotransacetylase-acetate kinase (PTA-AK) pathway was disrupted. As a consequence, two mutant strains were constructed, *N. gonorrhoeae* MS11 Δ*pta*::*kan*$^r$ and *N. gonorrhoeae* Δ*ackA*::*kan*$^r$, one with a lower acetyl-phosphate concentration and another with a higher concentration, respectively.

The *pta* gene (NGFG00350, NGO0214) catalyses the reversible reaction of acetyl-CoA to acetyl-phosphate. By mutating this gene, the synthesis of acetyl-phosphate is inhibited and the intracellular concentration decreases. Contrary, the mutant Δ*ackA* (NGFG00758, NGO1521) causes an increase of the intracellular acetyl-phosphate concentration since this enzyme catalyses the reversible reaction of acetyl-phosphate to acetate (Verdin and Ott, 2013).

Acetylation is a reversible post-translational modification, and deacetylation is either non-enzymatic or enzymatic. The first deacetylases were found in eukaryotic cells for the deacetylation of histones and are divided in classes according to their cofactor molecule, zinc or NAD (Grabiec and Potempa, 2018; Narita, Weinert and Choudhary, 2019). In bacteria, the classification is the same, histone-family like deacetylases (HDAC) and sirtuin CobB, respectively. Studies have preferred the study of CobB and have found that it regulates the activity of metabolic enzymes and transcriptional regulators (Pisithkul,

Patel and Amador-Noguez, 2015; Ren *et al.*, 2016; Macek *et al.*, 2019; Parks and Escalante-Semerena, 2020; Wang *et al.*, 2020). In this study, I studied the role of the not explored HDAC and analysed for the first time the acetylome of an isogenic strain Δ*hdac*.

A gonococcus mutant of the histone deacetylase-like (*hdac*) gene (NGFG00325, NGO0187) was constructed. This enzyme reverses acetylation by removing the acetyl group, and has shown to be important in the bacterial virulence and pathogenesis due to epigenetic modifications of the host cells (Grabiec and Potempa, 2018; Zughaier, Rouquette-Loughlin and Shafer, 2020).

The mutants were constructed by disrupting the genes with a kanamycin resistance gene (*kan*$^r$). PCR and DNA sequencing were performed to prove the mutant construction.

The *N. gonorrhoeae* MS11 Δ*pta*::*kan*$^r$ and *N. gonorrhoeae* Δ*ackA*::*kan*$^r$ strains were obtained as part of my MSc. Molecular Medicine project when the project was started (Felix-Diaz Parga, 2017).

A previous study performed a similar approach by analysing the acetylome of *N. gonorrhoeae* MS11 Δ*ackA*, however, the acetylome coverage showed in the study was lower compared to ours (Post *et al.*, 2017). Moreover, this was the first study in *N. gonorrhoeae* where Δ*pta* and Δ*hdac* mutants were constructed and their acetylome analysed.

## 3.2 Results

### 3.2.1 Characterisation of *N. gonorrhoeae* MS11 Δ*pta* and Δ*ackA*

The characterisation of the three strains of *N. gonorrhoeae* MS11 was conducted by assessing the enzymatic activity of phosphotransacetylase (Pta) and acetate kinase (AckA), and by determining the concentration of acetyl-phosphate (AcP). This was done in order to prove that the mutation on the *pta* and *ackA* genes provoked biological effect on the enzymatic activity and as consequence, a disruption of the acetyl-phosphate concentration.

The mutated strains showed no enzymatic activity with respect to their mutated proteins. The AckA activity of the Δ*pta* strain decreased 45% than the WT, while the Pta activity of the Δ*ackA* strain decreased 78% compared to the WT strain (table 3.1).

**Table 3.1 Pta and AckA activity of the three strains of *N. gonorrhoeae* MS11**

| Strain | Pta ($nmol^{-1}min^{-1}mg^{-1}$) | AckA ($nmol^{-1}min^{-1}mg^{-1}$) |
|---|---|---|
| *N. gonorrhoeae* MS11 WT | 1789.43 ± 267.38 | 9.78 ± 5.64 |
| *N. gonorrhoeae* MS11 Δ*pta* | 0 | 5.41 ± 3.86 |
| *N. gonorrhoeae* MS11 Δ*ackA* | 396.56 ± 87.94 | 0 |

n=3.

Since the activity of the enzymes was null, a change on the AcP production was expected. Therefore, the concentration of AcP was quantified as mention in section 2.8. *N. gonorrhoeae* MS11 Δ*pta* showed a significant 0.7 fold decrease, while the Δ*ackA* strain resulted in a significant 1.3 fold increase (fig. 3.1). Even though, the concentration of AcP was lower in the Δ*pta* it was not fully depleted, this could have been due to the sensitivity of the assay that also detects ATP molecules and if the samples preparation is not fully clean a signal of ATP could affect the result.

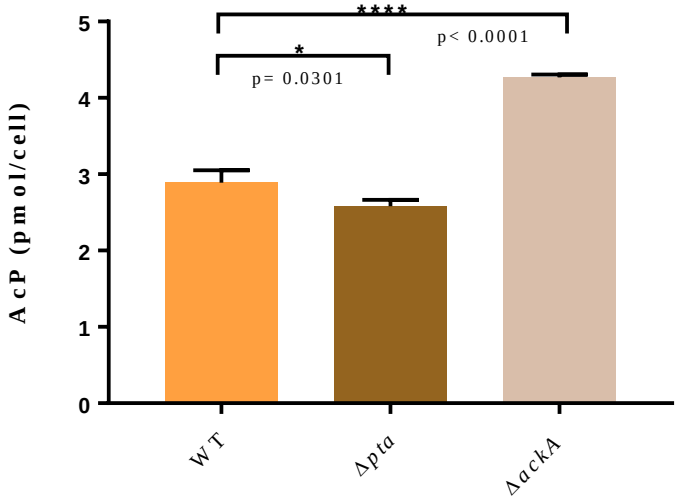


**Figure 3.1 PTA-AK pathway controls the concentration of acetyl-phosphate.** The concentration was quantified from cell free extracts obtained from each strain of *N. gonorrhoeae* MS11 grown on BHI broth for 10 h. A standard curve of AcP was used to calculate the concentration of AcP in pmoles per cell. The number of cells was measured by the $OD_{600}$ of the WT, Δ*pta*, and Δ*ackA* strains with values of 0.332, 0.170 and 0.244, respectively, being an $OD_{600}$ of 1.0 equal to $8x10^8$ cells/ml. Measurements were performed by triplicate. Δ*ackA* strain showed a significant higher concentration of AcP and Δ*pta* a significant lower concentration, both compared to the WT.

Due to the change of AcP concentration in the two strains, a western blot using anti-acetyllysine antibodies was performed. This antibody binds to the lysine residue of proteins that are acetylated. Since AcP was described as the molecule involved in the non-enzymatically acetylation (Klein *et al.*, 2007; Wolfe, 2016) a different pattern of acetylation was expected. The immunoblot loaded with normalised concentrations of proteins (fig 3.2b), showed that the Δ*ackA* had an increase of 16.5 fold in the intensity of the bands compare to the WT and the Δ*pta* showed a decreased of band intensity of 0.9 fold (fig 3.2c).

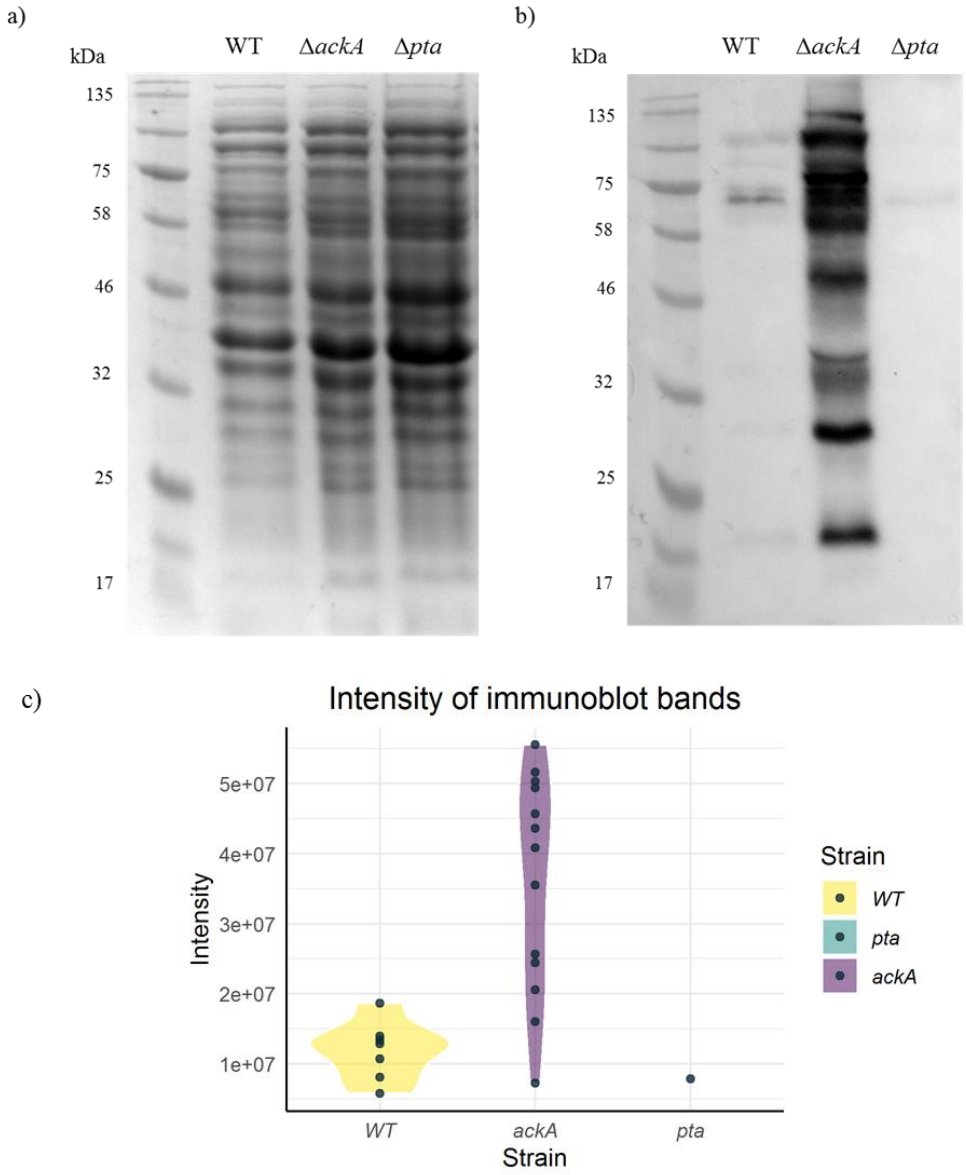


**Figure 3.2 Immunoblot for acetylated proteins using an anti-acetyllysine antibody**. Strains of *N. gonorrhoeae* MS11 were grown in BHI-Y for 24 h and protein extract was quantified and loaded on SDS-PAGE gels. **a)** SDS-PAGE with 10 µg of proteins; **b)** immunoblot with 45 µg of protein. The bands correspond to the acetylated proteins screened with the antibody; **c)** the immunoblot was analysed with the Image Lab software to calculate the number of bands and intensity, each point correspond to a band on the immunoblot (7, 13, 1) for each strain (WT, *ΔackA, Δpta*), respectively.

These three experiments confirmed that the two mutants led to a change in the levels of acetyl-phosphate and the level of protein lysine acetylation. Hence, the strains were analysed to identify the sites of the proteins that are acetylated by acetyl-phosphate.

### 3.2.2 Construction of *Neisseria gonorrhoeae* MS11 Δ*hdac*::*kan*$^r$

The gene *hdac* (NGFG00325, NGO0187) of the gonococcus was mutated by inserting the kanamycin resistance gene (*kan*$^r$) by annealing PCR, inserting the resistance marker at the nucleotide position 468. The primers were designed to overlap 25 and 26 bp between the *hdac* segments and *kan*$^r$. Additionally, once base pair was added to the hdac2-R primer in order to complete the DNA uptake sequence (DUS). In total, *hdac* possesses two of these sequences, however, the second DUS has one base pair that is out of the translating sequence (fig. 3.3). The homologous recombination frequency following transformation of the bacteria is increased with the presence of complete a DUS (Hamilton and Dillard, 2006; Duffin and Seifert, 2010; Spencer-Smith *et al.*, 2016).

The three fragments were gel purified due to the amplification of other amplicons (fig. 3.3b). The fragments were then used for the annealing PCR. This amplicon was further gel purified in order to avoid any unspecific amplicons, sequenced and then used for the transformation of *N. gonorrhoeae* MS11.

Several mutants were obtained after the agar spot transformation but only five colonies were selected for DNA sequencing, confirming the construction of the mutant isogenic strain. In the next sections the possible targets of this enzyme will be described.

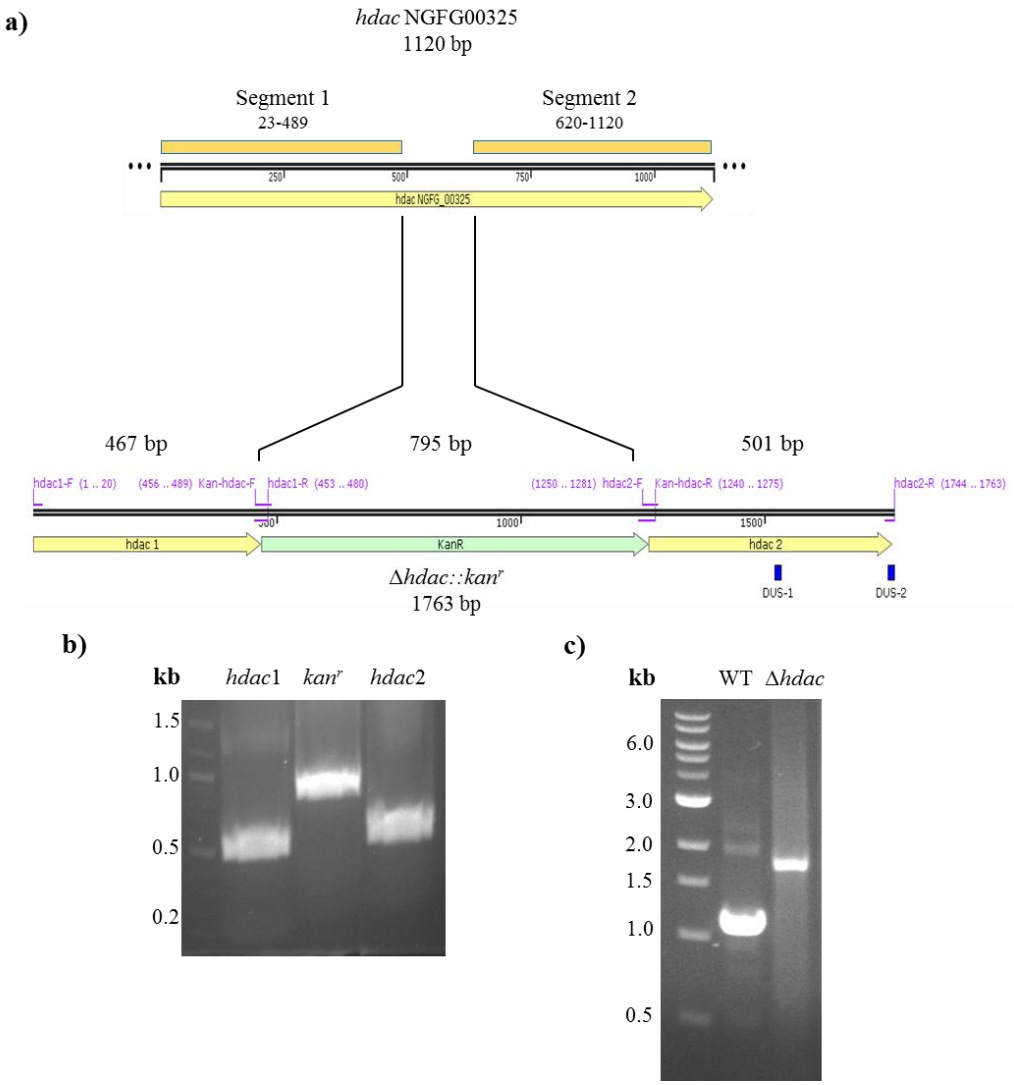


**Figure 3.3 Design and construction of *N. gonorrhoeae MS11* Δ*hdac::kan*$^r$. a)** The *hdac* gene was amplified in two different sections (yellow bars) of 467 and 501 bp, respectively. The first segment starts at position 23 and ends at position 489, while the second segment starts in the position 620 and ends at position 1120. The kanamycin resistance gene (green bar) was amplified from a gonococcus strain possessing the marker. The three amplicons were used as template for the annealing PCR. Four primers from six used, shown in magenta colour, were designed with overlapping sequences to obtain the construct. At the bottom of the mutant gene diagram are shown the location of the two DUS in blue colour. **b)** 1.5% agarose gel loaded with the three segments. **c)** 1% agarose gel loaded with the *hdac* and Δ*hdac::kan*$^r$ amplicons showing a band size of 1220 and 1763 bp, respectively. Two different temperatures were used for the annealing of the overlapping and non-overlapping primers at 60 and 52° C, respectively.

### 3.2.3 Acetylome of *Neisseria gonorrhoeae* MS11

The acetylome of the wild type strain was analysed first before the determination of the acetyl-phosphate dependant acetylation sites. The acetylome of *N. gonorrhoeae* MS11 was determined by LC-MS/MS. Using mass spectrometry 1,254 proteins were identified, representing the 59% coverage of the proteome that possesses 2,106 proteins, higher than the average coverage of 21% calculated from 9 studies. From the identified proteins, 3,752 acetylation sites were identified in 1,017 proteins corresponding to the 48.3% of the proteome (fig. 3.4).

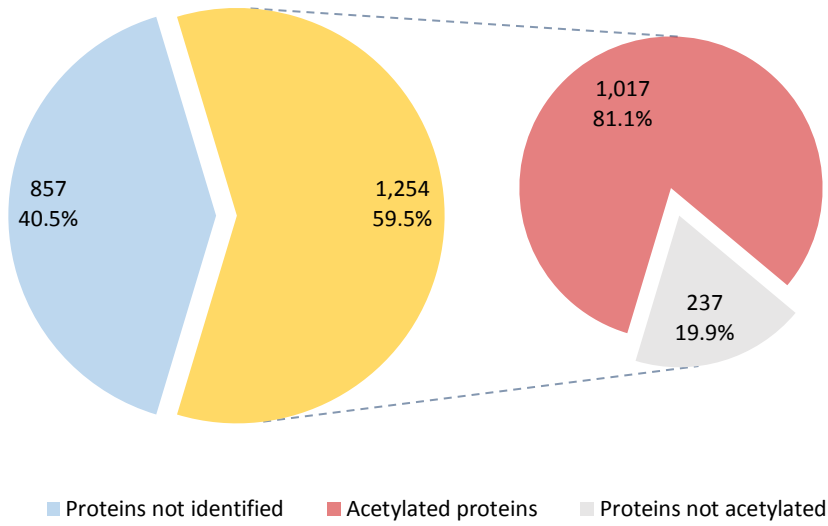


**Figure 3.4 Number of identified proteins of *N. gonorrhoeae* MS11 by mass spectrometry.** Protein extracts enriched with anti-acetyl lysine antibodies were analysed in quadruplicates by LC-MS/MS. The spectra of *N. gonorrhoeae* MS11 was analysed with the software MaxQuant using the proteome database downloaded from UniProt and 1,254 proteins were identified. The parameters of the software Perseus to localise class I acetylation sites were set to a localisation probability of > 0.75 and a score difference >5, identifying 3,752 class I acetylation sites in 1,017 proteins.

The 50% of acetylated proteins had a length of 186-436 amino acids and possessed between 1 to 5 acetylation sites (fig. 3.4a). The median size of the proteins increased to

the number of acetylation sites (fig. 3.4b). However, the fitness of the correlation between the length and number of acetylation sites was low (fig. 3c).

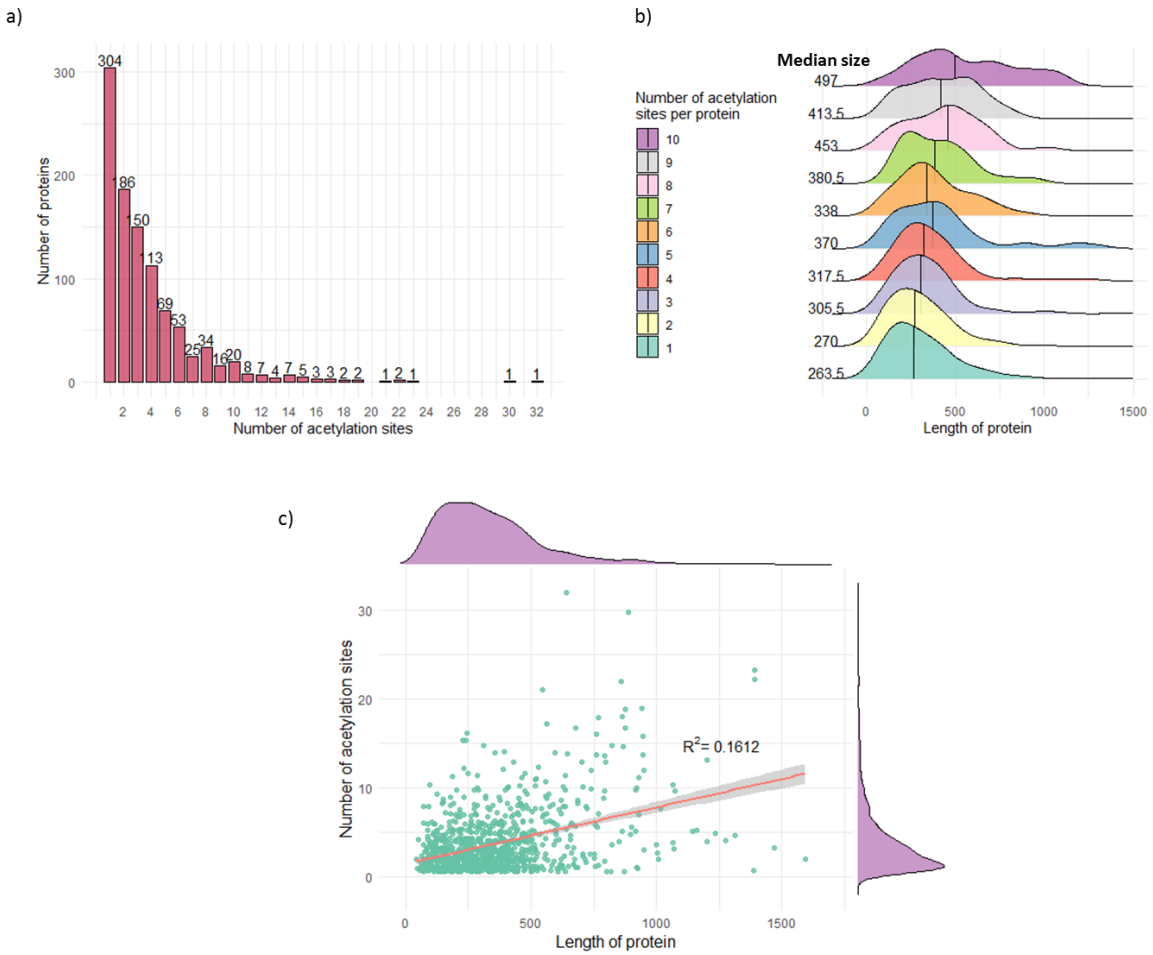


**Figure 3.5 Distribution of acetylated proteins.** **a)** Distribution of acetylated proteins according to the number of acetylation sites. **b)** Distribution of proteins with 1 to 10 acetylation sites. Lines within the plot show the median size of the proteins. **c)** Correlation between the length of proteins and number of acetylation sites. The plot shows the distribution for each variable. A linear regression model showed a fitness of 0.1612 and a correlation of 0.401.

The number of lysines/acetylation sites ratio showed that 21% of proteins are acetylated in 10% of the total lysines (fig. 3.5a). Further analysis to determine the correlation between the lengths of protein and number of acetylation sites, surprisingly showed no

correlation. In order to analyse this, a correlation between acetylated lysines, number of total lysines and protein length showed an $R^2$ of 0.007 (fig. 3.5b).

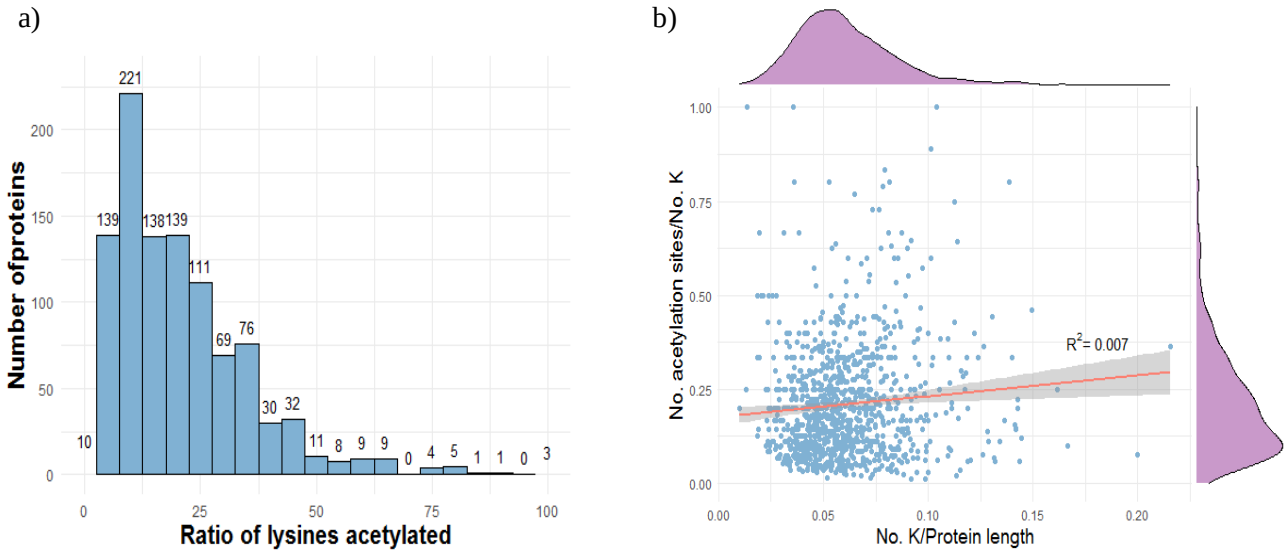


**Figure 3.6 Correlation of acetylation sites and protein length. a)** Distribution of acetylated lysines ratio. The ratio was calculated by dividing the number of acetylated lysines to the number of total lysines. The data was obtained using the UniProt entry to download the protein sequences by data mining. **b)** Correlation between acetylated lysines/number of total lysines, and number of lysines/protein length ratios. A linear regression model is shown in red line and the distribution of both axis are shown. The correlation value was 0.083.

The distribution of the 3,752 acetylation sites within the protein showed that the density of acetylation occurs at a higher rate by the middle of the sequence with the highest peak of acetylation at the C-terminus of the protein (fig. 3.6).

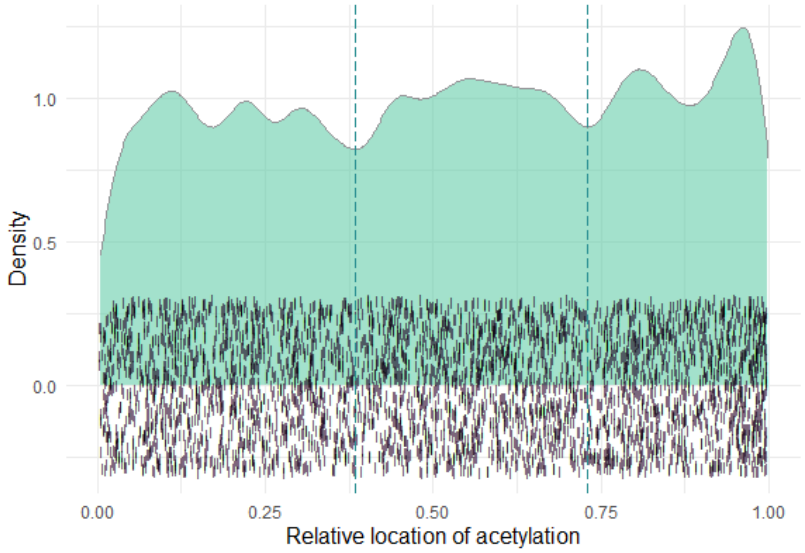


**Figure 3.7 Relative location of acetylation sites.** The plot shows the density of the acetylation sites in the relative location to the protein length. The plot is divided in three regions of highest density of acetylation. The first is in the N-terminus (left) area from the relative location of 0 to 0.38; the second, by the middle of the sequence from the relative location 0.38 to 0.73 where it shows a constant density; and the third region corresponding to the C-terminus (right), where the highest density is observed. The values were obtained by dividing the position of acetylation to the length of the protein. The parameters used for the analysis were a Gaussian method for the kernel density estimate with and adjust value of 0.5. The dashed lines intercept the two sites with the lowest density. The 3,752 sites are shown at the bottom of the plot.

The 3,752 sequence windows, which are the sequence of peptides detected by the mass spectrometer flanking the acetylation sites on each side, were analysed to determine the sequence motif of the acetylation sites. The acetylation site is considered the position 0 and the analysis of the 4 amino acids flanking the acetylated lysine on each side, showed that the most probable amino acids to flank the acetylation site are leucine and glutamic acid, both at the position -1 (fig. 3.6a-b).

Interestingly, the probability to find more negative charged amino acids for the first 4 amino acids downstream is higher than upstream, contrary to upstream, where the

probability is higher for the positive charged amino acids. Downstream the probability for negative and positive charged amino acids is 0.1695 and 0.072. Upstream the probability for negative and positive charged amino acids is 0.1095 and 0.1775 (fig 3.7b).

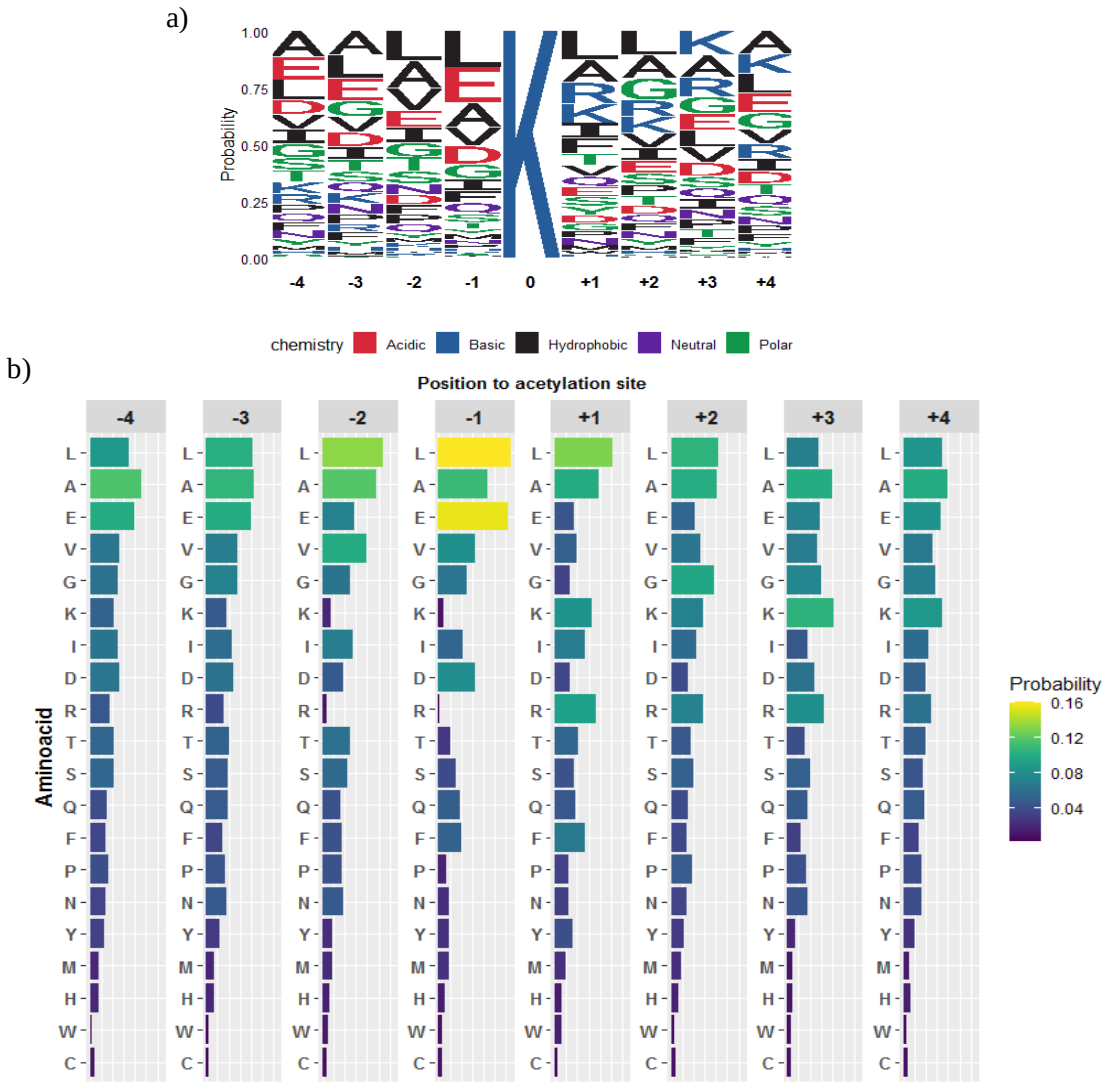


**Figure 3.8 Flanking amino acids of the acetylation site. a)** Sequence motif of the 3,752 acetylation sites. The logo shows the probability of the 4 amino acids flanking the acetylated lysine. The sequence motif was generated with the ggseqlogo package of R. **b)** Probability of each amino acid for each position flanking the acetylated lysine. The minus side showed a higher probability of negative charged amino acid while in the plus side was of positive charged amino acids.

#### 3.2.3.1 Enrichment analysis

All of the proteins that were identified with an acetylation site were analysed for enrichment of pathways using the DAVID bioinformatics tool. The enrichment analysis showed that the PTM acetylation was found in several metabolic processes (fig 3.9).

A figure of 55 biological processes were identified as significantly enriched. The areas with the highest enrichment scores were metabolic processes related to pyruvate, pyrimidines, aspartic acid, and translation. These processes contained 18, 16, 18, and 80 proteins, respectively. The area with the highest number of proteins was metabolic processes with 503.

For the molecular function annotations, 39 terms were enriched and interestingly, 28 of them were related to binding functions. rRNA binding was the term with the highest enrichment score.

Finally, 17 terms were enriched for cellular components. The three terms with the highest enrichment score were ribosome-related containing more than 50 proteins each.

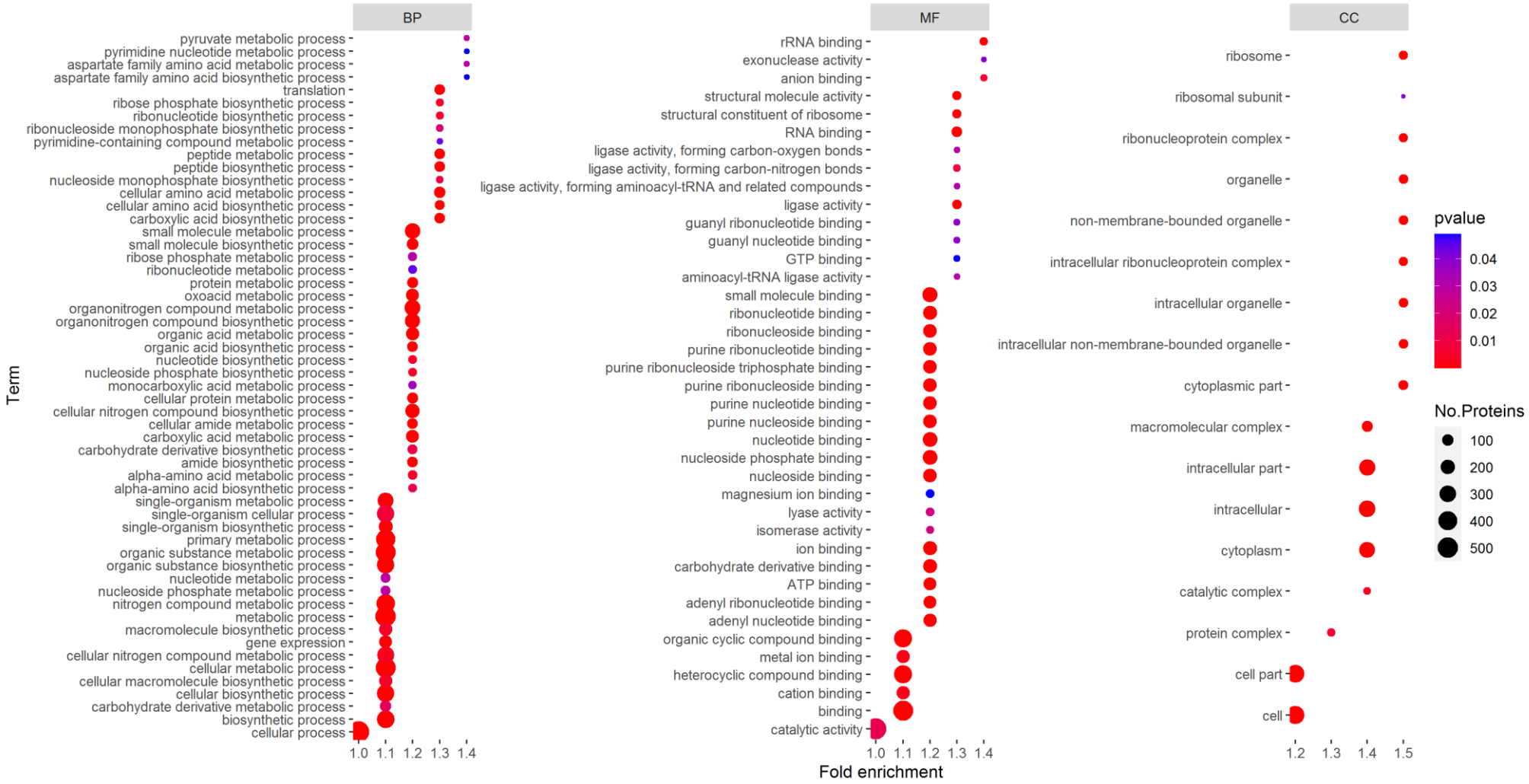


**Figure 3.9 Enrichment of gene ontology annotations of *N. gonorrhoeae* MS11 acetylome.** The enrichment was performed using the Database for Annotation, Visualization and Integrated Discovery (DAVID) v6.8. From the 1,017 protein entries, 591, 426 and 730 were found for biological process (BP), molecular function (MF) and cellular component. The plots show the enrichment score for terms with a significance difference (*p* value <0.05) and the size of each point correspond to the number of genes found in each term.

An interaction network of the KEGG pathways was analysed in order to observe clusters where acetylation could be involved. The network shows a cluster that includes glycolysis, TCA cycle, and propanoate metabolism; and in the centre of the cluster is the pyruvate metabolism pathway. Out of this cluster we found pathways involved in translation, purine metabolism, pentose phosphate pathway and interestingly, pili biosynthesis labelled as flagellar assembly by the software (fig 3.10).

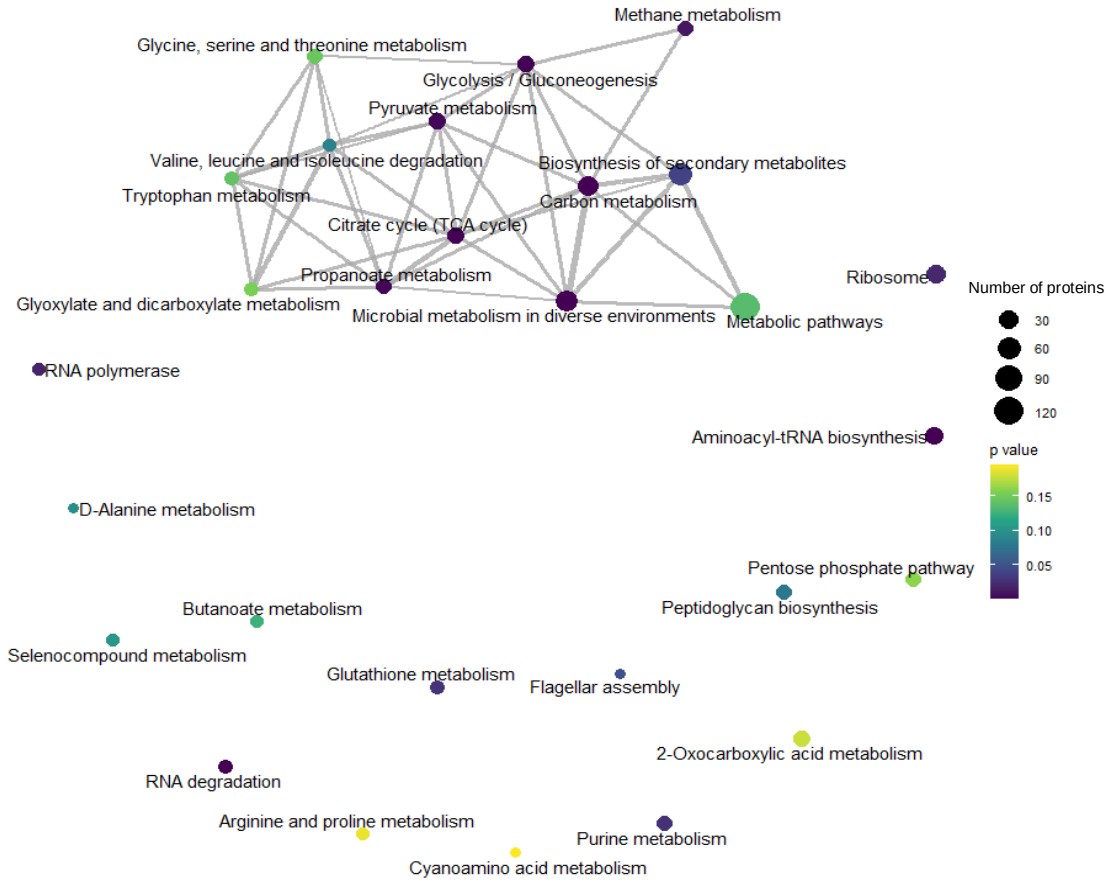


**Figure 3.10 KEGG pathways network of the *N. gonorrhoeae* MS11 acetylome**. At the top of the network is shown a cluster composed by the central metabolic pathways whereas the TCA cycle, pyruvate metabolism, glycolysis/gluconeogenesis and carbon metabolism have the highest number of edges. Surrounding the cluster are shown pathways that are not sharing proteins. Each pathway is coloured depending on the *p* value which shows the significance according to the times the protein appears in the acetylome and the size correspond to the number of proteins. The edges connect to each pathway when proteins are shared and the thickness increases with the number of shared proteins.

Acetylation has shown to modify the activity of some enzymes and their conformational structure (Xiong and Guan, 2012; Šoštarić *et al.*, 2018). Therefore, proteins with 10 or more acetylation sites were filtered from the data set to observe to which pathways they correspond. In fig. 3.11 are shown the 44 proteins that are involved in 45 different pathways which correlate to the cluster observed in fig. 3.10. Showing that proteins in common among these pathways that contain a high number of acetylation sites.

The enzymes with the highest number of acetylation sites were the chaperonin protein DNA K, pyruvate dehydrogenase E1 component, DNA-directed RNA polymerase subunit beta, 60 kDa chaperonin, alanine t-RNA ligase and 2-oxoglutarate dehydrogenase with 32, 30, 23, 20, 19 and 18 acetylation sites, respectively.

Interestingly, 5 different t-RNA ligases possessed high number of acetylation involved aminoacyl-tRNA biosynthesis. In addition, the other pathways that shown proteins with high acetylation sites were the ones in carbon metabolism (TCA cycle, glycolysis/gluconeogenesis and pyruvate metabolism), and nucleotide metabolism (purine and pyrimidine).

A table showing proteins with 5 or more acetylation sites and the pathways they participate are shown in the supplement table 8.1.

Once the acetylome was analysed in the WT, the next step was to analyse the different constructed mutants to see the role of acetyl-phosphate and the histone deacetylase family protein in the acetylation of *N. gonorrhoeae.*

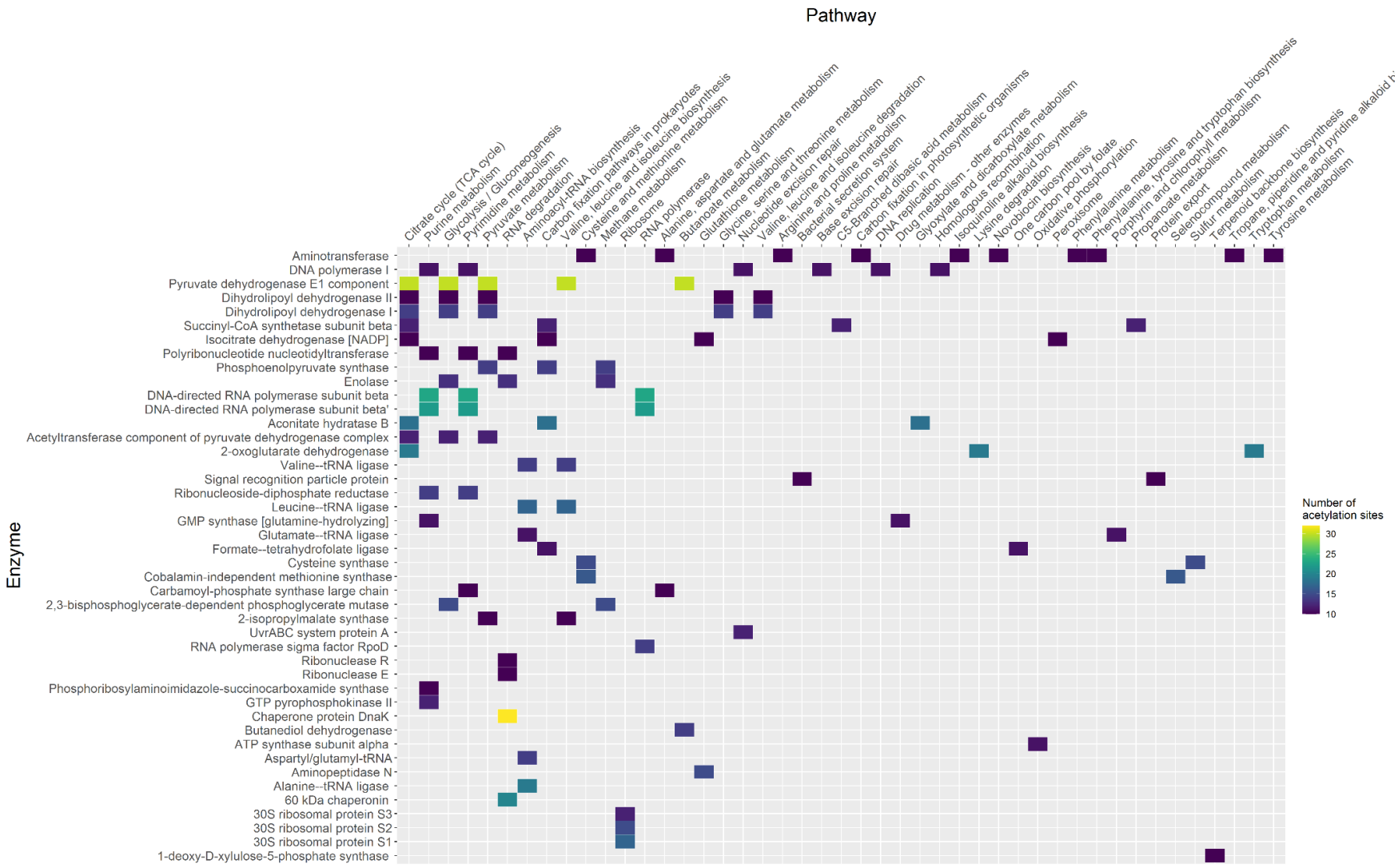


**Figure 3.11 Correlation between proteins with high acetylation sites number and pathways in *N. gonorrhoeae* MS11.** Proteins with 10 or more acetylation sites are sorted in descending order according to the number of KEGG pathways they are involved and the pathways are sorted in descending order according to the number of enzymes. The tiles are coloured respective to the number of acetylation sites the protein possesses.

### 3.2.4 Acetylome of isogenic mutants of *N. gonorrhoeae* MS11

In this section the validation of the mass spectrometry and the analysis of the acetylome of the three isogenic mutant strains of the gonococcus is described. *N. gonorrhoeae* MS11 Δ*ackA* and Δ*pta* were used to identify the acetyl-phosphate-dependent acetylation sites and the strain of *N. gonorrhoeae* MS11 Δ*hdac* was studied to determine possible targets of this deacetylase enzyme. As mention previously, this study involved the investigation of two novel mutant constructs of *N. gonorrhoeae,* Δ*pta* and Δ*hdac* the two latter strains were constructed for the first time for this study

#### 3.2.4.1 Validation of mass spectrometry experiment

The four strains of *N. gonorrhoeae* MS11, WT, Δ*hdac*, Δ*ackA* and Δ*pta*, were grown in chemical defined medium supplemented with 10 mM glucose until mid-logarithmic phase was reached. Four independent replicate cell free extracts (CFE) were obtained for each strain, counting the WT strain as well, 16 CFE were analysed through mass spectrometry. In order to validate the experiment, before the CFEs were enriched with the antibody, the proteome of the samples were analysed to determine the expression of the proteins among the 16 CFEs and identify any difference.

The 16 replicates were evaluated by doing a correlation of the values of intensity to determine if any replicate had to be excluded. A correlation value lower than 0.75 was set to exclude a sample. However, all the replicates showed a correlation value higher than 0.75. The samples that showed the lowest correlation value were the replicates 1 from the isogenic strains Δ*pta* and Δ*hdac*. The rest of the replicates showed a correlation value above 0.89 (fig. 3.12).

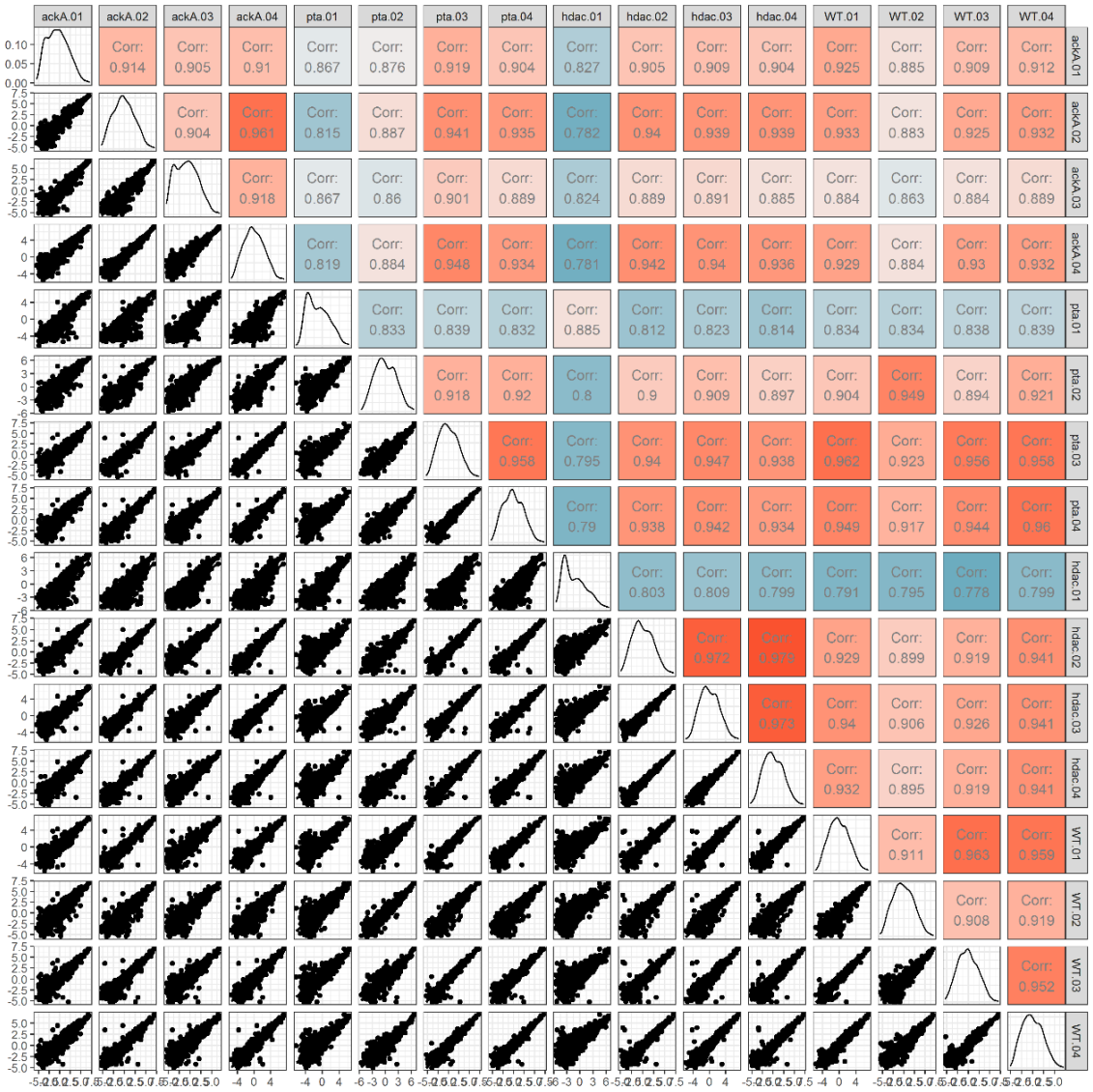


**Figure 3.12 Correlation of CFE for sample validation.** The CFE from the 4 replicates of the 4 *N. gonorrhoeae* strains were processed for mass spectrometry to determine the acetylome. Before the enrichment of acetylated peptides, aliquots were taken to determine the proteome and compare the correlation between samples. The 16 samples were correlated by a Pearson correlation analysis using the intensity values. On the left side of the plot are the correlation plots, in the middle arranged in diagonal are the distributions of the proteins on each sample and on the right side are the Pearson correlation coefficients.

### 3.2.4.2 Descriptive analysis of the acetylome

The samples after validation were analysed to determine the acetylome. The CFE were enriched using anti-acetyllysine antibodies that identify the acetylated peptides. The intensity given for each acetylation site for the 16 samples were analysed with the Student´s t-test. This is a two-tailed test that compares the means between samples taking the WT strain as the reference value to determine if the acetylated peptide was significantly increased or decreased. To discard type I errors, a t-test adjusted for multiple sample comparison was calculated using a permutation-based FDR of 1%. Applying this FDR we filtered potential false positive acetylation sites.

A volcano plot in figure 3.13 shows the significant different acetylation sites according to the fold change difference to the WT. The plot correlates the negative logarithm of the *p* -value and the fold change of acetylation.

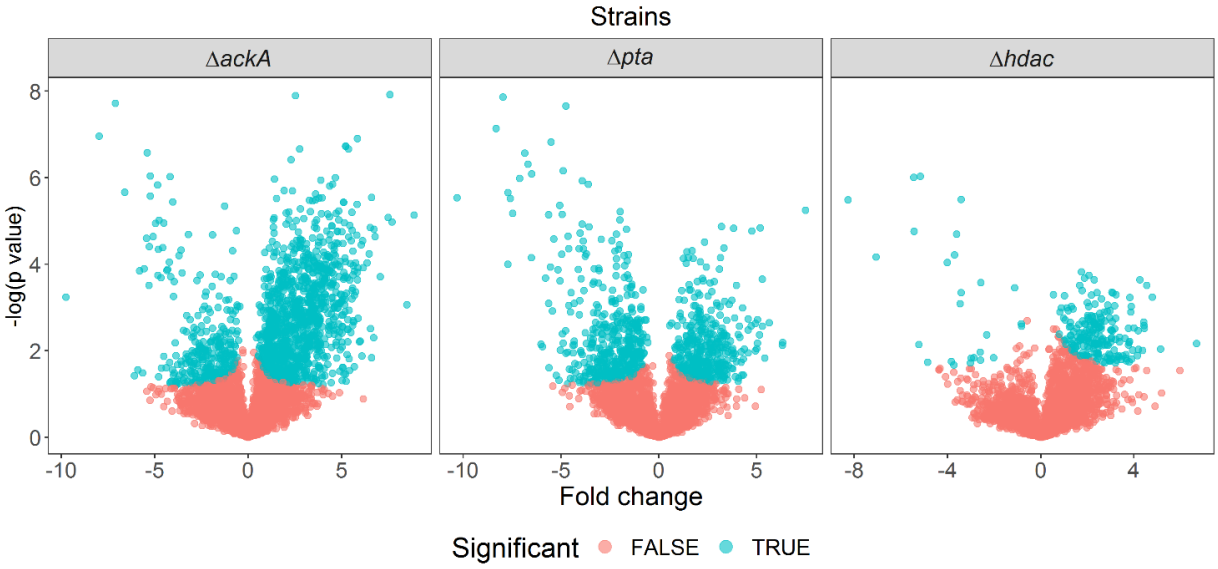


**Figure 3.13 Volcano plot for acetylation sites in *N. gonorrhoeae* MS11.** The plot shows the acetylation sites that are significantly decreased (left side) or increased (right side) compared to the WT strain determined by the two-tailed Student´s test. The S0 parameter was set to 0.1 and the false discovery rate to 0.05. Acetylation sites that showed a significant difference are blue coloured while the red are non-significant.

In table 3.2 are shown the number of proteins that showed significant different acetylation sites compared to the common acetylation profile of the WT strain that considers the abundance of proteins. This acetylation sites were classified by the number of proteins which showed significant increased and decreased acetylation sites. The total number of significant acetylation sites was 3,752. From these sites, we observed sites with significant increase and decrease in acetylation. As expected, the isogenic strain Δ*ackA* showed a higher number of significant increased acetylation sites as in the Δ*hdac* strain, and in the Δ*pta* strain more acetylation sites were found significantly decreased. The table with the proteins with two or more significant different acetylation sites are found on the supplement table 8.2.

The significant different acetylation sites were used through the rest of the study for the analysis and determination of the sites potentially regulated by acetyl-phosphate.

**Table 3.2 Number of significant proteins and acetylation sites in the isogenic mutant strains of *N. gonorrhoeae* MS11.** The percentage next to the total number of proteins and acetylation sites is compared to the total number found in the three strains. The percentage of the other values are respective to the total number from each strain.

| Strain | Significant proteins | | | Significant acetylation sites | | |
|---|---|---|---|---|---|---|
| | Total (n=1,017) | Increased | Decreased | Total (n=3,752) | Increased | Decreased |
| **Δ*ackA*** | 638 (62.7%) | 531 (83.2%) | 235 (36.8%) | 1,369 (36.5%) | 1369 (77.7%) | 305 (22.3%) |
| **Δ*pta*** | 527 (51.8%) | 277 (52.6%) | 330 (62.6%) | 847 (22.6%) | 387 (45.7%) | 460 (53.3%) |
| **Δ*hdac*** | 184 (18.1%) | 164 (89.1%) | 26 (14.1%) | 235 (6.3%) | 209 (88.9%) | 26 (11.1%) |

The median fold change of acetylation in the three isogenic mutant strains is 2.24, -1.09 and 2.07 in Δ*ackA*, Δ*pta* and Δ*hdac*, respectively (fig. 3.14b). However, when the

acetylation sites are divided into the type of fold change (increased or decreased) the median values are similar among the strains (fig. 3.14c).

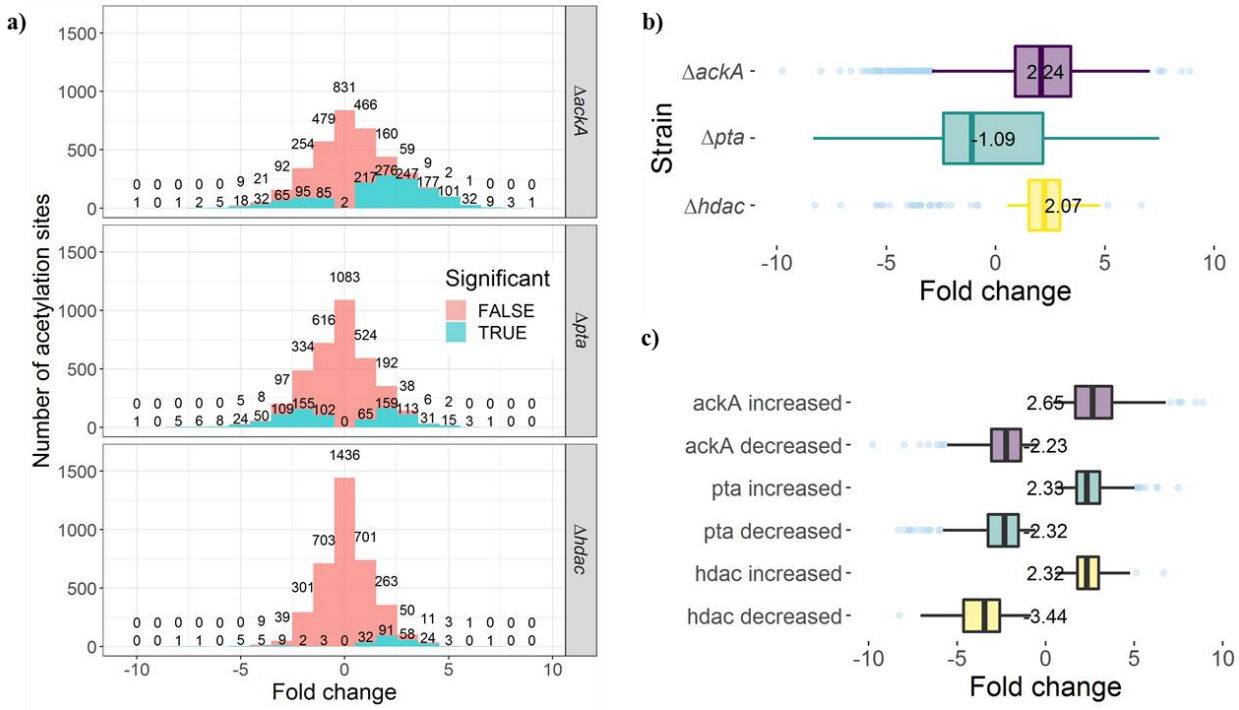


**Figure 3.14 Distribution and median of acetylation sites in the isogenic mutant strains of *N. gonorrhoeae* MS11. a)** Distribution of the acetylation sites according to the fold change. **b)** Boxplot of all the significant sites from the three isogenic mutant strains. Δ*ackA* and Δ*hdac* have a median of fold change on the positive side, while Δ*pta* on the negative side. **c)** The distribution of the acetylation sites showed that the significant sites are divided in two by increased and decreased acetylation. Therefore, the median size was calculated for each division considering increased when the fold changed was higher than 0 and decreased when lower than 0. The median fold changes are shown for the three strains.

In order to analyse the location of acetylation in the protein. The site of acetylation was calculated relatively to the length of the protein, being 0 the N-terminus and 1 the C-terminus (fig. 3.15). The location of acetylation between strains showed a different pattern of acetylation compared to the WT (fig. 3.7). Suggesting that acetylation by acetyl-phosphate occurs in surface expose lysines.

The Δ*ackA* isogenic strain showed a different pattern of distribution of the location. The middle part corresponding from 0.385 to 0.73 showed lower density than the WT in that area but the final section (0.73-1.0) showed the highest region of density with the highest density of 1.23. Analysis of the sequence motifs of the three sections, showed that in all the sections, the two amino acids that had the highest probability at position -1 were leucine (L) and glutamic acid (E), a hydrophobic and a negative charged amino acid, respectively. Overall, the probability of the arginine increases the closer to the C-terminus of the protein (fig. 3.15).

Contrary to Δ*ackA*, the two lowest points in Δ*pta* were at a similar location to the WT strain, however, the densities were different. In the middle section, the highest density in the decreased acetylation of Δ*pta* was 1.30 and in the increased was 1.24. The sequence motifs in the decreased acetylation of Δ*pta*, opposite to Δ*ackA*, showed that the two amino acids at position -1 with the highest probability were E and L in three sections. On the increased acetylation of Δ*pta*, the sequence motifs changed on the three sections and the amino acids with the highest probability at postion-1 were arginine, leucine and alanine. However, at the third section arginine is the third most probable (fig 3.15).

The density of increased acetylation sites in Δ*hdac* showed the highest density in the N-terminus of 1.23. In the middle section a peak is observed however is lower that the first section with a density of 1.08. As in the first two cases the two most probable amino acids at position -1 were L and E. However, in the second and third sections it is observed that the amino acid arginine is found as the first option in several positions (fig 3.15).

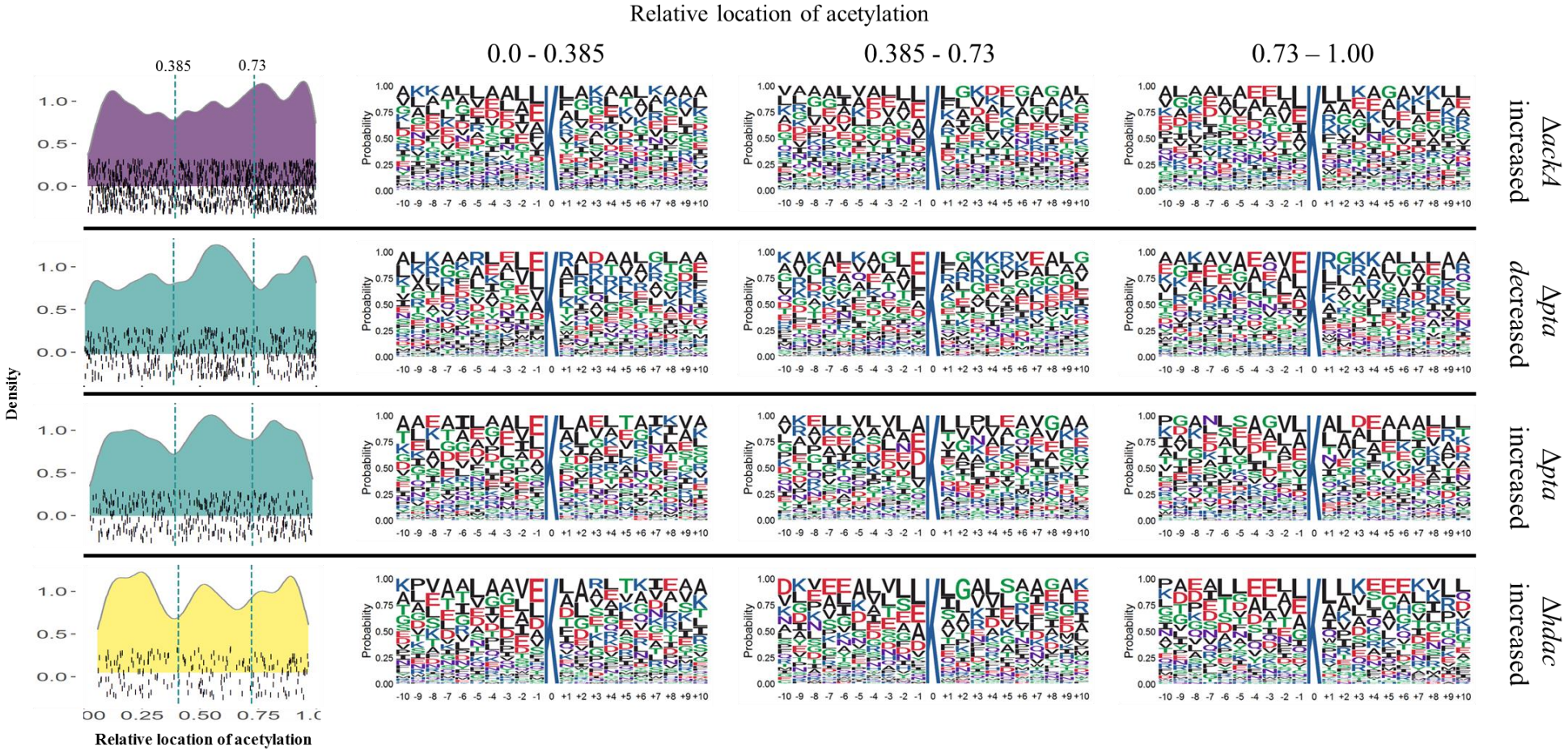


**Figure 3.15 Analysis of the sequence motifs for the acetylation sites in the three isogenic strains of *N. gonorrhoeae* MS11.** The plot shows the density of the significant acetylation sites in the relative location to the protein length. The plots are divided in three regions as in the WT. The values were obtained by dividing the position of the acetylation site to the length of the protein. The parameters used for the analysis were a Gaussian method for the kernel density estimate with and adjust value of 0.5. The dashed lines intercept the two sites with the lowest density. The significant different acetylation sites are shown at the bottom of the plot. The sequence motifs were generated with the ggseqlogo package of R by filtering the data to select the sequence windows of section of the density plot. The size of each amino acid correspond to the probability of the amino acid to be at the position surrounding the acetylation site.

### 3.2.5 Acetyl-phosphate dependent acetylation in *N. gonorrhoeae* MS11

In nature, two types of acetylation occur as post-translational modifications on protein. The first is enzymatically, by the action of acetyltransferases an acetyl group binds to the Nε-lysine residue using acetyl-CoA as donor. The second is non-enzymatically, the acetyl group is donated by the high energy molecule acetyl-phosphate (Verdin and Ott, 2013; Ouidir, Kentache and Hardouin, 2016; Wolfe, 2016). In this section, utilising the data obtained from the acetylome of the isogenic mutant Δ*ackA* and Δ*pta*, we determined the acetylation sites dependent of acetyl-phosphate.

In this study, the acetyl-phosphate dependent acetylation sites were defined as the unique acetylation sites found in both Δ*ackA* and Δ*pta* that showed a significant (*p* value <0.05) increased and decreased of fold change, respectively, in at least three of the four biological replicates.

The proteins and acetylation sites of both strains were analysed by a Venn diagram, identifying 409 and 424, respectively (fig. 3.16a-b). The selection of highly regulated acetylation sites by acetyl-phosphate was determined by analysing the increased and decreased acetylation sites from Δ*ackA* and Δ*pta*, respectively. From this classification, 117 unique acetylation sites were found in 107 proteins (fig. 3.16 c).

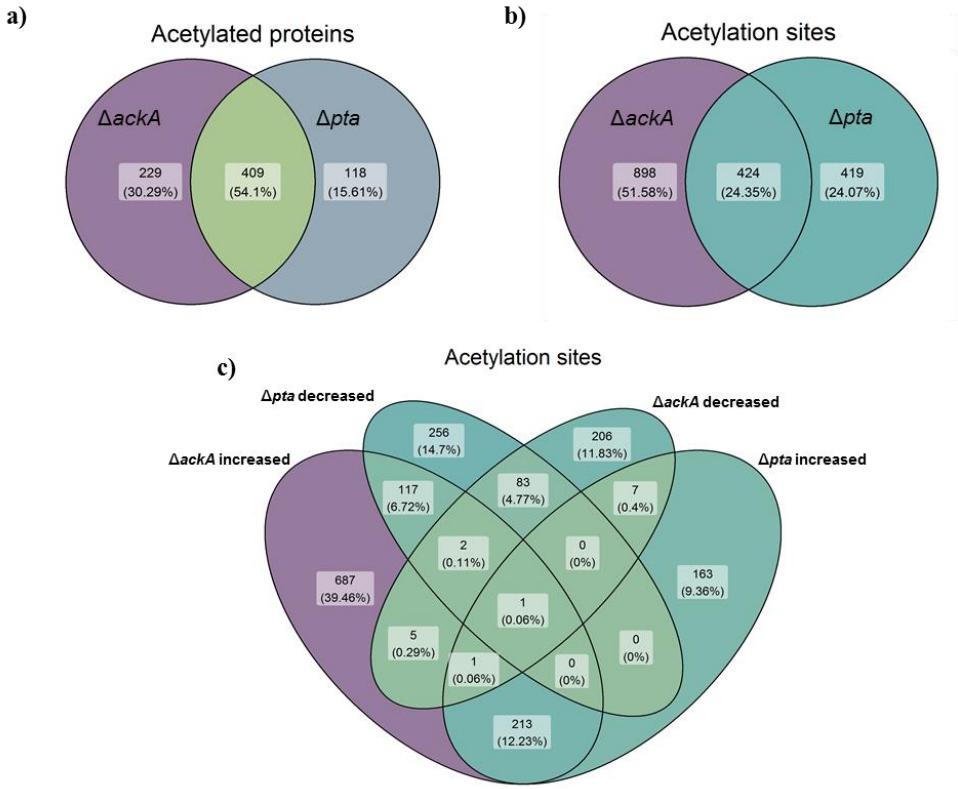


**Figure 3.16 Identification of unique acetyl-phosphate-dependent acetylation sites in *N. gonorrhoeae* MS11.** Venn diagrams of proteins and acetylation sites from the strains Δ*ackA* and Δ*pta*. **a)** 409 unique proteins were shared between both strains, and **b)** 424 acetylation. **c)** Acetylation sites were divided in increased and decreased depending on the fold difference. The overlapping acetylation sites from Δ*ackA* with an increased fold difference and the decreased from Δ*pta* are the highly regulated acetyl-phosphate dependent sites. A total of 117 unique acetylation sites were found in 102 proteins**.**

The sequence windows from the 117 acetylation sites were analysed to determine the sequence motif. This sequence motif shows the amino acids that are flanking the acetyl-phosphate dependent acetylation site.

At the position -1, the amino acid with the highest probability was glutamic acid with 0.198 and at position +1 was arginine with 0.178. At position +3 and +4, lysine has the highest probability due to the presence of multiple acetylation sites (fig. 3.17a-b).

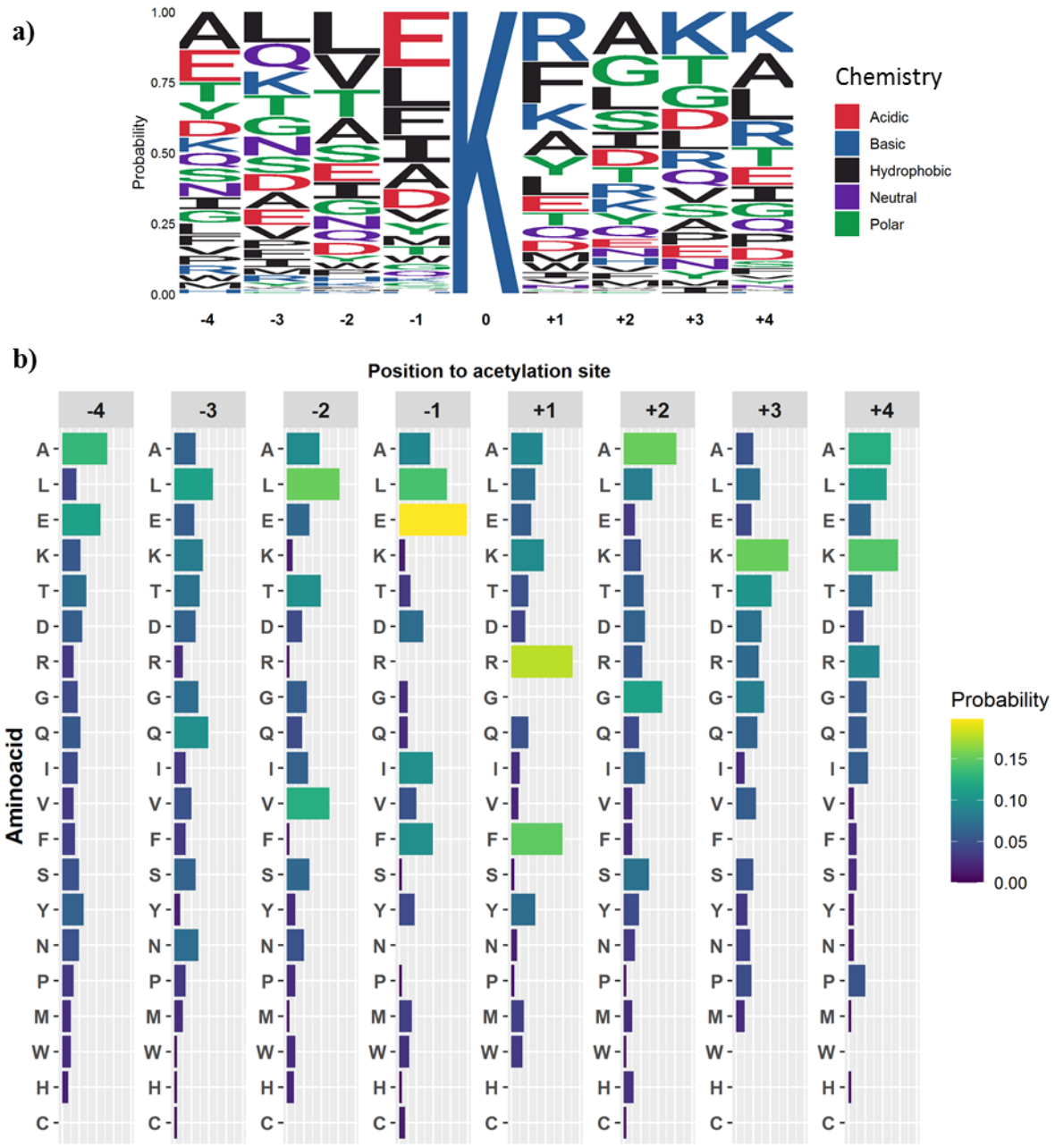


**Figure 3.17 Sequence motif of acetyl-phosphate dependent acetylation sites. a)** Sequence motif generated from the 117 unique sequence windows of the classified acetylation sites. The sequence motif shows the first 4 amino acids flanking the acetylation site and the size correspond to the probability to be in that position. The sequence motif was generated using the ggseqlogo package of R. **b)** Probability of each amino acid for the positions flanking the acetylation sites.

From 102 proteins, 88 showed one acetyl-phosphate dependent sites and 14 two. The mean fold change was 2.02 and -2.23, and the median was 1.52 and -1.99, in Δ*ackA* and Δ*pta*, respectively (fig. 3.18a-b).

The analysis of gene ontologies showed that the molecular function term with the highest number of proteins with acetyl-phosphate dependent sites was ATP binding with 38 proteins. However, seven more terms were related to molecule binding function. The KEGG pathways with the highest number of protein were pyruvate metabolism and methane metabolism with 7 proteins each. Other carbon metabolism pathways with five proteins were glycolysis and gluconeogenesis. Thirty four of the proteins are found in the cytoplasm, 11 are integral components of membrane (fig. 3.18c). The only biological process with more than 5 proteins was translation. A table with the terms with more than two proteins is find in the supplement table 8.3.

An enrichment analysis of the identified proteins with an AcP-dependent site was performed. The biological process with the highest enrichment score were processes related to tRNA aminoacylation. Five of the terms were related to metabolic processes. For the molecular function we found that 65% of the terms were related to binding function. The cellular components of these proteins were found in the cytoplasm (fig. 3.19)

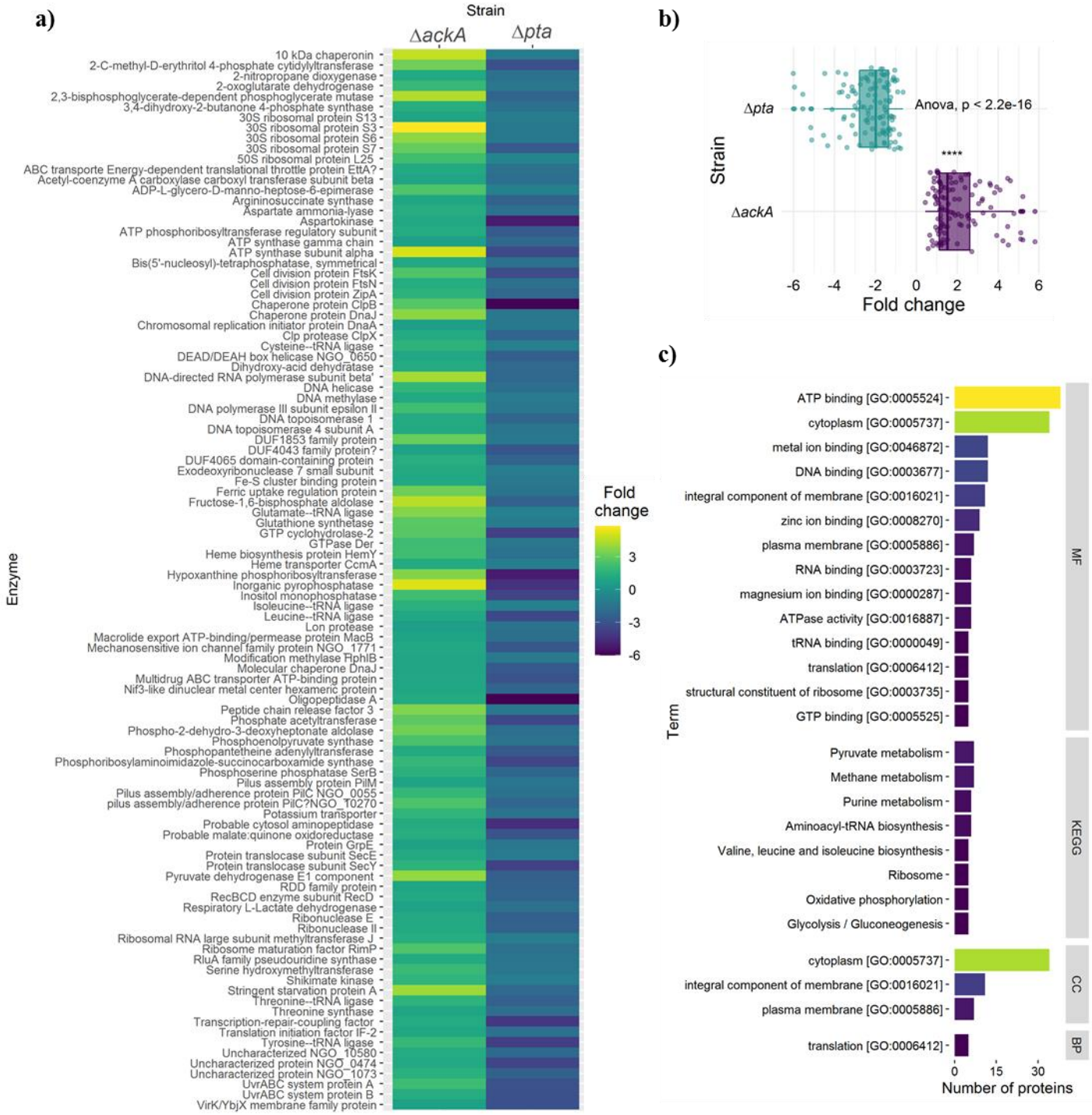


**Figure 3.18 Acetyl-phosphate dependent sites. a)** Proteins classified as acetyl-phosphate dependent for acetylation. The same acetylation site was found on both strains with a significant difference of the fold change. **b)** Boxplot showing the fold change of each acetylation site. An ANOVA test shows a significant difference between the fold changes in both strains. **c)** Gene ontology analysis showing the terms with more than five proteins in molecular function (MF), KEGG pathways (KEGG), cellular component (CC), and biological process (BP).

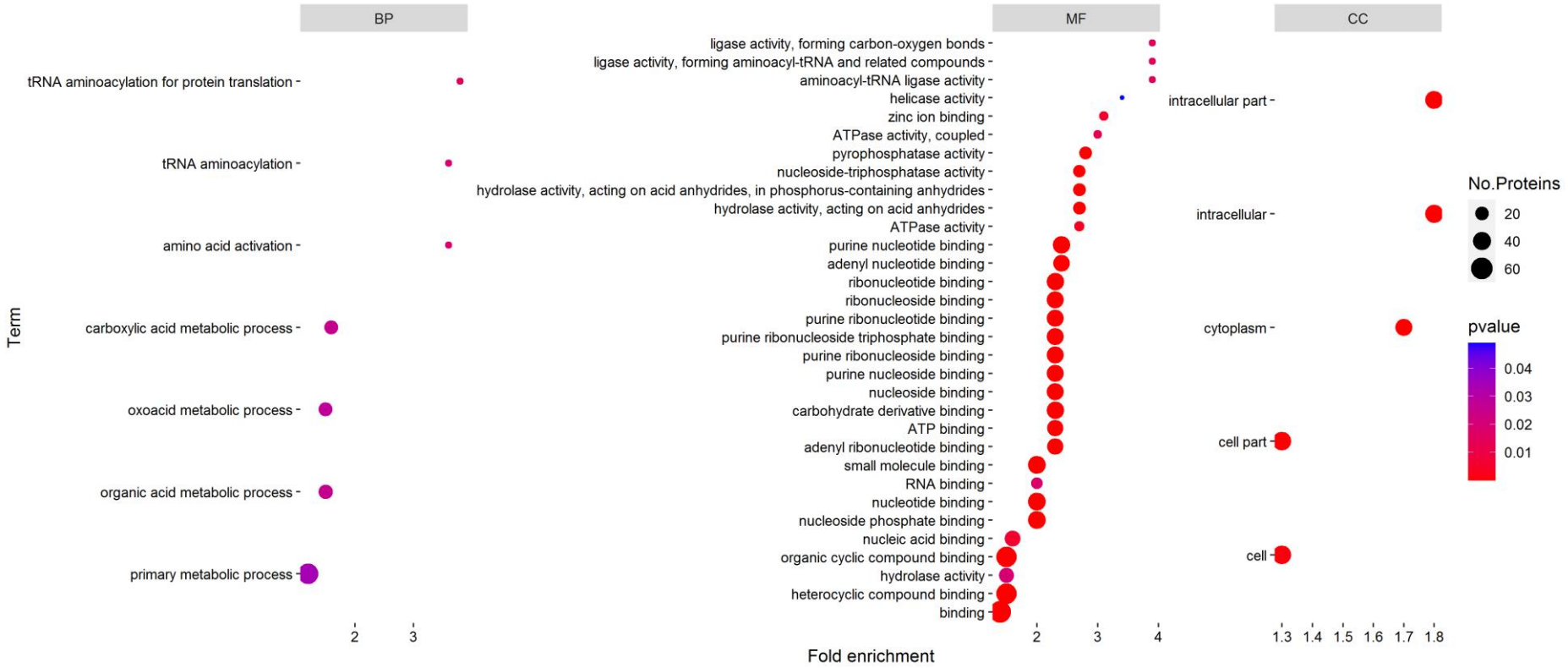


**Figure 3.19 Enrichment analysis of the gene ontologies for the proteins with acetyl-phosphate- dependent sites.** The analysis was performed using the DAVID website which identifies the annotations and perform a statistical analysis to identify the enriched terms. In the plot are shown the significant terms (*p* value <0.05) for biological process (BP), molecular function (MF) and cellular component (CC)

#### 3.2.5.1 Determination of targets for the gonococcal histone deacetylase-like protein

Histone deacetylase-like proteins (HDAC) are a family of enzymes that removes the acetyl group from the N-ε-lysine residue. These enzymes were first discovered in eukaryotic cells and classified in different classes (Grabiec and Potempa, 2018). Their main target are histones to block the transcription of genes. Recently, several HDACs have been found in prokaryotes and a 2020 study in *N. gonorrhoeae*, found that the gonococcal HDAC NGO0187, same gene that was used in this study, plays a role in the regulation of the host gene expression (Jiang *et al.*, 2017; Zughaier, Rouquette-Loughlin and Shafer, 2020)

For the identification of the possible targets of HDAC, all the acetylation sites with a significant fold change were classified according to the difference, increased or decreased. Since the action of the HDAC is to deacetylate proteins, the possible targets were classified as the unique acetylation sites that showed a significant increase in the isogenic mutant strain Δ*hdac*. Thirty four unique acetylation sites in 34 proteins were classified with this criteria and therefore the possible targets of HDAC (fig. 3.20).

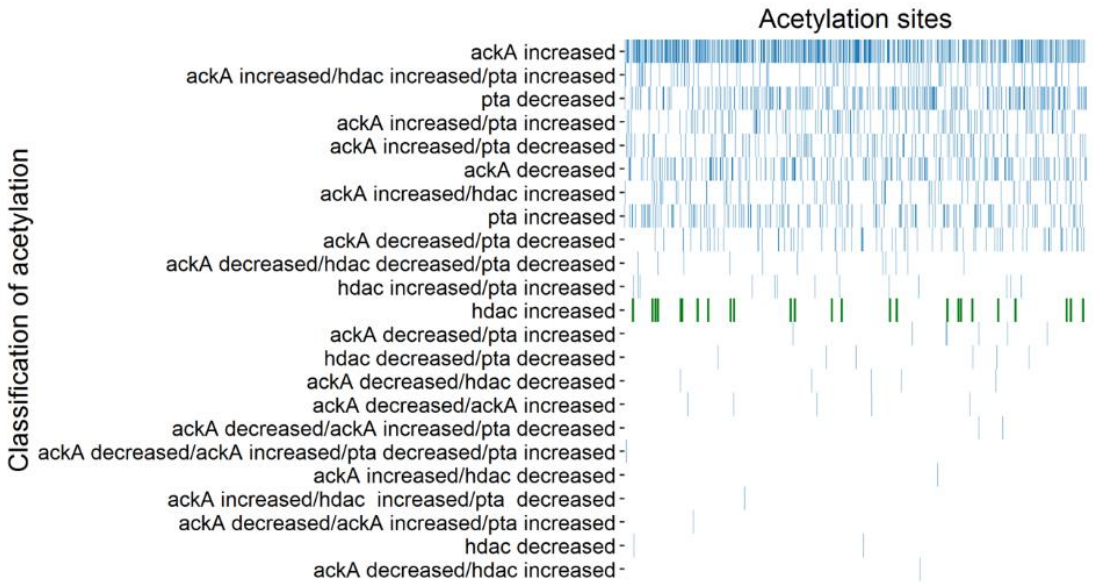


**Figure 3.20 Identification of the possible targets of HDAC.** The acetylation sites found in the three isogenic mutant strains Δ*ackA,* Δ*pta,* and Δ*hdac* were classified according to the fold change difference. From the 2,451 acetylation sites (blue), 34 (green) were unique for Δ*hdac.*

The sequence windows of the 34 acetylation sites showed a similar sequence motif as the acetyl-phosphate dependent sites. At the position -1 the amino acid with the highest probability was glutamic acid with 0.28 and at position +1 was isoleucine with 0.24 probability. Different to the acetyl-phosphate dependent sites, the HDAC targets sequence motifs also present a negative charge amino acid at position -2. The amino acid aspartic acid showed a probability of 0.20 (fig 3.21).

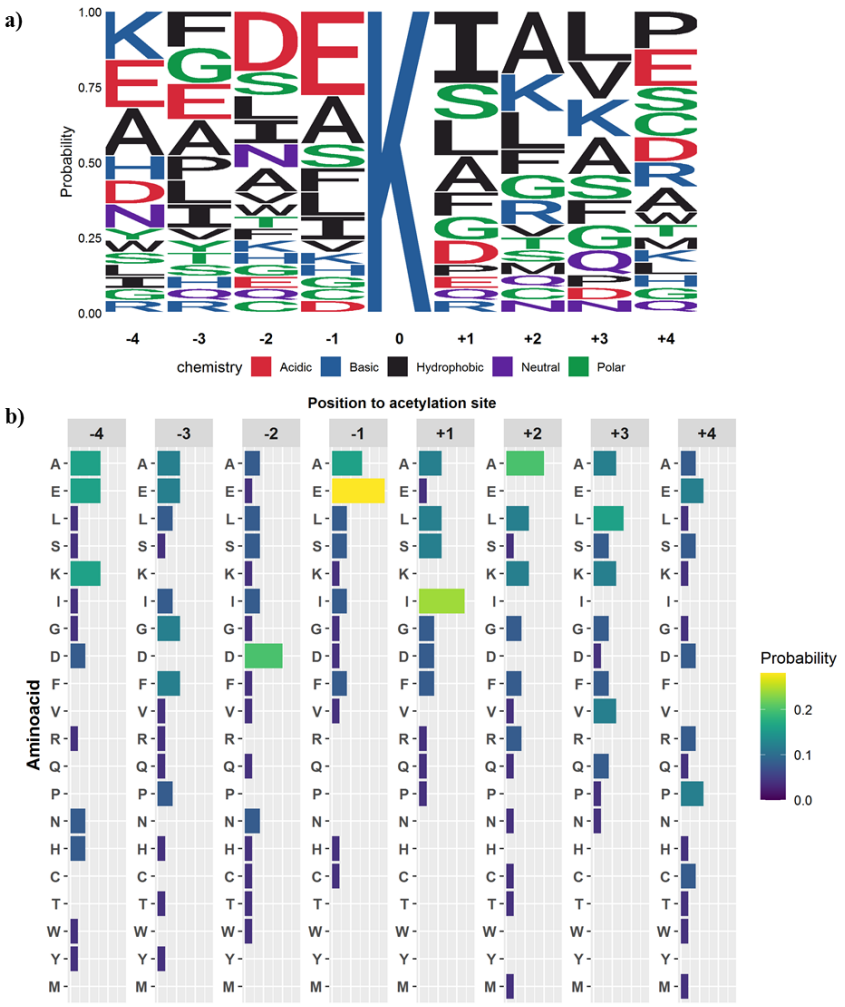


**Figure 3.21 Sequence motif and probability for the HDAC targets. a)** Sequence motif generated from 25 unique sequence windows. The sequence motif shows the first 4 amino acids flanking the acetylation site and the size correspond to the probability to be in that position. The sequence motif was generated using the ggseqlogo package of R. **b)** Probability of each amino acid for the positions flanking the acetylation sites.

From the identified proteins with an acetylation site susceptible to HDAC (fig. 3.22a) three tRNA ligases are involved in translation, both ribosomes (50S and 30S) showed one target site in one subunit. Interestingly, the enzyme phosphotransacetylase showed higher acetylation in K450, furthermore, the porin B, a protein involved in the virulence of the gonococcus, showed one site.

The gene ontologies of the identified proteins showed a diversity of functions, however, the term translation was the only biological process with two proteins the rest showed only one. The molecular function with the highest number of proteins was ATP binding with eleven proteins followed by zinc ion binding, tRNA binding and magnesium ion binding. Purine and pyrimidine metabolism presented three proteins. The complete heat map with all the enzymes and terms is found in the supplement fig 8.1.

A network analysis of the KEGG pathways and biological processes showed a cluster for processes related to translation and tRNA metabolism, including the tRNA ligases for valine (*valS*), alanine (*alaS*), and glutamate (*gltX*). Pyruvate metabolism and TCA cycle, contained one enzyme each biotin carboxylase and 2-oxoglutarate dehydrogenase, respectively (fig. 3.22b).

The enrichment analysis showed 4 biological process terms with metabolic and biosynthetic metabolic processes. All the molecular functions are binding related except for one which has ATPase activity. tRNA binding showed the highest enrichment score. Finally, the majority of the proteins were found in the cytoplasm (fig. 3.23).

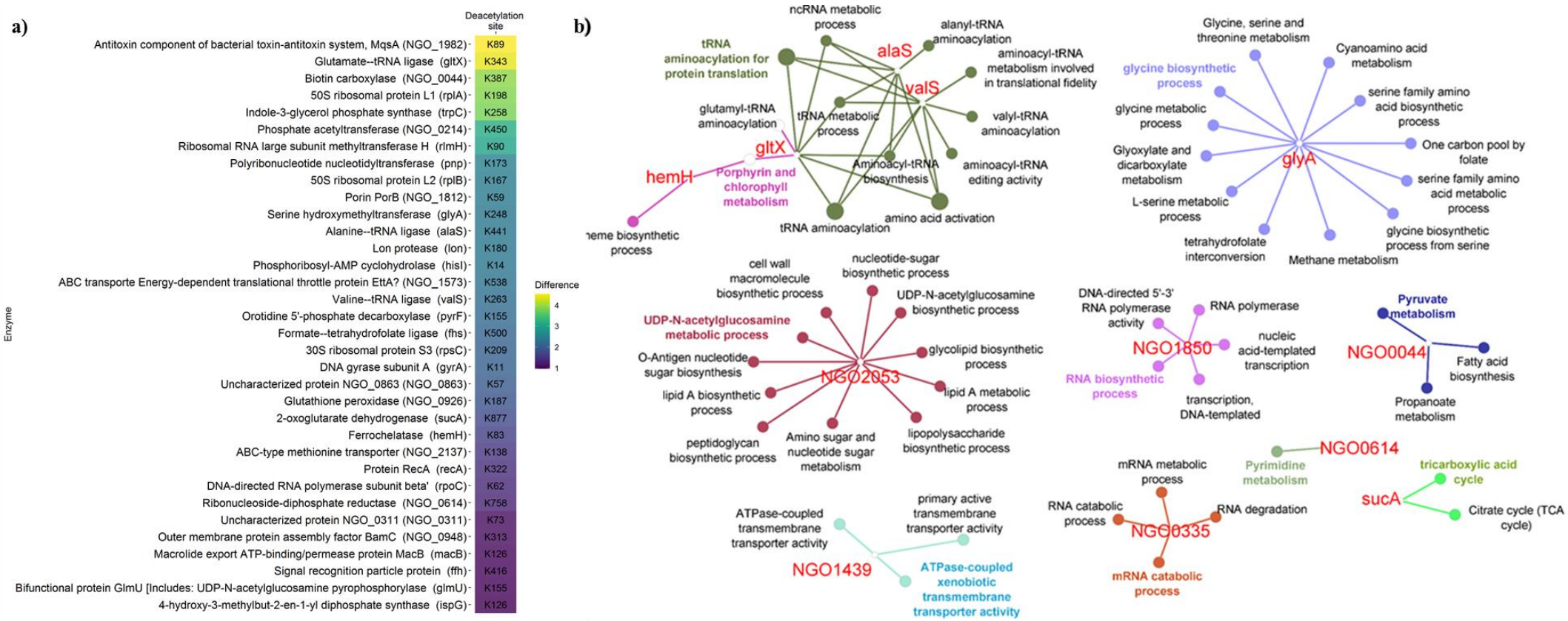


**Figure 3.22 Protein targets of HDAC and network analysis. a)** List of the possible deacetylation sites of the protein HDAC in *N. gonorrhoeae* MS11. The list shows the protein name and the gene name. The tiles are filled according the fold change difference and the deacetylation position site is found inside of the tile. **b)** A network of the identified enzymes was created using ClueGo on the software Cytoscape. The network shows the biological processes in black and in colour the KEGG pathways. In red are the identified genes. The parameters for the network were a minimum of 1 gene and 4% of the total genes for each term.

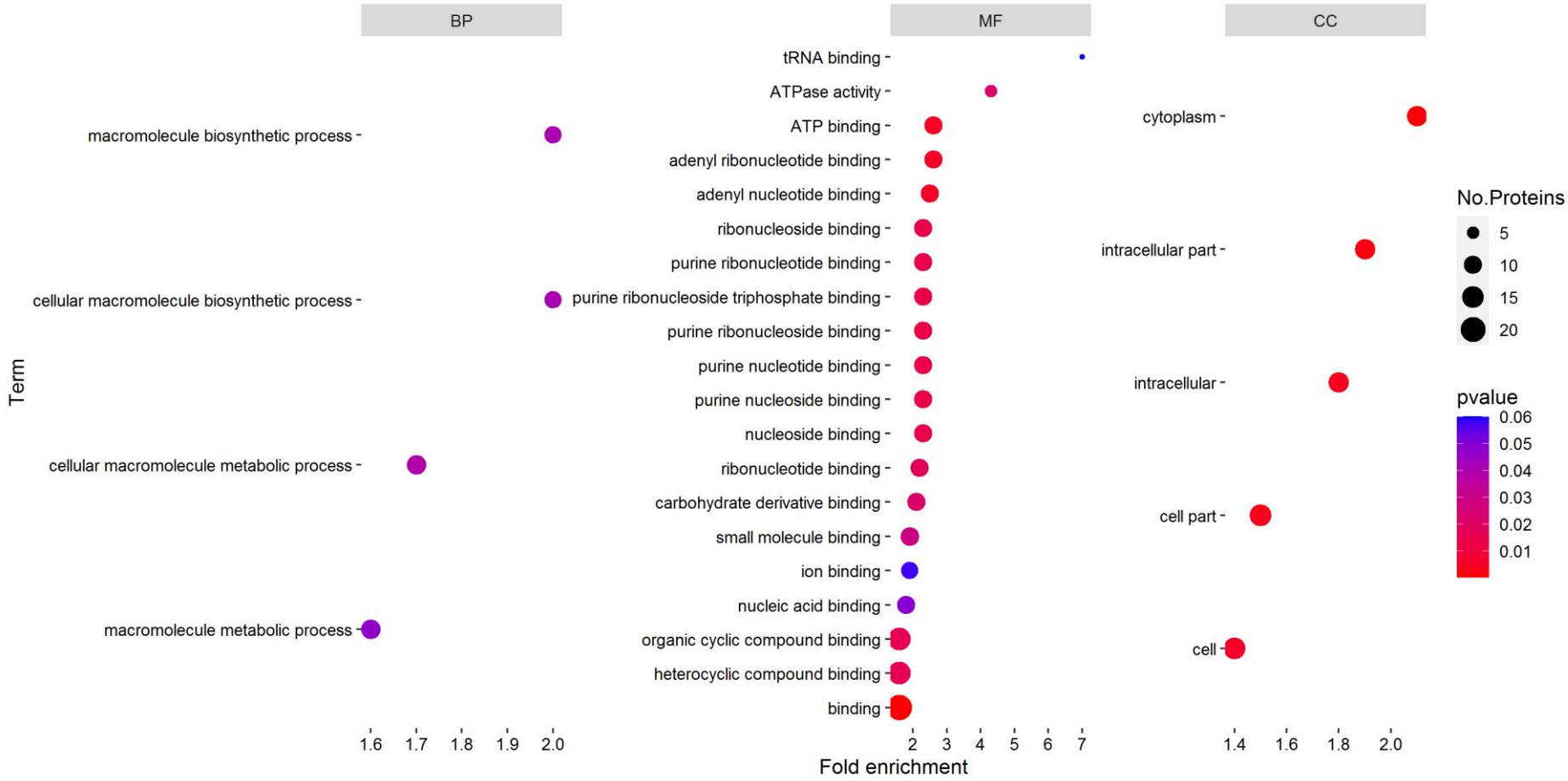


**Figure 3.23 Enrichment analysis of the gene ontologies for the HDAC targets.** The analysis was performed using the DAVID website which identifies the annotations and perform a statistical analysis to identify the enriched terms. In the plot are shown the significant terms ($p$ value <0.05) for biological process (BP), molecular function (MF) and cellular component (CC)

## 3.3 Discussion

From the discovery of the first histone deacetylase in 1996, to the discovery of the non-enzymatic acetylation in both eukaryotic and prokaryotic cells, a door was opened to explore new types of enzymatic regulations (Verdin and Ott, 2013, 2015; Wagner and Payne, 2013; David G Christensen *et al.*, 2019). The development of new technologies such as mass spectrometry, has made that studies like proteomics be more affordable and with better resolution. For instance, two studies of acetylation in *E.coli* in 2008 and 2013, identified 125 and 1,070 acetylation, respectively (Yu *et al.*, 2008; Zhang *et al.*, 2013).

In this study, the acetylome of the wild type strain and three isogenic mutants of *N. gonorrhoeae* MS11 was analysed. The coverage of identified proteins and acetylation sites overtakes the acetylome of the last acetylome study made by Post *et al.*, 2017. The total coverage of identified proteins increased by 55% and 40% for acetylation sites (fig. 3.24). Post study and this study share in common 444 and 1,345, proteins and acetylation sites, respectively, corresponding to the 43.7% and 35.8%, respectively. Moreover, in this study we analysed four samples for each strain, including Δ*pta* and Δ*hdac*, one more biological replicate than Post study.

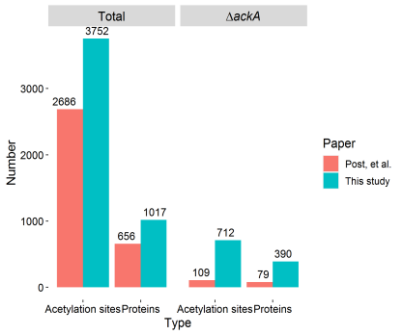


**Figure 3.24 Comparison of identified proteins and acetylation sites. The data correspond to three and four biological replicates from the Post, et al. paper and this study.**

Comparing data from the most recent papers that made immunoaffinity enrichment and mass spectrometry, we observed that this study shows the highest coverage and the number of biological replicates is as high as one more study (table. 3.3). This difference in coverage was possible due to the high number of biological replicates, the number of strains analysed and the protocol established at the BIOMICS facilities of the University of Sheffield.

**Table 3.3 Comparison of studies with bacterial acetylomes.**

| Organism | Acetylation sites | Proteins | Coverage | Growth medium | Growth phase | Replicates | Reference |
|---|---|---|---|---|---|---|---|
| ***Clostridium acetobutylicum*** | 458 | 254 | 6.60% | Minimal medium with glucose | Logarithmic, transitional and stationary | 3 biological | Xu *et al.*, 2018 |
| ***Salmonella* Typhimurium** | 1,259 | 631 | 13.30% | LB broth | Early logarithmic | 1 biological | Li *et al.*, 2018 |
| ***Bacillus subtilis*** | 1,355 | 629 | 15.03% | Fresh minimal medium supplemented with glucose | Logarithmic | 4 biological | Kosono *et al.*, 2015 |
| ***Brenneria nigrifluens*** | 1,866 | 737 | 17.30% | Tryptic soy broth | Stationary | 6 technical | Li *et al.*, 2020 |
| ***Streptococcus pneumoniae*** | 653 | 392 | 20.50% | Toddy-Hewitt broth with 0.5% yeast extract medium | Stationary | 2 biological | Liu *et al.*, 2018 |
| ***Escherichia coli* BW25113** | 3,840 | 978 | 23.87% | M9 minimal medium 0.4% Glucose | Stationary | 3 biological | Schilling *et al.*, 2019 |
| ***Vibrio alginolyticus*** | 2,883 | 1,178 | 27.17% | LB broth | Logarithmic | NA | Pang *et al.*, 2020 |
| ***Neisseria gonorrhoeae* MS11** | 2,686 | 656 | 31.15% | GC broth supplemented with 1% IsoVitaleX and Kellogg's supplement | Stationary | 3 biological | Post *et al.*, 2017 |
| ***Vibrio cholerae* V52** | 3,402 | 1,240 | 34.67% | LB broth | Mid-logarithmic and stationary | 2 biological | Jers *et al.*, 2018 |
| ***Neisseria gonorrhoeae* MS11** | 3,752 | 1,017 | 48.29% | Chemically defined with glucose | Mid-logarithmic | 4 biological | This study |

Comparing the data from the Post study, 1213 acetylation sites in 444 proteins are in both acetylomes. From this 689 were significantly different in 327 proteins. From the 1,017 proteins, the 70% showed more than 1 acetylation site analogous to other study, where they found 72%. The proteins with >20 acetylation were six, chaperone protein DnaK (DnaK), pyruvate dehydrogenase E1 component (AceE), DNA-directed RNA polymerase subunit beta (RpoB), chaperone protein ClpB (ClpB), DNA-directed RNA polymerase subunit beta (RpoC) and 60 kDa chaperonin (GroEL), which four of these proteins have been also identified with a high number of acetylation sites (Yu *et al.*, 2008; Kuhn *et al.*, 2014; Post *et al.*, 2017).

DnaK and GroEL are chaperones which function is to fold proteins, these proteins are specially synthesised during a heat shock that causes the denaturation of proteins and that the chaperones refold to their native conformation. The two chaperones have shown to be regulated by levels of acetyl phosphate. In two studies made on a Δ*ackA*Δ*pta* mutant of *E. coli* they found increased transcription levels, however, their activity was reduced. The idea that ATP was affecting their activity was discarded when they found that the levels between the WT and the mutants were not significantly different (Mizrahi, Biran and Ron, 2006, 2009).

The enrichment analysis showed similar results as in other bacteria species. The biological processes with the highest enrichment score were metabolic process for pyruvate, pyrimidine and aspartate followed by translation. The first two terms were also found in *S. enterica* serovar Typhimurium, although in their study they only analysed one biological repetition, the protein extract was also collected during exponential growth (Li *et al.*, 2018). In *V. cholerae* translation was also one of the terms with the highest enrichment score and the sample was extracted during logarithmic phase (Jers *et al.*, 2018).

The 78% of molecular function terms were related to the binding of molecules, which has been also shown in several bacterial acetylomes (Liu *et al.*, 2016, 2018; Jers *et al.*, 2018). Acetylation has shown to be involved in the regulation of gene transcription by inhibiting the binding of transcription gene regulators to their gene targets. Some examples are the inhibition of the regulator of the two-components system in *S. enterica* Typhimurium by the acetylation of K102 and K201 (Ren *et al.*, 2016; Koo *et al.*, 2020); acetylation of the nucleoid-associated protein HU, which helps in the DNA compaction, decreases the interaction with the DNA in *Mycobacterium tuberculosis* (Ghosh *et al.*, 2016); and in a recent study in *E.coli*, acetylation showed to be involved in the synthesis of proteins. The threonine aminoacyl tRNA synthetase was mutated to have a specific lysine acetylated, this enzyme produced mischarged amino acids which affect the synthesis of the peptide chain (Chen *et al.*, 2019). Acetylation of aminoacyl-tRNA ligases has also shown an inhibition of their activity in *E. coli* (Barnoy *et al.*, 2017; Ye *et al.*, 2017; Chen *et al.*, 2019)

In this study, we identified the 20 amino acids tRNA ligases but only 18 showed significant different acetylation sites (supplement table 8.4) and from 53 ribosomal proteins from both subunits, 44 possessed significant acetylation sites. This explains the high enrichment score of the cellular component for ribosomes which in total showed 250 and acetylation sites.

Acetylation is present in the central metabolism of *N. gonorrhoeae* MS11. The interaction network of KEGG pathways showed a cluster with pathways of the central metabolism. This means that enzymes with acetylation sites are shared among pathways. The analysis of 3 pathways (TCA cycle, glycolysis, and pyruvate metabolism) showed that almost all of the proteins belonging to these pathways were identified in the acetylome of the gonococcus. In fact, it has been shown in other bacteria that the acetylation of enzymes

from the central metabolism controls the metabolic flux. In *Salmonella enterica* and *E. coli* the enzymes of the central metabolism were all acetylated and found that it regulates the carbon flux and the enzymatic activity (Wang *et al.*, 2010; Zhang *et al.*, 2013; Pisithkul, Patel and Amador-Noguez, 2015).

### 3.3.1 Acetylation affects chemical properties of proteins

Acetylation has shown to regulate the activity of metabolic enzymes by either changing the conformational structure of the protein, modifying net charges or inhibiting the interaction with the substrate (Xiong and Guan, 2012; Lin *et al.*, 2013; Baeza, Smallegan and Denu, 2015; Ghosh *et al.*, 2016; Bontemps-Gallo *et al.*, 2018; Chen *et al.*, 2019; Barbosa Leite *et al.*, 2020). The general approach to determine if an acetyl-phosphate dependent site regulates the activity of an enzyme is by mutating the lysine to another amino acid usually non-charged or by site directed acetylation (Venkat, Gregory, Gan, *et al.*, 2017; Barbosa Leite *et al.*, 2020). In a study of *Trypanosoma brucei*, the parasite that causes sleeping sickness in human, the activity of the glycolysis enzyme aldolase was shown to be decreased in the mutants where lysine was mutated to the polar uncharged amino acid glutamine in the positions K157Q and K163Q. They found a change in the pocket where the substrate binds, and a change on the surface net charge to the negative side (Barbosa Leite *et al.*, 2020).

In *N. gonorrhoeae*, we observed a changed to a more negative charge net on all the identified proteins. The positive and negative charged amino acids were quantified in all the sequences from the identified proteins in the acetylome, since lysine is a positive charged amino acid when acetylated it is neutralised and a negative charge is added to the net protein charge. In fig 3.25, we observe that the linear regression model shifts to the negative charged amino acids when the lysines are acetylated and therefore, the positive

charge is neutralised. Studies have shown that this changes caused by acetylation stabilise proteins and increase the interaction protein-protein (Lin *et al.*, 2013; Ree, Varland and Arnesen, 2018).

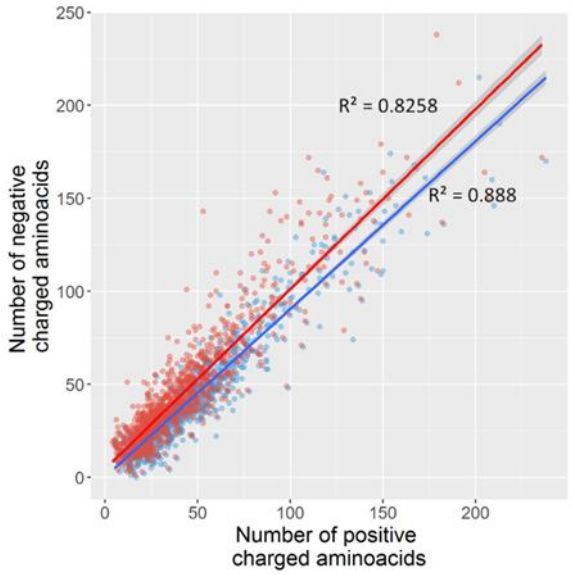


**Figure 3.25 Acetylation decreases the charge of a protein by neutralising positive residues.** Protein sequences were obtained and the amino acids with negative and positive charge were counted and plot. The blue and red dots are the number of charged amino acids before and after acetylation, respectively. Linear regression and the r square are shown for each condition.

In this study, we analysed the distribution of the acetylation location in the proteins. We observed that the distribution was divided in 3 regions, the extreme regions showed a higher number of acetylation sites than in the middle, supporting the hypothesis that non-enzymatic acetylation is a PTM where the access to enzyme is limited (Kuhn *et al.*, 2014; Baeza, Smallegan and Denu, 2015; David G Christensen *et al.*, 2019). Indeed, we observed that in Δ*ackA* the increased acetylation is in all regions, while in Δ*pta* the majority of the decreased acetylation is in the middle region of the protein presumably where the access for acetylation is difficult to access. Similar, the acetylation sites of Δ*hdac* were found at a higher density at the N and C-terminus of proteins. That area is

where the enzyme might be acting because in the middle it cannot access for deacetylation.

The specific mechanism of non-enzymatic acetylation still unrevealed, however, there is a proposal that acetyl-phosphate dependent acetylation occurs in lysines that are located close to acidic amino acid (Kuhn *et al.*, 2014; Carabetta and Cristea, 2017). Indeed, we found that approximately 20% of acetyl-phosphate dependant sites were next to a residue of glutamic acid.

### 3.3.2 Neisserial histone- deacetylase like protein

We identified from mass spectrometry 34 unique sites with a significant increase acetylation in Δ*hdac*. The logo sequence of the amino acids flanking the acetylation showed a similar distribution and probability of the amino acids found in Δ*ackA* and Δ*pta*, with a glutamic acid next to the lysine. These lysine acetylation sites could be possible targets of HDAC. Enzymes involved in tRNA binding was the molecular function to be enriched suggesting that tRNA proteins are regulated by Hdac. In *E. coli* it was found that lecucyl-tRNA and arginyl-tRNA were negatively regulated by AcP-dependent acetylation and that the deacetylase CobB was responsible of removing the acetyl to activate the tRNAs (Ye *et al.*, 2017). Venkat showed in two studies that acetylation of tyrosil-tRNA, and threonyl-tRNA impairs their enzymatic activity and suggests that CobB deacetylates the enzymes to activate them (Venkat, Gregory, Gan, *et al.*, 2017; Chen *et al.*, 2019). In *N. gonorrhoeae* glutamate, alanine, and valine-tRNA ligase acetylation was increased in the isogenic strain Δ*hdac*.

Other relevant proteins that suggest to be deacetylated by Hdac were biotin carboxylase, 2-oxoglutarate dehydrogenase and phosphotransacetylase. The three enzymes are involved in acetyl-CoA metabolism, tricarboxylic acid cycle (TCA) and the PTA-AK

pathway, respectively. In *Mycobacterium tuberculosis*, isocitrate lyase, the enzyme of the glyoxylate shunt, showed to be positively regulated by the deacetylase CobB (Bi *et al.*, 2017). In *E. coli*, malate dehydrogenase and isocitrate dehydrogenase, both enzymes from TCA, also showed an increase of activity when deacetylated by CobB (Venkat, Gregory, Sturges, *et al.*, 2017; Venkat *et al.*, 2018).

Phosphotransacetylase (Pta), the protein that produces acetyl-phosphate, showed an increase of acetylation in the lysine site K450 in the isogenic strain Δ*hdac*. This site is located in the active site of the protein. This result is discuss in the next chapter where a regulation of Pta by the deacetylase HDAC is proposed.

# Chapter 4

## Role of acetyl-phosphate in the metabolism of *Neisseria gonorrhoeae* MS11

# 4 Role of acetyl phosphate in the metabolism of *N. gonorrhoeae* MS11

## 4.1 Introduction

Bacterial metabolism is known to be regulated by post-translational modifications (PTM), including, glycosylation, phosphorylation, and acetylation among others (Duan and Walther, 2015; Pisithkul, Patel and Amador-Noguez, 2015). The interest in bacterial lysine acetylation has increased during the last 20 years (fig. 1) and studies have shown interesting findings suggesting that acetyl-phosphate is the precursor molecule for ATP, acetylation of metabolic enzymes is conserved among different bacterial species, acetyl phosphate has a dual role for acetylation and phosphorylation of proteins, lysine acetylation regulates the metabolic flux and bacterial virulence (Wanner and Wilmes-Riesenberg, 1992; Wang *et al.*, 2010; Pisithkul, Patel and Amador-Noguez, 2015; Nakayasu *et al.*, 2017; Ren *et al.*, 2017; Camprubi *et al.*, 2018)

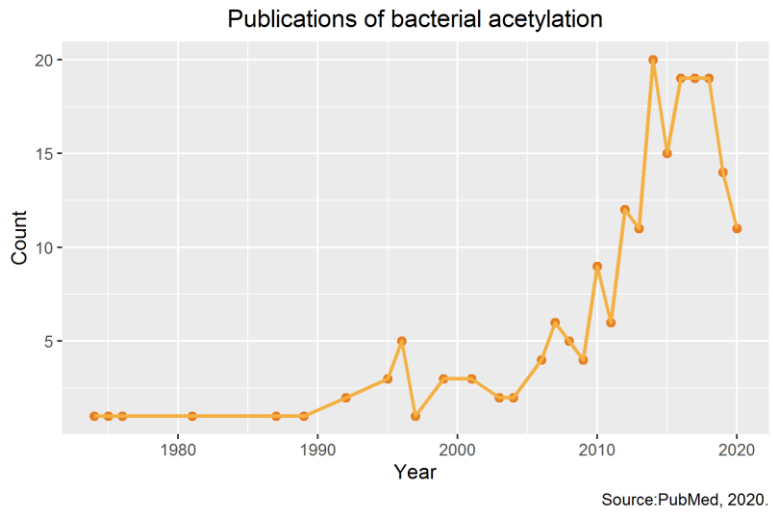


**Figure 4.1 Number of publications related to bacterial lysine acetylation.** The data corresponds to the search on PubMed from the period 1974-2020 using acetyl-phosphate, acetylation, and bacterial as keywords for the search.

Acetyl-phosphate is the intermediate metabolite from the phosphotransacetylase-acetate kinase pathway (PTA-AK) metabolite that is synthesised by the enzyme phosphate acetyltransferase which converts Acetyl-CoA to acetyl-phosphate, using inorganic phosphate and realising CoA-SH, acetyl-phosphate is then metabolised to acetate by acetate kinase realising ATP (fig. 4.2) (Kuhn *et al.*, 2014; Wolfe, 2016; David G Christensen *et al.*, 2019).

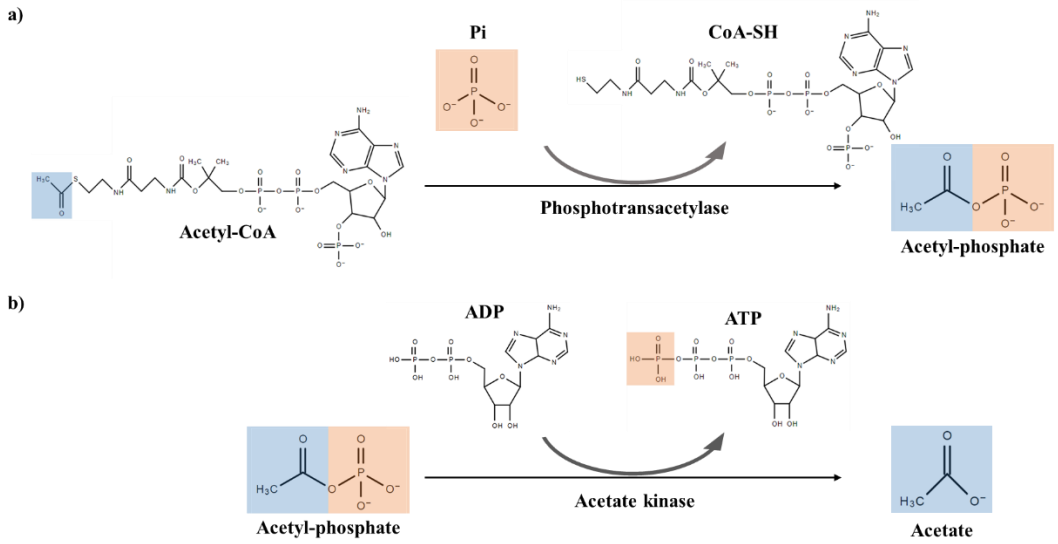


**Figure 4.2 Reactions in the PTA-AK pathway. a)** Reaction metabolised by phosphotransacetylase (NGO0214) synthesising acetyl-phosphate, **b)** and then converted to acetate by acetate kinase (NGO0977).

Acetyl-phosphate is a high energy molecule that has shown a balance between stability and reactivity. A study shown that acetyl-phosphate is more stable at cooler temperatures and hydrolysis increases when temperature is increased. Also they have shown that it has a dual role as an acetyl donor, and phosphate donor especially to nucleotides (Camprubi *et al.*, 2018). Due to its high free energy it reacts with residues of lysines where it can acetylate in two ways; the Nα and Nε, being the latter reversible and the most common lysine acetylation (fig. 3) (Hentchel and Escalante-Semerena, 2015).

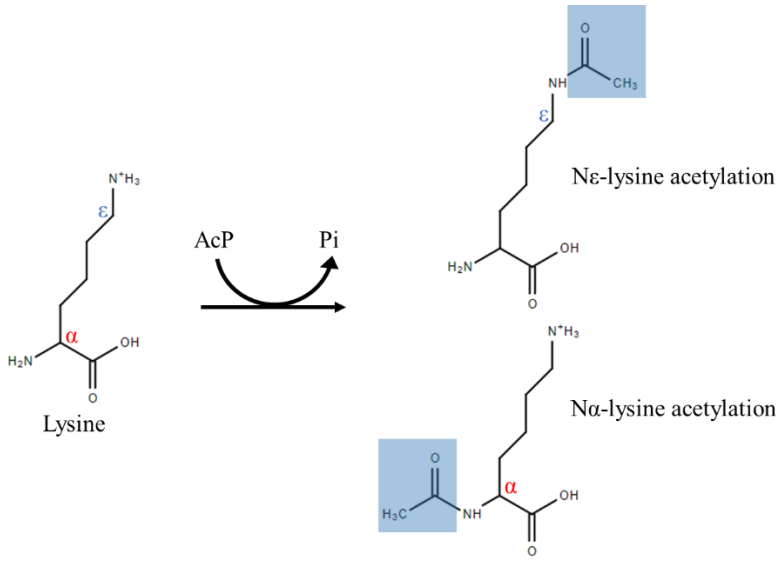


**Figure 4.3 Types of lysine acetylation.** The acetylation of residues of lysine occurs in the Nα (bottom) and Nε (top).

The majority of acetylated enzymes have been identified to be involved in metabolic processes in *E. coli*, *S. enterica*, *B. subtilis*, *M. tuberculosis* and *S. aureus* (Wang *et al.*, 2010; Sadykov *et al.*, 2013; Hentchel and Escalante-Semerena, 2015; Schilling *et al.*, 2015). The acetylation leads to changes on the surface charge and in the conformation of the binding pocket to substrates and ligand, inhibiting the activity of the enzymes (Nakayasu *et al.*, 2017; Barbosa Leite *et al.*, 2020).

*N. gonorrhoeae* is an obligate human pathogen that mainly colonises the genito-urinary tract. *N. gonorrhoeae* has adapted to survive in this niche, which is characterised by limited nutrient sources, and the organism metabolises the carbon sources that are available. It is a fastidious microorganism that grows in microaerobic conditions. However, it also grows in anaerobic conditions using the nitrite and nitric oxide reductase to metabolise nitrite to nitrous oxide ($N_2O$) by a denitrification pathway (Knapp and Clark, 1984; Overton *et al.*, 2006; Quillin and Seifert, 2018). Glucose, pyruvate, and lactate are the only carbon sources that the bacteria metabolises, the latter is considered

to influence the pathogenicity and virulence of *N. gonorrhoeae* (Stephen A. Morse, Stein and Hines, 1974; Yates *et al.*, 2000; Smith, Tang and Exley, 2007; Li *et al.*, 2010; Atack *et al.*, 2014).

In this chapter, we analysed the effect of acetylation by acetyl-phosphate in the metabolism of *N. gonorrhoeae*. We found that PTA-AK pathway is a possible escape pathway during overflow metabolism. We determined, that the consumption of lactate increases acetylation compared to other carbon sources. Structural and docking analysis of enzymes, showed a possible regulation of the central metabolic pathways by the acetylation of lysines present in the active site of proteins.

## 4.2 Results

### 4.2.1 Acetyl-phosphate dependent acetylation is enriched in central metabolic pathways

In this chapter, the analysis to determine the effect of lysine acetylation in the metabolism of *N. gonorrhoeae* MS11 was based on the data obtained from mass spectrometry. The enzymes with acetylation sites that showed a significantly difference in fold change of acetylation were selected for this chapter. Since the level of acetyl-phosphate was different in the mutants Δ*ackA* and Δ*pta* we could determine the role of these two enzymes in the regulation of the metabolism.

An enrichment analysis of metabolic pathways was performed using the data of fold change in the acetylation. The analysis was performed using the package BiocManager on R. The package uses the database of KEGG pathways and performs an enrichment analysis utilising the values from levels of acetylation.

The analysis showed an enrichment of the carbon metabolism in the mutants Δ*ackA* and Δ*pta*, from these the central metabolic pathways were found. Entner-Doudoroff, gluconeogenesis, pyruvate metabolism and TCA cycle were enriched. The mutant Δ*ackA* showed an increased enrichment of pyruvate metabolism, and gluconeogenesis was both increased and decreased, this is due to the mutant showed sites that were significantly increased and decreased in acetylation. The mutant Δ*pta* showed an increase in gluconeogenesis, pyruvate metabolism and TCA cycle. The mutant Δ*hdac* showed an increased enrichment in the pyruvate metabolism (fig. 4.4).

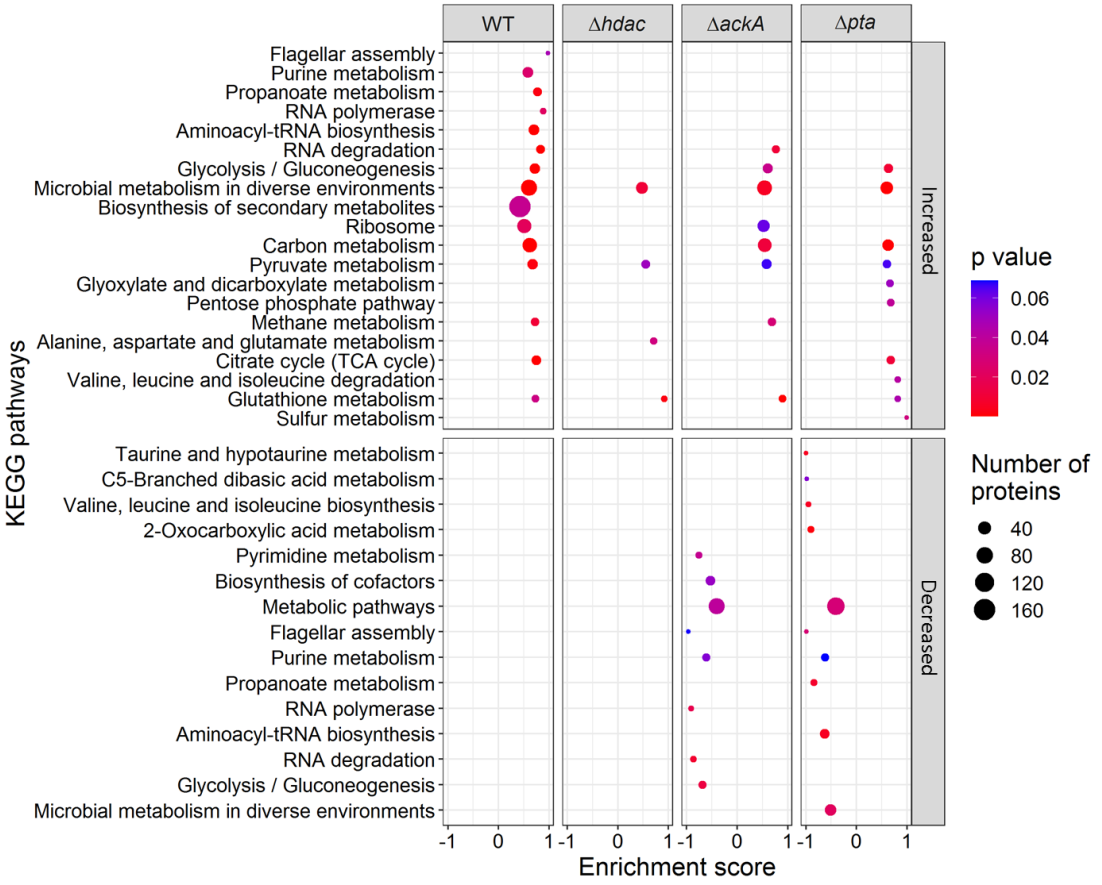


**Figure 4.4 Enrichment analysis of KEGG pathways for the acetylated enzymes in *N. gonorrhoeae* MS11.** The enzymes with significantly different acetylation were divided in increased and decreased depending the level of fold change in the acetylation. The enrichment of the WT strain was determined using all the identified acetylation sites.

Different studies have shown an alteration of central metabolism pathways and in the metabolism flux due to the disruption of the PTA-AK pathway (D. G. Christensen *et al.*, 2019; Schütze *et al.*, 2020), therefore, the isogenic mutant strains were grown in glucose, lactate and pyruvate, reported to be the only carbon sources that the gonococcus metabolises (Stephen A. Morse, Stein and Hines, 1974). The strains were cultured overnight on a chemically defined medium with 10 mM glucose and then transferred to the same medium supplemented with the carbon sources to test their growth during 10 h. Samples were taken every hour and the optical density at 600 nm was measured.

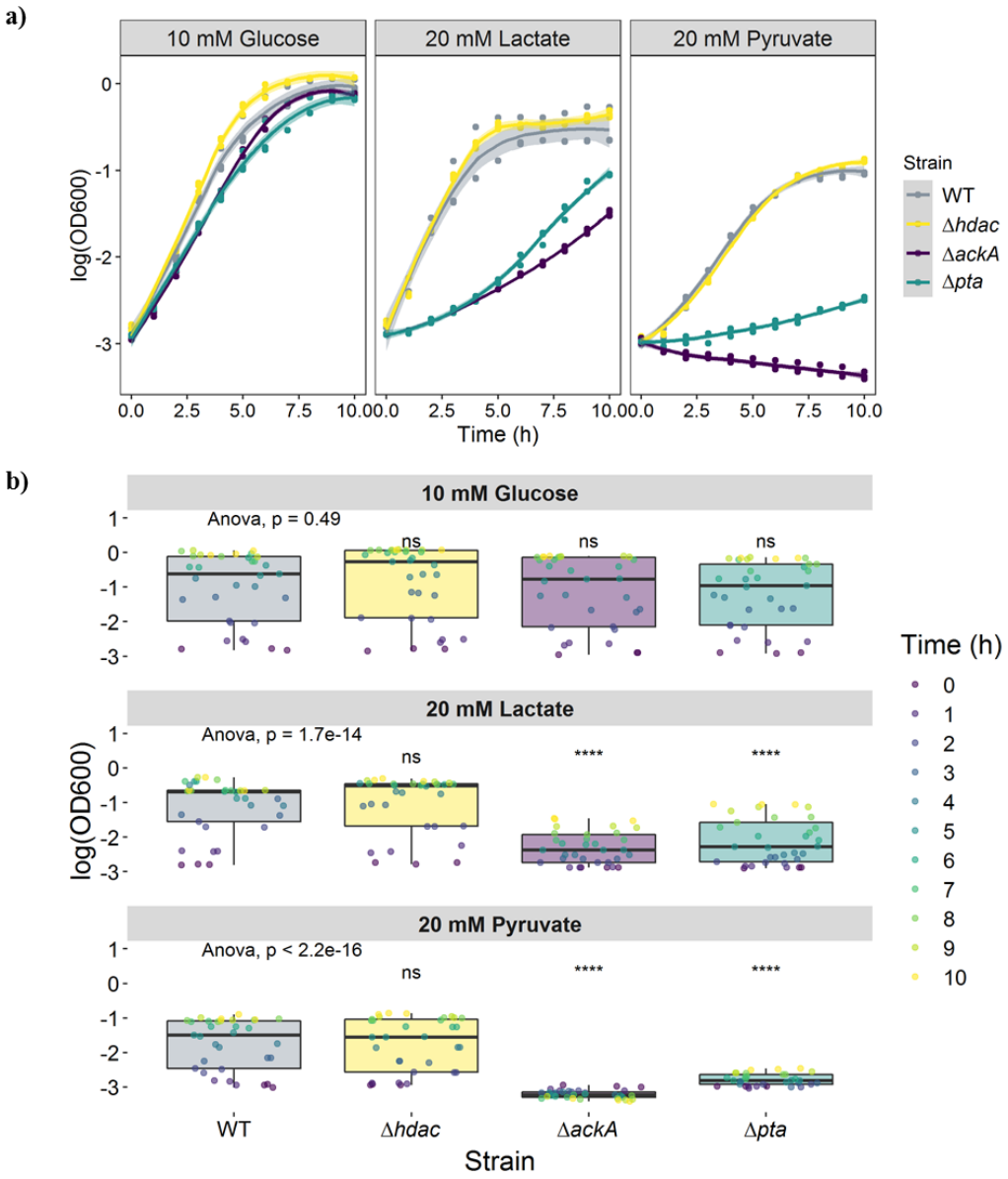


**Figure 4.5 Growth curves of *N. gonorrhoeae* MS11 in glucose, lactate, and pyruvate.** Strains of *N. gonorrhoeae* MS11 were grown for 10 h at 37 °C with shaking in a chemically defined medium supplemented with a carbon source. Samples were taken every hour and read in a spectrophotometer. **a)** Growth curves of the 4 strains growing on the three different carbon sources. The plot shows the standard deviation of the curves. **b)** The growth of the isogenic strains were compared to the WT growth and a T test was performed. The ANOVA test demonstrated if the carbon source showed a significance difference among all the data. ns, no significance; **** *p* value < 0.0001.

The growth of the strains was compared to the WT growth in the three different carbon sources. In glucose, no significant difference was shown overall, however, a significance difference in all the strains was observed at 2 and 3 h of growth (supplement table 2.4). Δ*hdac* showed an increased growth, contrary to Δ*ackA* and Δ*pta*. In lactate and pyruvate, only the growth of Δ*ackA* and Δ*pta* was significantly different with a reduction of the growth (fig 4.5 a-b).

The growth rates on every carbon source were calculated for each strain. The doubling time of all strains were significantly different to the WT on all the carbon sources.

In glucose, the doubling time of the WT was 1.13 h. The isogenic strain Δ*hdac* reduced the doubling time by 1.04 fold, while the doubling time was increased by 1.25 and 1.3 fold by the isogenic strains Δ*ackA* and Δ*pta*, respectively, all compared to the WT doubling time (fig. 4.6a) .

The doubling time in lactate was 1.19 h in the WT, the doubling time of Δ*hdac* showed no significance difference, however, the doubling time of Δ*ackA* and Δ*pta* was significantly slower (fig. 4.6a).

The doubling time in pyruvate by the WT strain was 2.06 h, and all isogenic strains showed a significance difference on the doubling time. Δ*hdac* increased the doubling time by 1.07 fold, and Δ*pta* in 6.66 fold. Interestingly, Δ*ackA* showed a negative doubling time, meaning that the bacteria were not growing, presenting a doubling time of -24.02 h (fig. 4.6a).

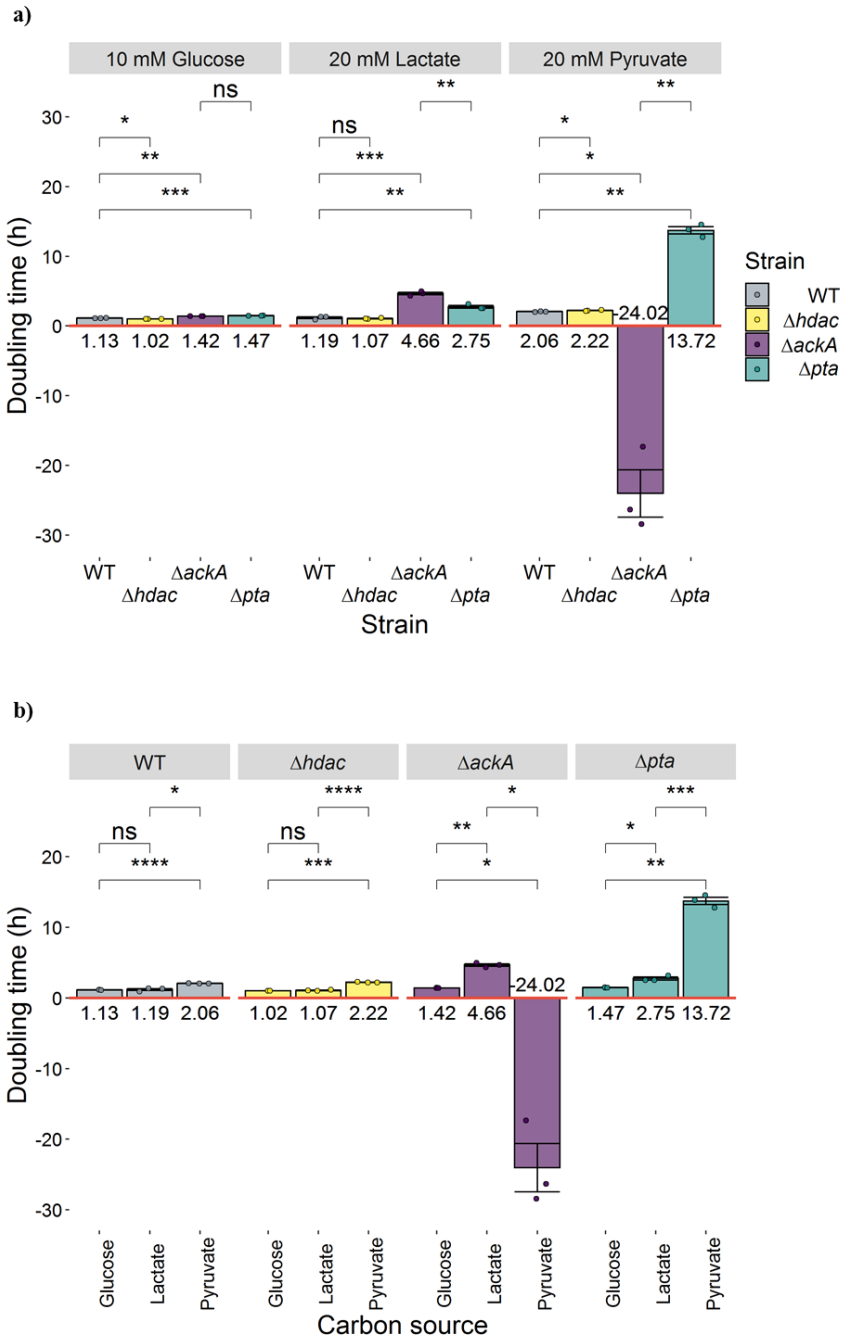


**Figure 4.6 Doubling time of *N. gonorrhoeae* MS11 and the isogenic strains in three carbon sources.** The exponential phase (EP) was different for each strain due to the growth patterns showed in each carbon source. Therefore, for WT and Δ*hdac* the EP was considered from 2 to 4 h in all carbon sources. However, for Δ*ackA* and Δ*pta* the EP was different in lactate and pyruvate. The EP was account from 6 to 8 h of growth, and in glucose from 2 to 4 h of growth. The doubling time was calculated using the generation time formula G= t/n. **a)** The times were compared between strains and **b)** by carbon source. ns, no significance; * *p* value < 0.05; ** *p* value < 0.01, *** *p* value < 0.001; **** *p* value < 0.0001.

The doubling time of each strain was compared to the growth on each carbon source. The WT and Δ*hdac* strains showed no significance difference in the doubling time growing in glucose and lactate, however, the doubling time was significantly increased when growing in pyruvate by 1.82 and 2.17 fold, respectively (fig. 4.6b).

The strain Δ*ackA* significantly increased the doubling time in lactate compared to the growth in glucose by 3.28 fold and in pyruvate no growth was observed. The Δ*pta* strain showed a significant increase in doubling time in both lactate and pyruvate compared to glucose, by 1.87 and 9.33 fold, respectively (fig. 4.6b).

In previous studies, bacteria was grown in different carbon sources and concluded that glucose stimulates the acetylation in *E. coli* and *S. enterica* and that the acetylation is increased in the central metabolic pathways controlling the activity of the enzymes (Wang *et al.*, 2010; Pisithkul, Patel and Amador-Noguez, 2015). Therefore, a western blot using the anti-acetyllysine antibody was used to observe if acetylation is modified in the growth of the three different carbon sources.

Samples of bacteria were taken after 10 h growing in the different carbon sources and a western blot was performed (fig. 4.7a). The intensity of the bands was analysed and then compared by a t-test. The Δ*pta* strain showed no bands after growing in each carbon source. The Δ*hdac* and Δ*ackA* strains showed no significant difference in the intensity of the bands when grown in glucose, however, it is shown a tendency to increase the intensity of the bands in both strains being Δ*ackA* the strain with higher intensity of the bands. Growth in lactate and pyruvate showed no significance difference between WT and Δ*hdac* although with a tendency to increase the intensity in the Δ*hdac* strain. Interestingly, the intensity of the bands was significantly increased in the Δ*ackA* strain. This means that both carbon sources increased acetylation compared to the growth in glucose (fig. 4.7b).

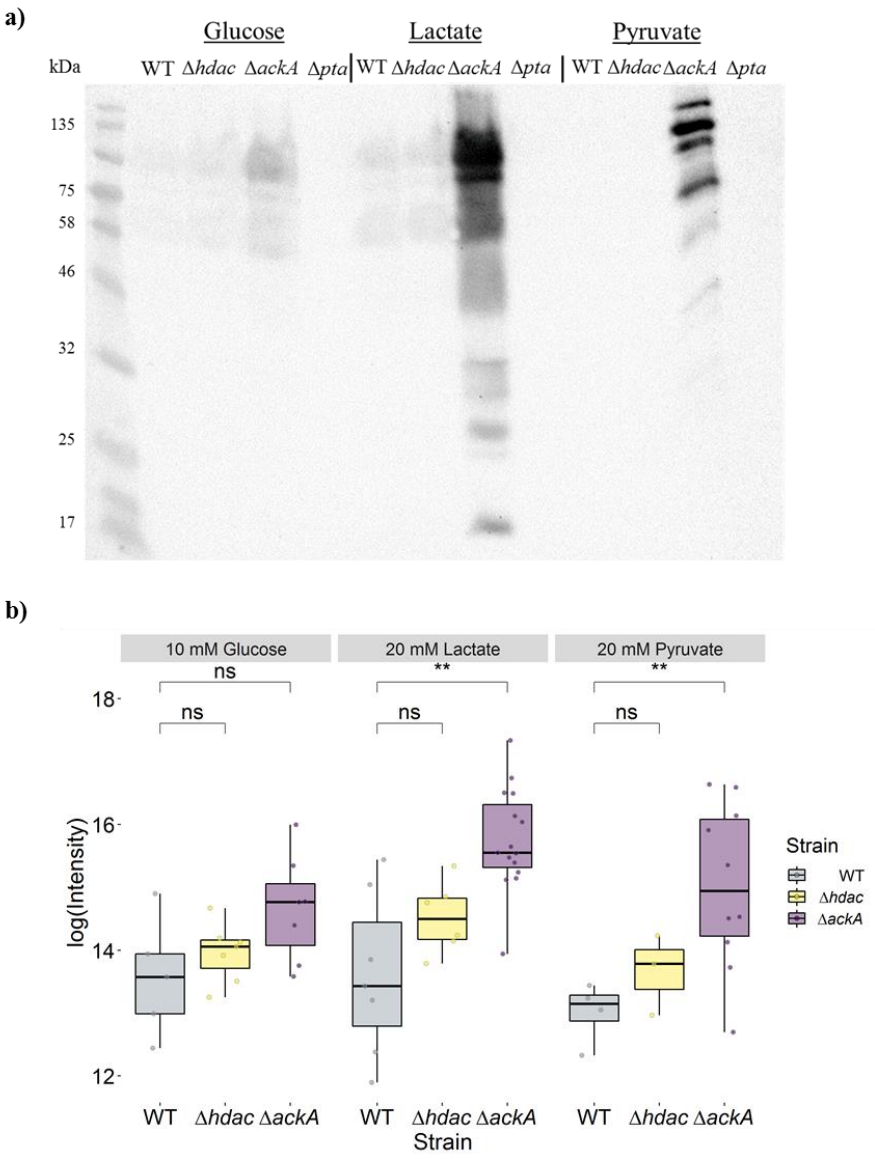


**Figure 4.7 Acetylation of proteins in *N. gonorrhoeae* MS11 in different carbon sources.** Samples of bacteria growing at 37 °C in a chemically defined medium supplemented with 10 mM glucose, 20 mM lactate or 20 mM pyruvate was taken for protein extraction. **a)** 100 µg of proteins was loaded in a SDS-PAGE for western blot using an anti-acetyllysine antibody to detect acetylated proteins. **b)** The intensity of the bands was analyse with the ImageLab® software and the intensities were compared between strains in the three different carbon sources with a t-test. ns, no significance, ** $p$ value < 0.01.

The intensities were then compared between each carbon to determine if the growing in different carbon sources modifies the acetylation on each strain. Overall, acetylation is not affected by the carbon source, however, a tendency to decrease acetylation is observed when the strains were grown in pyruvate. The only strain that showed a significant difference in the intensity of acetylation was Δ*ackA*. The growth in lactate increased the acetylation compared when grown in glucose (table 4.1).

**Table 4.1 Comparison in the acetylation of isogenic strains of *N. gonorrhoeae* MS11 growing in different carbon sources.** A western blot with 100 µg of proteins was analysed to determine the intensity of the bands. The values were compared among carbon sources for each strain using t-test.

| Strain | Comparison | | *p* value | Significance |
|---|---|---|---|---|
| | Carbon 1 | Carbon 2 | | |
| **WT** | Glucose | Lactate | 0.594 | ns |
| | Glucose | Pyruvate | 0.268 | ns |
| | Lactate | Pyruvate | 0.176 | ns |
| **Δ*hdac*** | Glucose | Lactate | 0.119 | ns |
| | Glucose | Pyruvate | 0.479 | ns |
| | Lactate | Pyruvate | 0.069 | ns |
| **Δ*ackA*** | Glucose | Lactate | 0.017 | * |
| | Glucose | Pyruvate | 0.194 | ns |
| | Lactate | Pyruvate | 0.287 | ns |

ns, no significance.

The difference of acetylation in the Δ*ackA* follows the hypothesis that lactate increases acetylation due to the presence of three different lactate dehydrogenases in *N. gonorrhoeae* which metabolise lactate to pyruvate and then to acetyl-CoA, the precursor for acetyl-phosphate (Atack *et al.*, 2014). During infection lactate is increased by the Warburg effect, where anaerobic glycolysis is stimulated synthesising a higher level of lactate that *N. gonorrhoeae* could use as carbon source. In fact, some bacteria have shown the stimulation of lactate when found intracellularly in PMN and *N. gonorrhoeae* have

shown a depletion of oxygen within HL-60 cells due to lactate metabolism, furthermore, growth of *N. gonorrhoeae* is increased when grown in glucose supplemented with lactate (Britigan *et al.*, 1988; Regan *et al.*, 1999; Kelly and O'Neill, 2015; Shi *et al.*, 2015).

The alteration to the metabolism of the three carbon sources in the different isogenic strains showed that the level of acetyl-phosphate is altering in the activity of the enzymes from the central metabolic pathways. Therefore, the enzymes from Entner-Doudoroff, gluconeogenesis, pyruvate metabolism, and TCA cycle enzymes were analysed in the acetylation sites identified by mass spectrometry.

### 4.2.2 PTA-AK pathway is a metabolic flux escape for carbon overflow

Enzymes from the central metabolic pathways are susceptible to acetylation and it is now recognised that it regulates the activity of the enzymes, but also the flux of the metabolism (Wang *et al.*, 2010; Pisithkul, Patel and Amador-Noguez, 2015; Schilling *et al.*, 2015, 2019; Bernal, Castaño-Cerezo and Cánovas, 2016; Venkat, Gregory, Sturges, *et al.*, 2017; Venkat *et al.*, 2018; D. G. Christensen *et al.*, 2019; Macek *et al.*, 2019; VanDrisse and Escalante-Semerena, 2019; Schütze *et al.*, 2020). Although it is not fully understood, it has been shown that the regulation of enzymes by acetylation is driven by a difference in the protein surface charge and changes in the conformational structure of the pockets were the substrates or cofactors bind.

Lysine is a positively charged amino acid that is susceptible to the nucleophilic attack of acetyl-phosphate to its charged amine group. As consequence, the positive charge is neutralised and interactions with surrounding amino acid residues is altered, furthermore, the addition of the acetyl group to lysine changes the conformation of the surface of the enzyme (Kuhn *et al.*, 2014; Nakayasu *et al.*, 2017). Barbosa Leite *et al.*, 2020, shown that the aldolase of *Trypanosoma brucei* is inhibited by the acetylation of K157 due to changes on the surface charge and conformation of the cavity pocket where the substrate binds.

In this section, enzymes of the central metabolic pathways were analysed for alterations in the conformation of the catalytic site and the interactions with the substrates and cofactors. We found that 96% of the enzymes from gluconeogenesis, pentose phosphate, Entner-Doudoroff, pyruvate metabolism, and TCA cycle pathways shown acetylation sites dependent on acetyl-phosphate.

The central metabolic pathways were obtained from the KEGG pathway database website (https://www.genome.jp/kegg/pathway.html) and the values of fold change for the

acetylation sites from mass spectrometry were mapped for each enzyme. Protein models of the enzymes were searched in the PDB database (https://www.rcsb.org/) and the acetylation sites detected by mass spectrometry were mapped on the 3D model of the enzymes to analyse any modification on the conformation of the enzyme or on the interaction with the substrates.

#### 4.2.2.1Gluconeogenesis

*Neisseria gonorrhoeae* process glucose through the Entner-Doudoroff pathway because the glycolysis pathway is not complete due to the lack of phosphofructokinase, however, gluconeogenesis is found in the gonococcus (Baart *et al.*, 2010). The gluconeogenesis pathway shown that all enzymes, except triosephosphate isomerase, possessed acetylation sites dependent to acetyl-phosphate. The enzymes with the highest number of significant different acetylation sites were 2, 3-bisphosphoglycerate dependent phosphoglycerate mutase (GMPA) and phosphoenolpyruvate synthase (NGO0200). The enzymes fructose-1,6-bisphosphate aldolase (NGO0034), GMPA, and phosphoenolpyruvate synthase (NGO0200) shown acetylation sites that are highly regulated by the PTA-AK pathways, this means, that in the Δ*ackA* and the Δ*pta* strains, the acetylation fold change was increased and decreased, respectively (fig. 4.8).

## Gluconeogenesis

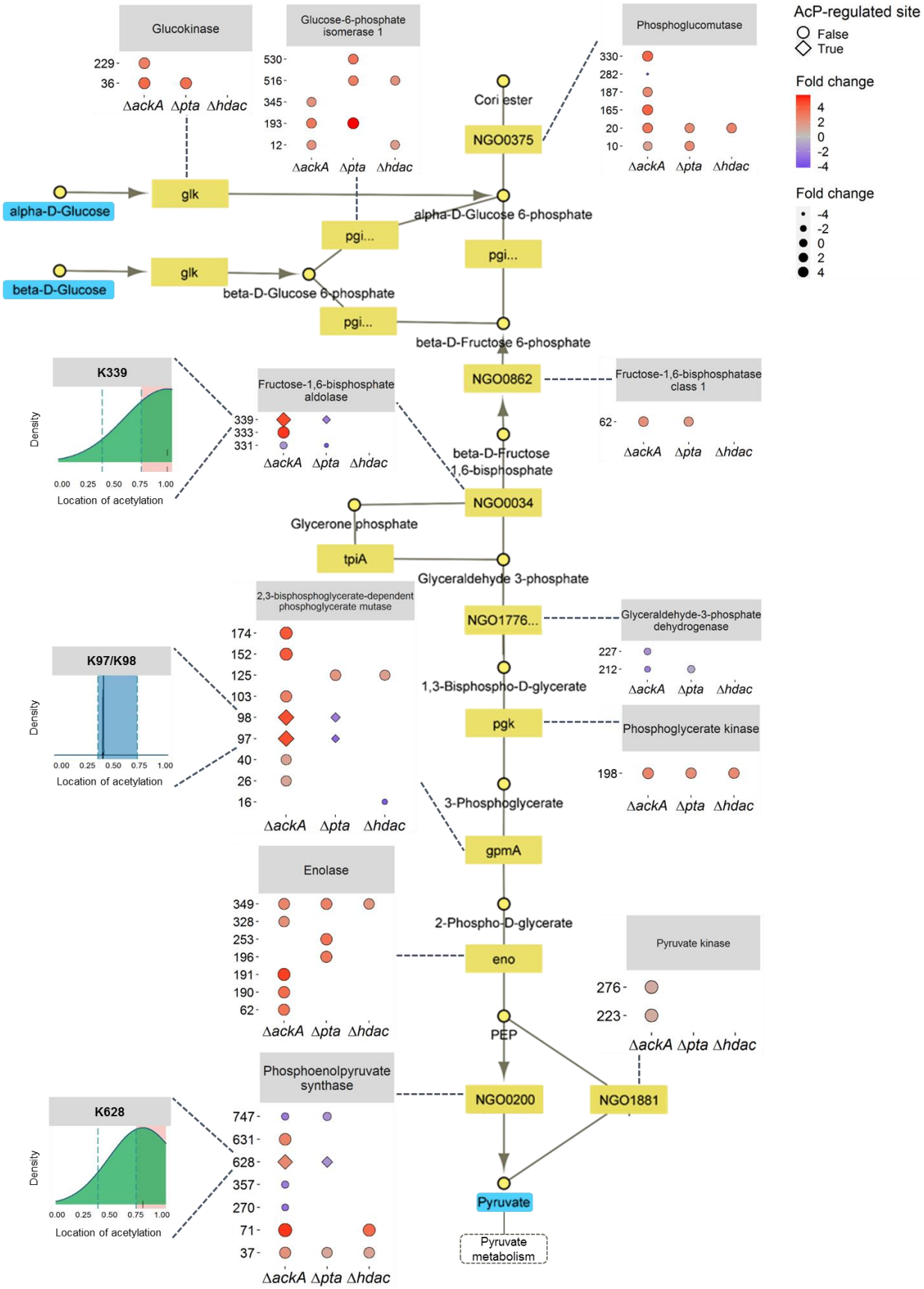

**Figure 4.8 Acetylation of the gluconeogenesis enzymes.** Gluconeogenesis pathway of *N. gonorrhoeae* was downloaded from KEGG pathway website with entry number ngo00010. The acetylation sites with a significant different fold change to the WT were mapped to each enzyme. The acetyl-phosphate regulated sites (square shape) were considered if it was found in both Δ*ackA* and Δ*pta*, and presenting a high and low fold change in acetylation, respectively, Thus, highly regulated sites were plotted to map them on the relative location of the protein, N-terminus, middle and C-terminus. Enzymes (yellow box); metabolites (yellow circles); carbon sources (blue box).

The only enzymes that have been crystallised for *N. gonorrhoeae* in this pathway are fructose-1, 6-bisphosphate aldolase (FBA) and GPMA, the crystals were obtained from the protein bank database (PDB) with the accession numbers, 5U4N and 5UM0, respectively. The acetylation sites were identified and the binding sites of the substrates were analysed by docking the enzymes. Both enzymes shown that lysine acetylation modified the substrate binding and the conformation of the pocket cavity.

The enzyme fructose-1,6-bisphosphate aldolase (FBA) catalyses the reversible conversion of fructose 1, 6 biphosphate to dihydroxyacetone phosphate and glyceraldehyde 3-phosphate and it is essential for gluconeogenesis and it plays an important role in pathogenic bacteria (Pegan *et al.*, 2013; Ziveri *et al.*, 2017; Barbosa Leite *et al.*, 2020). The acetylation sites of FBA were mapped on the protein and the acetylation site K202 was located in the active site. Although this acetylation site was found in the *N. gonorrhoeae* WT and no significant differences were found in the isogenic mutants, it is relevant to show how acetylation affects the interactions of the enzyme when it is acetylated. Three residues from the active site form hydrogen bonds with K202, however, when the lysine is acetylated, only one hydrogen bond remains. Furthermore, acetylation reduced the surface of the pocket cavity by 13.62 $Å^2$ (fig. 4.9).

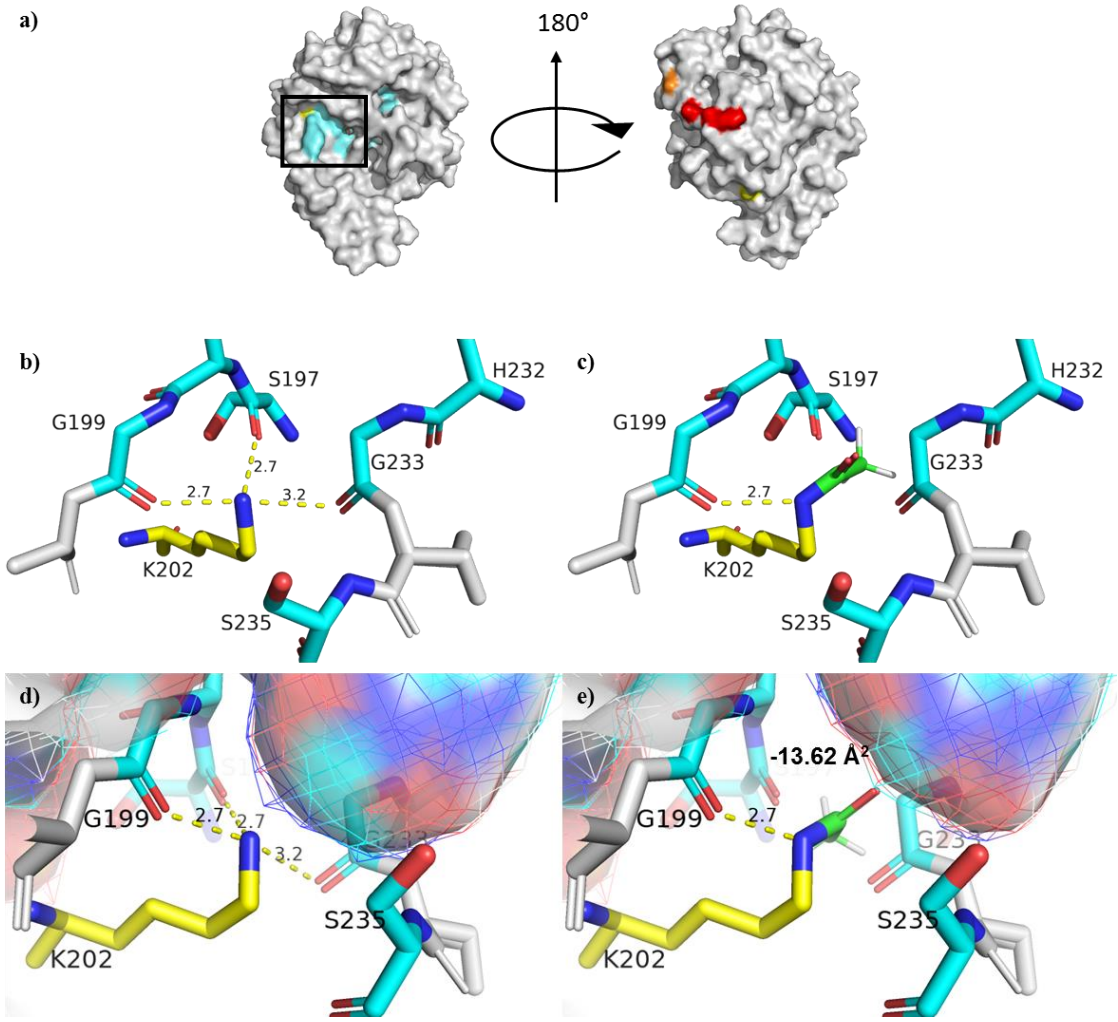


**Figure 4.9 K202 acetylation of fructose-1, 6-bisphosphate aldolase changes the surface area and hydrogen bonds of catalytic sites. a)** FBA crystal with a resolution of 1.6 Å downloaded from the PDB with an accession number 5U4N. The active site was located (cyan, box) and the acetylation sites were identified for the WT (yellow), Δ*ackA* (red), and AcP regulated (orange). **b)** K202 site (yellow) in the active site interacts by hydrogen bonds (yellow dashed lines) with G199, S197 and G233. **c)** The acetylation of K202 (green) causes the loss of two hydrogen bonds and a change of the pocket cavity by decreasing the surface area (d, e).

The enzyme 2, 3-bisphosphoglycerate-dependent phosphoglycerate mutase (GPMA) catalyses the reversible reaction of 3-phosphoglycerate to 2-phospho-D-glycerate. Studies have shown that the activity of GPMA is regulated by acetylation (Hallows, Yu and Denu, 2012; Xu *et al.*, 2014). The crystal model of the neisserial protein was obtained from PDB and analysed. The acetylation in K97 was shown to be affected by the PTA-AK pathway since the fold change of acetylation was significantly increased and decreased in the isogenic strains Δ*ackA* and Δ*pta*, respectively.

The acetylation of K97 modifies the conformation of the pocket cavity and the interactions with the substrate 3-phosphoglycerate. The *in silico* analysis showed that the substrate binds to the enzyme by nine hydrogen bonds to 6 amino acids residues , including K97. When the lysine residue is acetylated, the cavity pocket changed the conformation and decreased the surface area for solvent molecules by 9.99 $Å^2$ (fig 4.10).

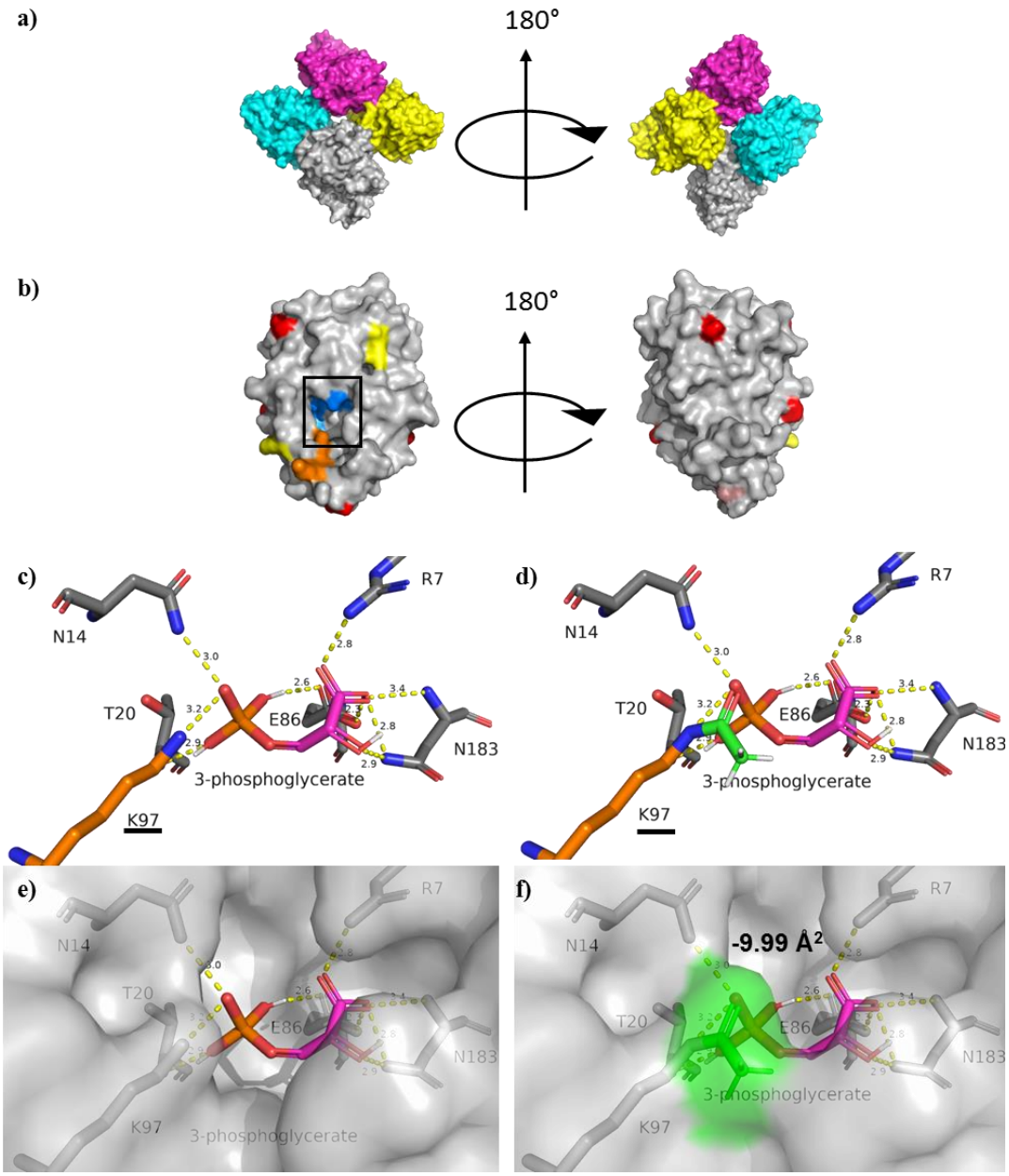


**Figure 4.10 Acetylation of K97 is acetyl-phosphate regulated in GPMA. a)** The model of the GPMA enzyme was downloaded from PDB with the accession code 5UM0 in the tetramer conformation. **b)** A monomer unit was isolated and the active site was located (blue, box) and the acetylation sites were identified for the WT (yellow), Δ*ackA* (red), and AcP regulated (orange). **c)** The substrate 3-phosphoglycerate was docked to the enzyme by *in silico* analysis showing nine hydrogen bonds including K97. **d)** The acetylation of K97 shows the same interactions with the six residues. **e)** The cavity pocket of the catalytic site, (f) showed a decreased of the surface of 9.99 $Å^2$ when K97 was acetylated (green).

The analysis of electrostatic potential surface (EPS) showed that acetylation is found in a cluster with a positive EPS. The acetylation of K97 also altered the EPS charge by neutralising the positive of the lysine and modifying the pocket cavity (fig 4.11).

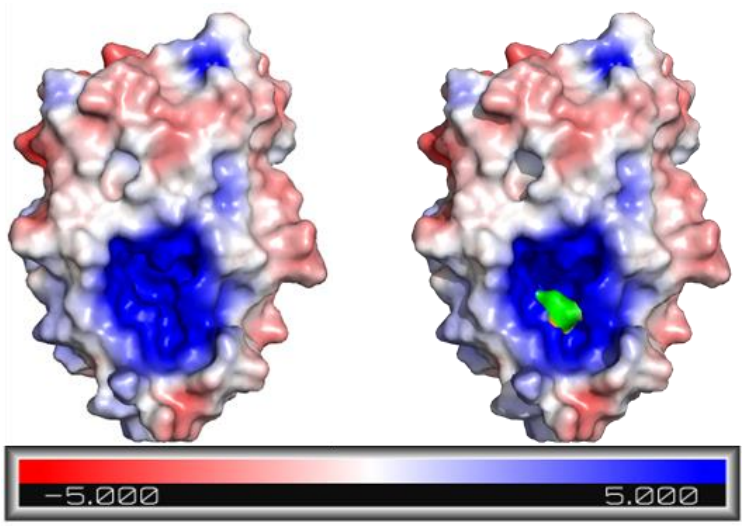


**Figure 4.11 Acetylation of K97 changes the electrostatic potential surface of GPMA.**

The model of the GPMA enzyme was downloaded from PDB with the accession code 5UM0. The EPS was calculated with PyMOL. The scale bar represents the charges on the surface of the protein. GPMA shows a cavity pocket with a positive charge (left) and the acetylation of K97 (green) causes a modification on the conformation on the pocket and the neutralisation of the positive charge of lysine (right).

Since the acetylation site was located in a cluster that showed a highly positive electrostatic potential surface, this suggested that acetylation could regulate the activity of enzymes that possess areas of highly positive electrostatic potential surface.

Therefore, the enzymes of all the gluconeogenesis pathway were analysed to determine the site whereas acetyl-phosphate dependant acetylation occurs depending on the electrostatic potential surface.

The protein models were obtained using PHYRE2, except FBA and GPMA, and showed that more than 90% of the residues possessed a modelling confidence higher than 90%. The significant different acetylation sites were located and determined if the location of acetylation was in the active site and if the lysine residue is a conserved site among different homologue sequences (fig 4.12).

The models showed that acetyl-phosphate dependant acetylation occurs on areas with a positive electrostatic potential. The sites that were close to the active site were analysed to determine if they are conserved in several species and to determine if the acetylation modified the pocket cavity of the active site (fig. 4.12).

The enzymes that showed acetylation in the active site were fructose 1, 6-biphosphate aldolase (FBA), phosphoglycerate kinase (PGK), 2, 3-bisphosphoglycerate-dependent phosphoglycerate mutase (GPMA), and pyruvate kinase (PK). All the acetylation sites were significantly increased in the Δ*ackA* strain (fig. 4.12).

The other enzymes showed a negative electrostatic potential in the active site and therefore, no acetylation was found in the active site of those enzymes (fig. 4.12).

The relation found on the electrostatic potential surface and acetylation among the gluconeogenesis enzymes, led that this analysis was used on all the next pathways to determine which enzymes had the potential to be further analysed.

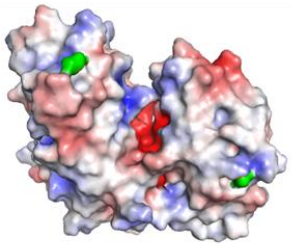
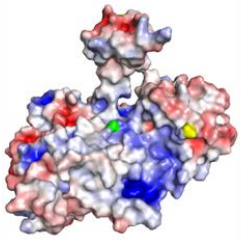
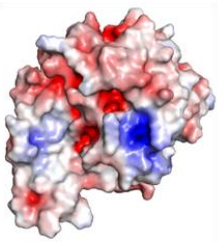
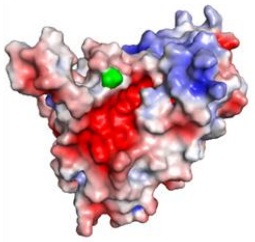
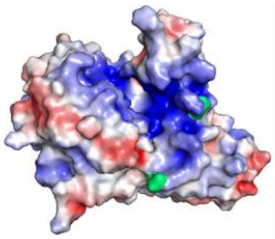

| Protein name | Glucokinase | Glucose-6-phosphate isomerase 1 | Fructose-1,6-bisphosphate aldolase | Fructose-1,6-bisphosphatase class 1 | Glyceraldehyde-3-phosphate dehydrogenase |
|---|---|---|---|---|---|
| Abbreviation | GLK | PGI | FBA | FBP | GAPDH |
| MW (Da) | 58057 | 26917 | 35420 | 24183 | 50423 |
| Modification of active site | No | No | Yes | No | No |
| K acetylation | - | - | 202 | 62 | - |
| Ratio of acetylated lysines | 26.7%(4/15) | 29.2%(7/24) | 35.3%(6/17) | 15.4%(2/13) | 10%(2/20) |
| Kollman charge | 8.0 | 12.0 | -7.4 | -3.0 | 5.0 |

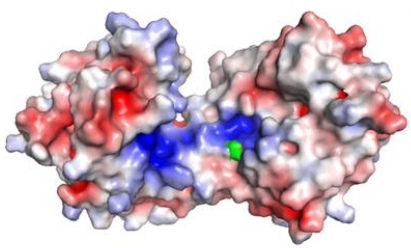
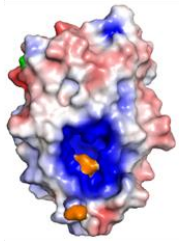
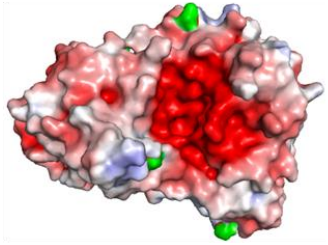
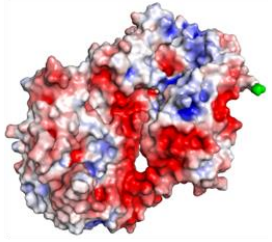
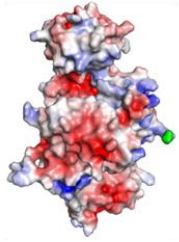

| Protein name | Phosphoglycerate kinase | 2,3-bisphosphoglycerate-dependent phosphoglycerate mutase | Enolase | Phosphoenolpyruvate synthase | Pyruvate kinase |
|---|---|---|---|---|---|
| Abbreviation | PGK | GPMA | ENO | PPSA | PK |
| MW (Da) | 85013 | 8165 | 26917 | 22678 | 57380 |
| Modification of active site | Yes | Yes | No | No | Yes |
| K acetylation | 198 | 97 | - | - | 235 |
| Ratio of acetylated lysines | 21.9%(7/32) | 83.3%(15/18) | 50%(13/26) | 32.6%(14/43) | 22.2%(4/18) |
| Kollman charge | -1.0 | -2.4 | -15.0 | -17.0 | -4.0 |

**Figure 4.12 Electrostatic potential surface (EPS) of enzymes from the gluconeogenesis pathway in *N. gonorrhoeae*.** The enzymes were modelled using PHYRE2 and the EPS was determined using PyMOL. The significant different acetylation sites were mapped for Δ*ackA* (green), Δ*pta* (yellow) and found in both strain with a higher and lower acetylation, respectively (orange). The modification to the active site was considered if the acetylation site was located within cavity pocket of the active site. On the table at the bottom it is shown the abbreviation of the protein name, the molecular weight in Daltons (Da), if the acetylation is found in the active site and the position of the residue, the ratio of acetylated lysines to total number of lysines found in the enzyme and the Kollman charge.

### 4.2.2.2Pentose phosphate pathway

The pentose phosphate pathway (PPP) runs parallel to glycolysis and it shares reactions with the Entner-Doudoroff pathway. PPP synthesises precursors for the synthesis of nucleotides and amino acids. It also produces pyruvate from fructose 6 phosphate. This pathway is important in *N. gonorrhoeae* because the glucose catabolism occurs through the Entner-Doudoroff pathway (Stephen A. Morse, Stein and Hines, 1974; Stincone *et al.*, 2015).

The acetylation sites of the PPP enzymes were analysed and the enzymes related to the Entner Doudoroff pathway showed levels of acetylation significantly higher. The enzymes glucose 6-phosphate 1-dehydrogenase (NGO0715), 6-phosphogluconolactonase (NGO0716), and phosphogluconate dehydratase (NGO0714) are involved in the biosynthesis of pyruvate and they presented a fold change of acetylation from 1.24 to 5.17 (fig 4.13).

For the enzymes that are involved in the biosynthesis of the nucleotide precursor phosphoribosyl pyrophosphate (PRPP) (Hove-Jensen *et al.*, 2017). All enzymes showed acetylation levels altered by acetyl-phosphate for exemption of ribulose-phosphate 3-epimerase (NGO0758). The enzyme that showed the highest level of acetylation was the ribose-phosphate pyrophosphokinase (NGO0441) with the sites K185 and K195 with fold change of 5.83 and 5.63, respectively (fig 4.13).

.

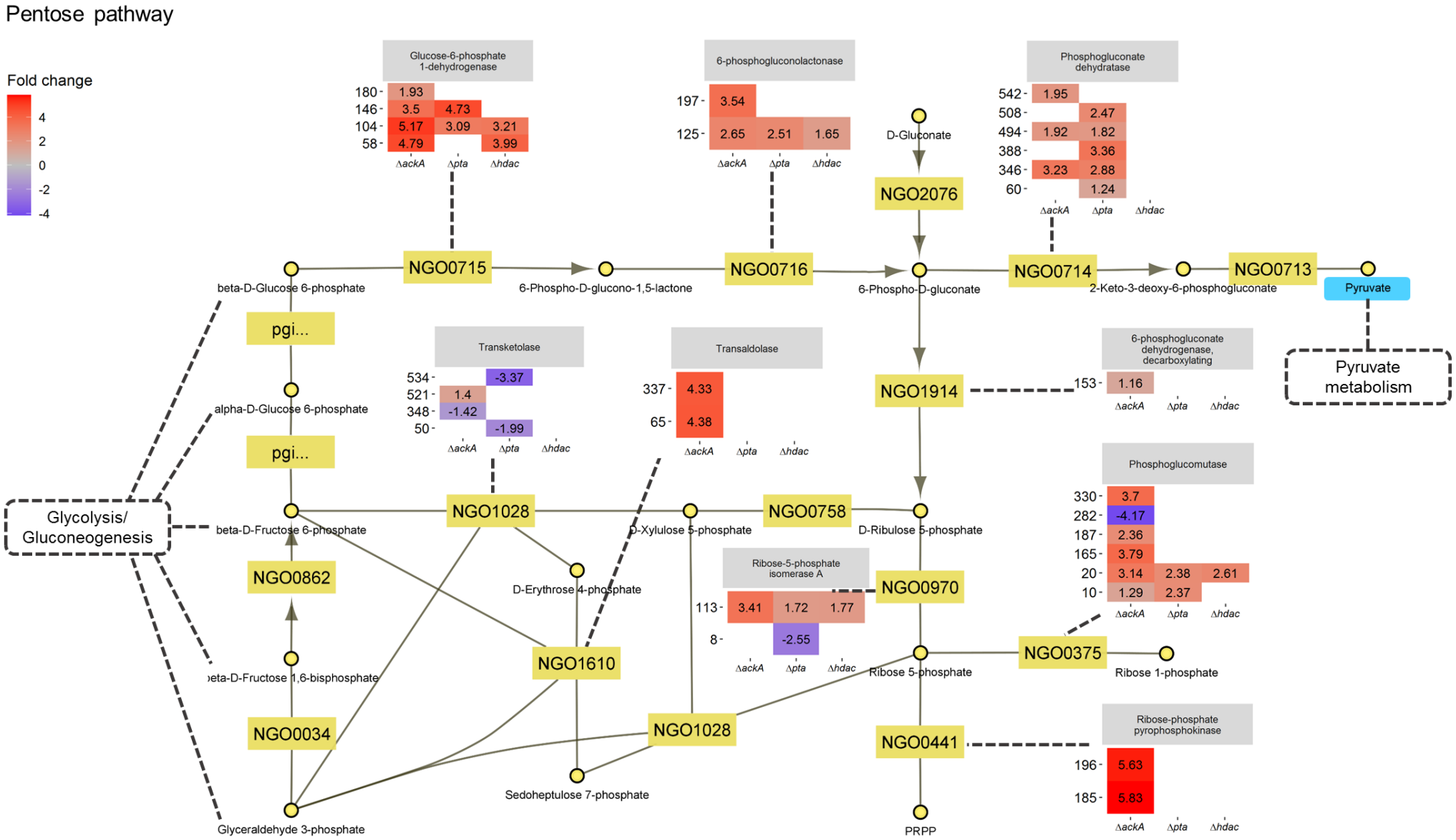
Pentose pathway
Fold change
4
2
0
-2
-4
Glucose-6-phosphate 1-dehydrogenase
180 1.93
146 3.5 4.73
104 5.17 3.09 3.21
58 4.79 3.99
ΔackA Δpta Δhdac
6-phosphogluconolactonase
197 3.54
125 2.65 2.51 1.65
ΔackA Δpta Δhdac
Phosphogluconate dehydratase
542 1.95
508 2.47
494 1.92 1.82
388 3.36
346 3.23 2.88
60 1.24
ΔackA Δpta Δhdac
D-Gluconate
NGO2076
NGO0715
NGO0716
NGO0714
NGO0713
beta-D-Glucose 6-phosphate
6-Phospho-D-glucono-1,5-lactone
6-Phospho-D-gluconate
2-Keto-3-deoxy-6-phosphogluconate
Pyruvate
Pyruvate metabolism
pgi...
alpha-D-Glucose 6-phosphate
pgi...
Transketolase
534 -3.37
521 1.4
348 -1.42
50 -1.99
ΔackA Δpta Δhdac
Transaldolase
337 4.33
65 4.38
ΔackA Δpta Δhdac
6-phosphogluconate dehydrogenase, decarboxylating
153 1.16
ΔackA Δpta Δhdac
NGO1914
Glycolysis/ Gluconeogenesis
beta-D-Fructose 6-phosphate
NGO1028
D-Xylulose 5-phosphate
NGO0758
D-Ribulose 5-phosphate
Phosphoglucomutase
330 3.7
282 -4.17
187 2.36
165 3.79
20 3.14 2.38 2.61
10 1.29 2.37
ΔackA Δpta Δhdac
NGO0862
D-Erythrose 4-phosphate
Ribose-5-phosphate isomerase A
113 3.41 1.72 1.77
8 -2.55
ΔackA Δpta Δhdac
NGO0970
NGO0375
Ribose 1-phosphate
beta-D-Fructose 1,6-bisphosphate
NGO1610
Ribose 5-phosphate
NGO0034
NGO1028
NGO0441
Ribose-phosphate pyrophosphokinase
196 5.63
185 5.83
ΔackA Δpta Δhdac
Sedoheptulose 7-phosphate
Glyceraldehyde 3-phosphate
PRPP

**Figure 4.13 Acetylation of the pentose phosphate pathway enzymes.** PPP of *N. gonorrhoeae* was obtained from KEGG pathway website with entry number ngo00030**.** The acetylation sites with a significant different fold change from the WT were mapped to each enzyme. The final metabolites of the pathway are phosphoribosyl pyrophosphate (PRPP), ribose 1-phosphate and pyruvate (blue box). This pathway is connected to gluconeogenesis, nucleotide biosynthesis and pyruvate metabolism. Thus, highly regulated sites were plotted to map them on the relative location of the protein, N-terminus, middle and C-terminus. Enzymes (yellow box); metabolites (yellow circles); carbon sources (blue box).

The EPS analysis showed that six out nine enzymes presented significant levels of acetylation in areas with positive electrostatic potential and that are located within the active site pocket. From the non-oxidative branch, the enzymes with an acetylation site within the active site were ribose-5-phosphate isomerase A (RPIA), phosphoglucomutase (PGM), and ribose-phosphate pyrophosphokinase (PRPS). These enzymes contribute to the biosynthesis of PRPP which it is used as a precursor for the synthesis of nucleotides and amino acids (fig. 4.14).

All the enzymes of oxidative branch, Entner-Doudoroff pathway, showed acetyl-phosphate dependent acetylation present in the active site. The enzymes were glucose-6-phosphate 1-dehydrogenase (G6PDH), 6-phosphogluconolactonase (PGLS), and phosphogluconate dehydratase (EDD) (fig. 4.14).

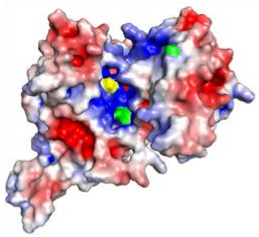
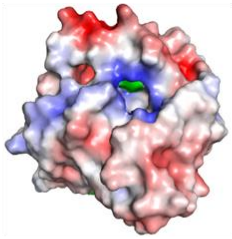
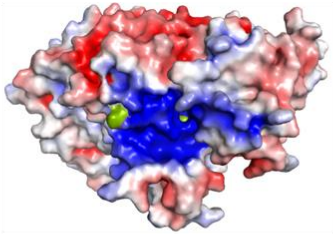
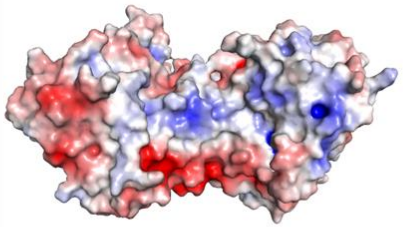
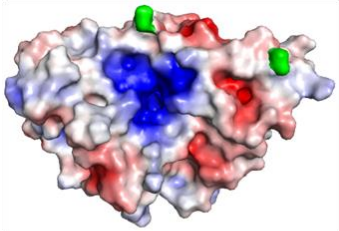

| Protein name | Glucose-6-phosphate 1-dehydrogenase | 6-phosphogluconolactonase | Phosphogluconate dehydratase | Transketolase | Transaldolase |
|---|---|---|---|---|---|
| **Abbreviation** | G6PDH | PGLS | EDD | TKT | TAL |
| **MW (Da)** | 153794 | 57351 | 57351 | 44578 | 85989 |
| **Modification in active site** | Yes | Yes | Yes | No | No |
| **K acetylation** | 146 | 197 | 346, 494 | - | - |
| **Ratio of acetylated lysines** | 30.8%(8/26) | 36.4%(4/11) | 29.6%(8/27) | 17.1%(6/35) | 15.8%(3/19) |
| **Kollman charge** | -5.0 | -3.0 | 14.0 | 2.0 | -2.0 |

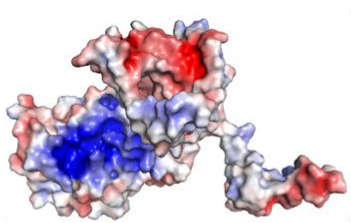
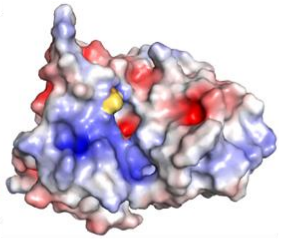
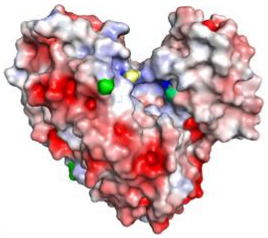
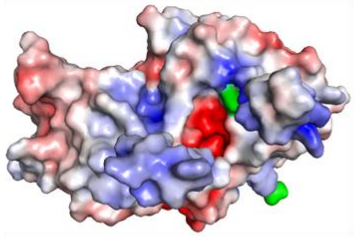

| Protein name | 6-phosphogluconate dehydrogenase, decarboxylating | Ribose-5-phosphate isomerase A | Phosphoglucomutase | Ribose-phosphate pyrophosphokinase |
|---|---|---|---|---|
| **Abbreviation** | PGD | RPIA | PGM | PRPS |
| **MW (Da)** | 30117 | 76944 | 155749 | 7078 |
| **Modification in active site** | No | Yes | Yes | Yes |
| **K acetylation** | - | 8 | 10, 282 | 196 |
| **Ratio of acetylated lysines** | 17.9%(5/28) | 31.2%(5/16) | 32%(8/25) | 36.4%(4/11) |
| **Kollman charge** | -5.0 | -4.0 | -6.0 | -2.0 |

**Figure 4.14 Electrostatic potential surface (EPS) of enzymes from the pentose phosphate pathway in *N. gonorrhoeae*.** The enzymes were modelled using PHYRE2 and the EPS was determined using PyMOL. The significant different acetylation sites were mapped for Δ*ackA* (green), and Δ*pta* (yellow). The modification to the active site was considered if the acetylation site was located within cavity pocket of the active site. On the table at the bottom it is shown the abbreviation of the protein name, the molecular weight in Daltons (Da), if the acetylation is found in the active site and the position of the residue, the ratio of acetylated lysines to total number of lysines found in the enzyme and the Kollman charge.

The crystals of two enzymes of the PPP were found on the PDB. These enzymes were transaldolase (NGO1610) and 6-phosphogluconolactonase (NGO0716), with the accession numbers 3CLM and 3HLI, respectively.

The transaldolase converts the glyceraldehyde 3-phosphate (G3P) and sedoheptulose 7-phosphate (S7P) to D-erythrose 4-phosphate (E4P) and beta D-fructose 6-phosphate (F6P) with the formation of a Schiff intermediate helped by the action of lysine (Samland and Sprenger, 2009). The active site was identified and a molecular docking for both substrates G3P and S7P was performed. By locating the binding sites of the two molecules, it was observed that any of the acetylation sites that are acetyl-phosphate dependent (K65 and K337) interacted with the substrates (fig 4.13).

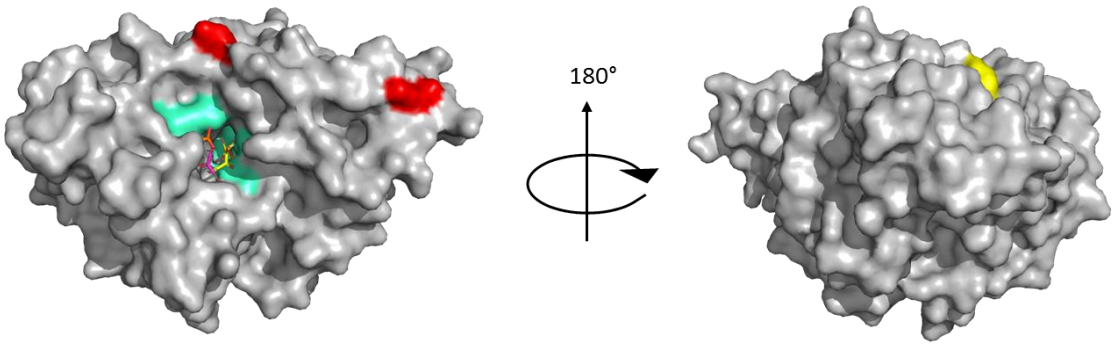


**Figure 4.15 Acetylation of K65 and K337 are outside the active site of the enzyme transaldolase in *N. gonorrhoeae*.** The model of enzyme transaldolase was downloaded from PDB with the access number 3CLM. The model has a resolution of 1.14 Å. The substrates glyceraldehyde 3-phosphate and sedoheptulose 7-phosphate were modelled and the energy was decreased to 0 kJ/mol. The molecular docking was selected to the lowest affinity energy. The acetylation sites with an increased found in the Δ*ackA* strain acetylation are located outside of the active sites (red), the acetylation site found in the WT (yellow) is not interacting with the active site (cyan).

Contrary, the active site of the enzyme 6-phosphogluconolactonase (NGO0716) showed to be affected by acetylation. 6-phosphogluconolactonase (PGLS) catalyses the second reaction of the PPP, which it is also involved in the Entner Doudoroff pathway. This reaction converts the 6-phospho D-glucono-1,5-lactone (6PGL) to 6-phospho D-gluconate (6PG) by an hydrolysis reaction (Miclet *et al.*, 2001).

The molecular docking showed that the substrate 6GPL possessed an affinity of -7.8 kcal/mol and that it interacts with 5 residues (G41, S44, D68, M134, and K197) by eight hydrogen bonds. Two of these bonds interact with a lysine residue K197 that showed higher acetylation in the isogenic strain Δ*ackA* by 3.54 fold change.

Interestingly, a conservation analysis of the site showed that from 447 homologue sequence, 407 contained the lysine K197 meaning a 91% conservation. The lysine K197 was acetylated *in silico* and showed the loss of two hydrogen bonds with the substrate 6GPL. Furthermore, the conformation of the pocket cavity of the active site was altered. The surface area for the access of solvent molecules was decreased by 51.52 $Å^2$ (fig. 4.14).

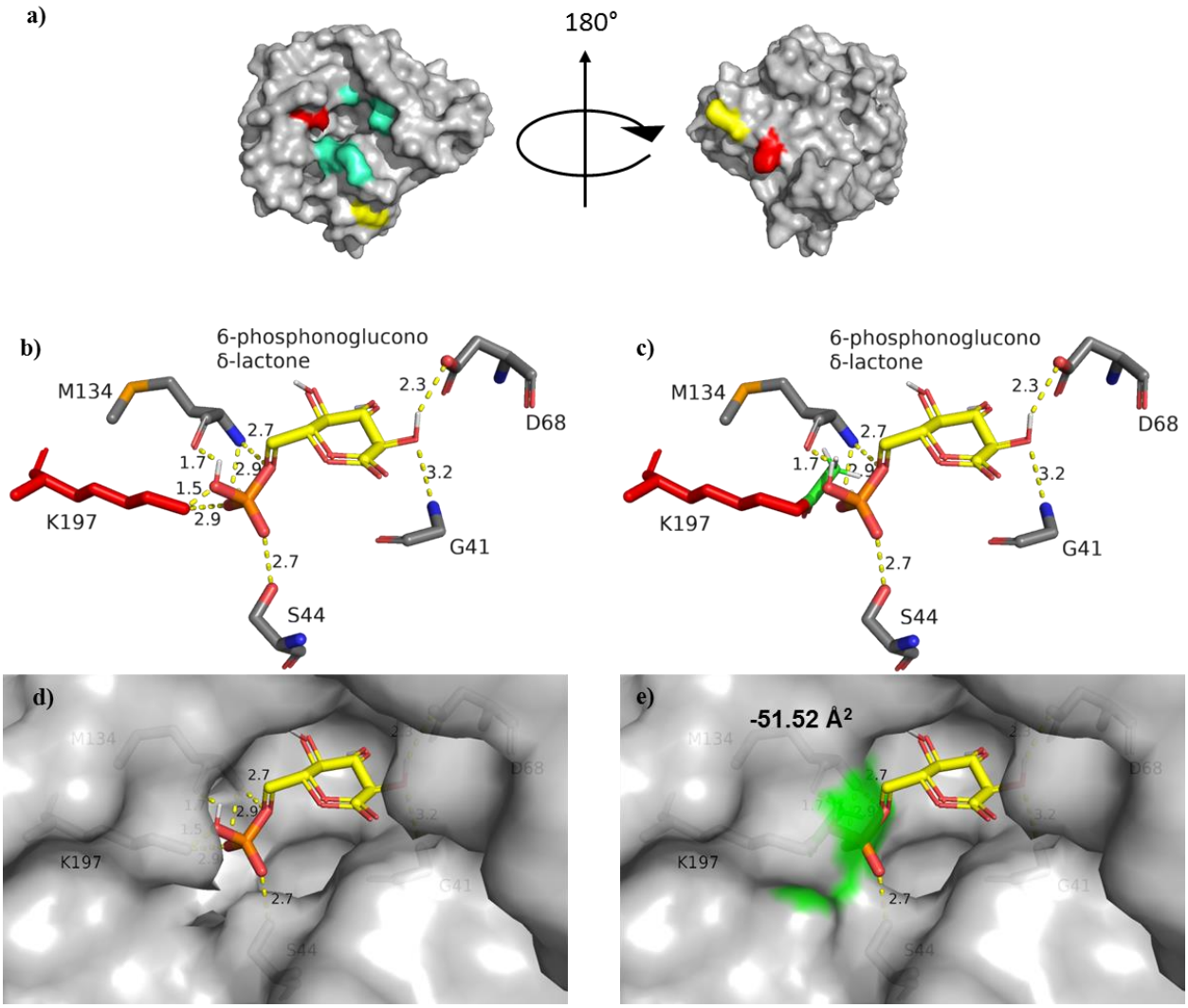


**Figure 4.16 Acetylation of the residue K197 in 6-phosphogluconolactonase in *N. gonorrhoeae* modifies the interaction and conformation of the active site. a)** The model of GPLS enzyme was downloaded from PDB with the accession code 3CLM. The catalytic residues were located (cyan) and the lysine residues that were acetylated were identified for the WT (yellow), and Δ*ackA* (red). **b)** The substrate 6-phospho D-glucono-1, 5-lactone (6PGL) was docked to the enzyme by *in silico* analysis showing eight hydrogen bonds including K197. **c)** The acetylation *in silico* of K97 showed a loss of two hydrogen bonds with K197. **d)** The cavity pocket of the catalytic site, **e)** showed a decreased of the surface by 51.52 $Å^2$ when K197 was acetylated (green).

### 4.2.2.3Pyruvate metabolism

The pyruvate metabolism is the core of the central metabolism, it is the connection between glycolysis and TCA cycle. In this pathway pyruvate is oxidative decarboxylated to form the metabolite acetyl-coenzyme A (acetyl-CoA), $CO_2$, and NADH ($H^+$). This transformation is catalysed by a complex of three different enzymes, known as pyruvate dehydrogenase complex (PDC) (De Kok *et al.*, 1998; Sauer and Eikmanns, 2005; Patel *et al.*, 2014).

The PDC is integrated by pyruvate dehydrogenase (E1) (*aceE*), dihydrolipoamide acetyltransferase (E2) (NGO0564), and dihydrolipoamide dehydrogenase (NGO0562). Each component has a specific role in the reaction. E1 decarboxylates pyruvate to form an enamine that then will acetylate a lipoyl residue in E2; then E2 transfers the acetyl group to the coenzyme A to form acetyl-CoA, and finally, the E3 transfers the electrons to produce NADH ($H^+$). In previous studies, the pyruvate dehydrogenase E1 has shown to have a great number of acetylation sites (Post *et al.*, 2017; Pang *et al.*, 2020).

In this pathway is also included the conversion of lactate to pyruvate. *N. gonorrhoeae* possesses three different lactate dehydrogenase that catalyses this reaction. Two are found on the membrane, and one in the cytosol. These enzymes are of particular interest due to the influence that lactate have shown in the pathogenesis and metabolism of *N. gonorrhoeae* (Parsons *et al.*, 1996; Atack *et al.*, 2014; Sigurlásdóttir *et al.*, 2017).

Furthermore, the PTA-AK pathway is found in pyruvate metabolism. Therefore, the study of these pathways are key to understand the role of acetyl-phosphate in the metabolism of *N. gonorrhoeae.*

All the enzymes of pyruvate metabolism pathway showed acetyl-phosphate dependent acetylation, except acetate kinase that showed a significantly decreased acetylation which it was due to the knocking out of the gene (fig. 4.15).

The enzyme that presented more acetylation sites altered by acetyl-phosphate was pyruvate dehydrogenase E1 with sixteen different acetylation sites. Two of those sites are highly regulated by the PTA-AK pathway because the level of acetylation was higher in the isogenic strain Δ*ackA* and lower in Δ*pta.* From the three lactate dehydrogenases, only the respiratory L-lactate dehydrogenase (NGO0639) showed a highly regulated acetylation site by PTA-AK pathway (fig. 4.15).

From the enzymes of the PTA-AK pathway only the phosphate acetyltransferase (NGO0214) showed acetylation sites dependent on acetyl-phosphate. Although acetate kinase (NGO0977) showed significant decreased acetylation on the sites K169 and K195, these are not relevant because the gene was knocked out therefore, the peptides were decreased due to the lack of enzyme production by the bacteria (fig. 4.15).

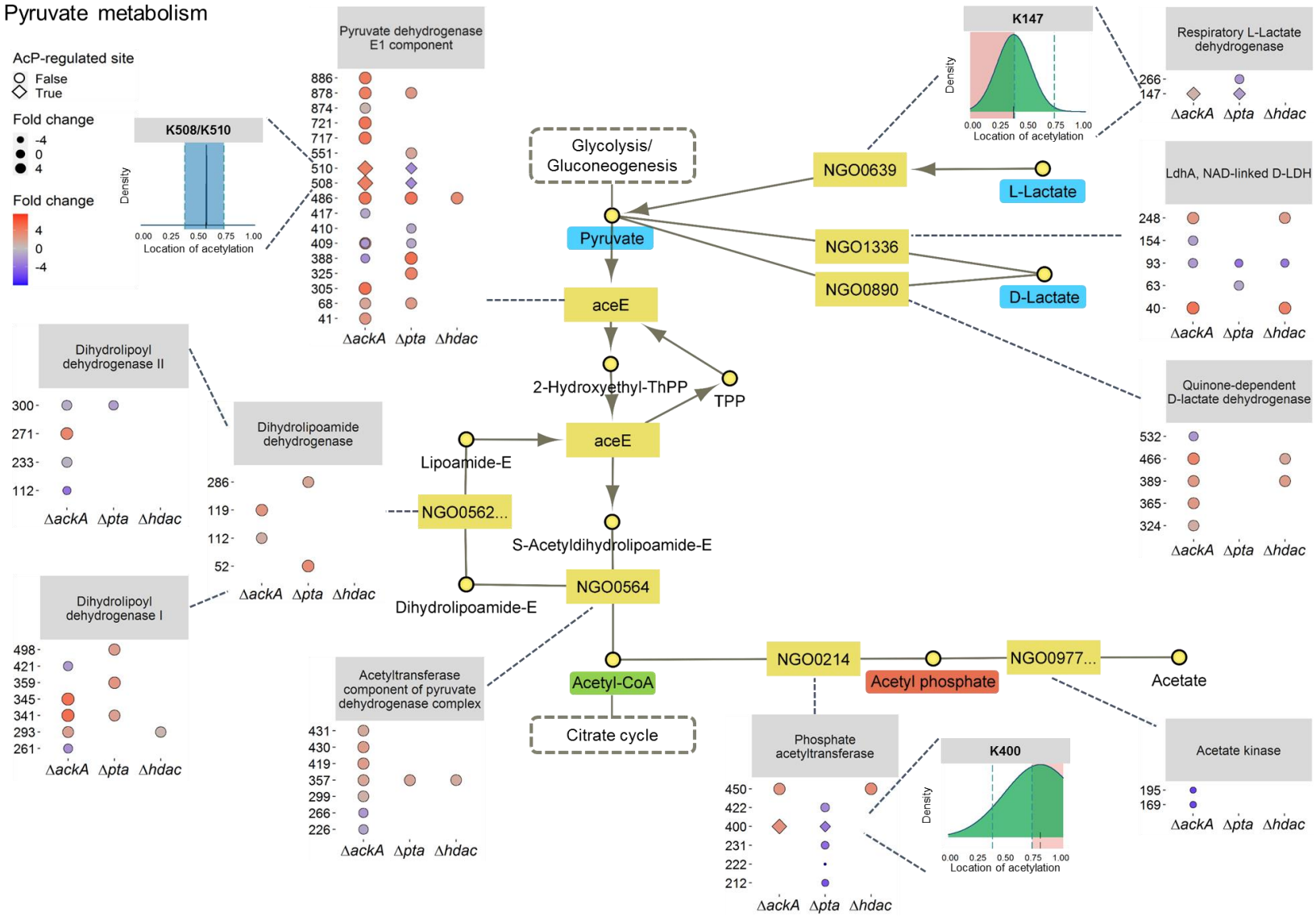
Pyruvate metabolism
AcP-regulated site
False
True
Fold change
-4
0
4
Fold change
4
0
-4
K508/K510
Density
0.00 0.25 0.50 0.75 1.00
Location of acetylation
Pyruvate dehydrogenase E1 component
886
878
874
721
717
551
510
508
486
417
410
409
388
325
305
68
41
ΔackA Δpta Δhdac
Glycolysis/ Gluconeogenesis
Pyruvate
aceE
2-Hydroxyethyl-ThPP
TPP
aceE
Lipoamide-E
NGO0562...
S-Acetyldihydrolipoamide-E
NGO0564
Dihydrolipoamide-E
Acetyltransferase component of pyruvate dehydrogenase complex
431
430
419
357
299
266
226
ΔackA Δpta Δhdac
Acetyl-CoA
Citrate cycle
NGO0639
L-Lactate
NGO1336
NGO0890
D-Lactate
K147
Density
0.00 0.25 0.50 0.75 1.00
Location of acetylation
Respiratory L-Lactate dehydrogenase
266
147
ΔackA Δpta Δhdac
LdhA, NAD-linked D-LDH
248
154
93
63
40
ΔackA Δpta Δhdac
Quinone-dependent D-lactate dehydrogenase
532
466
389
365
324
ΔackA Δpta Δhdac
Dihydrolipoyl dehydrogenase II
300
271
233
112
ΔackA Δpta Δhdac
Dihydrolipoamide dehydrogenase
286
119
112
52
ΔackA Δpta Δhdac
Dihydrolipoyl dehydrogenase I
498
421
359
345
341
293
261
ΔackA Δpta Δhdac
NGO0214
Acetyl phosphate
NGO0977...
Acetate
Phosphate acetyltransferase
450
422
400
231
222
212
ΔackA Δpta Δhdac
K400
Density
0.00 0.25 0.50 0.75 1.00
Location of acetylation
Acetate kinase
195
169
ΔackA Δpta Δhdac

**Figure 4.17 Acetylation of the pyruvate metabolism enzymes.** The pyruvate metabolism of *N. gonorrhoeae* was obtained from KEGG pathway website with entry number ngo00620**.** The acetylation sites with a significant different fold change to the WT were mapped to each enzyme. The acetyl-phosphate regulated sites (square shape) were considered if it was found in both Δ*ackA* and Δ*pta*, and presenting a high and low fold change in acetylation, respectively. Thus, highly regulated sites were plotted to map them on the relative location of the protein, divided by N-terminus, middle and C-terminus. The pathway shows the name of the gene by either the abbreviation or the locus (yellow box), the metabolites (yellow circles) and the carbon source used by *N. gonorrhoeae* (blue box). The intermediate metabolite of the PTA-AK pathway, acetyl-phosphate is highlighted in red.

The EPS analysis of the enzymes from the pyruvate metabolism showed that six enzymes possessed acetyl-phosphate dependent acetylation sites in the active site. Some of them with a percentage of conservation. However, all these sites found in the active site showed a positive electrostatic surface charge (fig. 4.18).

The enzymes that presented these acetylation sites were LdhA, NAD-linked D-LDH (LDHA), quinone-dependent D-lactate dehydrogenase (LDHD), pyruvate dehydrogenase E1 component (PDE1), dihydrolipoamide dehydrogenase (DLD), acetyltransferase component of pyruvate dehydrogenase complex (DLAT), and phosphate acetyltransferase (PTA) (fig. 4.18).

The ratio of acetylated lysines to the total number of lysines in the enzymes of this pathway was 27.7%. However, the enzyme PDE1 showed a ratio of 62.5%, and interestingly, all of the pyruvate dehydrogenase complex showed in total 191 acetylated lysine residues from which 72 showed a significant different fold change of acetylation in the different strains (fig. 4.18).

The lysine residues identified to be conserved were found in DLAT and PTA, with a conservation percentage of 35 and 81% among 1001 and 429 different sequences, respectively. The acetylation sites that suggest to be altering the active site and therefore, the interaction with the substrate were K357 and K450, respectively. K357 was found with a significant increase acetylation in Δ*ackA*, Δ*pta*, and Δ*hdac* with a fold change of 1.56, 1.57 and 1.32, respectively. Since DLAT mechanism action is complex due to the involvement of the enzymes of the pyruvate dehydrogenase complex, the prediction of acetylation in the binding interaction was not performed (fig. 4.18).

However, the two enzymes LDHA and PTA were modelled and analysed for the binding interaction, since LDHA showed an unusual acetylation pattern in the active

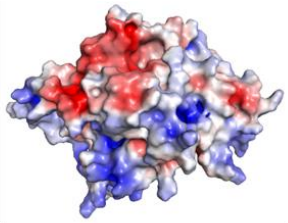
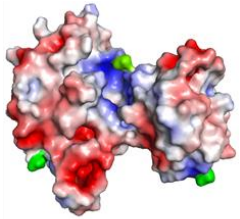
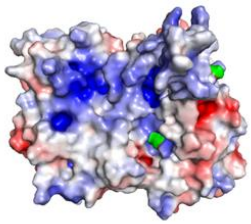
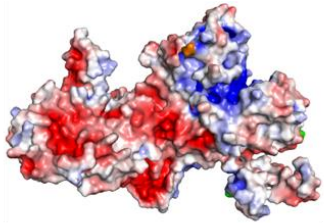
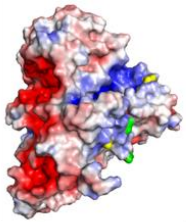
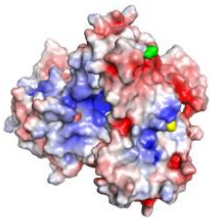

| Protein name | Respiratory L-Lactate dehydrogenase | LdhA, NAD-linked D-LDH | Quinone-dependent D-lactate dehydrogenase | Pyruvate dehydrogenase E1 component | Dihydrolipoyl dehydrogenase I | Dihydrolipoyl dehydrogenase II |
|---|---|---|---|---|---|---|
| **Abbreviation** | LLDD | LDHA | LDHD | PD E1 | PD E2 | PD E2 |
| **MW (Da)** | 13360 | 155749 | 16460 | 36797 | 33292 | 69355 |
| **Modification in active site** | No | Yes | Yes | Yes | - | - |
| **K acetylation** | NA | 154 | 466 | 388 | - | - |
| **Ratio of acetylated lysines** | 14.3%(4/28) | 27.8%(5/18) | 23.7%(9/38) | 62.5%(30/48) | 35%(14/40) | 27%(10/37) |
| **Kollman charge** | 5.0 | -0.7 | 19.0 | -1.0 | -8.0 | 4.0 |

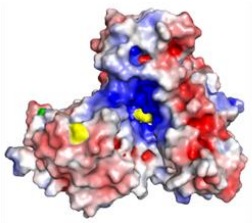
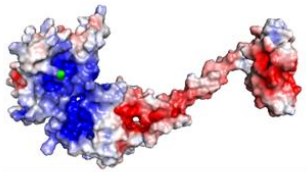
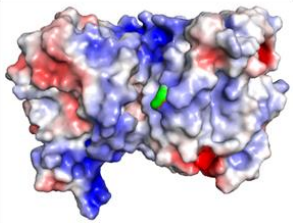
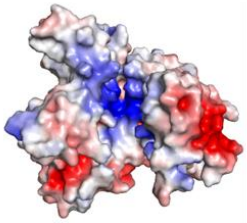
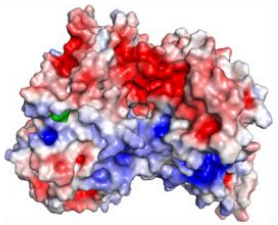

| Protein name | Dihydrolipoamide dehydrogenase | Acetyltransferase component of pyruvate dehydrogenase complex | Phosphate acetyltransferase | Acetate kinase | Phosphoenolpyruvate carboxylase |
|---|---|---|---|---|---|
| **Abbreviation** | DLD | DLAT | PTA | AK | PEPcx |
| **MW (Da)** | 106333 | 21350 | 14990 | 57351 | 155749 |
| **Modification in active site** | Yes | Yes | Yes | No | No |
| **K acetylation** | 52 | 357 | 450 | - | - |
| **Ratio of acetylated lysines** | 25%(6/24) | 28.6%(12/42) | 22.2%(6/27) | 23.8%(5/21) | 15%(6/40) |
| **Kollman charge** | 7.0 | -20.0 | -9.0 | 1.0 | 18.0 |

**Figure 4.18 Electrostatic potential surface (EPS) of enzymes from the pyruvate metabolism in *N. gonorrhoeae*.** The enzymes were modelled using PHYRE2 and the EPS was determined using PyMOL. The significant different acetylation sites were mapped for Δ*ackA* (green), and Δ*pta* (yellow). The modification to the active site was considered if the acetylation site was located within cavity pocket of the active site. On the table at the bottom it is shown the abbreviation of the protein name, the molecular weight in Daltons (Da), if the acetylation is found in the active site and the position of the residue, the ratio of acetylated lysines to total number of lysines found in the enzyme and the Kollman charge. The sites where the active site was not determined were identified with "-".

The location of the acetylation sites showed that the enzymes $NAD^+$-linked D-LDH (LDHA) and phosphate transacetylase (PTA) were affected on the active site by acetylation. The proteins were modelled with PHYRE2 with a confidence modelling higher than 90% in the 99 (fig. 4.16a) and 65% (fig. 4.18a) of the sequence residues, respectively.

The enzyme LDHA is a cytosolic lactate dehydrogenase that catalyses the reversible reaction of D-lactate to pyruvate with the reduction of $NAD^+$ (Atack *et al.*, 2014). Contrary to the previous enzymes where the acetylation inhibited the binding to the substrate, the structure prediction an *in* silico analysis suggests that acetylation increases the binding to the substrate. The enzyme showed a significant reduction of acetylation in the residue K154 by 1.54 fold in the Δ*ackA* strain (fig. 4.16).

The substrates $NAD^+$ and lactate were docked in the active site of the enzyme and $NAD^+$ showed five hydrogen bonds to four residues (G153, K154, I155 and S233). One of the hydrogen bonds interacts with K154 and when the lysine was acetylated *in silico*, the hydrogen bond was replaced by two bonds, increasing the number of hydrogen bonds from five to six (fig. 4.16).

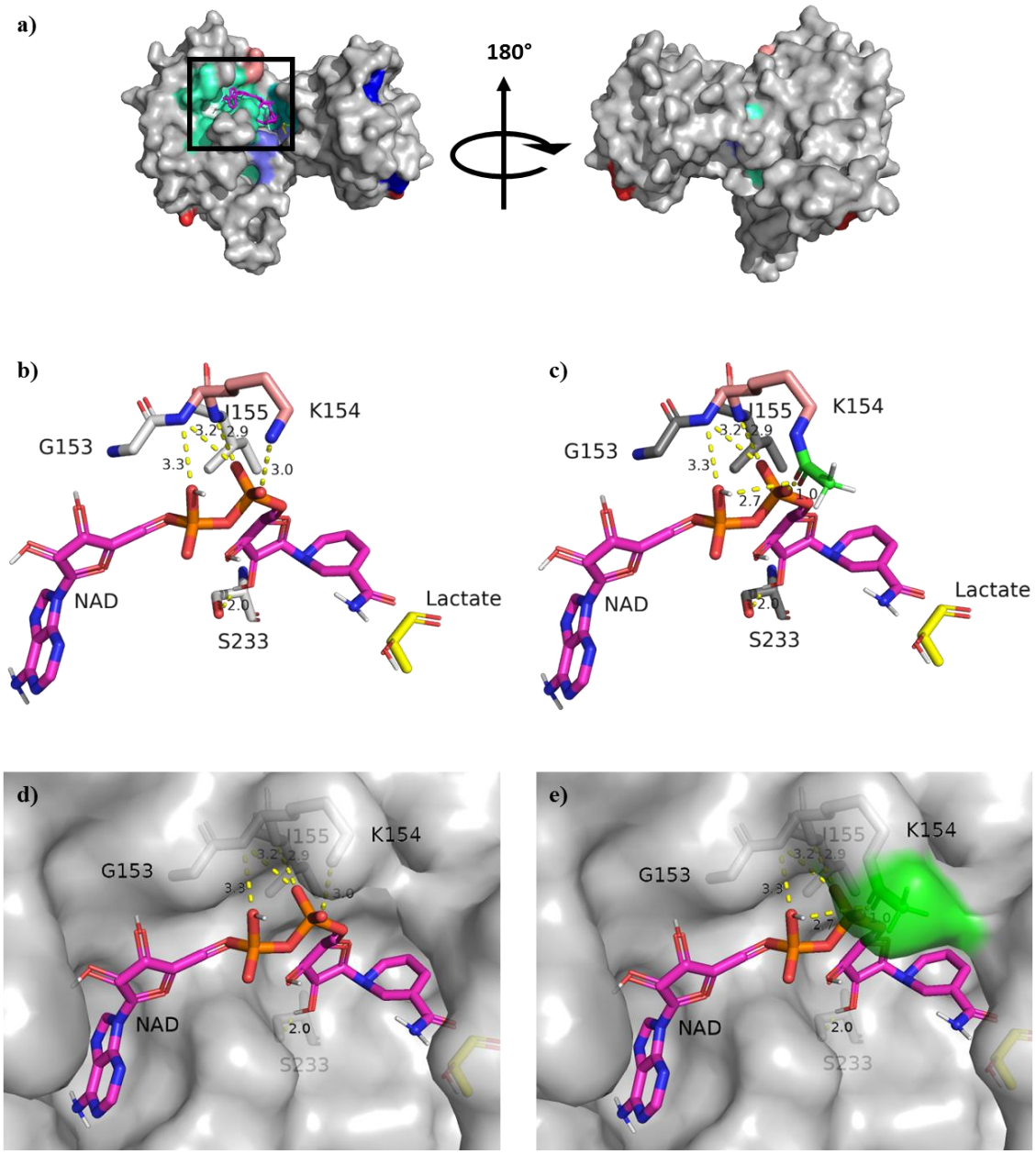


**Figure 4.19 Acetylation of K154 interacts with the substrate of LDHA in *N. gonorrhoeae.* a)** The modelling of LDHA was created using PHYRE2. The catalytic residues were located (cyan) and the lysine residues that were acetylated were identified for the WT (yellow), increased acetylation in *Δpta* (blue), decreased acetylation in Δ*ackA* (salmon), and increased acetylation in Δ*ackA* (red,). **b)** The substrates NAD (magenta) and lactate (yellow) were docked to the enzyme by *in silico* analysis showing five hydrogen bonds including K154. **c)** The acetylation *in silico* of K154 showed interaction with $NAD^+$. **d)** The cavity pocket of the catalytic site, **e)** when acetylated showed a change in the conformation of the cavity pocket of the active site (green).

The enzyme PTA is part of the short pathway PTA-AK that catalyses the conversion of acetyl-CoA to pyruvate with the generation of the intermediate metabolite acetyl-phosphate and the release of CoA. Acetyl-phosphate is the responsible molecule of non-enzymatic acetylation (Verdin and Ott, 2013; Wolfe, 2016).

The predictive model of PTA was analysed to find possible interactions with the substrate. The model presented a percentage confidence of 65% of residues modelled higher than 90% due to the presence of 175 amino acids in the N-terminus that have not been modelled from a crystal. However, discarding the first 175 amino acids, the modelling confidence increases to more than 90% compared with 429 homologue sequences.

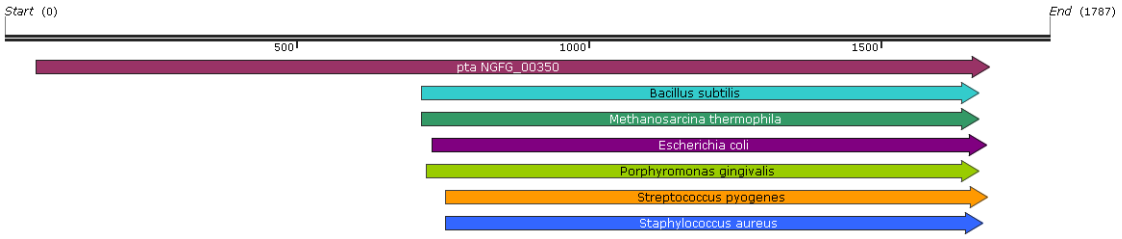


**Figure 4.20 Alignment of PTA with different bacterial species.** The sequence of phosphate transacetylase (PTA) from *N. gonorrhoeae* MS11 was aligned to the sequence of PTA from 6 species of different bacteria. The sequence of the gonococcus contains 175 amino acids additional to the other sequences.

The enzyme showed a significant increase of acetylation in the lysine residue K450, located the active site, in the isogenic strain Δ*ackA*. The molecular docking of the substrate acetyl-CoA showed interactions with seven residues (T302, N446, Y449, K450, G462, S476, and G478) forming seven hydrogen bonds. One of the hydrogen bonds is with K450 which showed an 81% conservation among 429 homologue sequences. Acetylation of the lysine residue *in silico* showed the depletion of the hydrogen bond and a change in the conformation of the pocket of the active site by decreasing the surface area for solvent molecules by 11.26 $Å^2$. The increase of acetylation was 2.65 fold in the strain Δ*ackA*, however, this same site was significantly increased by 3.15 fold in the Δ*hdac* strain. This suggests the site is deacetylated by HDAC (fig. 4.18).

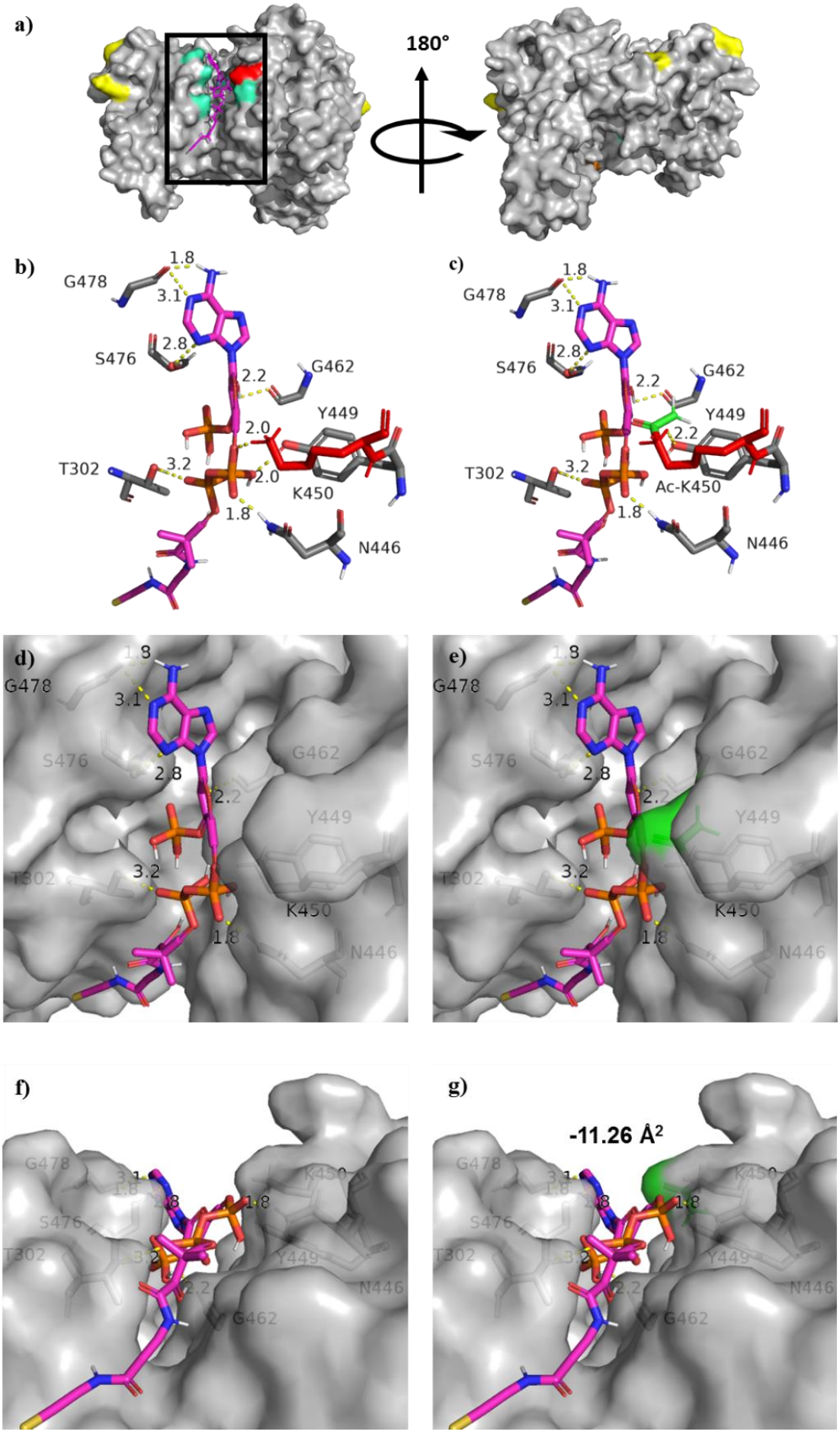
a)
180°
b)
G478
S476
T302
G462
Y449
K450
N446
c)
Ac-K450
d)
e)
f)
g)
-11.26 Å²

**Figure 4.21 Acetylation of K450 residue of phosphate transacetylase is predicted to alter the interaction with the substrate and the conformation of the active site. a)** Predictive model of PTA using PHYRE2. The active site was located (cyan, box) and the acetylation sites were identified for the WT (yellow), and Δ*ackA* (red). **b)** The substrate acetyl-CoA was docked to the enzyme by *in silico* analysis, showing seven hydrogen bonds including the residue K450. **c)** The acetylation *in silico* of K450 showed a loss of a hydrogen bond to K450. **d)** Aerial view of the cavity pocket of the catalytic site, **e)** showed a decreased of the surface area when K197 was acetylated (green). **f)** Lateral view of the active site with substrate, and **g)** after acetylation of K450 showing a decrease of surface area by 11.26 $Å^2$.

The second enzyme of the PTA-AK pathway is acetate kinase (AK). The enzyme catalyses the reversible conversion of acetyl-phosphate to acetate with the production of one molecule of ATP (Verdin and Ott, 2013). The predictive model of the enzyme possessed a 100% of residues modelled at >90% confidence. The active site was located and by molecular docking the predictive binding sites of the substrates acetyl-phosphate and ADP were identified.

The acetylation sites of the enzyme were located, which only were found in the WT strain. Two sites of acetylation (K169 and K197) showed a significant lower acetylation, however, these sites were decreased due to the sequence of the mutant that some parts were deleted from the WT sequence. The rest of the acetylation sites found in the WT strain are located outside of the active site and K47 is located near the acetylation site but the data from mass spectrometry showed no acetylation difference in any of the isogenic strains (fig. 4.19).

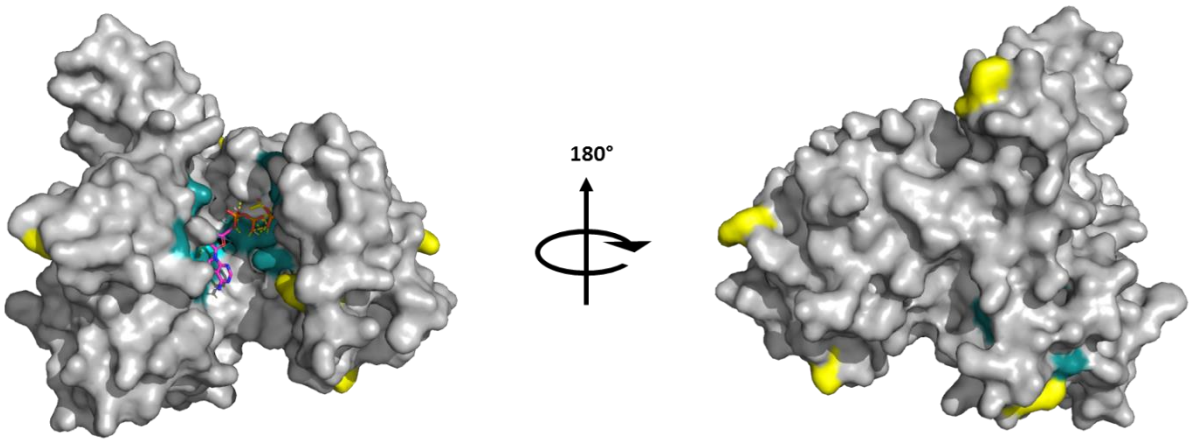


**Figure 4.22Acetate kinase model of *N. gonorrhoeae*.** The model was constructed with PHYRE2 and the active site (cyan) was used to the molecular docking of the substrates ADP (magenta) and acetyl-phosphate (yellow). Then the acetylation sites were located for the WT strain (yellow). The only acetylation site close to the active site was K47

### 4.2.2.4TCA cycle

The TCA cycle is the final pathway of the central metabolic pathway. In this pathway merges the oxidation of carbohydrates, amino acids and lipids and it is the pathway where the highest number of ATP molecules for the obtainment of energy. The pathway starts with a molecule of acetyl-CoA that will suffer a number of steps to be finally decarboxylated into $CO_2$ (Akram, 2014).

The analysis of acetylation of the TCA cycle enzymes showed that all presented significant different levels of acetylation in the isogenic strains. Aconitate hydratase B (NGO1231), isocitrate dehydrogenase (NGO1082), and 2-oxoglutarate dehydrogenase (SUCA) were the enzymes that presented the highest number of acetyl-phosphate dependent sites with 18, 10, and 19 sites, respectively (fig. 4.23).

2-oxoglutarate and malate quinone reductase showed that the acetylation site K563 and K218, respectively, are regulated by the PTA-AK pathway, since the fold change of acetylation was higher in the isogenic strain Δ*ackA* and decreased in Δ*pta* (fig. 4.23).

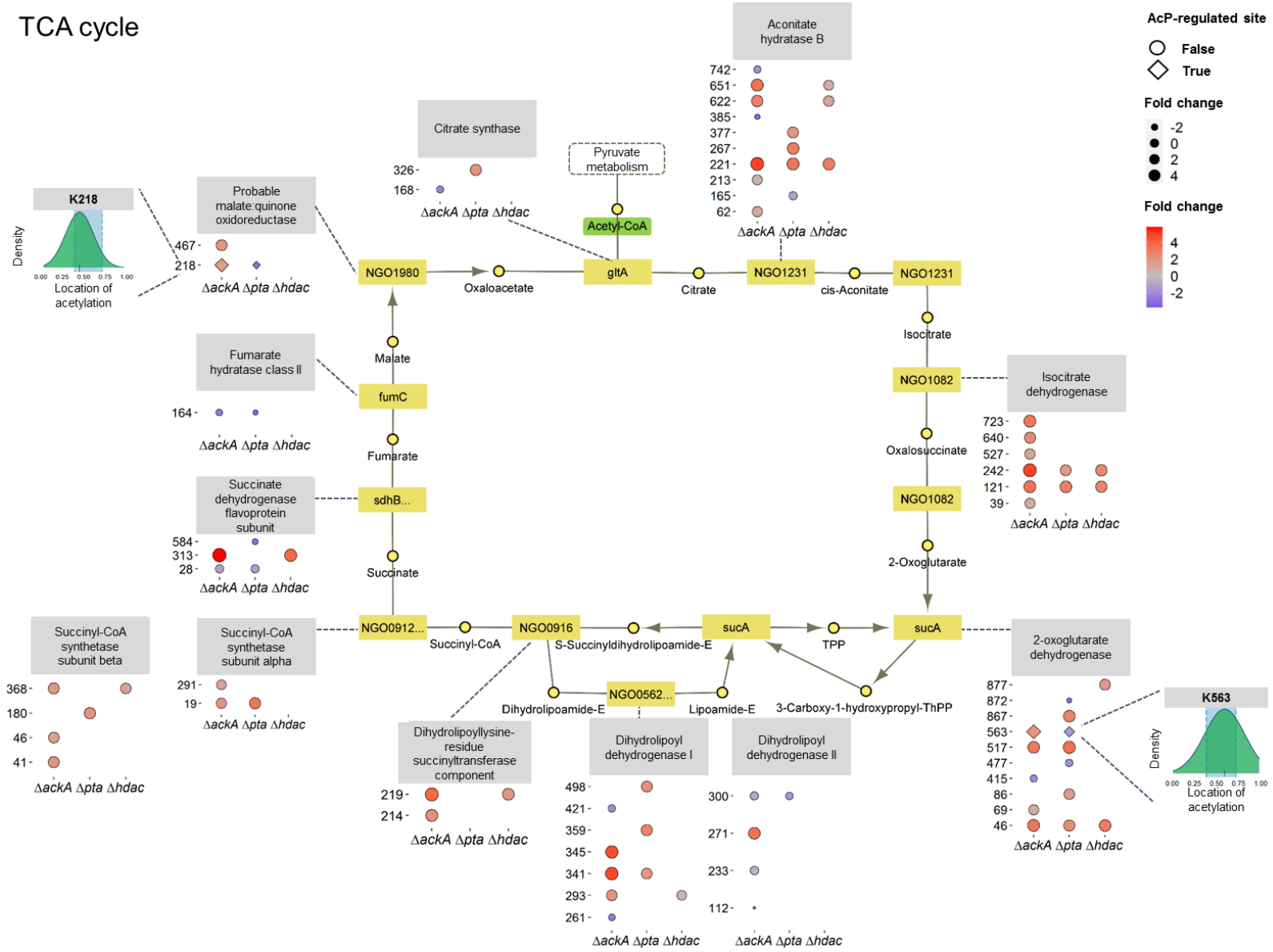
TCA cycle
AcP-regulated site
False
True
Fold change
-2
0
2
4
Fold change
4
2
0
-2
Aconitate hydratase B
742
651
622
385
377
267
221
213
165
62
ΔackA Δpta Δhdac
Citrate synthase
326
168
ΔackA Δpta Δhdac
Pyruvate metabolism
Acetyl-CoA
K218
Density
0.00 0.25 0.50 0.75 1.00
Location of acetylation
Probable malate:quinone oxidoreductase
467
218
ΔackA Δpta Δhdac
NGO1980
Oxaloacetate
gltA
Citrate
NGO1231
cis-Aconitate
NGO1231
Isocitrate
Malate
Fumarate hydratase class II
fumC
164
ΔackA Δpta Δhdac
Fumarate
NGO1082
Isocitrate dehydrogenase
723
640
527
242
121
39
ΔackA Δpta Δhdac
Oxalosuccinate
Succinate dehydrogenase flavoprotein subunit
sdhB...
584
313
28
ΔackA Δpta Δhdac
Succinate
NGO1082
2-Oxoglutarate
Succinyl-CoA synthetase subunit beta
368
180
46
41
ΔackA Δpta Δhdac
Succinyl-CoA synthetase subunit alpha
291
19
ΔackA Δpta Δhdac
NGO0912...
Succinyl-CoA
NGO0916
S-Succinyldihydrolipoamide-E
sucA
TPP
sucA
2-oxoglutarate dehydrogenase
877
872
867
563
517
477
415
86
69
46
ΔackA Δpta Δhdac
K563
Density
0.00 0.25 0.50 0.75 1.00
Location of acetylation
Dihydrolipoamide-E
NGO0562...
Lipoamide-E
3-Carboxy-1-hydroxypropyl-ThPP
Dihydrolipoyllysine-residue succinyltransferase component
219
214
ΔackA Δpta Δhdac
Dihydrolipoyl dehydrogenase I
498
421
359
345
341
293
261
ΔackA Δpta Δhdac
Dihydrolipoyl dehydrogenase II
300
271
233
112
ΔackA Δpta Δhdac

**Figure 4.23 Acetylation of the TCA cycle enzymes.** The TCA cycle of *N. gonorrhoeae* was obtained from KEGG pathway website with entry number ngo00020**.** The acetylation sites with a significant different fold change to the WT were mapped to each enzyme. The acetyl-phosphate regulated sites (square shape) were considered if it was found in both Δ*ackA* and Δ*pta*, and presenting a high and low fold change in acetylation, respectively, Thus, highly regulated sites were plotted to map them on the relative location of the protein, divided by N-terminus, middle and C-terminus. The pathway shows the name of the gene by either the abbreviation or the locus (yellow box), the metabolites (yellow circles) and, the metabolite that initiates the cycle acetyl-CoA (green).

The electrostatic potential surface analysis demonstrated that citrate synthase (CS) and dihydrolipoyllysine residue succinyltransferase component of 2-oxoglutarate dehydrogenase complex (DLST) possessed a positive EPS cluster where acetylation could have occurred. However, only DLST showed that the site K214 was in this cluster. This cluster suggests to be an active site of the enzyme, but the conserved amino acids were found in another area which possesses a negative EPS (fig. 4.24).

Contrary to the previous pathways where enzymes showed acetylation sites in the active site, none of the enzymes from the TCA cycle showed acetylation sites that were significant different in the active site (fig. 4.24).

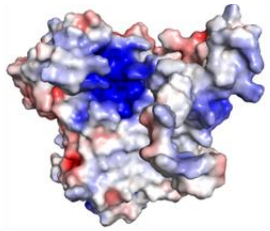
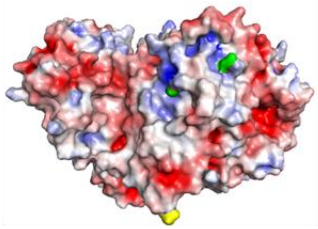
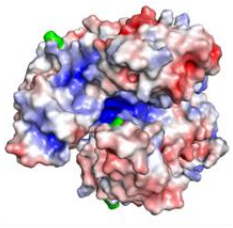
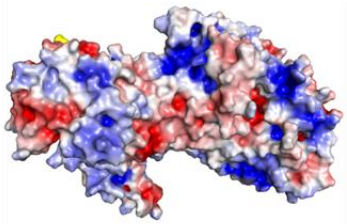
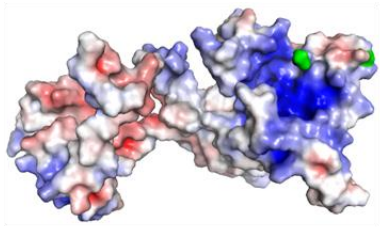

| Protein name | Citrate synthase | Aconitate hydratase B | Isocitrate dehydrogenase [NADP] | 2-oxoglutarate dehydrogenase | Dihydrolipoyllysine-residue succinyltransferase component of 2-oxoglutarate dehydrogenase complex |
|---|---|---|---|---|---|
| Abbreviation | CS | ACNB | IDH | OGDH | DLST |
| MW (Da) | 36797 | 32453 | 39017 | 12564 | 68803 |
| Modification in active site | No | No | Yes | No | - |
| K acetylation | - | - | 120 | - | - |
| Ratio of acetylated lysines | 21.1%(4/19) | 31.6%(18/57) | 18.5%(10/54) | 32.8%(19/58) | 16.7%(4/24) |
| Kollman charge | 9.0 | -3.0 | 2.0 | 18.0 | -13.4 |

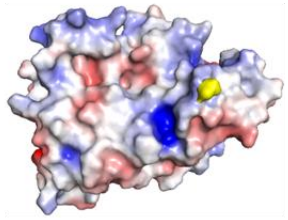
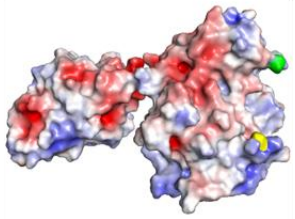
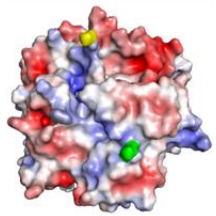
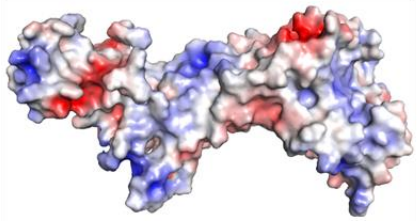
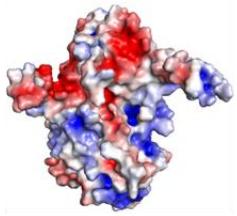

| Protein name | Succinyl-CoA synthetase subunit alpha | Succinyl-CoA synthetase subunit beta | Succinate dehydrogenase flavoprotein subunit | Fumarate hydratase class II | Probable malate:quinone oxidoreductase |
|---|---|---|---|---|---|
| Abbreviation | SUCLG1 | SUCLG2 | SDHA | FUMC | MQO |
| MW (Da) | 9820 | 24177 | 41362 | 77951 | 41511 |
| Modification in active site | - | - | No | No | No |
| K acetylation | - | - | - | - | - |
| Ratio of acetylated lysines | 31.6%(6/19) | 38.7%(12/31) | 25.8%(8/31) | 14.3%(3/21) | 12%(3/25) |
| Kollman charge | 0.0 | -4.0 | 6.0 | 4.0 | 1.8 |

**Figure 4.24 Electrostatic potential surface (EPS) of enzymes from the TCA cycle in *N. gonorrhoeae*.** The enzymes were modelled using PHYRE2 and the EPS was determined using PyMOL. The significant different acetylation sites were mapped for Δ*ackA* (green), and Δ*pta* (yellow). The modification to the active site was considered if the acetylation site was located within cavity pocket of the active site. On the table at the bottom it is shown the abbreviation of the protein name, the molecular weight in Daltons (Da), if the acetylation is found in the active site and the position of the residue, the ratio of acetylated lysines to total number of lysines found in the enzyme and the Kollman charge. The sites where the active site was not determined were identified with "-".

## 4.3 Discussion

In this chapter the role of acetyl-phosphate in the acetylation of the enzymes from the central metabolic pathways (CMP) and the effect acetylation possesses in growth and carbon utilisation was described.

The general approach was to identify the pathways where acetylation was increased and decreased by an enrichment analysis in the three isogenic strains. From the enriched pathways we found that all the CMP were found at least in one mutant, which corresponds to a phenomena that has been described previously in other studies (Zhang *et al.*, 2008; Xiong and Guan, 2012; Schilling *et al.*, 2015, 2019; Reverdy *et al.*, 2018; David G Christensen *et al.*, 2019). In fact, a study analysed the acetylation of 48 different bacterial species and determined that acetylation is highly conserved among bacteria for the regulation of the enzymes from the CMP (Nakayasu *et al.*, 2017).

In this study, we found that 96% of the total enzymes corresponding to the CMP presented acetyl-phosphate dependent acetylation sites. This supports the idea presented by Nakayasu *et al.*, 2017, that acetylation was one of the first regulation system for the enzymes belonging to the metabolic pathways. Interestingly, it was determined that acetyl-phosphate is the ancestor of ATP for the obtainment of energy. The molecule acetyl-phosphate was synthesised non-biologically and it showed to phosphorylate proteins just in the presence of water. In the study also, acetyl-phosphate was able to phosphorylate ADP to ATP (Camprubi *et al.*, 2018). Duan and Walther, 2015, proposed that each post translational modification (PTM) has a specific role in the cell. By the analysis of networks and enrichment of biological processes for each PTM they showed that proteins that have more phosphorylation sites, are more prone to interact with other proteins. This would suggest that the main role of acetylation in bacteria is to regulate the enzymes of the central

metabolic pathways, as described previously in several studies (Castaño-Cerezo *et al.*, 2009a, 2015; Wang *et al.*, 2010; Kim *et al.*, 2013; Sadykov *et al.*, 2013; Choudhary *et al.*, 2014; Venkat, Gregory, Sturges, *et al.*, 2017; Venkat *et al.*, 2018). This hypothesis is supported by the results found in the analysis of acetylation of the enzymes from each pathway from CMP.

The growth in different carbon sources showed a changed in the phenotype in *N. gonorrhoeae* and revealed that acetylation is important in the control of carbon metabolism. Furthermore, this is the first time that PTA-AK mutants were grown in lactate and pyruvate. In glucose, although all the strains grew, the isogenic strains Δ*ackA* and Δ*pta* presented a significant lower growth during the first 3 and 4 h, respectively. Therefore, the doubling time was significantly slower. This effect has been observed in other studies where the *pta* gene was mutated in *E. coli* and observed a slower growth in glucose compared to the WT (Chang *et al.*, 1999; Mizrahi, Biran and Ron, 2006). While in the strain Δ*hdac* the doubling time was significantly faster. In a study of a deacetylase mutant of *Mycobacterium tuberculosis* the growth was faster in fatty acids suggesting that the deacetylation of isocitrate lyase increased the metabolism and therefore the speed of growth (Bi *et al.*, 2017).

However, the growth phenotype changed radically when these two isogenic strains were grown in lactate and pyruvate. In bacteria, the oxidation of glucose leads to the formation of pyruvate and finally to acetyl-CoA. The unbalance of carbon catabolism and respiration leads to the accumulation of products, and this is known as carbon overflow (Castaño-Cerezo *et al.*, 2009b, 2015; Schilling *et al.*, 2015; Bernal, Castaño-Cerezo and Cánovas, 2016; De Mets, Van Melderen and Gottesman, 2019). The accumulation of products is found in the pyruvate node where pyruvate is converted to acetyl-CoA. Since acetyl-CoA is not metabolised through the TCA cycle due to the carbon overflow, it is reconverted into

pyruvate causing the intracellular accumulation and extracellular release of pyruvate (Wolfe, 2005).

PTA-AK pathway plays an important role in metabolism as the escape valve to handle the carbon overflow by producing and releasing acetate extracellularly, a phenomenon known as the acetate switch (Chang *et al.*, 1999; Wolfe, 2005; Bernal, Castaño-Cerezo and Cánovas, 2016; Schütze *et al.*, 2020). This switch in bacteria has been extensively studied and it has been related to the pathogenicity, virulence, biofilm formation, and response to stress. However, when the PTA-AK pathway has been altered by constructing mutants, the bacteria have shown a difference in their phenotypes. For instance, bacterial growth is decreased and there is a presence of secretion of lactate, pyruvate and formate instead of acetate (Holms, 1996; Dittrich, Bennett and San, 2008; Niu *et al.*, 2014; Castaño-Cerezo *et al.*, 2015; Bernal, Castaño-Cerezo and Cánovas, 2016). Indeed, a slower growth was observed in both the Δ*ackA* and Δ*pta* isogenic strains.

Although, the acetate switch has been longer studied, the reason for this change of metabolism has not been fully understood. However, in this study I proposed a mechanism that regulates the acetate switch by the acetylation of the first enzyme of the PTA-AK pathway.

As mention previously, the acetate switch occurs when there is carbon overflow due to an increase of substrates to be oxidised which leads to the secretion of other by products including pyruvate and lactate. This occurs in the pyruvate node, where the pyruvate is converted into acetyl-CoA through a series of reactions catalysed by the pyruvate dehydrogenase complex (PDC). This complex is encoded in an operon formed by the enzymes pyruvate dehydrogenase, dehydrolipoyl acetyltransferase, and dehydrolipoyl dehydrogenase (De Kok *et al.*, 1998; Yang, Bennett and San, 1999). This complex is

transcriptionally regulated by the repressor PdhR, which activity is inhibited in presence of pyruvate (Ogasawara *et al.*, 2007). Interestingly, in an *E. coli* Δ*pta* strain, the levels of PdhR were decreased by 10 fold compared to the WT but the PDC activity was increased. In this study, the researchers proposed a post translational modification as the regulatory mechanism of PdhR (Castaño-Cerezo *et al.*, 2009a). Contrary to *E. coli*, *N. gonorrhoeae* lacks the gene *pdhR* upstream to the PDC operon and the regulation of the PDC transcription has not been described (fig 4.25). However, the analysis of the upstream sequence of the gonococcus operon showed the palindromic sequences where PdhR binds the PDC promoter in *E. coli*. This could suggest that a different inhibition for the transcription of the *aceEF-lpd* operon occurs in *N. gonorrhoeae* or that the regulation of the activity of the PDC is directly on the enzymes by post translational modifications.

Interestingly, in the proteome of *N. gonorrhoeae* Δ*pta* we found a decrease in the expression of the dehydrolipoyl acetyltransferase, the component E2 of the PDC. Thus, the change of expression suggests that a transcriptional regulator repressor is regulated by acetylation and that it is active when it is deacetylated. The transcriptional regulators have shown an affinity to DNA, however, when they suffer acetylation the positive charge of the lysine residue that interacts with the negative charge of the phosphodiester backbone of DNA is inhibited and the proteins detach from the DNA. This phenomenon has been observed in several transcriptional regulators and DNA-binding proteins as histones (Kuhn *et al.*, 2014; Ghosh *et al.*, 2016; Sang *et al.*, 2017; Brosh, 2019; Ren *et al.*, 2019; Koo *et al.*, 2020). Indeed, a GntR transcriptional regulator (NGO1360) with a similar structure is found in the neisserial genome, however, it is found upstream from the *ace* operon, this regulator is flanking lactate-permease and the mtrCDE operon. This transcriptional regulator showed a decreased of acetylation in the site K252 in Δ*pta*. The decrease of acetylation increases the biding to DNA as mention previously. Therefore, repressing the

transcription of the *ace* operon. Indeed, qPCR of the component 2 of the PDC showed a decreased expression in Δ*pta* (table 5.1).

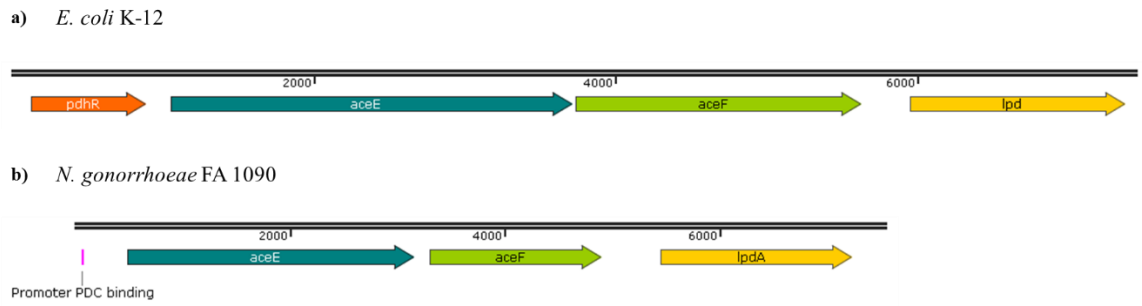


**Figure 4.25 *aceEF-lpd* operon.** The sequence from both operons were obtained from NCBI and the genes were mapped. a) The operon of *E. coli* K-12 possesses the *pdhR* gene downstream to the *aceE*. b) *N. gonorrhoeae* FA 1090 lacks of the *pdhR* in the operon. *pdhR*, pyruvate dehydrogenase transcriptional repressor; *ace*, pyruvate dehydrogenase E1; *aceF*, dehydrolipoyl acetyltransferase; *lpd*, dehydrolipoyl dehydrogenase.

Pyruvate dehydrogenase E1 (AceE) is one of the few enzymes that presented one of the highest number of acetylation sites. *Vibrio alginolyticus*, *Bacillus subtilis*, *Salmonella enterica* serovar Typhimurium, *E. coli* and *N. gonorrhoeae* have also shown high numbers of acetylation sites, suggesting a regulation of the enzyme by post translational modifications (Yu *et al.*, 2008; Kuhn *et al.*, 2014; Kosono *et al.*, 2015; Pang *et al.*, 2020). Indeed, phosphorylation of pyruvate dehydrogenase causes the inhibition of the enzyme (Sgrignani *et al.*, 2018). However, post translational modifications are not the only regulating mechanisms. Pyruvate dehydrogenase is also repressed at high concentration of acetyl-CoA and NADH (Hansen and Henning, 1966; Schwartz and Reed, 1970).

The regulation of the pyruvate node has been described, however, this does not explain the underlying mechanism of the carbon overflow. Furthermore, this explanation has not taken in account why in PTA-AK mutants the metabolism is slowed down and there is an increase of lactate and pyruvate secretion in other bacteria. It has been accepted that it is a

combination of different regulatory mechanisms involving catabolic repression, post translational modification but none of the studies have considered that this regulation could be driven by the acetylation of the PTA-AK pathway.

### 4.3.1 Carbon overflow is possibly regulated by acetylation of Pta

The analysis of the enzyme models to map all the acetyl-phosphate dependent sites, showed that some of the acetylation sites are found in the active sites and that this could be affecting the binding of the substrate. Thus, acetylation could possibly inhibit the enzyme activity. Indeed, some studies have reported the inhibition of the enzymatic activity by lysine acetylation. For instance, the acetylation of K55 decreased the activity of isocitrate dehydrogenase in *E. coli* (Venkat *et al.*, 2018); the deacetylation of the isocitrate lyase by the deacetylase CobB increases its activity in *E. coli* (Castaño-Cerezo *et al.*, 2014); DNA topoisomerase I reduced the binding to DNA when acetylated (Zhou *et al.*, 2018); and in *Mycobacterium tuberculosis* a similar effect was observed in the nucleoid-associated protein HU (Ghosh *et al.*, 2016). Interestingly, some studies have shown that acetylation stabilises protein-protein interactions, improves protein folding, and increases enzymatic activity (Lin *et al.*, 2013; Venkat, Gregory, Sturges, *et al.*, 2017; Ree, Varland and Arnesen, 2018).

Different studies have shown that acetylation neutralises the positive charge of the lysine residues and a change in the conformation of the active site (Tzeng *et al.*, 2004; Lu *et al.*, 2011; Xiong and Guan, 2012; Baeza, Smallegan and Denu, 2016; Nakayasu *et al.*, 2017; Barbosa Leite *et al.*, 2020). Moreover, the site of acetylation has been attributed to the sequence or to the secondary structure of the protein, finding the majority of acetylation in alpha helices (Lu *et al.*, 2011; Carabetta and Cristea, 2017). In a study conducted by Lu *et al.*, 2011, they modified the sequence of proteins by *in silico* mutagenesis to change lysine

residues that had been shown to be acetylated to other amino acids. They found that lysine residues stabilises the alpha helix structure, however, when acetylated the alpha helix is destabilised.

However, no study has considered the electrostatic charge surface (EPS) of the proteins as a clue to identify the location of acetylation. Only one study reported that the EPS was changed by the acetylation in the active site of the fructose 1,6-bisphosphate aldolase in *Trypanosoma brucei* (Barbosa Leite *et al.*, 2020). EPS accounts for the stability and conformation of the proteins, the charges that amino acids possess determine the interaction with neighbouring proteins and substrates (Strickler *et al.*, 2006; Tsai *et al.*, 2016; Vascon *et al.*, 2020). The analysis of EPS in all the central metabolic pathways showed that acetyl-phosphate dependent acetylation occurs in positive EPS.

The analysis of the 2,3-bisphosphoglycerate-dependent phosphoglycerate mutase (GPMA) revealed that acetylation occurred exactly in a cluster that showed a positive EPS. Furthermore, this cluster was found in the active site. The acetylation of K97 was shown to be highly regulated by acetyl-phosphate. Interestingly, in humans the acetylation of K100 in this enzyme was shown to inhibit its activity and it was regulated by a deacetylase Sirt1 (Hallows, Yu and Denu, 2012). The alignment of both sequences showed that the lysine residue is conserved in both organisms, however, in *N. gonorrhoeae* the regulation is by the acetyl-phosphate acetylation. This could suggest the evolution of the enzymatic activity regulation (fig. 4.26). This idea is supported by the evidence provided by Nakayasu *et al.*, 2017, where they found that acetylation sites were conserved among several bacterial species, and that 67% of enzymes from glycolysis and the TCA cycle were acetylated in active sites.

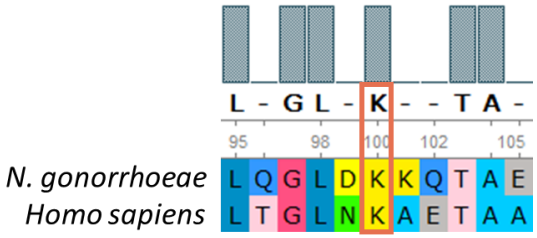


**Figure 4.26 Alignment of phosphoglycerate mutase sequences.** The sequences from *N. gonorrhoeae* (Uniprot: Q5F7C0) and *Homo sapiens* (Uniprot: P18669) were aligned by Clustal W and the site K100 showed to be conserved in both sequences.

The EPS analysis and acetylation mapping on the different enzymes of the central metabolic pathways suggests that enzymes from the Embden Meyerhof Parnas (glycolysis/gluconeogenesis), Entner-Doudoroff and pyruvate metabolism could be inhibited by acetyl-phosphate due to the acetylation of lysine residues that are part of the active sites. However, the enzymes from the TCA cycle did not present acetyl-phosphate dependent acetylation sites that could inhibit the enzymatic activity.

The aim to construct both isogenic mutant strains, Δ*ackA* and Δ*pta*, was not only to create strains of *N. gonorrhoeae* MS11 with different concentration of acetyl-phosphate but also used to observe the role of the acetate switch in the gonococcus. In this study, I propose a mechanism for the role of the PTA-AK pathway and the intermediate acetyl-phosphate in the regulation of the central metabolic pathway by the acetylation of enzymes (fig 4.27).

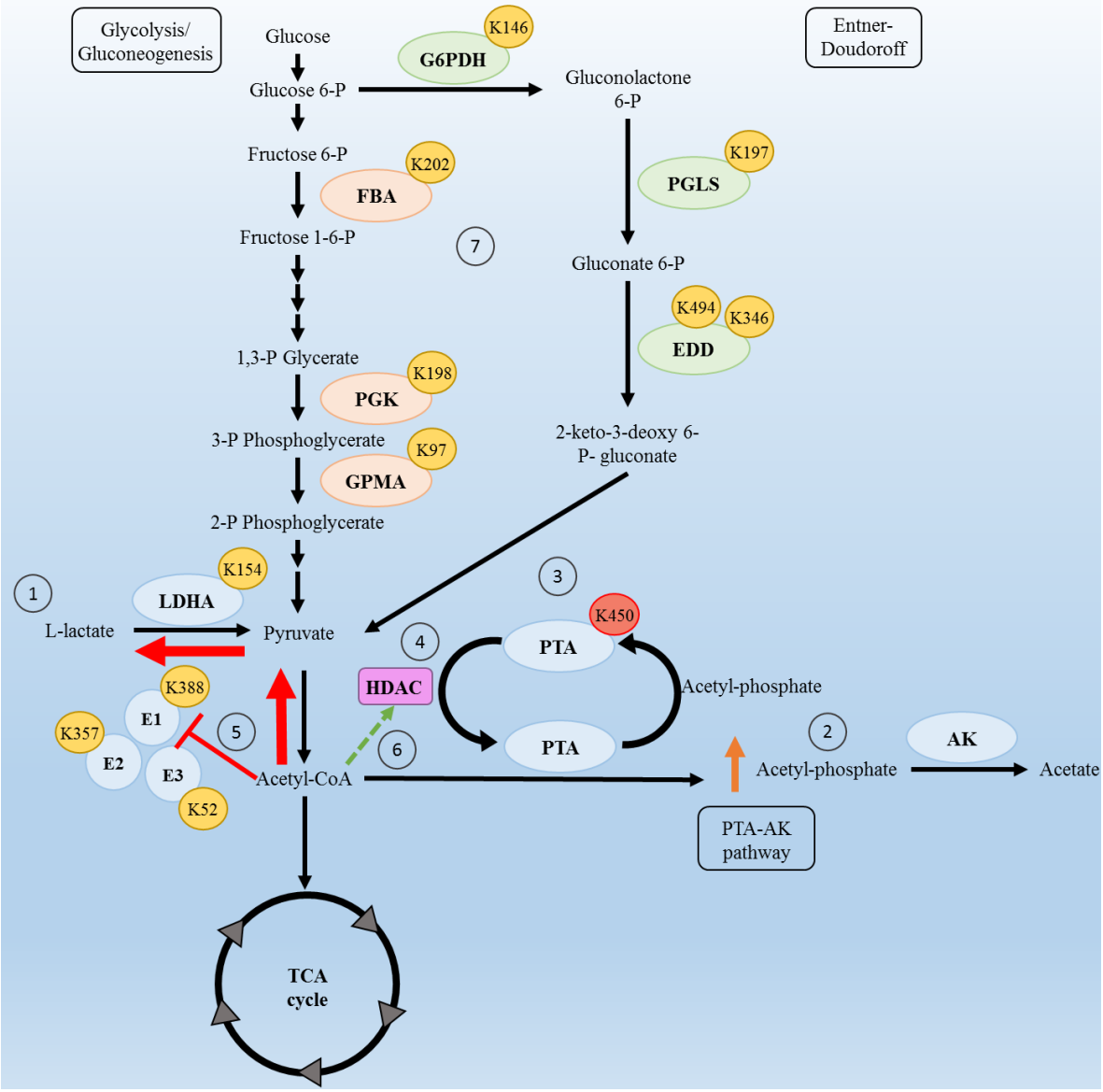


**Figure 4.27 Proposal of the regulation of the central metabolic pathway by acetylation.** The PTA-AK pathway converts acetyl-CoA to acetate with the production of acetyl-phosphate as intermediate metabolite. **1)** During carbon overflow, the TCA cycle is saturated and acetyl-CoA accumulates. One mechanism to deal with carbon overflow is to convert acetyl-CoA to pyruvate and lactate which then they are secreted. **2)** However, PTA-AK pathway is used as the secondary pathway to release the load of acetyl-CoA accumulation. This causes the increase of acetyl-phosphate concentration since the enzymatic activity of acetate kinase is lower than phosphotransacetylase. As consequence, acetyl-phosphate dependent acetylation increases and lysine residues of the enzymes are acetylated, some of them found in the active site. Acetylation

inhibits the activity of the enzymes. **3)** Phosphotransacetylase suggests an inhibition caused by the acetylation of K450, molecular docking showed interactions between K450 and the substrate acetyl-CoA. Moreover, this post translational modification alters the conformation of the active site pocket. K450 is a conserved residue found in 81% of the sequences analysed. **4)** In the isogenic strain Δ*hdac*, the fold change of acetylation for K450 was higher than in Δ*ackA* suggesting that this is a target for the histone deacetylase like protein (HDAC). Therefore, the acetylation by acetyl-phosphate and deacetylation by HDAC could be the regulatory mechanism for PTA. The acetylation of PTA causes the enzymatic inhibition, thus, the acetyl-CoA further accumulation. **5)** Acetyl-CoA inhibits the pyruvate dehydrogenase complex enzymatic activity which stops the carbon flux towards the TCA cycle. **6)** The accumulation of acetyl-CoA activates the activity of HDAC and the increase of acetyl-phosphate leads to a global acetylation of the CMP. **7)** However, this was only found to inhibit the enzymes from glycolysis, Entner-Doudoroff pathway and pyruvate metabolism. This suggests carbon overflow is regulated by the acetylation of the enzymes to halt the production of acetyl-CoA and favour the activity of the TCA cycle to oxidise the pool of acetyl-CoA and to maintain the homeostasis of the bacteria metabolism. When the levels of acetylation decrease due to the reduction of acetyl-CoA, the central metabolic pathway is re-activated. The enzymes show the acetyl-phosphate dependent acetylation sites that are located in the active site (yellow circle) and that were significantly increased. FBA, fructose-1,6-bisphosphatase class 1; PGK, phosphoglycerate kinase; GPMA, 2,3-bisphosphoglycerate-dependent phosphoglycerate mutase; G6PDH, glucose-6-phosphate 1-dehydrogenase; PGLS, 6-phosphogluconolactonase; EDD, Phosphogluconate dehydratase; E1, pyruvate dehydrogenase component E1; E2, dehydrolipoyl acetyltransferase; E3, dehydrolipoyl dehydrogenase; HDAC, histone deacetylase-like protein; PTA, phosphotransacetylase; AK, acetate kinase.

The metabolism of glucose in *N. gonorrhoeae* is catabolised through the Entner-Doudoroff pathway (EDP) (Stephen A. Morse, Stein and Hines, 1974; Chen *et al.*, 1989; Mizuno *et al.*, 2016). Interestingly, three from the four enzymes of the EDP showed an increase of acetyl-phosphate dependent acetylation in the active site, modifying the conformation of the cavity pocket and the interaction with the substrates. Moreover, this enzymes shown the highest fold change from the rest of the CMP. Entner-Doudoroff pathway is considered as the precursor of glycolysis, thus, the regulation of this pathway suggests that is driven by the ancient molecule acetyl-phosphate (Romano and Conway, 1996; Nakayasu *et al.*, 2017; Camprubi *et al.*, 2018).

The enzymes from gluconeogenesis that showed acetylation in the active site were fructose-1,6-bisphosphate aldolase (FAB), phosphoglycerate kinase (PGK), and 2,3-bisphosphoglycerate-dependent phosphoglycerate mutase (GPMA).

From these three enzymes FBA has an important role in the CMP of bacteria, thus the regulation of FBA is relevant. In glycolysis, FBA acts as the control point, it is also a transcriptional regulator for the transcription of genes involved in host redox homeostasis and immune response (Shestov *et al.*, 2014; Ziveri *et al.*, 2017). Fructose 1,6-bisphosphate, the product of FBA, has shown to regulate the activity of lactate dehydrogenase, acetate kinase, and phosphoenolpyruvate carboxylase (Sauer and Eikmanns, 2005; Puri *et al.*, 2014; Kim, Ahn and Burne, 2015). In *E. coli*, FBA has shown high levels of acetylation compared to other enzymes, however they showed that the enzymatic activity was not altered (Zhang *et al.*, 2013; Schütze *et al.*, 2020). Contrary to our results where acetylation suggests to inhibit the activity of FBA. Indeed, in *Trypanosoma brucei* it was determined that acetylation of K157 inhibits the activity due to a change in the conformation of the active site that inhibits the binding of the substrate (Barbosa Leite *et al.*, 2020).

The pyruvate metabolism showed the highest number of acetylation sites and it has been shown that the pyruvate node is the bottleneck for carbon overflow (Castaño-Cerezo *et al.*, 2009b; Bernal, Castaño-Cerezo and Cánovas, 2016). The accumulation of acetyl-CoA inhibits the activity of the pyruvate dehydrogenase complex, therefore, it is halted the conversion to pyruvate (Yang, Bennett and San, 1999; D. G. Christensen *et al.*, 2019; Schütze *et al.*, 2020). In this scenario, PTA-AK pathway converts acetyl-CoA to acetate to release the metabolism from carbon overflow, effect known as acetate switch. The acetate switch generates high levels of acetyl-phosphate (Wolfe, 2005; Valgepea *et al.*, 2010; Bernal, Castaño-Cerezo and Cánovas, 2016).

In this study, we propose that the increase of acetyl-phosphate led to the inhibition of the phosphotransacetylase (PTA) enzyme. K450 showed an increase of acetyl-phosphate dependent acetylation. This residue is located in the active site, moreover, it is a conserved site that showed 81% of conservation among 439 sequences of different species. Interestingly, the PTA activity was decreased in the Δ*ackA* isogenic strain which possessed high levels of acetyl-phosphate production (396.56 ± 87.94 $nmol^{-1}min^{-1}mg^{-1}$). The reduction of the enzymatic activity was by 4.5 folds compared to the WT (1789.43 ± 267.38. $nmol^{-1}min^{-1}mg^{-1}$) (table 3.1). Indeed, the growth of *N. meningitidis* in pyruvate showed that the enzymatic activity of PTA was decreased in pyruvate growth compared to glucose (Leighton *et al.*, 2001). The molecular docking revealed that this site interacts with acetyl-CoA and that the acetylation of K450 modifies the conformation of the active site, blocking the binding to the substrate. Although, this suggests that the enzymatic activity of PTA is regulated by acetylation further studies are needed to determine the role of K450.

Since K450 only showed an increase of acetylation in the strain Δ*ackA*, and no significant decrease of acetylation was found in Δ*pta*. This suggested that the deacetylation of K450

is enzymatically regulated. Indeed, the isogenic strain Δ*hdac* showed a higher fold change of acetylation in K450 compared to Δ*ackA*. In chapter 3, it was described the possible targets of HDAC and the site K450 of PTA was a candidate. This supports the idea that PTA is deacetylated by HDAC to activate the enzyme during carbon overflow when high levels of acetyl-phosphate are found. As mention previously, acetyl-CoA is accumulated during carbon overflow. Interestingly, it was demonstrated that acetyl-CoA activates HDAC (Vogelauer *et al.,* 2012). This suggests that the regulation of PTA is driven by negative feedback and HDAC.

Curiously, acetyl-phosphate dependent acetylation was only observed in the phase of the oxidation of glucose to acetyl-CoA, suggesting that acetylation only inhibits the enzymes for the formation of acetyl-CoA and TCA cycle is favoured to metabolise acetyl-CoA. In TCA cycle, only isocitrate dehydrogenase presented acetylation by acetyl-phosphate near the active site. Interestingly, a study conducted in *E. coli* showed the activation of isocitrate dehydrogenase when acetylated, contrary to what it has been described in enzymes from glycolysis, pentose phosphate pathway and pyruvate metabolism (Venkat *et al.*, 2018). However, in *N. meningitidis*, Leighton *et al.*, 2001, measured the enzymatic activity of the TCA cycle and PTA-AK pathway enzymes when the bacteria grew on either glucose or pyruvate. All enzymes showed a decreased in the enzymatic activity when growth in pyruvate compared to glucose. This suggests that increase of acetylation slows down the global enzymatic activity of the central metabolic pathways, however, TCA cycle enzymes are not inhibited by the acetylation of the active sites, as observed in this study. Indeed, in *Staphylococcus aureus* it was observed that metabolites from the TCA cycle were increased when the PTA-AK pathway was inactivated. Furthermore, they found a 4 fold increase of citrate synthase enzyme, the first enzyme that catalyses the conversion of acetyl-CoA to citrate (Sadykov *et al.*, 2013). As mention previously,

pyruvate accumulates during carbon overflow, thus, the growth in pyruvate resembles the conditions of carbon overflow due to the imbalance between oxidation and respiration.

Therefore, the proposed regulation of carbon overflow is that the increase of acetylation inhibits the production of acetyl-CoA by acetylating the active sites and blocking the binding of the substrates in the enzymes from glycolysis, Entner-Doudoroff and pyruvate metabolism. The PTA-AK pathway is also inhibited by the acetylation of the site K450 in PTA which blocks the production of acetate. This directs the flux of acetyl-CoA to TCA cycle where acetyl-phosphate acetylation was not found in the active sites of the enzymes. The depletion of acetyl-CoA leads to the decrease of acetyl-phosphate dependent acetylation, causing the reactivation of the production of acetyl-CoA. As consequence, the balance between oxidation and cellular respiration.

### 4.3.2 Future work

In order to prove this mechanistic proposal and to determine that in fact, ED and pyruvate metabolism is regulated by acetyl-phosphate. Enzymatic assay to measure enzymatic activity from each isogenic mutants must be performed. By analysing the enzymatic from each isogenic mutant would be possible to compare it to the WT and observe any increase or decrease of the activity. Furthermore, if any statistically significant difference is observed, the next step would be to perform site directed mutagenesis to determine if the lysine that showed to be acetylated by mass spectrometry and the structure analysis is indeed important for the regulation of the enzyme. The enzymes would it be more interesting to analyse in detail are pyruvate dehydrogenase, due to its high number of acetylation sites, and phosphotransacetylase, since the site K450 is locates in the active site and the histone deacetylase-like protein shows to target that site. This approach follows different studies where they have performed site-directed mutagenesis to change

the lysine residue that is acetylated for a neutral aminoacid as glutamine that mimics the structure of lysine (Venkat *et al.*, 2018). In a study conducted in *Trypanosoma brucei* the lysine of the aldolase active site was mutated by a glutamine, a polar uncharged amino acid that contains an amine group as lysine. They found that the enzymatic activity was decreased, showing that acetylation regulates the activity of aldolase (Barbosa Leite *et al.*, 2020). Therefore, this technique could be applied to enzyme Pta, G6PDH, EDD, and the PDC. If the enzymatic activity is altered, this would indicate that acetylation of the lysine regulates the activity.

# Chapter 5

## Role of acetyl-phosphate in the virulence of *Neisseria gonorrhoeae* MS11

# 5 Role of acetyl phosphate in the virulence of *N. gonorrhoeae* MS11

## 5.1 Introduction

Sexually transmitted infections (STI) are a major public health issue, the World Health Organisation (WHO) has estimated that every year, 376 million people get a STI (WHO, 2019b). In 2016, 86.9 million cases corresponded to the STI gonorrhoea, caused by the bacteria *N. gonorrhoeae* (Rowley *et al.*, 2019). The WHO has taken action due to the high prevalence and incidence of STI and has set a goal to reduce 90% of cases of gonorrhoea by 2030 (WHO, 2019a). However, since the discovery of azithromycin resistance of *N. gonorrhoeae* in 2009 in Japan, the number of cases with gonococcal resistant strains has increased (Yahara *et al.*, 2018). This has caused a surge of cases worldwide, in 2020, the UK reported the highest number of cases of gonorrhoea since it started to record data in 1918. The number increased from 56,232 in 2018 to 70,936 in 2019, this meant an increase of 26% (Wise, 2020).

*N. gonorrhoeae* is an obligate human pathogen that has evolved at the same time as human which has led the bacteria to adapt for survival. Therefore, it possesses many mechanisms to evade the immune system (Stern *et al.*, 1986; Lu *et al.*, 2018; Quillin and Seifert, 2018). Furthermore, it has shown to modulate the differentiation and regulation of immune system cells (Chen and Seifert, 2011; Ortiz *et al.*, 2015; Château and Seifert, 2016). The virulence of the gonococcus has been studied, however, the relation with acetylation has not been studied deeply.

In this chapter, we explore different mechanisms that might be altered by acetylation and an enzyme has been proposed as target to combat *N. gonorrhoeae*.

## 5.2 Results

In this chapter we analysed the effect of acetylation in the virulence of *N. gonorrhoeae*. Assays included proteomics, RT-qPCR, *Galleria mellonella* and human monocyte-derived macrophages (MDM), antibiotics resistance by disc diffusion and *in vitro* microscopy.

### 5.2.1 Acetylation alters the intracellular survival of *N. gonorrhoeae*

Macrophages (MΦ) are the first line of defence in the innate immunity. MΦ polarise depending on the infection, M1- MΦ shows a strong microbicidal activity and releases proinflammatory cytokines, while M2- MΦ is polarised during parasite infection, reduces inflammation and modulates the immune response (Boorsma, Draijer and Melgert, 2013; Duque and Descoteaux, 2014). *N. gonorrhoeae* is a pathogen with the capacity to survive intracellularly in polymorphonuclear cells and macrophages through different mechanism evading the immune response of the cells (Johnson and Criss, 2013; Atack *et al.*, 2014; Château and Seifert, 2016; Ritter and Genco, 2018). Interestingly, *N. gonorrhoeae* has been shown to modulate the polarisation and apoptosis of MΦ, and the production of cytokines, which makes the investigation of acetylation in *N. gonorrhoeae* an important area of study (Ortiz *et al.*, 2015).

Monocyte-derived macrophages (MDM) were isolated from healthy volunteer donors and infected with the 4 different isogenic strains of *N. gonorrhoeae* MS11. The assay was first optimised to determine the concentration of gentamicin and saponin to perform the experiment, as well as the growth curve in BHI to grow the bacteria prior to the infection of the MDM.

Gentamicin, the antibiotic that was used to kill the extracellular bacteria for the killing assay, was tested in the fours strains at 20, 50, 60, 70, 80, 90, 100 and 200 µg/mL and the

concentration that inhibited the growth by 99.98% was gentamicin 100 µg/mL. The optimisation was also performed for the detergent saponin, used to dissolve the MDM´s membrane. We tested the saponin at 0.5, 1, 1.5 and 2 % and 1.5% saponin that was ultimately used showed no effect in bacterial viability.

The growth in BHI showed that the mid-logarithmic phase was at 4 h, time used to collect the bacteria for the infection of the MDMs (fig. 5.1).

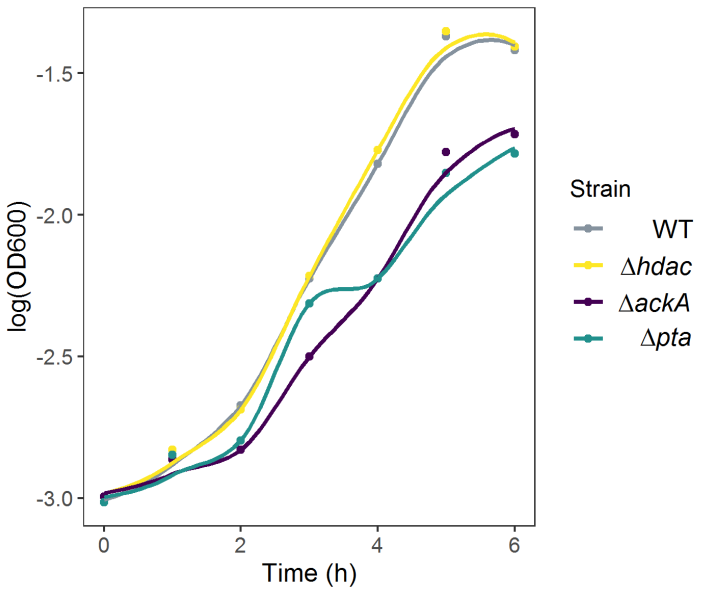


**Figure 5.1 Growth curve of isogenic strains of *N. gonorrhoeae* in BHI.** The strains were grown at 37 °C with shaking and the optical density (OD) was read at 600 nm every hour to determine the mid-logarithmic phase.

Once the conditions were standardised, MDM were infected with an MOI of 5 of the isogenic strains of *N. gonorrhoeae* MS11. The MDM were processed at 2 and 3 h post-infection to quantify the number of alive intracellular bacteria. The colony formation units were normalised to the initial inoculum. It was found that the isogenic strain Δ*ackA* after 2 h of infection was phagocytosed significantly higher than WT, although Δ*pta* was not significantly higher, it showed a tendency to be found in a higher amount compared to

the WT and Δ*hdac* strains. However, after 3 h post-infection, Δ*pta* was phagocytosed significantly higher than the three other strains (fig 5.2).

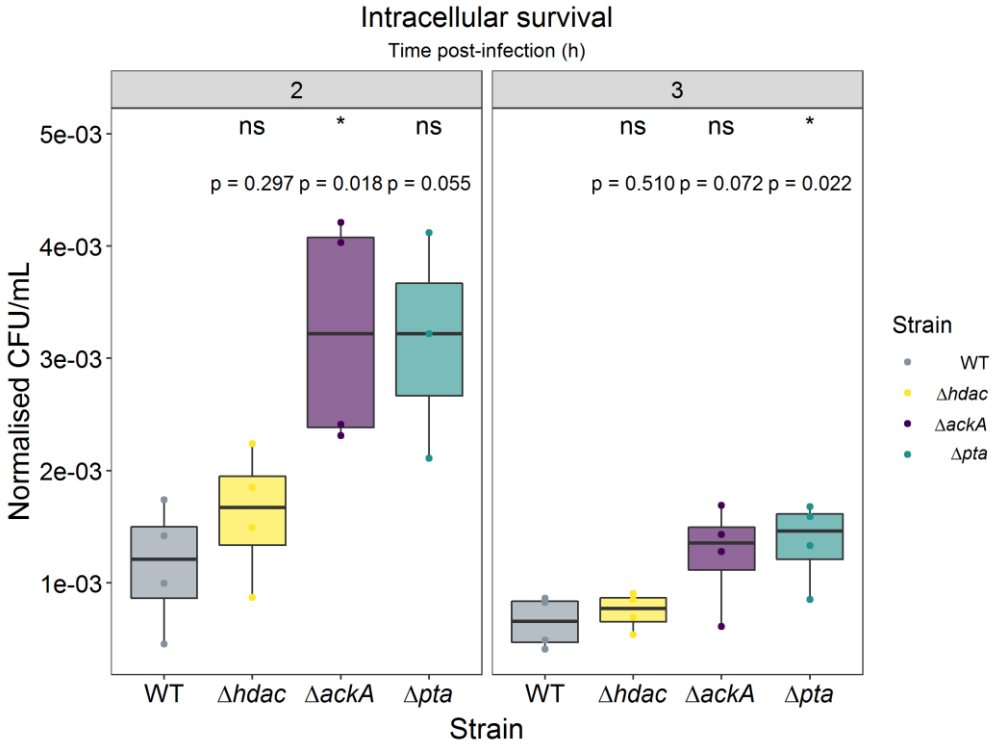


**Figure 5.2 Intracellular survival of *N. gonorrhoeae* in MDM.** MDM obtained after 14 days of differentiation were infected with the isogenic strains of *N. gonorrhoeae* with an MOI of 5. The MDM were lysed after 2 and 3 h post-infection and the dilutions $10^{-3}$ and $10^{-4}$ were plated by Miles-Misra technique to quantify the number of colony formation units (CFU) that were intracellular. The CFU/mL was normalised to the initial inoculum. A Student's t-test was performed for statistical analysis, setting the WT strain as the reference. The *p* value and significance are found at the top of the graph the experiment was performed with 3 technical replicates and 4 biological replicates each.

### 5.2.2 Acetylation in *N. gonorrhoeae* affects immune system evasion

In order to escalate the analysis of the intracellular survival of *N. gonorrhoeae*, fluorescence microscopy was employed. After several trials to obtain a neisserial strain that synthesises the green fluorescence protein (GFP) that resulted in no success (supplement fig 8.2), it was decided to label the bacteria with a fluorescence dye. Indeed,

the decision was a better approach for the purpose of the experiment to observe the phagocytosis of *N. gonorrhoeae* by monocyte-derived- macrophages (MDM).

MDM were stained with NucBlue which dyes the nuclei and the bacteria were stained with pHrodo. The latter is a pH sensitive dye, this molecule binds to the membrane surface of bacteria and emits low fluorescence at neutral pH and high fluorescence at acid pH. Therefore, this dye is used to observe phagocytosis, when MΦ engulf pathogens they are encapsulated in the phagosome which fuses with granules that acidify the phagosome in order to kill the pathogen (Lindner, Burkard and Schuler, 2020). In this experiment, the isogenic strains of *N. gonorrhoeae* were labelled with pHrodo, when the bacteria are found extracellularly they don´t emit fluorescence, however, when phagocytosed by the MDM the environment changes to an acidic pH which activates the fluorophore of pHrodo (green) and emits fluorescence a green fluorescence that is detected by the camera of the microscope (fig 5.3).

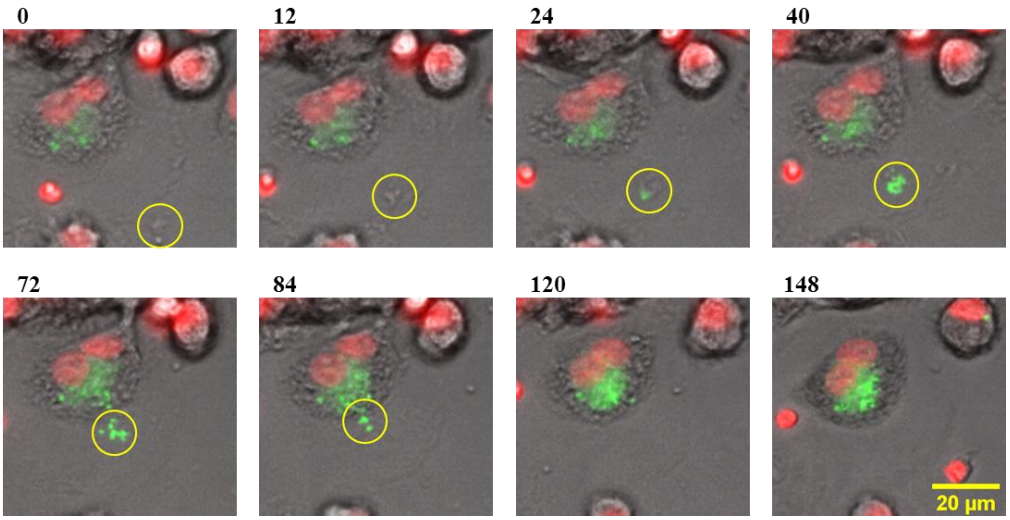


**Figure 5.3 Phagocytosis of *N. gonorrhoeae* labelled with pHrodo.** The images taken with a fluorescence microscope show the process of phagocytosis in MDM (red nucleus) and how pHrodo is activated by the decrease of the pH when the phagosome fuses with the lysosome to form the phagolysosome, emitting fluorescence. The process is indicated in minutes and inside the yellow circle is shown the engulfed bacteria.

MDM were infected with an MOI of 5 and a control condition was set with non-infected MDM. Pictures were taken every 4 min for 7.5 h using a 20x objective. Five locations at the centre of the well were chosen for each strain and a control which was MDM without bacteria. The nuclei are observed in a red colour and phagocytosed bacteria in green (fig. 5.3). The control showed no particles engulfed just a green background due to pHrodo traces. The four isogenic strain of *N. gonorrhoeae* showed phagocytosis of bacteria. In the fig. 5.4 is shown a location for each strain and the control. It was observed that the number of phagocytosed bacteria increased with time.

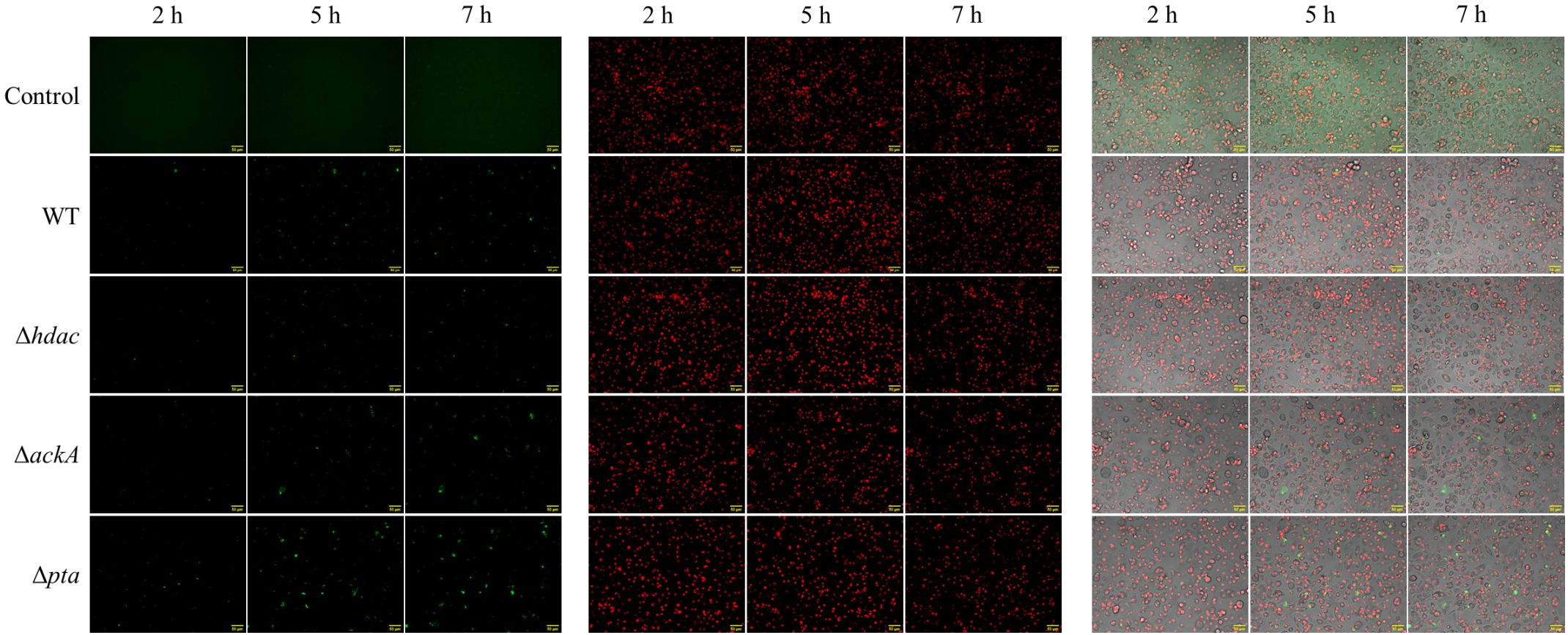


**Figure 5.4 Fluorescence microscopy for *in vitro* phagocytosis of *N. gonorrhoeae* MS11 by MDM.** *In vitro* microscopy of MDM phagocytising *N. gonorrhoeae*. Pictures were taken with a 20x objective every 4 minutes for 7.5 h in a fluorescent microscope in a chamber with $CO_2$ at 37 °C. The bacteria were stained with pHrodo dye (green, left) and MDM with NucBlue (red, middle), and the image was merged with the bright field channel and the two fluorescent channels (right). The diagram shows the MDM control which was not infected, and the MDM infected with each of the four isogenic strains of *N. gonorrhoeae* MS11. The pictures are from 2, 5 and 7 h post-infection. The bar scale at the bottom right indicates 50 µm.

The images were analysed using ImageJ as described in section 2.15.2. Briefly, the file was adjusted to a certain threshold to detect only the desired component of the image (nuclei or bacteria), the image was then masked and the particles were analysed to quantify the number of either nuclei of bacteria in the image.

The analysis was divided for the number of cells and bacteria by splitting the image in channels, according to the dye used. The average size of more than 894,000 nuclei showed two populations across all conditions, with an average size of 38 $\mu m^2$ and 67 $\mu m^2$ (fig. 5.5a). The total area was analysed and comprises the total area that cells or bacteria occupy in the image. In cells, we observed two peaks in the density of the total area at 38 $\mu m^2$ and 67 $\mu m^2$ and the total area decreased after 5 h in all conditions. However, cells infected with *N. gonorrhoeae* MS11 WT increased in number and the number stabilised after 6 h post-infection. In bacteria, the total area detected, corresponded to the bacteria phagocytosed by MDM (fig. 5.5b-c). Phagocytosis was similar for all the strains at 2 h post- infection except for *N. gonorrhoeae* M11 Δ*pta* which was increased. However, the differences in the level of phagocytosis across the four strains changed after 4 h of infection and the tendency continued until the 7 h. The strains Δ*ackA* and Δ*hdac* were significantly less phagocytosed compared to the WT. Interestingly, the isogenic strain Δ*pta* was phagocytosed significantly higher than WT (fig 5.5d).

The ratio between the total area of cells and bacteria showed that cells infected with *N. gonorrhoeae* M11 Δ*pta* was higher compared to the WT, while it was lower in the isogenic strains Δ*ackA* and Δ*hdac* after 6 and 7 h post-infection. Curiously, the curve for ratio of number of cells and bacteria showed the similar pattern, however, in the WT it was observed that the curve flattened from 5 h post-infection. The relation between total area and number of cells and bacteria showed that in the isogenic strain Δ*pta* the relation was lower (fig. 5.5e-h).

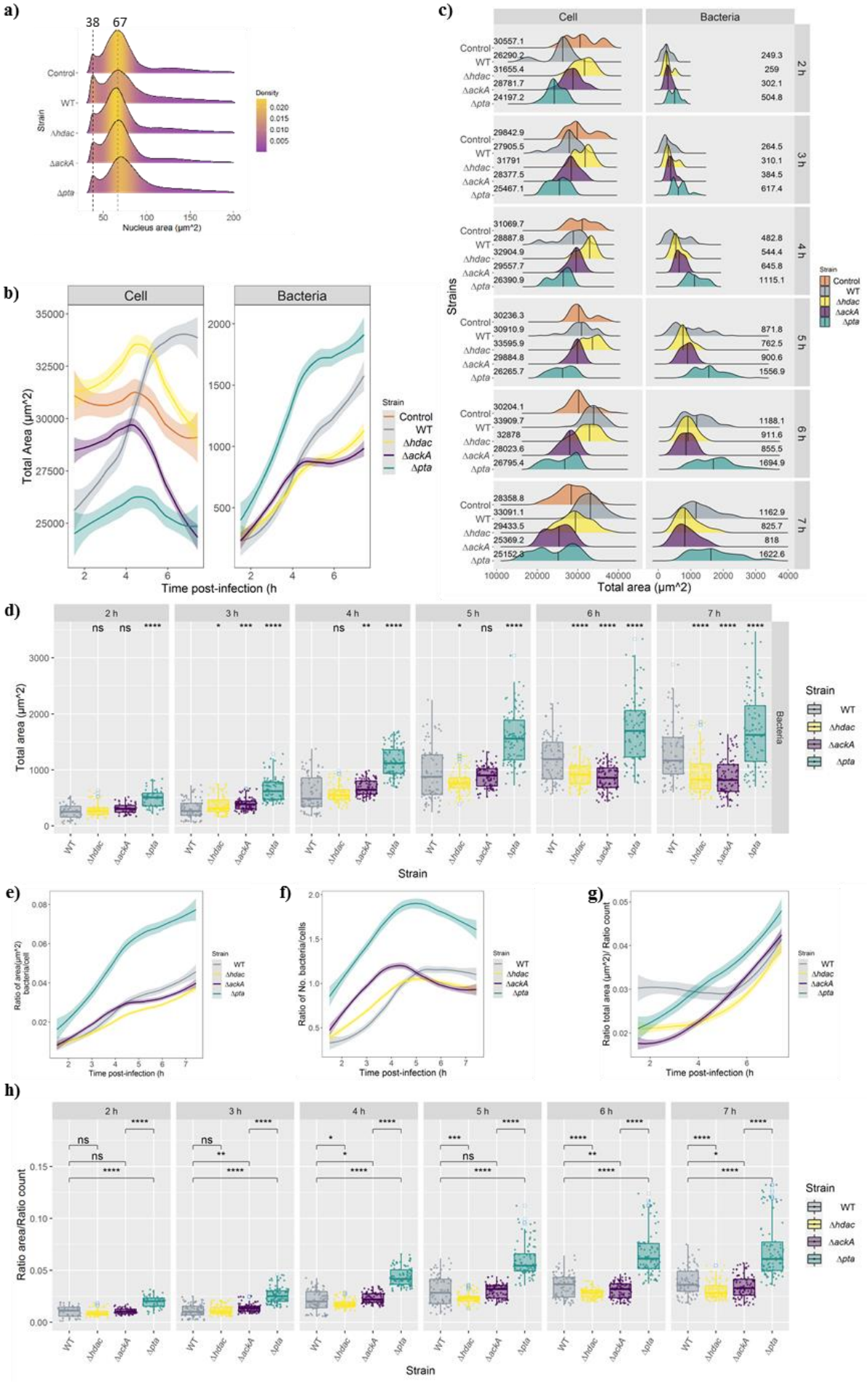
a)
38
67
Control
WT
Δhdac
ΔackA
Δpta
Strain
Density
0.020
0.015
0.010
0.005
50
100
150
200
Nucleus area (μm^2)
b)
Cell
Bacteria
Total Area (μm^2)
Time post-infection (h
Strain
Control
WT
Δhdac
ΔackA
Δpta
c)
Cell
Bacteria
Strains
2 h
3 h
4 h
5 h
6 h
7 h
Total area (μm^2)
d)
Total area (μm^2)
Bacteria
Strain
e)
Ratio of area(μm^2) bacteria/cell
Time post-infection (h
f)
Ratio of No. bacterial/cells
Time post-infection (h
g)
Ratio total area (μm^2)/ Ratio count
Time post-infection (h
h)
Ratio area/Ratio count
Strain

**Figure 5.5 Analysis of fluorescence microscopy. a)** Density of average size of the nuclei for the five conditions. The two highest peaks show the two most frequent average sizes of cells in $\mu m^2$. **b)** Total area of cells and bacteria. **c)** Density plots of the total area of cells and bacteria for every hour. **d)** Boxplot comparing the total area of bacteria phagocytosed every hour. **e)** Ratio of total area between cells and bacteria. **f)** Ratio of number of cells by number of bacteria. **g)** Relation between the ratios of total area and count. **h)** Boxplot for the comparison of the relation between total area and number. For the statistical analysis *N. gonorrhoeae* WT was set as reference and a T-test was performed. The significance is shown at the top of the plots. ns, no significance;*, *p* value <0.05; **, *p* value <0.01; ***, *p* value <0.001; ****, *p* value < 0.0001.

This experiment was only performed once due to the beginning of the pandemic and no further technical replicates where performed. The experiment and analysis performed was from 5 different images taken from 2 different wells. Although, it is not enough replicates to conclude a result, this experiment shows that acetylation could be involved in the virulence of *N. gonorrhoeae*. Since the isogenic strains Δ*ackA* and Δ*hdac* were less phagocytosed and Δ*pta* more phagocytosed, this could suggest that acetylation is correlated to the evasion of phagocytosis.

### 5.2.3 Pili biosynthesis and a two-component system is possibly altered by acetylation

*N. gonorrhoeae* is an obligate human pathogen and possesses the ability of intracellular survival. In order to colonise new tissues, the gonococcus binds to the cells and it is internalised. *N. gonorrhoeae* possesses different molecules that are involved in the binding to host cells including Opa proteins, porins, lipooligosaccharides, and type IV pili (Edwards and Apicella, 2002, 2004; Edwards, 2010; Criss and Seifert, 2012; Sintsova *et al.*, 2015; Quillin and Seifert, 2018).

In order to regulate the synthesis of these adhesion molecules and other virulence factors, bacteria possess a number of transcriptional regulatory systems including two-component systems (TCS). TCS function as sensors for chemical and physical signals from the environment. The TCS are formed by of two proteins, a sensor kinase and a response regulator. When an external signal is detected by the bacteria the sensor kinase phosphorylates the response regulator which leads to a response, usually in the transcription of a gene. Previous studies have shown that AcP can act as a direct phosphoryl donor of the response regulator of TCS (Klein *et al.*, 2007; Mitrophanov and Groisman, 2008).

*N, gonorrhoeae* is reported to have three TCS; NtrXY (NGO1866, NGO1867) and NarPQ (NGO0752, NGO0753), these TCS regulate the expression of genes involved in the respiration and the adaptation to anaerobic environment, respectively; and MisRS (NGO0177, NGO0176) which is involved in the virulence of the gonococcus, this TCS regulates the synthesis of membrane proteins when the gonococcus is in stress conditions (Overton *et al.*, 2006; Atack *et al.*, 2013; Gangaiah *et al.*, 2017).

From the previous experiment it was suggested that acetylation is involved in the virulence of the bacteria by evading phagocytosis. Therefore, we examined the expression of genes and proteins of the molecules involved in the adhesion to cells, as well as a killing assay in the animal model of *Galleria mellonella* to observe the virulence of the isogeneic strains of *N. gonorrhoeae* MS11.

Interestingly, we found that proteins that are involved in the synthesis or as a component of the type IV pili were expressed significantly different only in the isogenic strains Δ*ackA* and Δ*pta*. The strain Δ*hdac* showed no significant difference in the expression of proteins. The isogenic strain Δ*ackA* showed a significant lower expression of the protein MafA (NGO0229) and an increase of the pilin protein PilA (NGO11165). While the strain Δ*pta* showed a significant decrease of the pilus assembly protein PilC (NGO0055). The protein decreased in both strains was the fimbrial protein pilin pilS2c1 (NGO10980) (fig 5.6).

**a)**

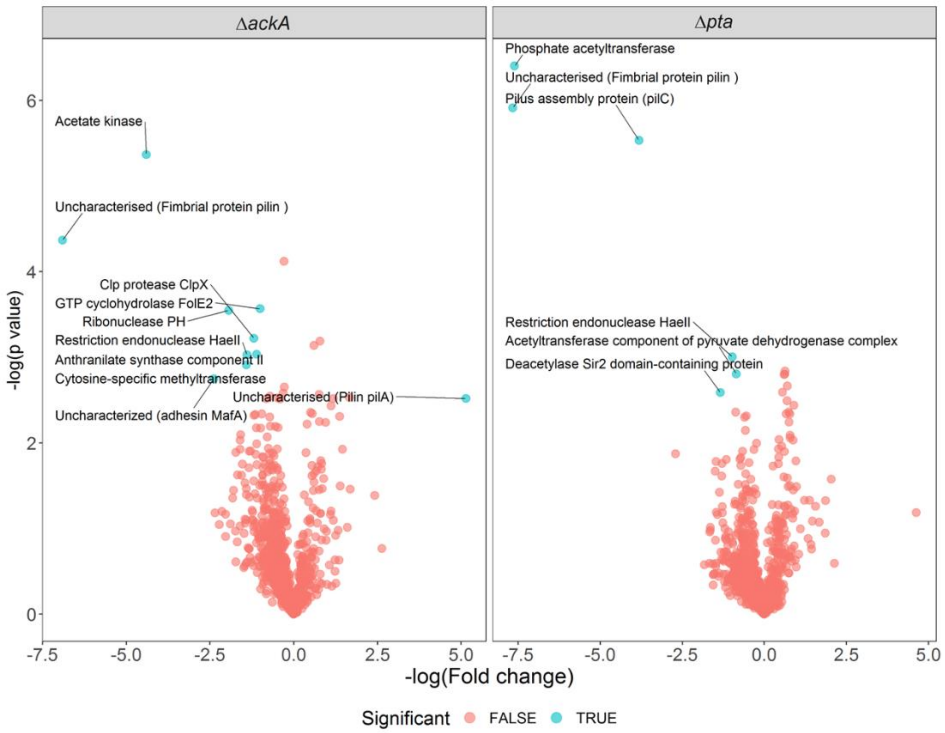


**b)**

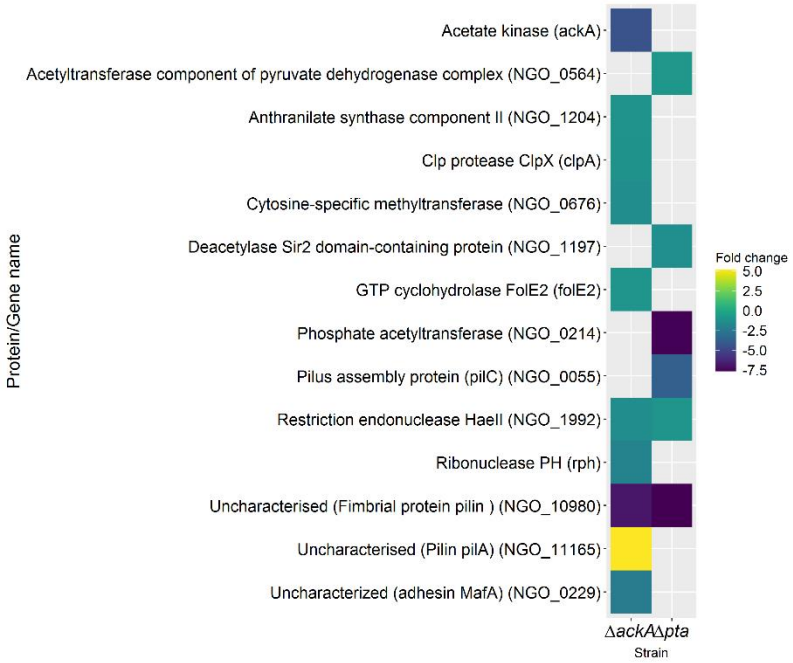


**Figure 5.6 Volcano plot of the proteome of *N. gonorrhoeae*. a)** Protein extracts of the isogenic strains were analysed by mass spectrometry and the expression was analysed. In red and blue are the non-significant and significant different proteins for the isogenic strains Δ*ackA* and Δ*pta*. The significant different proteins are labelled with the name and abbreviation. **b)** Significant different expressed proteins identified from mass spectrometry. The gene name or locus is shown next to the protein name. Experiment with 4 technical replicates.

To observe if acetylation alters the virulence of *N. gonorrhoeae,* a killing assay using *G. mellonella* was performed. *G. mellonella,* commonly known as wax moth, is an insect that has been used for the study of bacterial pathogenesis and virulence (Leuko and Raivio, 2012; Loh *et al.*, 2013; Mizerska-Dudka and Andrejko, 2014; Tsai, Loh and Proft, 2016).

To determine the median lethal dose ($LD_{50}$) of *N. gonorrhoeae* MS11 and if *N. gonorrhoeae* MS11 killed *G. mellonella*, groups of 15 larvae were infected with different concentrations of *N. gonorrhoeae* MS11. After 144 h a 60% survival was observed with the concentration of bacteria at $10^8$ CFU/mL (fig. 5.7a). This concentration was then used for the infection with the isogenic mutant strains.

The virulence of the neisserial strains WT, Δ*pta*, and Δ*ackA* were compared (fig 5.7b). The non-infected group of the larvae showed a survival of 100%. However, the larvae infected with Δ*ackA* died 3 times faster compared to the WT and with a similar percentage of survival of 27% compared to the 60% of the WT. In contrast, the isogenic Δ*pta* strain showed after 6 days post-infection a survival percentage of 87%, higher than the WT and similar to the group infected with PBS. In order to prove the survival of the gonococcus within the larvae, samples of haemolymph from each group were plated on CHO and GC-Kanamycin agar plates. Gram staining revealed the presence of diplococcus suggesting that the three strains of *N. gonorrhoeae* MS11 were viable from larvae.

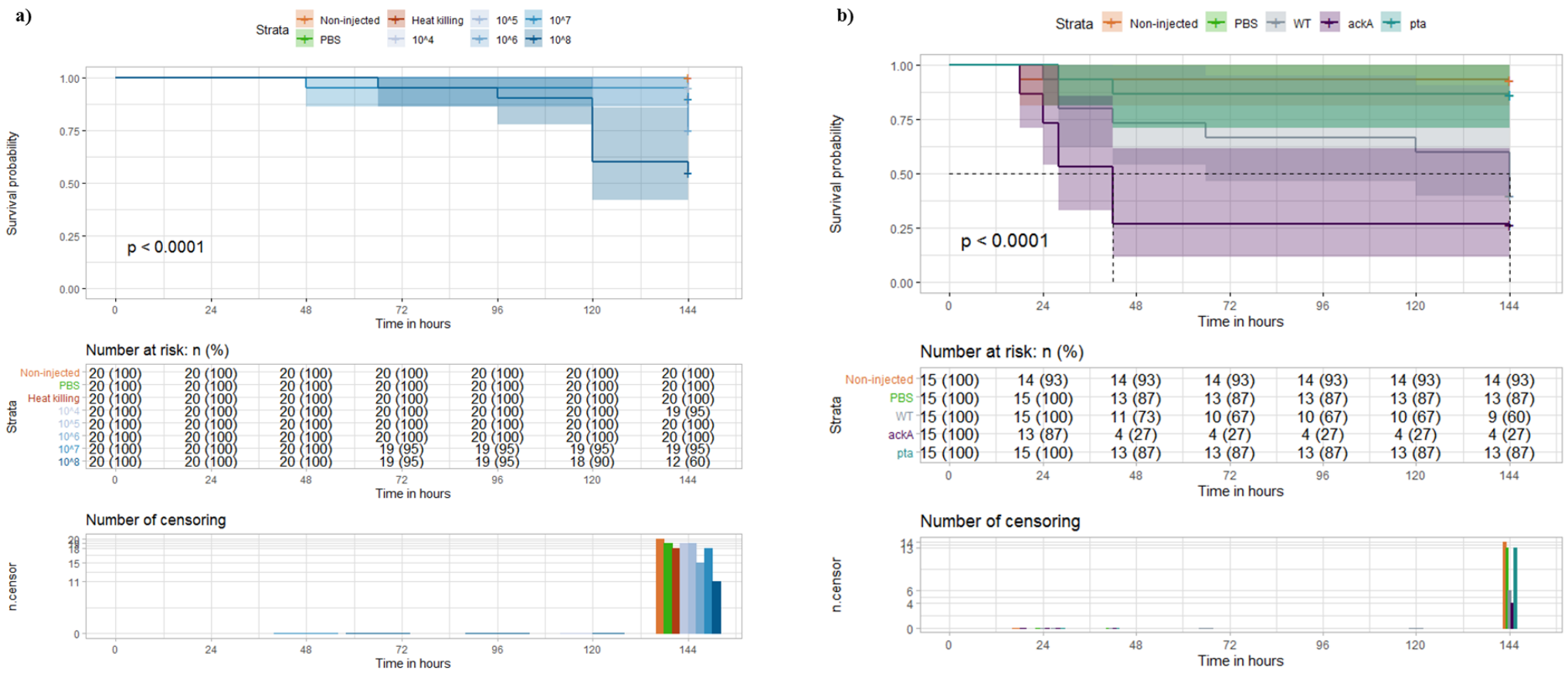


**Figure 5.7 Killing assay of *Galleria mellonella* infected with *N. gonorrhoeae*.** Survival graph at top showing the percentage of survival for 6 days of experiment recording results every 24 h. The table in the middle shows the number of larvae at risk of dying and the bottom graph shows the number of alive larvae for each day. **a)** Groups of 20 larvae were infected each with 10 µL of different gonococcus concentration. Three groups were used as control; one infected with PBS; non-infected; and to observe if the larvae dead was indeed caused by live bacteria the bacterial growth was heat killed at 95 °C for 10 min. After 6 days post-infection a survival of 55% was only observed in the group of larvae infected with the highest dilution infected with approximately 3.14x105 CFU. The t-test showed a significant difference between for the larvae infected with $10^8$ CFU. **b)** Larvae were infected with the three strains. WT, Δ*pta*, Δ*ackA* strains. The group inoculated with Δ*pta* showed a higher survival than WT, similar to the control group infected with PBS. In contrast, Δ*ackA* was the strain with the lowest survival. The t-test shows a significant difference of the survival between larvae infected with Δ*ackA* and WT.

Since pili proteins and the virulence of the gonococcus showed alteration. The expression of genes related to pili biosynthesis and the two-component system were quantified. The primers for RT-qPCR were designed using Primer Blast website. In order to prove that the primers were specific, PCR was performed using as template the gDNA from the fours neisserial strains. All set of primers showed specificity except PilEuss2 and PilS2c1 (fig 5.8a-c). However, after RT-qPCR the gene PilS2c1 showed specificity (fig 5.8d). RNA was extracted from the 4 neisserial strains and a gel was run to prove the extraction (fig 5.8e). Thus, the RT-qPCR was standardised by doing a standard curve using as housekeeping gene the 16S rRNA. It was determined that best RNA concentration for the RT-qPCR was 0.1 ng due to the CT value which was higher than 10 (fig 5.8f).

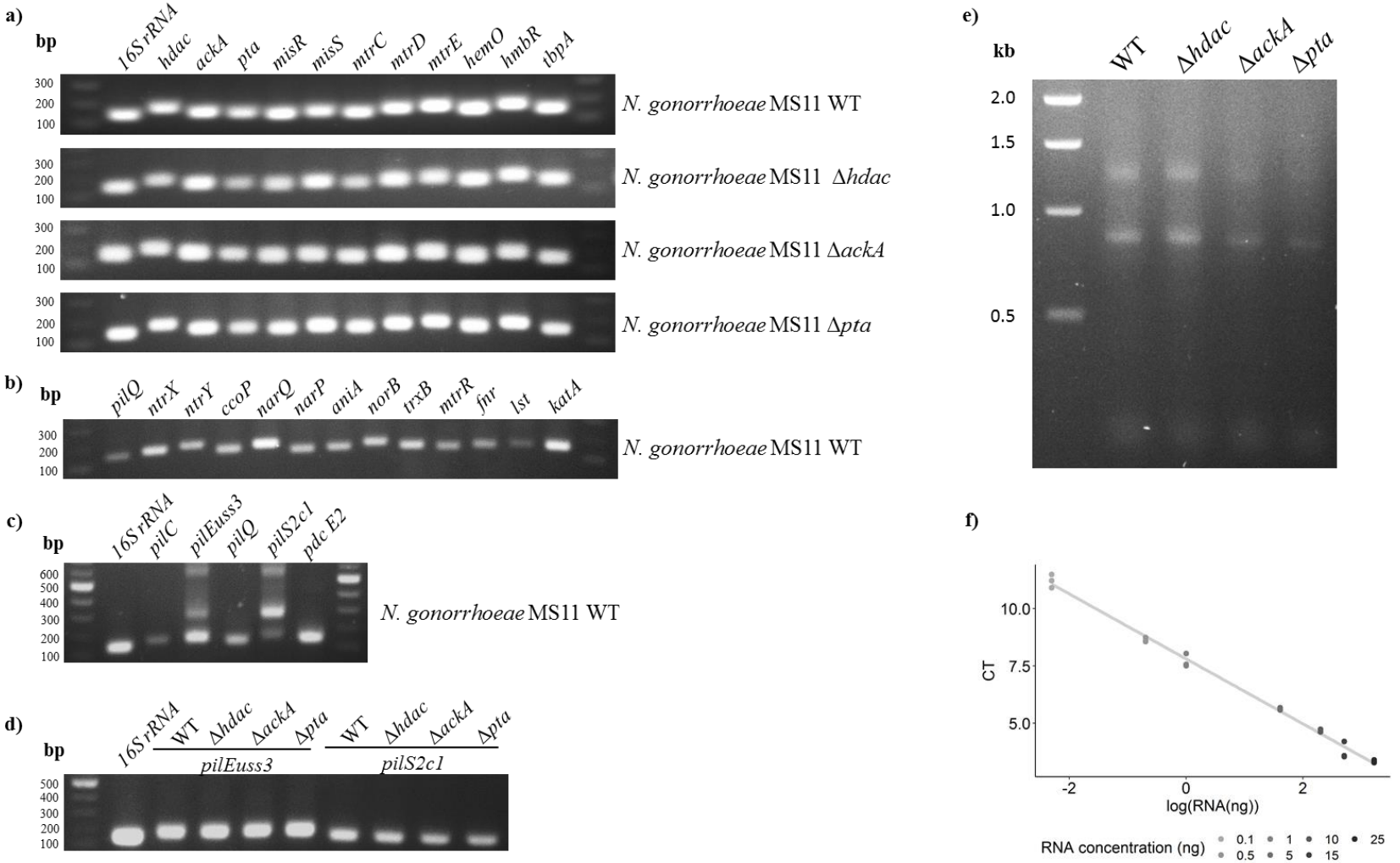


**Figure 5.8 Quality control of primers for RT-qPCR of genes involved in virulence of *N. gonorrhoeae*. a)** Agarose gel of the genes amplified by PCR of the four neisserial isogenic strains. **b)** PCR of genes involved in two-component system and oxidative stress. **c)** PCR of genes involved in pili biosynthesis and pyruvate metabolism. **d)** Amplification of pilEuss3 and pilSc1 after RT-qPCR. **e)** Agarose gel of RNA extraction from fours isogenic strains. **f)** Standard curve of RNA concentration using 16SrRNA as housekeeping gene; n=3.

In total, 23 genes were quantified from the fours isogenic strains. The relative mRNA expression was calculated from the quantification of the WT mRNA expression (supplement fig 8.3). The mRNA from TCS genes showed significant different expression especially in the regulator proteins. The genes *narP* and *ntrX* showed a significant decrease of expression in the isogenic mutant ΔackA, while an increase of the regulator *misR* was observed in this strain. The isogenic strain Δpta showed a significant decreased of *ntrX*.

Expression of genes controlled by the *misSR* TCS showed significant differences. Genes involved in iron acquisition were expressed at a higher level compared to the WT. The mutant Δ*ackA* showed a significant increase of *hemO* and *tbpA* a relative expression of 1.8 and 1.5, respectively. While Δpta showed an increase in *hmbR* and *tbpA* with an expression of 3.3 and 3.6, respectively. The unique gene from the multidrug efflux pump that showed a significant difference was *mtrD* in the strain Δpta with a relative expression of 1.7. Interestingly, the results of genes involved in the pili biosynthesis corresponded to the proteome. The gene *pilS2c1* showed a significant decrease in ΔackA and Δpta with a relative expression of 0.2 and 0.3, respectively. *pilQ* showed a significant decrease in the three isogenic strains Δhdac, ΔackA, and Δpta (table 5.1).

**Table 5.1 Gene expression in isogenic strains of *N. gonorrhoeae* MS11.** Gene expression was quantified by RT-qPCR and the relative expression level of mRNA was determined from *N. gonorrhoeae* MS11 WT gene expression. The relative expression was compared by t-test statistical analysis. The table shows the genes that showed a significant decreased or decreased expression, followed by the significance and the mean of the relative mRNA expression and the standard deviation. Each gene expression was replicated 3 to 5 times.

| Type | Gene | Δ*hdac* | Δ*ackA* | Δ*pta* |
|---|---|---|---|---|
| PTA-AK pathway | *ackA* | ns/0.662 ± 0.273 | ns/1.03 ± 0.241 | ns/0.98 ± 0.323 |
| | *pta* | ns/0.939 ± 0.452 | Increased */1.56 ± 0.331 | ns/1.514 ± 0.518 |
| Pyruvate metabolism | *aceE E2* | ns/0.998 ± 0.231 | Decreased **/0.349 ± 0.032 | Decreased **/0.293 ± 0.022 |
| Transcriptional repressor | *fnr* | ns/0.754 ± 0.126 | Decreased **/0.56 ± 0.02 | Decreased */0.758 ± 0.093 |
| | *mtrR* | ns/0.503 ± 0.393 | ns/0.777 ± 0.205 | ns/1.486 ± 0.268 |
| TCS | *misR* | ns/0.831 ± 0.198 | Increased **/2.308 ± 0.341 | ns/1.233 ± 0.376 |
| | *misS* | ns/1.071 ± 0.925 | ns/1.558 ± 0.478 | ns/1.997 ± 0.568 |
| | *narP* | Decreased */0.701 ± 0.02 | Decreased **/0.563 ± 0.032 | ns/0.921 ± 0.126 |
| | *narQ* | ns/0.657 ± 0.507 | ns/0.637 ± 0.315 | ns/1.317 ± 0.401 |
| | *ntrX* | Decreased */0.776 ± 0.025 | Decreased **/0.388 ± 0.092 | Decreased **/0.672 ± 0.019 |
| | *ntrY* | ns/0.78 ± 0.213 | Decreased */0.609 ± 0.03 | Increased */1.35 ± 0.059 |
| Oxidative stress | *ccoP* | ns/0.725 ± 0.328 | ns/0.698 ± 0.721 | Decreased */0.442 ± 0.221 |
| | *kat* | Decreased */0.452 ± 0.008 | Decreased */0.317 ± 0.127 | ns/0.691 ± 0.178 |

| | | | | |
|---|---|---|---|---|
| Iron acquisition | *hemO* | ns/0.749 ± 0.12 | Increased */1.837 ± 0.312 | ns/1.282 ± 0.597 |
| | *hmbR* | Increased */1.986 ± 0.481 | ns/1.624 ± 0.543 | Increased **/3.344 ± 0.643 |
| | *tbpA* | Increased */1.584 ± 0.077 | Increased */1.516 ± 0.283 | Increased **/3.635 ± 0.916 |
| Multidrug efflux pump | *mtrC* | ns/0.673 ± 0.264 | ns/1.16 ± 0.381 | ns/1.152 ± 0.251 |
| | *mtrD* | ns/0.704 ± 0.448 | ns/0.931 ± 0.181 | Increased **/1.696 ± 0.101 |
| | *mtrE* | ns/0.737 ± 0.093 | ns/1.384 ± 0.264 | ns/0.988 ± 0.282 |
| Pili biosynthesis | *pilEuss3* (NGO_11165) | ns/0.495 ± 0.258 | ns/0.739 ± 0.519 | ns/1.186 ± 0.33 |
| | *pilQ* | Decreased */0.546 ± 0.258 | Decreased **/0.324 ± 0.26 | Decreased **/0.398 ± 0.238 |
| | *pilS2c1* (NGO_10980) | ns/0.915 ± 0.407 | Decreased **/0.247 ± 0.159 | Decreased **/0.316 ± 0.261 |
| Sialyltransferase | *lst* | ns/1.104 ± 0.426 | ns/0.9 ± 0.626 | ns/1.26 ± 0.784 |

ns, no significance;*, $p$ value <0.05; **, $p$ value <0.01

Interestingly, the acetylome showed significant different acetylation in several virulence factors, including pili, two-component system protein, iron-acquisition protein and transporters, porin and multidrug efflux pumps (supplement fig 8.4).

The proteins type IV pilin (NGO_0465) and pilus assembly protein PilP (NGO_0095) showed the highest number of significant increased acetylation sites compared to the other pili proteins. The isogenic strain Δ*ackA* showed more acetylation sites in the PilP protein (fig 5.9). This protein is related to the protein PilQ for the polymerisation of the pili (Drake, Sandstedt and Koomey, 1997; Chen *et al.*, 2004).

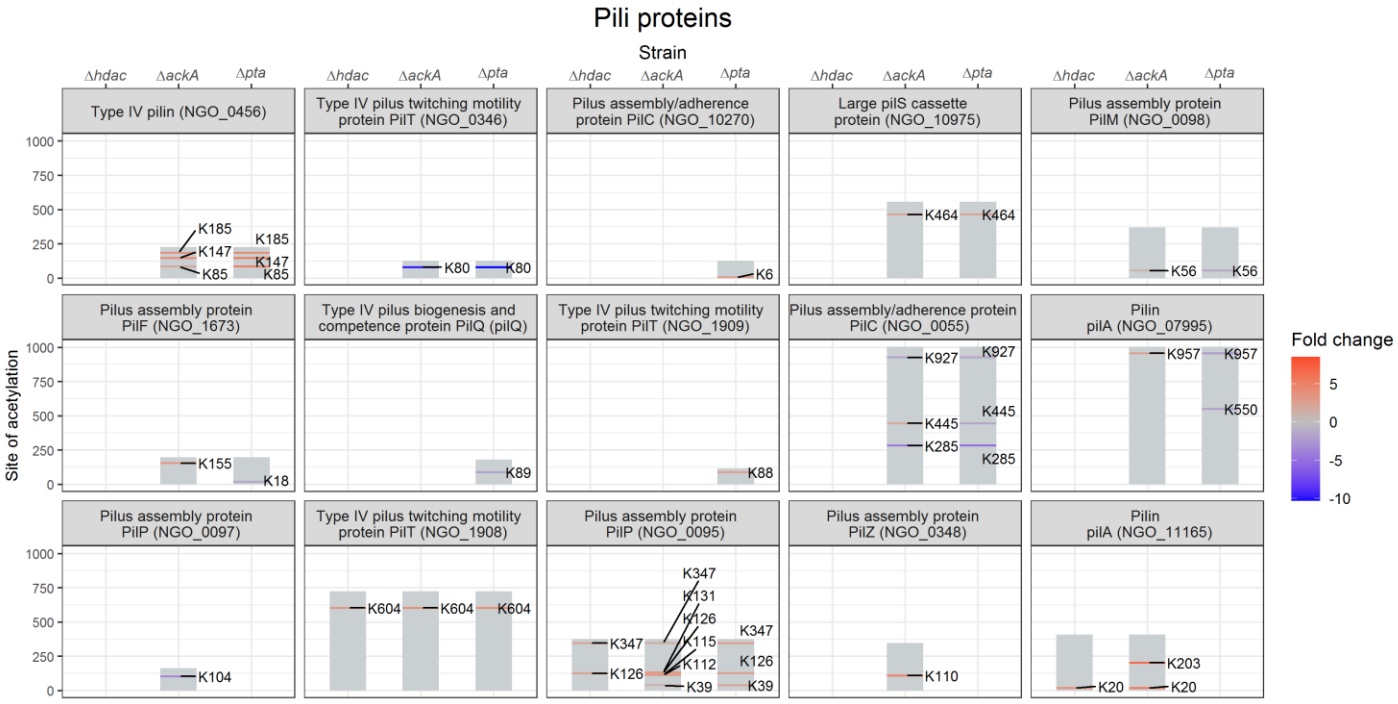


**Figure 5.9 Acetylation sites of pili-related proteins.** The significant different acetylation sites of the pili-related proteins were identified. Each plot shows the protein name and locus. The tiles are fill with a gradient according to the fold change in acetylation. The bar at the background shows the length of the protein.

Finally the antibiotic resistance of the isogenic strains was performed by the method of disc diffusion for the growth inhibition. Five different families of antibiotics were tested. Beta-lactam and cephalosporin are a family of antibiotics that inhibit the bacterial wall synthesis. Δ*ackA* and Δ*pta* showed significant decrease of resistance to the six antibiotics (fig 5.10a). Aminoglycoside, fluoroquinolone and naphtacene are a family of antibiotics that inhibit protein synthesis by binding to the ribosomes and the latter inhibits replication. From the three different antibiotics used, only Δ*ackA* and Δ*pta* showed a significant decrease of resistance to ciprofloxacin which inhibits replication. (fig 5.10b). Interestingly, Δ*hdac* showed no significance difference to any antibiotic.

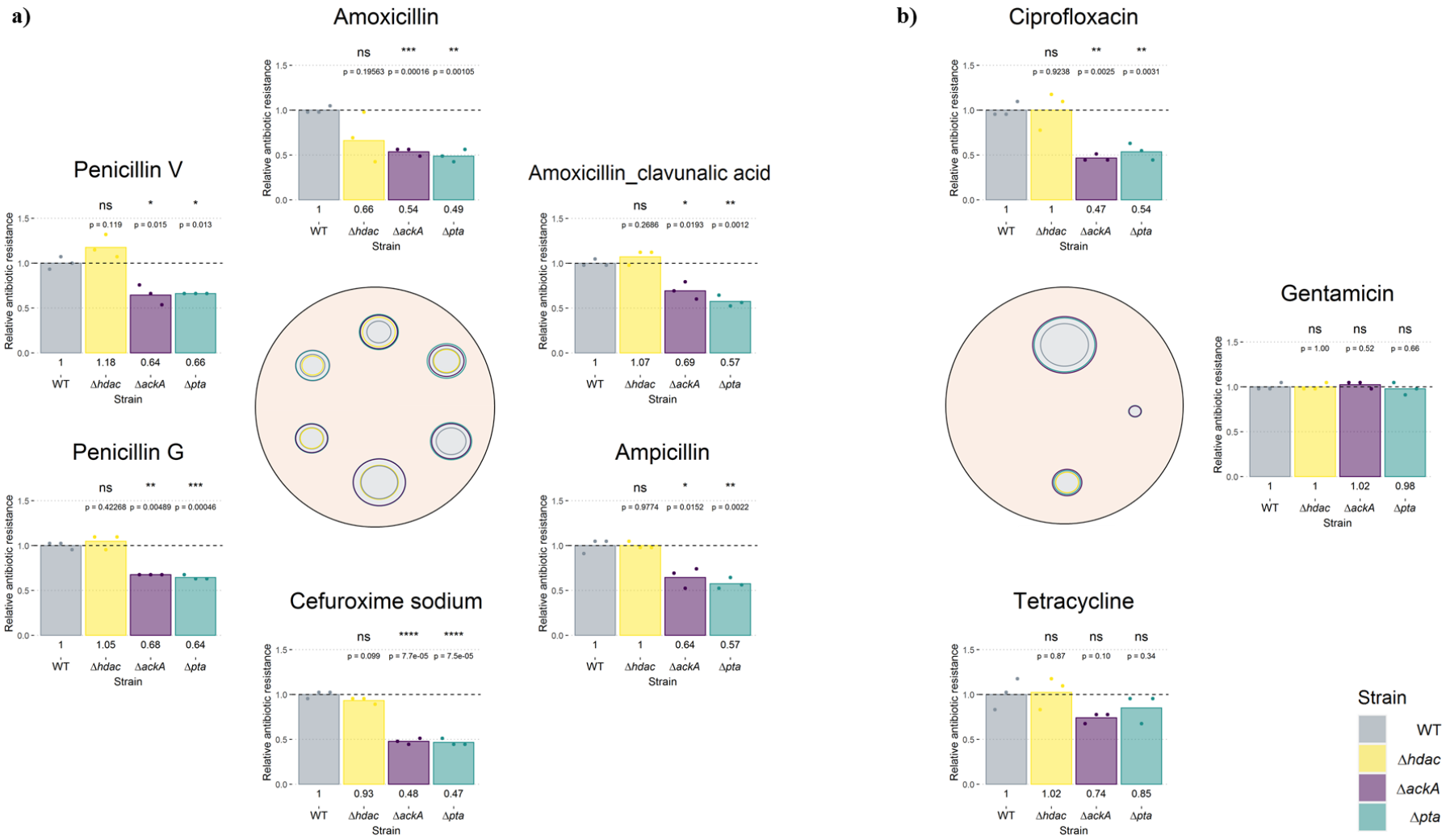


**Figure 5.10 Antibiotic resistance of *N. gonorrhoeae* MS11.** The disc diffusion test for antibiotic resistance was performed in the four isogenic strains of *N. gonorrhoeae* MS11. Bacterial suspensions with an $OD_{600}$ of 0.1 were plated on GC agar and incubated at 37 °C for 24 h at 5% $CO_2$. The halo of inhibition was measured and the relative resistance of the strains was calculated (bottom). The diameter of inhibition is illustrated for each strain and the relative resistance is represented in columns. The relative expression of the WT was considered as 1 for to use as reference for the calculation of the other strains **a)** Antibiotics for the inhibition of bacterial wall (beta-lactam and cephalosporin)..**b)** Antibiotics for the inhibition of protein synthesis and bacterial replication (aminoglycoside, naphtacene and fluoroquinolone). Replicates of 3 was performed and a T-test was performed for statistical analysis. The significance and *p* value are shown at the top of the plots. ns, no significance;*, *p* value <0.05; **, *p* value <0.01; ***, *p* value <0.001; ****, *p* value < 0.0001.

### 5.2.4 Phosphotransacetylase crystallisation

The increment of new antibiotic resistant strains has led the necessity for new approaches to combat the development and spread of these strains. *N. gonorrhoeae* is currently is considered by the WHO a high risk bacteria due to the concerning increase of cases of neisserial strains resistant to azithromycin and ceftriaxone, the current treatment against the gonococcus (Grad *et al.*, 2016; Yahara *et al.*, 2018; Rowley *et al.*, 2019).

The previous results observed in the isogenic mutants, showed that the strain Δ*pta* is more susceptible to phagocytosis and to be less virulent compared to the WT and opposite to the behaviour of Δ*ackA*, which showed more resistance to phagocytosis. Although these experiments need further replicates and more analysis. I proposed in this study to target the enzyme phosphotransacetylase for drug discovery to inhibit its activity. Therefore, the protein was cloned into a strain of *E. coli* BL21 for the overexpression (supplement fig 8.6), thus it was purified and finally, crystallised for the discovery of the structure.

The structure of the *N. gonorrhoeae* MS11 phosphotransacetylase or any *N. gonorrhoeae* has never been crystallised. In comparison to other sequences, the neisserial Pta protein contains approximately 120 more amino acids. This sequence is similar to a domain for the biosynthesis of biotin (fig 5.11).

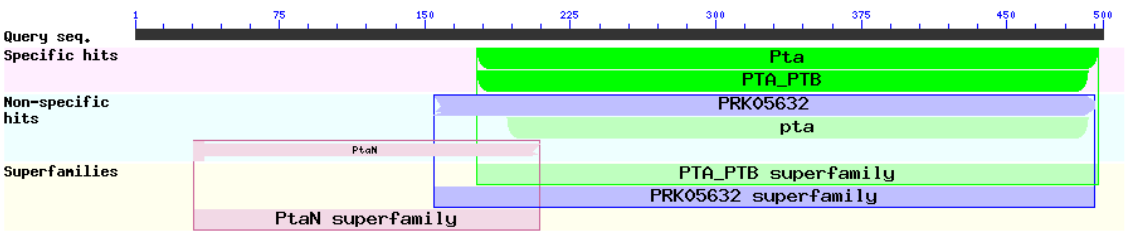


**Figure 5.11 Domains of neisserial Pta.** The protein sequence of Pta was blasted and the domains were searched on the website NCBI. The protein show to different domain. The first domain is a PtaN superfamily domain that belongs to a BioD-like N-terminal domain which function is the biosynthesis of biotin. The next domain is the phosphate acetyltransferase domain which catalyses the reaction of acetyl-CoA to acetyl-phosphate.

The expression of Pta was through the system of pET28a which induces the transcription of the insert by the addition of the inducer IPTG. Briefly, *E. coli* DH5α was used for the obtainment of the protein expression vector pET28a. *E. coli* XL1-blue was transformed with the vector containing the *pta* gene since this bacterium possesses a high transformation rate. The third strain was *E. coli* BL21-DE3, a bacterium that used for the overexpression of the Pta protein. In order to determine the best concentration of IPTG the expression of *pta* was induced with 0.1 and 1 mM IPTG (fig 5.12a-b). However, the insoluble phase showed presence of the overexpressed Pta. Therefore, different conditions were tested. The growth temperature was decreased and the IPTG concentration was increased. Glucose was also added in order to favour the induction of the protein, however, the expression was reduced when glucose was added. It was determined that the optimal condition for the protein expression was with 0.25 mM IPTG growing at 18 °C for 18 h (fig 5.12c).

For the purification of the protein, different columns were used. The protein was modified with 6 histidine at the C-terminus of the protein to purify it. It was determined that 150 mM imidazole was the optimal concentration for the elution of the protein from the His-Trap column (fig 5.12d). The bacteria were grown and the synthesis of protein induced, the bacteria were sonicated and the cell free extract was passed through the His-Trap column (fig, 5.12e), the eluate was then passed through two ion exchange columns (monoQ and monoS) with a positive and negative charge to discard proteins from the extract (fig 5.12f). The final purification step was the separation of the protein by gel filtration which separates the proteins by size, obtaining a single band of the desired protein Pta with a molecular weight of 52.1 kDa.

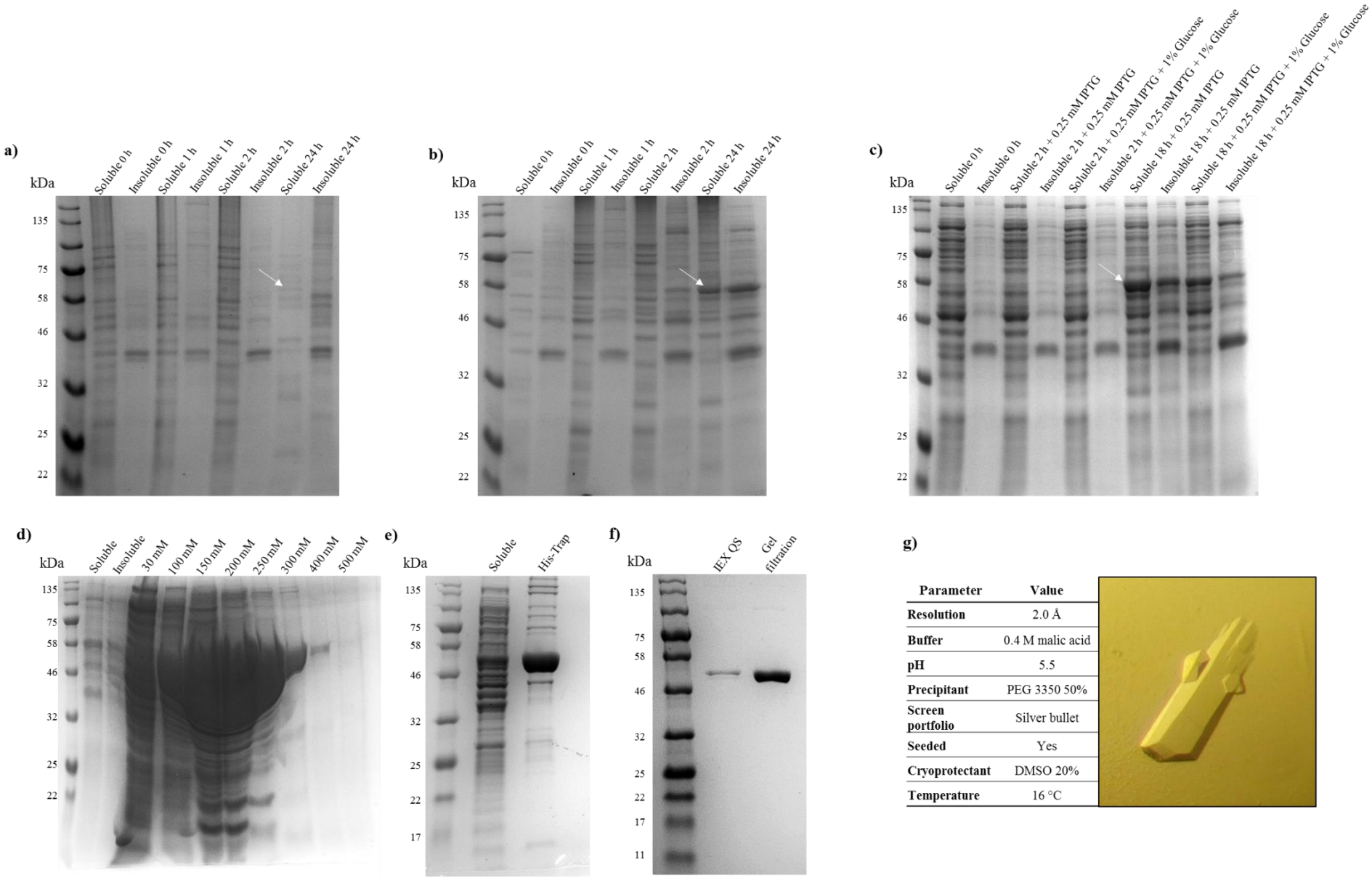


**Figure 5.12 Optimisation of expression, purification and crystallisation of *N. gonorrhoeae* Pta. a-b)** Induction of Pta expression by using 0.1 and 1 mM IPTG, respectively. **c)** Cell free extracts of bacteria induced with 0.25 mM IPTG with and without 1% glucose at 18 °C. **d)** Optimisation of elution buffer concentration. **e)** Purification of cell free extract through a His-Trap column. **f)** Purification through ion exchange Q and S columns and finally through a gel filtration column. **g)** Conditions of the crystallisation and picture of the crystal obtained.

The crystallisation was optimised after several combinations of conditions. The final condition that resulted in the crystallisation of Pta was using acid malic, the precipitant PEG, the utilisation of the screening portfolio silver bullet which are different buffers. The protein was also seeded to improve the formation of crystals. After two weeks, crystals were observed and collected to send them to the synchrotron Diamond Light Source, located in Oxford, UK (fig 5.12g). The processing of the crystal in the X-ray machine and the preparation to send it to the synchrotron was performed by Dr. Domen Zafred which kindly helped me during the whole process of expression, purification and crystallisation of the protein.

The crystal sent showed a resolution of 2.0 Å. The data obtained from the synchrotron was analyse on the WinCOOT- CCP4 software. The electron density cloud obtained from the synchrotron was refined and structure was obtained. The structure shows that the sites affected by acetyl-phosphate, K400 andK450, are located in the same coordinate as the PHYRE2 predicted model (fig 5.13).

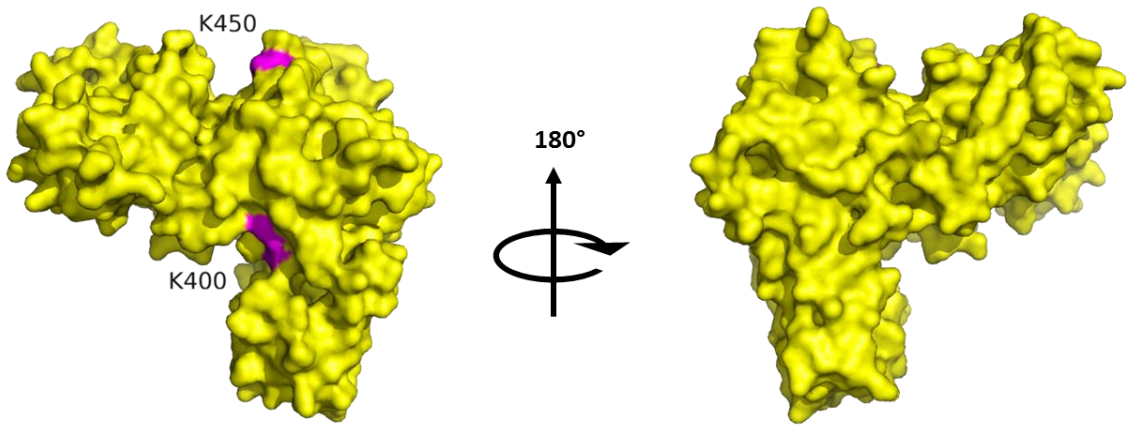


**Figure 5.13 Predicted structure of the crystal of the *N. gonorrhoeae* Pta (NGFG0350).** The predicted model of Pta obtained by Phyre2 was used as a template to model the crystal utilising the electron density obtained from the X-ray crystallography obtained from the synchrotron. The file .mtz was used on the WinCOOT- CCP4 software for the refinement of the structure. The sites K400 and K450 are shown in magenta colour.

## 5.3 Discussion

The disease gonorrhoea was one of the first ever infections recorded in history. The characteristic white purulent liquid was first described in the bible and from then the bacteria has been able to adapt to humans not only biologically but adapting into our intelligence and technology. The surge of antibiotic resistant strains has brought it to the attention of the worldwide public health. The World Health Organisation (WHO) has classified *N. gonorrhoeae* as a high risk bacteria due to the increase of incidence and antibiotic resistant cases. However, the gonococcus not only is effective in human invasion due to the resistance, it possesses several mechanisms that confers the ability to evade the immune system and survive within cells (Johnson and Criss, 2011; Criss and Seifert, 2012; Yahara *et al.*, 2018; W. J. Kim *et al.*, 2019; WHO, 2019a).

In this chapter, we focused in two particular pathogenic features of *N. gonorrhoeae*, intracellular survival and immune system evasion. For the study of intracellular survival, monocyte-derived macrophages (MDM) were used since the study of bacterial phagocytosis is more reliable in primary cells than in cell lines like THP-1 and U937 (Château and Seifert, 2016). MDM infected with Δ*ackA* showed a significant increase in the number of intracellular bacteria at 2 h post-infection, while the number of intracellular bacteria was increased in the Δ*pta* strain after 3 h of infection, both were compared to the WT. Although these results showed that an imbalance of acetyl-phosphate production altered their ability to be phagocytosed, the performance of the gentamicin protection assay (GPA) still generating conflict among researches. Studies have shown that the use of gentamicin is not reliable since the membrane of cells is permeable molecules of the antibiotic passes through the membrane and kill the intracellular bacteria, other researchers claim that gentamicin is present in the phagosome when phagocytosis occurs during GPA and that gentamicin enters the cell through phagosomes, indeed these results

have been confirmed in *Yersinia pestis* and *Streptococcus pyogenes* (Flannagan, Heit and Heinrichs, 2016; VanCleave *et al.*, 2017; J.-H. Kim *et al.*, 2019).

However, two different studies on *N. gonorrhoeae* were performed using the GPA with a gentamicin concentration of 200 µg/mL and this showed the viability of the gonococcus when the cells were plated. Contrary to this study where an MOI of 5 was used, other studies utilised an MOI of 100 and 1000, and the CFU counted intracellularly after the GPA was of 1% from the initial inoculum. However, the ratio of intracellular bacteria corresponds to the one from Ortiz *et al.*, 2015, proving that *N. gonorrhoeae* can survive at a high concentration of gentamicin during the GPA (Leuzzi *et al.*, 2005; Ortiz *et al.*, 2015).

In order to investigate the phagocytosis assay further and to observe it in real time, fluorescence microscopy in real time was used, infecting MDM with the four strains of *N. gonorrhoeae*. Different techniques are used to observe the phagocytosed bacteria, however, to observe them in real time the bacteria are labelled. The majority of studies tended to use fluorescein isothiocyanate (FITC), however, this method is not recommended since both extracellular and intracellular bacteria emits fluorescence. In 2009, a novel label was found using a pH sensitive dye. pHrodo was used to observe the phagocytosis of apoptotic cells. Several studies have now used this labelling to observe the phagocytosis of bacteria in real-time. The rationale of using this label is that bacteria that are phagocytosed enter to the phagosome and this matures through the fusion with lysosomes to generate the phagolysosome. As consequence of the fusion, the internal pH drops and the dye is activated to emit fluorescence that is recognised by the microscope (Miksa *et al.*, 2009; Weiss and Schaible, 2015; Lenzo *et al.*, 2016; Lindner, Burkard and Schuler, 2020).

The real-time fluorescence microscopy showed that acetylation might be involved in the regulation of *N. gonorrhoeae* to inhibit apoptosis and to synthesise pili. The curve of number of MDM cells showed a similar pattern across all the isogenic mutant strains and the control, however, the number of MDM infected with *N. gonorrhoeae* MS11 WT significantly increased compared to the rest of the conditions which showed a decrease in the number of cells after 4.5 h post-infection.

Macrophages (MΦ) are the first line of defence during infections, these cells are polarised into M1 or M2 MΦ depending on the activation of the cells. M1- MΦ possess a proinflammatory and high microbicidal activity and M2- MΦ is the anti-inflammatory type which is necessary for the healing (McWhorter *et al.*, 2013). Interestingly, it has been shown that *N. gonorrhoeae* suppresses the production of TNF-α, molecule that activates the immune response. Instead, it induces the production of immunoregulatory cytokines (Escobar *et al.*, 2013). In 2015, it was then found that this production of immunoregulatory cytokines like IL-6 and IL-10 coordinates the polarization of MΦ to a M2- MΦ type. Furthermore, they observed an induction of the programmed death ligand (PD-L1) which acts as an immunosuppressive molecule that suppresses the activity of lymphocytes T, observation found in several studies. (Zhu *et al.*, 2012; Escobar *et al.*, 2013; Ortiz *et al.*, 2015; Escobar, Rodas and Acuña-Castillo, 2018).

This immunoregulatory induction could explain the observation done by Leuzzi *et al.*, 2005 where the intracellular survival of *N. gonorrhoeae* was longer in MDM, a result shown in this study. Furthermore, the analysis of nuclei size showed the presence of two cell line populations, the cells with the 38 $\mu m^2$ nuclei size could be lymphocytes, and these cells might be regulated by the PD-L1 leading to the neisserial intracellular survival. Interestingly, image analysis showed the division of MDM infected with *N. gonorrhoeae* MS11 WT suggesting that gonococcus not only modulates the polarization of MΦ but

also induces the cellular division and that modulation is altered by changes in the acetylation of proteins since the other isogenic mutants showed the same pattern number as the control which was MDM non-infected.

Antigenic variation is an immune evasion mechanism of *N. gonorrhoeae* to be phagocytosed. This mechanism allows to synthesise a great number of proteins that vary in few amino acids and that prevent to the protein being recognised by antibodies due to the level of variation, this is found mainly in the synthesis of opacity proteins (Opa) and pili (Haas and Meyer, 1986; Rudel *et al.*, 1992; Stein *et al.*, 2015). Pili in *N. gonorrhoeae* confers the capacity to adhere and colonise epithelial cells, furthermore is has shown to be correlated to the adhesion to T cells, therefore, pili biosynthesis is important in the virulence of the gonococcus (Merz and So, 2000; Winther-Larsen *et al.*, 2001; Plant and Jonsson, 2006). However, other studies have shown that pili biogenesis inhibits the adhesion to macrophages (Escobar, Rodas and Acuña-Castillo, 2018).

In this study we found differences in the expression of pili-related proteins and genes among the isogenic strains. PilE is the major pilus component also known as pilin and it required for epithelial adherence together with PilC which has been shown to be necessary for pili biogenesis and they were found significantly increased and decreased in Δ*ackA* and Δ*pta*, respectively (Rudel *et al.*, 1992; Obergfell and Seifert, 2016). Pilus biogenesis is required to cross the bacterial outer membrane and this is possible by the action of PilQ a channel that transports pili and DNA. The *pilQ* mRNA was significantly decreased in both Δ*ackA* and Δ*pta* mutant strains. Interestingly, it was described that PilP is involved in the synthesis of PilQ, indeed a mutant Δ*pilP* showed the phenotype of a non-pilated strain, however, in this same study it is claimed that PilP is not involved in the synthesis of PilQ (Drake, Sandstedt and Koomey, 1997; Tammam *et al.*, 2011). Furthermore, PilP showed significant increase acetylation site in the Δ*ackA* isogenic strain. This difference

in the acetylation could be the responsible for the altering of the pili biogenesis and therefore, less phagocytosis compared to Δ*pta*. Indeed, it was found that acetylation of PilT altered the viability of *N. gonorrhoeae* showing that acetylation of pili-related proteins modifies their activity (Hockenberry *et al.*, 2018).

The infection of *G. mellonella*, resulted in an antagonistic response. The Δ*ackA* killed faster than the WT and with a similar survival percentage, while the Δ*pta* resulted in a ~90% survival. A study shown that infection of *G. mellonella* with *E. coli* mutated in the Cpx envelope stress regulator (CpxR) lost the ability to cause a lethal infection compare to the WT (Leuko and Raivio, 2012). In *N. gonorrhoeae* there are homologues of the Cpx TCS, called MisRS, where similar to other TCS, the response regulator can be phosphorylated by AcP (Mitrophanov and Groisman, 2008; Lima *et al.*, 2016). The results of the larvae killing assay showed a difference in the virulence of the mutant strains. The TCS is involved in the regulation of expression of virulence factor, suggesting that the MisRS can be altered by levels of acetyl-phosphate. MisRS was shown to be responsible for the resistance to cationic antimicrobials peptides (CAMP) and some antibiotics in *N. gonorrhoeae*. Levels of *mtrCDE*, genes encoding an efflux pump, were shown to be lower in a *misR* mutant and as consequence the susceptibility to CAMP and aminoglycosidases increased (Justin L Kandler *et al.*, 2016). The relation of this to our results are that *G. mellonella* has been reported to produce antimicrobial peptides (AMP). These AMP are gloverins and cecropins, which act on the LPS by inhibiting the conformation of the outer membrane (Vogel *et al.*, 2011). ).

In this study, *misR* was increased in Δ*ackA*, however, none of the *mtrcCDE* genes were significantly different. Interestingly, the Δ*pta* isogenic strain showed a significant increase in *mtrD*, *hmbR* and *tbpA*, the two latter are genes controlled by *misRS* and involved in iron acquisition, a virulence factor in the intracellular survival of *N.*

*gonorrhoeae* (Zhao *et al.*, 2010; Zughaier, Kandler and Shafer, 2014; Justin L. Kandler *et al.*, 2016; Post *et al.*, 2017). Ren *et al.*, 2016 showed that acetylation of the homologue of *misR* in *Salmonella* Typhimurium inhibits DNA binding and therefore demonstrated a decrease in the transcription of genes. Furthermore, these results are similar as a study performed in *N. gonorrhoeae* (Post *et al.*, 2017). A recent study has shown that MisRS is required by *N. gonorrhoeae*, for a successful colonisation of mice and that it is involved in the upregulation of porin synthesis for serum resistance (Gangaiah *et al.*, 2017). Moreover, the disc diffusion experiment showed a significant decrease of antibiotic resistance in the isogenic strains Δ*ackA* and Δ*pta*, especially in the beta-lactams and cephalosporin antibiotics.

The resistance to this antibiotics can be driven by the efflux pump encoded in the *mtrCDE* operon, this operon is regulated by the TCS MisRS and the expression is repressed by MtrR (Cámara *et al.*, 2012; Justin L Kandler *et al.*, 2016; Handing *et al.*, 2018). Interestingly, a study showed that the level of MisR does not affect the expression of *mtrCDE* (Justin L Kandler *et al.*, 2016). Indeed in the Δ*ackA* the expression of *misR* was increased, however the expression of MtrCDE were not altered. MtrR, is a transcriptional repressor that is autoregulated by the expression of MtrR, interestingly, it also controls the expression of the pili related operon *pilMNOPQ* in *N. gonorrhoeae* (Folster *et al.*, 2007). However, a recent study showed that expression of MtrR also regulates the expression of the repressor GdhR, a transcriptional regulator of central metabolic enzymes (Rouquette-Loughlin *et al.*, 2017b). Although, *mtrR* expression was not altered in the different isogenic strains, the acetylation was indeed increased in Δ*ackA*. This might suggest that the acetylation of MtrR is more important in the regulation of the transcription of genes rather than the expression (supplement 8.5). Indeed, since it has been shown that acetylation of transcriptional regulators inhibits DNA binding (Thao *et*

*al.*, 2010; Ghosh *et al.*, 2016; Ren *et al.*, 2016; Sang *et al.*, 2017), the acetylation of several transcriptional regulators in Δ*ackA* leads to the increase of synthesis of several genes, which leads to a better fitness to colonise and infect cells.

Although the gene expression of the genes was different between strains, a specific pattern for each strain was not observed. We would´ve expected from the role that has acetylation in the transcriptional factors, a decrease of gene expression, since it has been shown that acetylation inhibits the protein-DNA binding (Ren *et al.*, 2016; Sang *et al.*, 2017; Li, Krishnan and Duncan, 2018; Koo *et al.*, 2020). Since global acetylation was altered, it cannot be determine that the gene expression is determine by the specific acetylation of the transcriptional regulators. Instead, a study of individual transcriptional regulators would be needed to determine if acetylation inhibits the binding to DNA. This could be approach by site-directed mutagenesis from a lysine to a glutamine. Then a electrophoretic mobility assay shift would show the ability of the transcriptional regulator to bind DNA by observing the electrophoretic gel (Ghosh *et al.*, 2016). This experiments should be done in the two-component system involved in the virulence of *N. gonorrhoeae* MisRS.

Although Δ*ackA* and Δ*pta* showed differences in the virulence. The strain with less acetylation presented more susceptibility to phagocytosis and a lower virulence to kill *G. mellonella*. Indeed, more studies are needed to better understand the role that acetylation possesses in the virulence, however, with the results obtained in this study and the results from the literature there is a consensus that bacteria with less acetylation expressed less virulence features. The next step to show that acetylation is involved in the virulence of *N. gonorrhoeae* would be to infect mice. This could be performed by infecting female mice intravaginally, and samples would be taken daily after 2 days post-infection to determine the CFU that were able to colonise the epithelium. If more CFU are observed

in the Δ*ackA* isogenic strain compared to the WT and less CFU in mice infected with Δ*pta* we could conclude that the virulence of *N. gonorrhoeae* is regulated by lysine acetylation (Gangaiah *et al.*, 2017).

I proposed in this study the enzyme Pta as an enzyme to further analyse as a possible target to treat gonorrhoea. Interestingly, a Pta mutant of *Salmonella enterica* serovar Typhimurium showed less virulence. Mice were infected intraperitoneal with the WT and the mutant and mice infected with the Pta mutant showed a significant longer survival compared to the group of mice infected with the WT (Kim *et al.*, 2006).

Contrary to other homologous Pta enzymes, the neisserial presents a BioD-like N-terminal domain that is related to the biosynthesis of biotin. A study in *S. enterica*, which also contains this domain, proposed that the domain is for the allosteric binding of NADH and pyruvate to regulate the enzymatic activity (Brinsmade and Escalante-Semerena, 2007). However, in *E. coli*, Pta lacks of this domain and the binding of this molecules was found in a P-loop NTPase domain, different to the BioD-like domain (Campos-Bermudez *et al.*, 2010). In the case of the Pta from *Salmonella* the structure was not obtained and although the paper concludes that the crystal will be performed no further publications were found for the structure. This is the first time that a PTA with a BioD-like N-terminal domain is crystallised.

# Chapter 6

## Overall conclusions

# 6 Overall conclusions

*N. gonorrhoeae* is an obligate human bacterium that has adapted and evolved to survive in our cells. This has led to the bacteria to get resistant at a point it has converted into a worldwide public health risk. Last year, 2020, a pandemic broke and the pandemic still going by the end of this thesis. The pandemic has brought millions of infected people and sadly, thousands of deaths. The rise of this type of pandemics is not new to human kind and it is not going to be the last one. In fact, it is predicted that the number one cause of deaths by 2050 will be bacterial infections, causing the death of a person every 3 seconds (O'Neill, 2016). This is mainly to the increment of bacterial antibiotic resistance due to the non-legislated and uncontrolled use of antibiotics in some countries and *N. gonorrhoeae* is on the high risk list of bacteria that required R&D of new drugs.

In this study, the acetylation of *N. gonorrhoeae* MS11 and the relation it possesses in the regulation of metabolism and virulence was investigated. Acetyl-phosphate, a reactive molecule that donates either the phosphoryl group for phosphorylation or the acetyl group for acetylation, we focused in the acetylation of proteins. It was shown that alteration in the phosphotransacetylase-acetate kinase pathway (PTA-AK pathway) led to a change in the intermediate metabolite acetyl-phosphate, and therefore, different acetylation sites were found in the isogenic strains Δ*hdac*, Δ*ackA*, and Δ*pta*, two with a higher acetylation and a lower acetylation, respectively. The experiments performed showed us that acetylation in *N. gonorrhoeae* is involved in enzymes of the central metabolic pathway, gene expression, and that it affects the immune system evasion (fig 6.1).

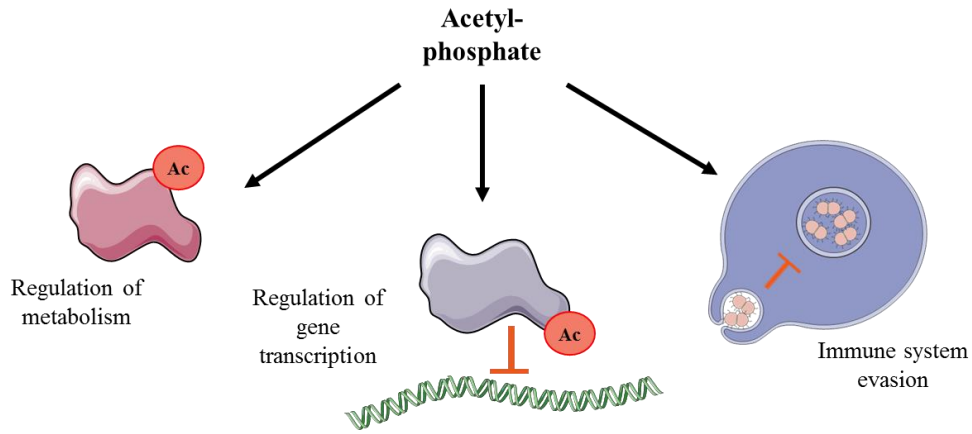


**Figure 6.1 Role of acetyl-phosphate in *N. gonorrhoeae*.** The experiments performed showed that acetylation is found in enzymes involved in metabolism, gene expression and virulence factors involved in immune system evasion. The acetylation of them suggest to cause an inactivation of activity or inhibition to DNA binding.

The acetylome allowed us to analyse the enzymes with a change in the acetylation pattern due to differences in intracellular acetyl-phosphate levels. The enrichment analysis showed that central metabolic were mainly affected by this change, therefore each enzyme of each central metabolic pathway was studied and it was possible to determine a regulation of the PTA-AK pathway. The data obtained from the acetylome showed that in the Δ*ackA* the majority of enzymes from gluconeogenesis, Entner-Doudoroff pathway and pyruvate metabolism were acetylated in the active sites. The *in silico* analysis of the structure and the binding to the substrate showed that some of these acetylation sites altered the conformation of the active site suggesting an inhibition of the enzymatic activity. However, enzymes from the TCA cycle showed no alteration in the active site. It was found that acetylation mainly occurs in clusters of the enzyme that show a positive electrostatic potential surface (EPS). The high concentration of acetyl-phosphate recreates the intracellular environment of the bacteria during carbon overflow, which leads to an increase of substrates including acetyl-phosphate. The information gathered from papers, and the growth curves and acetylome from our study, resulted in the proposal

of a regulatory mechanism of the PTA-AK pathway. The regulation involves the acetylation of the phosphotransacetylase (Pta) in the lysine K450 which is conserved in bacteria, being the histone- deacetylase like protein (HDAC) the predicted enzyme that could reactivate Pta activate by the deacetylation of K450 (fig 6.2).

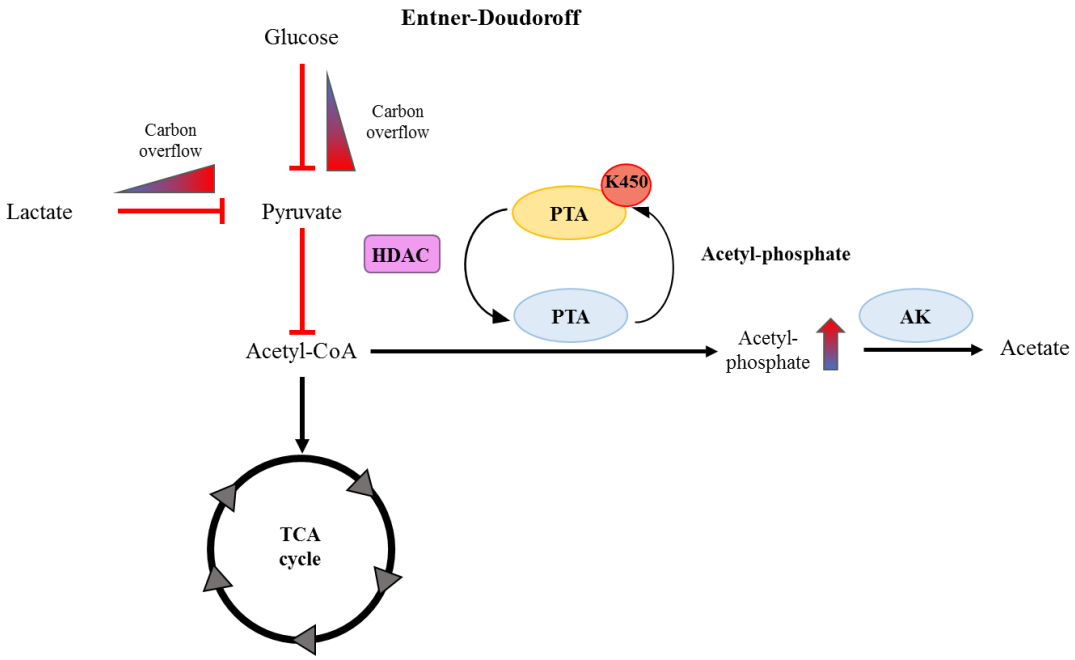


**Figure 6.2 Proposal of a regulatory mechanism of the PTA-AK pathway in *N. gonorrhoeae*.** During carbon overflow the enzymes from the TCA cycle saturate and the metabolites from the previous pathways accumulate. This leads to an accumulation of acetyl-CoA that is redirected to the PTA-AK pathway. Levels of acetyl-phosphate increase leading to an increase of the acetylation, causing an enzymatic inhibition of enzymes from the Entner-Doudoroff pathway, and pyruvate metabolism. The acetylation also was found in Pta in the site K450. This is a conserved site among bacteria and it is found in the active site where acetyl-CoA binds. The acetylation of Pta blocks the enzymatic activity, however, it was found that this site could be a target for the HDAC enzyme, suggesting a regulation of Pta. When the levels of the metabolite diminish due to the TCA cycle activity, the intracellular concentration of acetyl-phosphate decreases and the previous pathways are reactivated.

The study of neisserial virulence showed that acetylation could be involved in the intracellular survival of the bacteria and the regulation gene expression. The killing assay and microscopy to observe phagocytosis showed a correlation between acetylation and

immune system evasion. This suggested that virulence factors could be altered by acetylation. It was found from the proteome that proteins involved in the Type IV pili (Tfp) biosynthesis were expressed at different levels. Since Tfp is involved in the binding to the cells, levels of mRNA pili-related genes were analysed. It was found that some of the genes were downregulated and that some of these genes showed a higher acetylation. Although it is not well understood how acetylation could alter the function of the pili components, a hypothesis of the difference in phagocytosis could be that the acetylation of the pilin changes the positive charges of the protein, and therefore the interactions with the cell are inhibited causing immune system evasion (fig. 6.3).

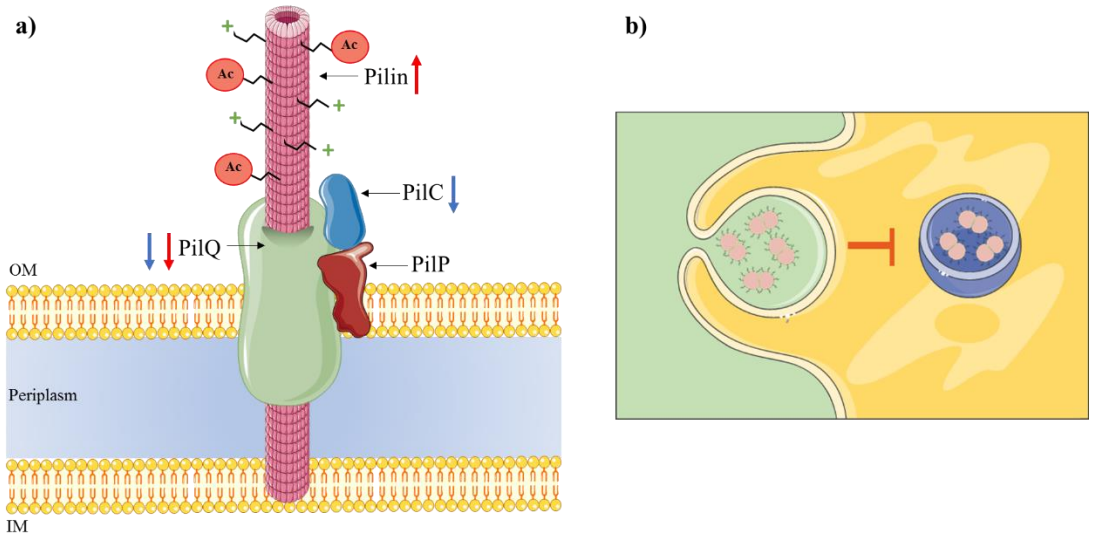


**Figure 6.3Acetylation of pili-biosynthesis proteins and electrostatic interactions.** The microscopy showed a correlation between acetylation and immune system evasion. Levels of protein related to pili-biosynthesis were overexpressed in Δ*ackA* and decreased in Δ*pta*. **a)** Diagram of the type IV pili structure, the pili is formed by monomers of pilin, and crosses both membranes through the channel PilQ assisted by the protein PilP, the stabilisation of the pili is driven by PilC. Levels of these proteins were expressed differently in Δ*ackA* (red) and Δ*pta* (blue). In Δ*ackA* the major pilin components showed an increase of acetylation in the sites K20 and K203 which could altered the electrostatic surface of the protein, **b)** interfering with the interaction with macrophages and further phagocytosis, leading to an immune system evasion.

The killing assay with *Galleria mellonella* showed an increase virulence the Δ*ackA* isogenic strain, while Δ*pta* showed a reduced virulence compared to WT. Some of the virulence factors are controlled by two-component system. Therefore, we analysed the expression of the TCS MisRS and its gene targets. We found an overexpression of MisR in Δ*ackA* and an overexpression of its targets in both isogenic strains. This could be due to the increase of acetyl-phosphate in Δ*ackA* that increased the activation of MisS and therefore the activation of MisR for gene transcription while in Δ*pta* the decrease of acetylation leads to a better binding between MisR and DNA. The genes studied for this TCS were genes involved in the efflux pump complex and iron acquisition (fig. 6.4).

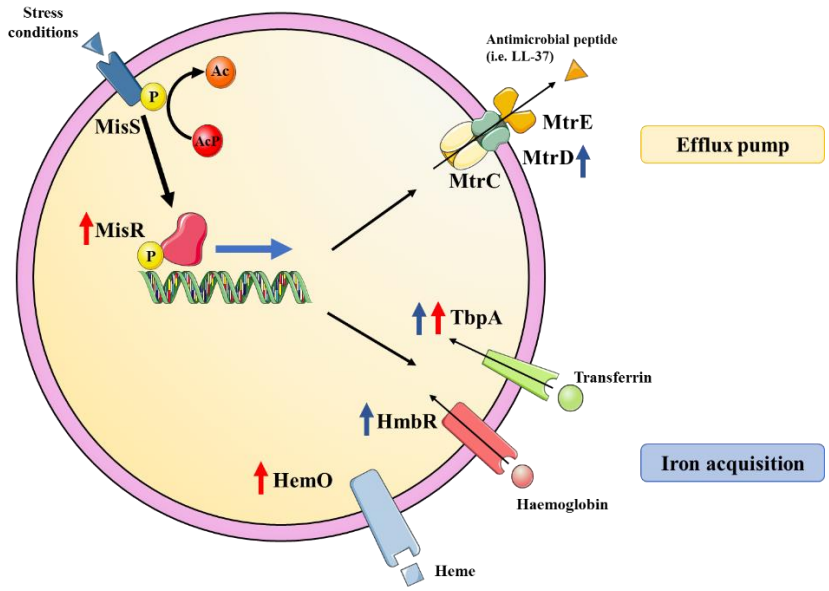


**Figure 6.4 Effect of acetylation in the two-component system MisRS in *N. gonorrhoeae*.** Two-components system are formed by a sensor (MisS) that detects changed in the environment and when they are activated they auto-phosphorylate, and acetyl-phosphate has been shown to be able to donate the phosphoryl group. This leads to the phosphorylation of the transcriptional regulator (MisR) that binds to the DNA for gene transcription. Some of the gene targets of the MisRS TCS are genes for the biosynthesis of the efflux pump MtrCDE, and genes for iron acquisition (TbpA, HmbR, and Hemo). This set of genes are involved in the virulence of *N. gonorrhoeae* for the transportation of molecules to the environment such as antibiotics and antimicrobial peptides, and iron acquisition, respectively. It was found that levels of these genes were overexpressed in Δ*ackA* (red) and Δ*pta* (blue).

Although more repetitions and further assays are required, these results demonstrate that acetylation could be an important post-translational modification to control the virulence of *N. gonorrhoeae*, since this has been shown in other bacteria. It was proposed that Pta could be a good target for an antibiotic due to these results, however, it could also be that an inhibition of Pta allows *N. gonorrhoeae* to disseminate more in the organism due to the action of macrophages to phagocytosed bacteria more and spread them. Therefore, it would be interesting to test the colonisation of the urinary genital tract of mice to observe any difference among the two isogenic strains possessing different levels of acetylation.

In any scenario, Pta has shown that it plays a key role in the regulation of acetyl-phosphate production which is linked to the regulation of metabolism and virulence due to the control of gene expression by the acetylation of transcriptional regulators. These are just the first steps in this study in our lab and it will be interesting what future generations find. However, I conclude with this study that Pta is a key enzyme for the pathogenesis of *N. gonorrhoeae*.

# References

# 7 References

Akram, M. (2014) 'Citric Acid Cycle and Role of its Intermediates in Metabolism', *Cell Biochemistry and Biophysics*, 68(3), pp. 475–478. doi: 10.1007/s12013-013-9750-1.

Allen, S. H. *et al.* (1964) 'Purification and Properties of Enzymes Involved in the Propionic Acid Fermentation.', *Journal of bacteriology*, 87(1), pp. 171–87. Available at: http://www.ncbi.nlm.nih.gov/pubmed/14102852.

Andersen, L. W. *et al.* (2013) 'Etiology and Therapeutic Approach to Elevated Lactate Levels', *Mayo Clinic Proceedings*, 88(10), pp. 1127–1140. doi: 10.1016/j.mayocp.2013.06.012.

Atack, J. M. *et al.* (2013) 'Characterization of an ntrX Mutant of Neisseria gonorrhoeae Reveals a Response Regulator That Controls Expression of Respiratory Enzymes in Oxidase-Positive Proteobacteria', *Journal of Bacteriology*, 195(11), pp. 2632–2641. doi: 10.1128/JB.02062-12.

Atack, J. M. *et al.* (2014) 'A role for lactate dehydrogenases in the survival of Neisseria gonorrhoeae in human polymorphonuclear leukocytes and cervical epithelial cells', *Journal of Infectious Diseases*, 210(8), pp. 1311–1318. doi: 10.1093/infdis/jiu230.

Baart, G. J. E. *et al.* (2007) 'Modeling Neisseria meningitidis metabolism: from genome to metabolic fluxes', *Genome Biology*, 8(7), p. R136. doi: 10.1186/gb-2007-8-7-r136.

Baart, G. J. E. *et al.* (2010) 'Expression of phosphofructokinase in Neisseria meningitidis', *Microbiology*, 156(2), pp. 530–542. doi: 10.1099/mic.0.031641-0.

Baeza, J., Smallegan, M. J. and Denu, J. M. (2015) 'Site-specific reactivity of nonenzymatic lysine acetylation', *ACS Chemical Biology*, 10(1), pp. 122–128. doi: 10.1021/cb500848p.

Baeza, J., Smallegan, M. J. and Denu, J. M. (2016) 'Mechanisms and Dynamics of Protein Acetylation in Mitochondria', *Trends in Biochemical Sciences*. Elsevier Ltd, 41(3), pp. 231–244. doi: 10.1016/j.tibs.2015.12.006.

Bakker, J., Nijsten, M. W. and Jansen, T. C. (2013) 'Clinical use of lactate monitoring in critically ill patients', *Annals of Intensive Care*, 3(1), pp. 1–8. doi: 10.1186/2110-5820-3-12.

Barak, R. and Eisenbach, M. (2001) 'Acetylation of the response regulator, CheY, is involved in bacterial chemotaxis', *Molecular Microbiology*, 40(3), pp. 731–743. doi: 10.1046/j.1365-2958.2001.02425.x.

Barbosa Leite, A. *et al.* (2020) 'Effect of lysine acetylation on the regulation of Trypanosoma brucei glycosomal aldolase activity', *Biochemical Journal*, 477(9), pp. 1733–1744. doi: 10.1042/BCJ20200142.

Barnoy, S. *et al.* (2017) 'The Galleria mellonella larvae as an in vivo model for evaluation of Shigella virulence', *Gut Microbes*. Taylor & Francis, 8(4), pp. 335–350. doi: 10.1080/19490976.2017.1293225.

de Barsy, M. and Greub, G. (2013) 'Functional genomics of intracellular bacteria', *Briefings in Functional Genomics*, 12(4), pp. 341–353. doi: 10.1093/bfgp/elt012.

Bennett, B. D. *et al.* (2009) 'Absolute metabolite concentrations and implied enzyme active site occupancy in Escherichia coli', *Nature Chemical Biology*, 5(8), pp. 593–599. doi: 10.1038/nchembio.186.

Bergman, P. *et al.* (2005) 'Neisseria gonorrhoeae downregulates expression of the human antimicrobial peptide LL-37', *Cellular Microbiology*, 7(7), pp. 1009–1017. doi: 10.1111/j.1462-5822.2005.00530.x.

Bernal, V., Castaño-Cerezo, S. and Cánovas, M. (2016) 'Acetate metabolism regulation in Escherichia coli: carbon overflow, pathogenicity, and beyond', *Applied Microbiology and Biotechnology*. Applied Microbiology and Biotechnology, 100(21), pp. 8985–9001. doi: 10.1007/s00253-016-7832-x.

Bi, J. *et al.* (2017) 'Modulation of Central Carbon Metabolism by Acetylation of Isocitrate Lyase in Mycobacterium tuberculosis', *Scientific Reports*. Nature Publishing Group, 7(1), p. 44826. doi: 10.1038/srep44826.

Bjerknes, R. *et al.* (1995) 'Neisserial porins inhibit human neutrophil actin polymerization, degranulation, opsonin receptor expression, and phagocytosis but prime the neutrophils to increase their oxidative burst', *Infection and Immunity*, 63(1), pp. 160–167.

Bontemps-Gallo, S. *et al.* (2018) 'Global Profiling of Lysine Acetylation in Borrelia burgdorferi B31 Reveals Its Role in Central Metabolism', *Frontiers in Microbiology*, 9(August), pp. 1–15. doi: 10.3389/fmicb.2018.02036.

Boorsma, C. E., Draijer, C. and Melgert, B. N. (2013) 'Macrophage heterogeneity in respiratory diseases', *Mediators of Inflammation*, 2013. doi: 10.1155/2013/769214.

Brinsmade, S. R. and Escalante-Semerena, J. C. (2007) 'In Vivo and in Vitro Analyses of Single-amino Acid Variants of the Salmonella enterica Phosphotransacetylase Enzyme Provide Insights into the Function of Its N-terminal Domain', *Journal of Biological Chemistry*. Â© 2007 ASBMB. Currently published by Elsevier Inc; originally published by American Society for Biochemistry and Molecular Biology., 282(17), pp. 12629–12640. doi: 10.1074/jbc.M611439200.

Britigan, B. E. *et al.* (1988) 'Phagocyte-derived lactate stimulates oxygen consumption

by Neisseria gonorrhoeae. An unrecognized aspect of the oxygen metabolism of phagocytosis.', *Journal of Clinical Investigation*, 81(2), pp. 318–324. doi: 10.1172/JCI113323.

Brosh, R. M. (2019) *Protein Acetylation, Definitions*. Edited by R. M. Brosh,. New York, NY: Springer New York (Methods in Molecular Biology). doi: 10.1007/978-1-4939-9434-2.

Brown, S. A., Palmer, K. L. and Whiteley, M. (2008) 'Revisiting the host as a growth medium', *Nature Reviews Microbiology*, 6(9), pp. 657–666. doi: 10.1038/nrmicro1955.

Buchakjian, M. R. and Kornbluth, S. (2010) 'The engine driving the ship: Metabolic steering of cell proliferation and death', *Nature Reviews Molecular Cell Biology*. Nature Publishing Group, 11(10), pp. 715–727. doi: 10.1038/nrm2972.

Bucki, R. *et al.* (2010) 'Cathelicidin LL-37: A multitask antimicrobial peptide', *Archivum Immunologiae et Therapiae Experimentalis*, 58(1), pp. 15–25. doi: 10.1007/s00005-009-0057-2.

Bullock, W. O., Fernandez, J. M. and Short, J. M. (1987) 'XL1-Blue: a high efficiency plasmid transforming recA Escherichia coli strain with β-galactosidase selection', *BioTechniques*, (5), pp. 376–378.

Burckhardt, R. M. and Escalante-Semerena, J. C. (2020) 'Small-Molecule Acetylation by GCN5-Related N -Acetyltransferases in Bacteria', *Microbiology and Molecular Biology Reviews*, 84(2), pp. 1–33. doi: 10.1128/MMBR.00090-19.

Cámara, J. *et al.* (2012) 'Molecular characterization of two high-level ceftriaxone-resistant Neisseria gonorrhoeae isolates detected in Catalonia, Spain', *Journal of Antimicrobial Chemotherapy*, 67(8), pp. 1858–1860. doi: 10.1093/jac/dks162.

Campos-Bermudez, V. A. *et al.* (2010) 'Functional dissection of Escherichia coli phosphotransacetylase structural domains and analysis of key compounds involved in activity regulation', *FEBS Journal*, 277(8), pp. 1957–1966. doi: 10.1111/j.1742-4658.2010.07617.x.

Camprubi, E. *et al.* (2018) 'Acetyl Phosphate as a Primordial Energy Currency at the Origin of Life', *Origins of Life and Evolution of Biospheres*. Origins of Life and Evolution of Biospheres, 48(2), pp. 159–179. doi: 10.1007/s11084-018-9555-8.

Carabetta, V. J. and Cristea, I. M. (2017) 'Regulation, Function, and Detection of Protein Acetylation in Bacteria', *Journal of Bacteriology*. Edited by W. Margolin, 199(16), pp. 1–15. doi: 10.1128/JB.00107-17.

Castaño-Cerezo, S. *et al.* (2009a) 'An insight into the role of phosphotransacetylase (pta) and the acetate/acetyl-CoA node in Escherichia coli', *Microbial Cell Factories*, 8(1), p. 54. doi: 10.1186/1475-2859-8-54.

Castaño-Cerezo, S. *et al.* (2009b) 'An insight into the role of phosphotransacetylase (pta) and the acetate/acetyl-CoA node in Escherichia coli', *Microbial Cell Factories*, 8(1), p. 54. doi: 10.1186/1475-2859-8-54.

Castaño-Cerezo, S. *et al.* (2015) 'Regulation of acetate metabolism in Escherichia coli BL21 by protein NE-lysine acetylation', *Applied Microbiology and Biotechnology*, 99(8), pp. 3533–3545. doi: 10.1007/s00253-014-6280-8.

Castaño-Cerezo, S. *et al.* (2014) 'Protein acetylation affects acetate metabolism, motility and acid stress response in Escherichia coli', *Molecular Systems Biology*, 10(11), p. 762. doi: 10.15252/msb.20145227.

Catenazzi, M. C. E. *et al.* (2014) 'A large genomic island allows Neisseria meningitidis

to utilize propionic acid, with implications for colonization of the human nasopharynx.', *Molecular microbiology*, 93(2), pp. 346–55. doi: 10.1111/mmi.12664.

Chan, S. H. J. *et al.* (2014) 'Acetate Kinase Isozymes Confer Robustness in Acetate Metabolism', *PLoS ONE*. Edited by D. Elias, 9(3), p. e92256. doi: 10.1371/journal.pone.0092256.

Chang, D.-E. *et al.* (1999) 'Acetate Metabolism in a pta Mutant of Escherichia coli W3110: Importance of Maintaining Acetyl Coenzyme A Flux for Growth and Survival', *JOURNAL OF BACTERIOLOGY*, 181(21), pp. 6656–6663. Available at: https://www.ncbi.nlm.nih.gov/pmc/articles/PMC94129/pdf/jb006656.pdf (Accessed: 28 July 2017).

Château, A. and Seifert, H. S. (2016) 'Neisseria gonorrhoeae survives within and modulates apoptosis and inflammatory cytokine production of human macrophages', *Cellular Microbiology*, 18(4), pp. 546–560. doi: 10.1111/cmi.12529.

Chen, A. and Seifert, H. S. (2011) 'Neisseria gonorrhoeae-Mediated Inhibition of Apoptotic Signalling in Polymorphonuclear Leukocytes', *Infection and Immunity*. Edited by J. N. Weiser, 79(11), pp. 4447–4458. doi: 10.1128/IAI.01267-10.

Chen, C. Y. *et al.* (1989) 'Physiology and metabolism of Neisseria gonorrhoeae and Neisseria meningitidis: implications for pathogenesis', *Clin.Microbiol.Rev.*, 2 Suppl(0893-8512 (Print)), pp. S35–S40. Available at: https://www.ncbi.nlm.nih.gov/pmc/articles/PMC358075/pdf/cmr00050-0045.pdf (Accessed: 31 July 2017).

Chen, H. *et al.* (2019) 'Site-Specifically Studying Lysine Acetylation of Aminoacyl-tRNA Synthetases', *ACS Chemical Biology*. American Chemical Society, 14(2), pp. 288–

295. doi: 10.1021/acschembio.8b01013.

Chen, I. *et al.* (2004) 'DNA uptake during bacterial transformation.', *Nature reviews. Microbiology*, 2(3), pp. 241–249. doi: 10.1038/nrmicro844.

Chittori, S., Savithri, H. S. and Murthy, M. R. N. (2012) 'Structural and mechanistic investigations on Salmonella typhimurium acetate kinase (AckA): identification of a putative ligand binding pocket at the dimeric interface', *BMC Structural Biology*, 12(1), p. 24. doi: 10.1186/1472-6807-12-24.

Choudhary, C. *et al.* (2014) 'The growing landscape of lysine acetylation links metabolism and cell signalling', *Nature Publishing Group*, 15. doi: 10.1038/nrm3841.

Christensen, D. G. *et al.* (2019) 'Mechanisms, Detection, and Relevance of Protein Acetylation in Prokaryotes', *mBio*, 10(2), pp. 1–20. doi: 10.1128/mbio.02708-18.

Christensen, David G *et al.* (2019) 'Post-translational Protein Acetylation: An Elegant Mechanism for Bacteria to Dynamically Regulate Metabolic Functions', *Frontiers in Microbiology*, 10(July), pp. 1–22. doi: 10.3389/fmicb.2019.01604.

Criss, A. K., Katz, B. Z. and Seifert, H. S. (2009) 'Resistance of Neisseria gonorrhoeae to non-oxidative killing by adherent human polymorphonuclear leucocytes', *Cellular Microbiology*, 11(7), pp. 1074–1087. doi: 10.1111/j.1462-5822.2009.01308.x.

Criss, A. K. and Seifert, H. S. (2012) 'A bacterial siren song: intimate interactions between Neisseria and neutrophils', *Nature Reviews Microbiology*. Nature Publishing Group, 10(3), pp. 178–190. doi: 10.1038/nrmicro2713.

Dillard, J. P. (2011) 'Genetic manipulation of Neisseria gonorrhoeae', *Current Protocols in Microbiology*, (SUPPL.23). doi: 10.1002/9780471729259.mc04a02s23.

Dittrich, C. R., Bennett, G. N. and San, K.-Y. (2008) 'Characterization of the Acetate-

Producing Pathways in Escherichia coli', *Biotechnology Progress*, 21(4), pp. 1062–1067. doi: 10.1021/bp050073s.

Drake, S. L., Sandstedt, S. A. and Koomey, M. (1997) 'PilP, a pilus biogenesis lipoprotein in Neisseria gonorrhoeae , affects expression of PilQ as a high-molecular-mass multimer', *Molecular Microbiology*, 23(4), pp. 657–668. doi: 10.1046/j.1365-2958.1997.2511618.x.

Duan, G. and Walther, D. (2015) 'The Roles of Post-translational Modifications in the Context of Protein Interaction Networks', *PLOS Computational Biology*. Edited by P. Radivojac, 11(2), p. e1004049. doi: 10.1371/journal.pcbi.1004049.

Duffin, P. M. and Seifert, H. S. (2010) 'DNA uptake sequence-mediated enhancement of transformation in Neisseria gonorrhoeae is strain dependent', *Journal of Bacteriology*, 192(17), pp. 4436–4444. doi: 10.1128/JB.00442-10.

Duque, G. A. and Descoteaux, A. (2014) 'Macrophage cytokines: Involvement in immunity and infectious diseases', *Frontiers in Immunology*, 5(OCT), pp. 1–12. doi: 10.3389/fimmu.2014.00491.

Dykhuizen, D. (2005) 'Species Numbers in Bacteria.', *Proceedings. California Academy of Sciences*, 56(6 Suppl 1), pp. 62–71. doi: 10.1007/s11103-011-9767-z.

Edwards, J. L. (2010) 'Neisseria gonorrhoeae survival during primary human cervical epithelial cell infection requires nitric oxide and is augmented by progesterone', *Infection and Immunity*, 78(3), pp. 1202–1213. doi: 10.1128/IAI.01085-09.

Edwards, J. L. and Apicella, M. A. (2002) 'The role of lipooligosaccharide in Neisseria gonorrhoeae pathogenesis of cervical epithelia: lipid A serves as a C3 acceptor molecule', *Cellular Microbiology*, 4(9), pp. 585–598. doi: 10.1046/j.1462-5822.2002.00212.x.

Edwards, J. L. and Apicella, M. a (2004) 'The Molecular Mechanisms Used by Neisseria

gonorrhoeae To Initiate Infection Differ between Men and Women', *Clinical Microbiology Reviews*, 17(4), pp. 965–981. doi: 10.1128/CMR.17.4.965.

Edwards, J. L., Entz, D. D. and Apicella, M. A. (2003) 'Gonococcal Phospholipase D Modulates the Expression and Function of Complement Receptor 3 in Primary Cervical Epithelial Cells', *Infection and Immunity*, 71(11), pp. 6381–6391. doi: 10.1128/IAI.71.11.6381-6391.2003.

Eisenreich, W. *et al.* (2010) 'Carbon metabolism of intracellular bacterial pathogens and possible links to virulence', *Nature Reviews Microbiology*. Nature Publishing Group, 8(6), pp. 401–412. doi: 10.1038/nrmicro2351.

El-Benna, J. *et al.* (2016) 'Priming of the neutrophil respiratory burst: role in host defense and inflammation', *Immunological Reviews*, 273(1), pp. 180–193. doi: 10.1111/imr.12447.

Enjalbert, B. *et al.* (2017) 'Acetate fluxes in Escherichia coli are determined by the thermodynamic control of the Pta-AckA pathway', *Scientific Reports*. Nature Publishing Group, 7(1), p. 42135. doi: 10.1038/srep42135.

Eschenbach, D. A. *et al.* (1989) 'Prevalence of hydrogen peroxide-producing Lactobacillus species in normal women and women with bacterial vaginosis.', *Journal of clinical microbiology*, 27(2), pp. 251–6. Available at: http://www.ncbi.nlm.nih.gov/pubmed/2915019.

Escobar, A. *et al.* (2013) 'Neisseria gonorrhoeae Induces a Tolerogenic Phenotype in Macrophages to Modulate Host Immunity', *Mediators of Inflammation*, 2013, pp. 1–9. doi: 10.1155/2013/127017.

Escobar, A., Rodas, P. I. and Acuña-Castillo, C. (2018) 'Macrophage-Neisseria

gonorrhoeae Interactions: A Better Understanding of Pathogen Mechanisms of Immunomodulation', *Frontiers in immunology*, 9(December), p. 3044. doi: 10.3389/fimmu.2018.03044.

Exley, R. M. *et al.* (2007) 'Lactate acquisition promotes successful colonization of the murine genital tract by Neisseria gonorrhoeae', *Infection and Immunity*, 75(3), pp. 1318–1324. doi: 10.1128/IAI.01530-06.

Faherty, C. S. and Maurelli, A. T. (2008) 'Staying alive: bacterial inhibition of apoptosis during infection', *Trends in Microbiology*, 16(4), pp. 173–180. doi: 10.1016/j.tim.2008.02.001.

Felix Diaz Parga, E. (2017) *The Role of Acetyl-Phosphate in the Pathogenesis of Neisseria gonorrhoeae*. University of Sheffield.

Fifer, H., Natarajan, U. and Unemo, M. (2016) 'Failure of Dual Antimicrobial Therapy in Treatment of Gonorrhea', *The New England journal of medicine*, 374(25), pp. 2504–2506. doi: 10.1056/NEJMc1514294.

Fisette, P. L. *et al.* (2003) 'The Lip Lipoprotein from Neisseria gonorrhoeae Stimulates Cytokine Release and NF-κB Activation in Epithelial Cells in a Toll-like Receptor 2-dependent Manner', *Journal of Biological Chemistry*, 278(47), pp. 46252–46260. doi: 10.1074/jbc.M306587200.

Flannagan, R. S., Cosío, G. and Grinstein, S. (2009) 'Antimicrobial mechanisms of phagocytes and bacterial evasion strategies', *Nature Reviews Microbiology*, 7(5), pp. 355–366. doi: 10.1038/nrmicro2128.

Flannagan, R. S., Heit, B. and Heinrichs, D. E. (2016) 'Intracellular replication of Staphylococcus aureus in mature phagolysosomes in macrophages precedes host cell

death, and bacterial escape and dissemination', *Cellular Microbiology*, 18(4), pp. 514–535. doi: 10.1111/cmi.12527.

Folster, J. P. *et al.* (2007) 'Differential Regulation of ponA and pilMNOPQ Expression by the MtrR Transcriptional Regulatory Protein in Neisseria gonorrhoeae', *Journal of Bacteriology*, 189(13), pp. 4569–4577. doi: 10.1128/JB.00286-07.

Foschi, C. *et al.* (2017) 'Vaginal Lactobacilli Reduce Neisseria gonorrhoeae Viability through Multiple Strategies: An in Vitro Study', *Frontiers in Cellular and Infection Microbiology*, 7(December), pp. 1–10. doi: 10.3389/fcimb.2017.00502.

Gangaiah, D. *et al.* (2017) 'Both MisR (CpxR) and MisS (CpxA) Are Required for Neisseria gonorrhoeae Infection in a Murine Model of Lower Genital Tract Infection', *Infection and Immunity*. Edited by S. M. Payne, 85(9), pp. 4690–4700. doi: 10.1128/IAI.00307-17.

Gao, L. *et al.* (1998) 'Lactate causes changes in gonococci including increased lipopolysaccharide synthesis during short-term incubation in media containing glucose', *FEMS Microbiology Letters*, 169(2), pp. 309–316. doi: 10.1016/S0378-1097(98)00448-0.

Ghosh, S. *et al.* (2016) 'Lysine acetylation of the Mycobacterium tuberculosis HU protein modulates its DNA binding and genome organization', *Molecular Microbiology*, 100(4), pp. 577–588. doi: 10.1111/mmi.13339.

Gill, M. J. *et al.* (1996) 'Functional Characterization of a Sialyltransferase-Deficient Mutant of Neisseria gonorrhoeae', *INFECTION AND IMMUNITY*, 64(8), pp. 3374–3378.

Gorrell, A., Lawrence, S. H. and Ferry, J. G. (2005) 'Structural and Kinetic Analyses of Arginine Residues in the Active Site of the Acetate Kinase from Methanosarcina

thermophila', *Journal of Biological Chemistry*, 280(11), pp. 10731–10742. doi: 10.1074/jbc.M412118200.

Grabiec, A. M. and Potempa, J. (2018) 'Epigenetic regulation in bacterial infections: targeting histone deacetylases', *Critical Reviews in Microbiology*. Informa Healthcare USA, Inc, 44(3), pp. 336–350. doi: 10.1080/1040841X.2017.1373063.

Grad, Y. H. *et al.* (2016) 'Genomic epidemiology of gonococcal resistance to extended-spectrum cephalosporins, macrolides, and fluoroquinolones in the United States, 2000-2013', *Journal of Infectious Diseases*, 214(10), pp. 1579–1587. doi: 10.1093/infdis/jiw420.

Gueriri, I. *et al.* (2008) 'The Pta-AckA pathway controlling acetyl phosphate levels and the phosphorylation state of the DegU orphan response regulator both play a role in regulating Listeria monocytogenes motility and chemotaxis', *Molecular Microbiology*, 70(6), pp. 1342–1357. doi: 10.1111/j.1365-2958.2008.06496.x.

Haas, R. and Meyer, T. F. (1986) 'The repertoire of silent pilus genes in neisseria gonorrhoeae: Evidence for gene conversion', *Cell*, 44(1), pp. 107–115. doi: 10.1016/0092-8674(86)90489-7.

Hallows, W. C., Yu, W. and Denu, J. M. (2012) 'Regulation of Glycolytic Enzyme Phosphoglycerate Mutase-1 by Sirt1 Protein-mediated Deacetylation', *Journal of Biological Chemistry*. Â© 2012 ASBMB. Currently published by Elsevier Inc; originally published by American Society for Biochemistry and Molecular Biology., 287(6), pp. 3850–3858. doi: 10.1074/jbc.M111.317404.

Hamilton, H. L. and Dillard, J. P. (2006) 'Natural transformation of Neisseria gonorrhoeae : from DNA donation to homologous recombination', *Molecular*

*Microbiology*, 59(2), pp. 376–385. doi: 10.1111/j.1365-2958.2005.04964.x.

Hanahan, D. (1983) 'Studies on Transformation of Escherichia coli with Plasmids', *J. Mol. Biol*, 166, pp. 557–580. Available at: https://ac.els-cdn.com/S0022283683802848/1-s2.0-S0022283683802848-main.pdf?_tid=6e5dee03-db83-4696-ba80-f7b8184f465b&acdnat=1530706157_2331a8b84846ba15db66839d3ff9a948 (Accessed: 4 July 2018).

Handing, J. W. *et al.* (2018) 'The MtrCDE Efflux Pump Contributes to Survival of Neisseria gonorrhoeae From Human Neutrophils and Their Antimicrobial Components', *Frontiers in Microbiology*, 9(November), pp. 1–12. doi: 10.3389/fmicb.2018.02688.

Hansen, R. G. and Henning, U. (1966) 'Regulation of pyruvate dehydrogenase activity in Escherichia coli K12', *Biochimica et Biophysica Acta (BBA) - Enzymology and Biological Oxidation*, 122(2), pp. 355–358. doi: 10.1016/0926-6593(66)90076-2.

Harvey, H. A. *et al.* (2001) 'Receptor-mediated endocytosis of Neisseria gonorrhoeae into primary human urethral epithelial cells: The role of the asialoglycoprotein receptor', *Molecular Microbiology*, 42(3), pp. 659–672. doi: 10.1046/j.1365-2958.2001.02666.x.

Hedges, S. R. *et al.* (1999) 'Limited Local and Systemic Antibody Responses toNeisseria gonorrhoeae during Uncomplicated Genital Infections', *Infection and Immunity* , 67(8), pp. 3937–3946. Available at: http://iai.asm.org/content/67/8/3937.abstract.

Hentchel, K. L. and Escalante-Semerena, J. C. (2015) 'Acylation of Biomolecules in Prokaryotes: a Widespread Strategy for the Control of Biological Function and Metabolic Stress.', *Microbiology and molecular biology reviews : MMBR*, 79(3), pp. 321–46. doi: 10.1128/MMBR.00020-15.

Hockenberry, A. M. *et al.* (2018) 'Perturbing the acetylation status of the Type IV pilus retraction motor, PilT, reduces Neisseria gonorrhoeae viability', *Molecular Microbiology*, 110(5), pp. 677–688. doi: 10.1111/mmi.13979.

Holms, H. (1996) 'Flux analysis and control of the central metabolic pathways in Escherichia coli', *FEMS Microbiology Reviews*, 19(2), pp. 85–116. doi: 10.1016/S0168-6445(96)00026-5.

Hongmei, Z. (2012) 'Extrinsic and Intrinsic Apoptosis Signal Pathway Review', in Pesek, K. (ed.) *Apoptosis and Medicine*. InTech, pp. 1–22. doi: 10.5772/50129.

Hove-Jensen, B. *et al.* (2017) 'Phosphoribosyl Diphosphate (PRPP): Biosynthesis, Enzymology, Utilization, and Metabolic Significance', *Microbiology and Molecular Biology Reviews*, 81(1), pp. 1–83. doi: 10.1128/MMBR.00040-16.

Ingram-Smith, C., Martin, S. R. and Smith, K. S. (2006) 'Acetate kinase: not just a bacterial enzyme', *Trends in Microbiology*, 14(6), pp. 249–253. doi: 10.1016/j.tim.2006.04.001.

Jers, C. *et al.* (2018) 'The Global Acetylome of the Human Pathogen Vibrio cholerae V52 Reveals Lysine Acetylation of Major Transcriptional Regulators', *Frontiers in Cellular and Infection Microbiology*, 7(JAN), pp. 1–13. doi: 10.3389/fcimb.2017.00537.

Jiang, Q. *et al.* (2017) 'AcuC, a histone deacetylase, contributes to the pathogenicity of Aeromonas hydrophila', *MicrobiologyOpen*, 6(4), pp. 1–12. doi: 10.1002/mbo3.468.

Johnson, M. B. and Criss, A. K. (2011) 'Resistance of Neisseria Gonorrhoeae to Neutrophils', *Frontiers in Microbiology*, 2(APR). doi: 10.3389/fmicb.2011.00077.

Johnson, M. B. and Criss, A. K. (2013) 'Neisseria gonorrhoeae phagosomes delay fusion with primary granules to enhance bacterial survival inside human neutrophils', *Cellular*

*Microbiology*, 15(8), pp. 1323–1340. doi: 10.1111/cmi.12117.

Johnson, S. R. *et al.* (1993) 'Characterization of a catalase-deficient strain of Neisseria gonorrhoeae: Evidence for the significance of catalase in the biology of N. gonorrhoeae', *Infection and Immunity*, 61(4), pp. 1232–1238.

Jordan, P. W., Snyder, L. A. and Saunders, N. J. (2005) 'Strain-specific differences in Neisseria gonorrhoeae associated with the phase variable gene repertoire', *BMC Microbiology*, 5(1), p. 21. doi: 10.1186/1471-2180-5-21.

Kandler, Justin L. *et al.* (2016) 'The genes that encode the gonococcal transferrin binding proteins, TbpB and TbpA, are differentially regulated by MisR under iron-replete and iron-depleted conditions', *Molecular Microbiology*, 102(1), pp. 137–151. doi: 10.1111/mmi.13450.

Kandler, Justin L *et al.* (2016) 'The MisR Response Regulator Is Necessary for Intrinsic Cationic Antimicrobial Peptide and Aminoglycoside Resistance in Neisseria gonorrhoeae', *Antimicrobial Agents and Chemotherapy*, 60(8), pp. 4690–4700. doi: 10.1128/AAC.00823-16.

Kanneganti, T.-D., Lamkanfi, M. and Núñez, G. (2007) 'Intracellular NOD-like Receptors in Host Defense and Disease', *Immunity*, 27(4), pp. 549–559. doi: 10.1016/j.immuni.2007.10.002.

Kelly, B. and O'Neill, L. A. J. (2015) 'Metabolic reprogramming in macrophages and dendritic cells in innate immunity', *Cell Research*. Nature Publishing Group, 25(7), pp. 771–784. doi: 10.1038/cr.2015.68.

Ketterer, M. R. *et al.* (2016) 'Desialylation of Neisseria gonorrhoeae Lipooligosaccharide by Cervicovaginal Microbiome Sialidases: The Potential for Enhancing Infectivity in

Men', *Journal of Infectious Diseases*, 214(11), pp. 1621–1628. doi: 10.1093/infdis/jiw329.

Kim, D. *et al.* (2013) 'The acetylproteome of Gram-positive model bacterium Bacillus subtilis', *Proteomics*, 13(10–11), pp. 1726–1736. doi: 10.1002/pmic.201200001.

Kim, J.-H. *et al.* (2019) 'Alternative Enzyme Protection Assay To Overcome the Drawbacks of the Gentamicin Protection Assay for Measuring Entry and Intracellular Survival of Staphylococci', *Infection and Immunity*. Edited by V. J. Torres, 87(5), pp. 1–16. doi: 10.1128/IAI.00119-19.

Kim, J. N., Ahn, S.-J. and Burne, R. A. (2015) 'Genetics and Physiology of Acetate Metabolism by the Pta-Ack Pathway of Streptococcus mutans', *Applied and Environmental Microbiology*. Edited by M. Kivisaar, 81(15), pp. 5015–5025. doi: 10.1128/AEM.01160-15.

Kim, M. S., Zhong, J. and Pandey, A. (2016) 'Common errors in mass spectrometry-based analysis of post-translational modifications', *Proteomics*, 16(5), pp. 700–714. doi: 10.1002/pmic.201500355.

Kim, W. J. *et al.* (2019) 'Neisseria gonorrhoeae evades autophagic killing by downregulating CD46-cyt1 and remodeling lysosomes', *PLoS Pathogens*, 15(2), pp. 1–18. doi: 10.1371/journal.ppat.1007495.

Kim, Y. R. *et al.* (2006) 'Mutation of Phosphotransacetylase but Not Isocitrate Lyase Reduces the Virulence of Salmonella enterica Serovar Typhimurium in Mice', *Infection and Immunity*, 74(4), pp. 2498–2502. doi: 10.1128/IAI.74.4.2498-2502.2006.

Klein, A. H. *et al.* (2007) 'The intracellular concentration of acetyl phosphate in Escherichia coli is sufficient for direct phosphorylation of two-component response

regulators', *Journal of Bacteriology*, 189(15), pp. 5574–5581. doi: 10.1128/JB.00564-07.

Knapp, J. S. and Clark, V. L. (1984) 'Anaerobic growth of Neisseria gonorrhoeae coupled to nitrite reduction', *Infection and Immunity*, 46(1), pp. 176–181.

De Kok, A. *et al.* (1998) 'The pyruvate dehydrogenase multi-enzyme complex from Gram-negative bacteria', *Biochimica et Biophysica Acta - Protein Structure and Molecular Enzymology*, 1385(2), pp. 353–366. doi: 10.1016/S0167-4838(98)00079-X.

Koo, H. *et al.* (2020) 'Regulation of gene expression by protein lysine acetylation in Salmonella', *Journal of Microbiology*, 58(12), pp. 979–987. doi: 10.1007/s12275-020-0483-8.

Kosono, S. *et al.* (2015) 'Changes in the acetylome and succinylome of Bacillus subtilis in response to carbon source', *PLoS ONE*. Public Library of Science, 10(6), pp. 1–24. doi: 10.1371/journal.pone.0131169.

Kuhn, M. L. *et al.* (2014) 'Structural, kinetic and proteomic characterization of acetyl phosphate-dependent bacterial protein acetylation', *PLoS ONE*, 9(4), pp. 1–26. doi: 10.1371/journal.pone.0094816.

Leighton, M. P. *et al.* (2001) 'An NMR and enzyme study of the carbon metabolism of Neisseria meningitidis', *Microbiology*, 147, pp. 1473–1482.

Lenzo, J. C. *et al.* (2016) 'Determination of Active Phagocytosis of Unopsonized Porphyromonas gingivalis by Macrophages and Neutrophils Using the pH-Sensitive Fluorescent Dye pHrodo', *Infection and Immunity*. Edited by B. A. McCormick, 84(6), pp. 1753–1760. doi: 10.1128/IAI.01482-15.

Leuko, S. and Raivio, T. L. (2012) 'Mutations That Impact the Enteropathogenic Escherichia coli Cpx Envelope Stress Response Attenuate Virulence in Galleria

mellonella', *Infection and Immunity*. Edited by S. M. Payne, 80(9), pp. 3077–3085. doi: 10.1128/IAI.00081-12.

Leuzzi, R. *et al.* (2005) 'Ng-MIP, a surface-exposed lipoprotein of Neisseria gonorrhoeae, has a peptidyl-prolyl cis/trans isomerase (PPlase) activity and is involved in persistence in macrophages', *Molecular Microbiology*, 58(3), pp. 669–681. doi: 10.1111/j.1365-2958.2005.04859.x.

Li, L. *et al.* (2018) 'First acetyl-proteome profiling of Salmonella Typhimurium revealed involvement of lysine acetylation in drug resistance', *Veterinary Microbiology*. Elsevier, 226(May), pp. 1–8. doi: 10.1016/j.vetmic.2018.09.024.

Li, Y. *et al.* (2010) 'Organization of the Electron Transfer Chain to Oxygen in the Obligate Human Pathogen Neisseria gonorrhoeae: Roles for Cytochromes c4 and c5, but Not Cytochrome c2, in Oxygen Reduction', *Journal of Bacteriology*, 192(9), pp. 2395–2406. doi: 10.1128/JB.00002-10.

Li, Y. *et al.* (2020) 'Acetylome analysis of lysine acetylation in the plant pathogenic bacterium Brenneria nigrifluens', *MicrobiologyOpen*, 9(1), pp. 1–11. doi: 10.1002/mbo3.952.

Li, Y., Krishnan, K. and Duncan, M. J. (2018) 'Post-translational regulation of a Porphyromonas gingivalis regulator', *Journal of Oral Microbiology*. Taylor & Francis, 10(1). doi: 10.1080/20002297.2018.1487743.

Lim, J. P. and Gleeson, P. A. (2011) 'Macropinocytosis: an endocytic pathway for internalising large gulps', *Immunology and Cell Biology*. Nature Publishing Group, 89(8), pp. 836–843. doi: 10.1038/icb.2011.20.

Lima, B. P. *et al.* (2011) 'Involvement of protein acetylation in glucose-induced

transcription of a stress-responsive promoter', *Molecular Microbiology*, 81(5), pp. 1190–1204. doi: 10.1111/j.1365-2958.2011.07742.x.

Lima, B. P. *et al.* (2016) 'In vitro evidence that RNA polymerase acetylation and acetyl Phosphate-Dependent CpxR phosphorylation affect CpxP transcription regulation', *FEMS Microbiology Letters*, 363(5), pp. 1–7. doi: 10.1093/femsle/fnw011.

Lin, R. *et al.* (2013) 'Acetylation Stabilizes ATP-Citrate Lyase to Promote Lipid Biosynthesis and Tumor Growth', *Molecular Cell*. Elsevier Inc., 51(4), pp. 506–518. doi: 10.1016/j.molcel.2013.07.002.

Lindner, B., Burkard, T. and Schuler, M. (2020) 'Phagocytosis assays with different pH-sensitive fluorescent particles and various readouts', *BioTechniques*, 68(5), pp. 245–250. doi: 10.2144/btn-2020-0003.

Liu, L. *et al.* (2016) 'Acetylome analysis reveals the involvement of lysine acetylation in biosynthesis of antibiotics in Bacillus amyloliquefaciens', *Scientific Reports*, 6(1), pp. 1–11. doi: 10.1038/srep20108.

Liu, Y.-T. *et al.* (2018) 'Comprehensive analysis of the lysine acetylome and its potential regulatory roles in the virulence of Streptococcus pneumoniae', *Journal of Proteomics*. Elsevier, 176(November 2017), pp. 46–55. doi: 10.1016/j.jprot.2018.01.014.

Loh, J. M. S. *et al.* (2013) 'Galleria mellonella larvae as an infection model for group A streptococcus', *Virulence*, 4(5), pp. 419–428. doi: 10.4161/viru.24930.

Lorenzen, D. R. *et al.* (2000) 'Neisseria gonorrhoeae porin modifies the oxidative burst of human professional phagocytes', *Infection and Immunity*, 68(11), pp. 6215–6222. doi: 10.1128/IAI.68.11.6215-6222.2000.

Lu, P. *et al.* (2018) 'A Subpopulation of Intracellular Neisseria gonorrhoeae Escapes

Autophagy-Mediated Killing Inside Epithelial Cells', *The Journal of Infectious Diseases*, in press(April), pp. 1–12. doi: 10.1093/infdis/jiy237.

Lu, Z. *et al.* (2011) 'Bioinformatic Analysis and Post-Translational Modification Crosstalk Prediction of Lysine Acetylation', *PLoS ONE*. Edited by N. J. Haslam. Public Library of Science, 6(12), pp. 1–9. doi: 10.1371/journal.pone.0028228.

Macek, B. *et al.* (2019) 'Protein post-translational modifications in bacteria', *Nature Reviews Microbiology*. Springer US, 17(11), pp. 651–664. doi: 10.1038/s41579-019-0243-0.

Massari, P. *et al.* (2002) 'Cutting Edge: Immune Stimulation by Neisserial Porins Is Toll-Like Receptor 2 and MyD88 Dependent', *The Journal of Immunology*, 168(4), pp. 1533–1537. doi: 10.4049/jimmunol.168.4.1533.

Massari, P. *et al.* (2003) 'Neisserial PorB is translocated to the mitochondria of HeLa cells infected with Neisseria meningitidis and protects cells from apoptosis', *Cellular Microbiology*, 5(2), pp. 99–109. doi: 10.1046/j.1462-5822.2003.00257.x.

Matthias, K. A. and Rest, R. F. (2014) 'Control of pili and sialyltransferase expression in Neisseria gonorrhoeae is mediated by the transcriptional regulator CrgA', *Molecular Microbiology*, 91(6), pp. 1120–1135. doi: 10.1111/mmi.12522.

Mavrogiorgos, N. *et al.* (2014) 'Activation of NOD receptors by Neisseria gonorrhoeae modulates the innate immune response', *Innate Immunity*, 20(4), pp. 377–389. doi: 10.1177/1753425913493453.

McCleary, W. R. and Stock, J. B. (1994) 'Acetyl phosphate and the activation of two-component response regulators', *Journal of Biological Chemistry*, 269(50), pp. 31567–31572.

Mcgee, D. J. and Rest, R. F. (1996) 'Regulation of Gonococcal Sialyltransferase, Lipooligosaccharide, and Serum Resistance by Glucose, Pyruvate, and Lactate', *INFECTION AND IMMUNITY*, 64(11), pp. 4630–4637.

McWhorter, F. Y. *et al.* (2013) 'Modulation of macrophage phenotype by cell shape', *Proceedings of the National Academy of Sciences*. National Academy of Sciences, 110(43), pp. 17253–17258. doi: 10.1073/pnas.1308887110.

Merz, A. J. and So, M. (2000) 'Interactions of Pathogenic Neisseriae with Epithelial Cell Membranes', *Annual Review of Cell and Developmental Biology*, 16(1), pp. 423–457. doi: 10.1146/annurev.cellbio.16.1.423.

De Mets, F., Van Melderen, L. and Gottesman, S. (2019) 'Regulation of acetate metabolism and coordination with the TCA cycle via a processed small RNA', *Proceedings of the National Academy of Sciences*, 116(3), pp. 1043–1052. doi: 10.1073/pnas.1815288116.

Miclet, E. *et al.* (2001) 'NMR Spectroscopic Analysis of the First Two Steps of the Pentose-Phosphate Pathway Elucidates the Role of 6-Phosphogluconolactonase', *Journal of Biological Chemistry*, 276(37), pp. 34840–34846. doi: 10.1074/jbc.M105174200.

Miksa, M. *et al.* (2009) 'A novel method to determine the engulfment of apoptotic cells by macrophages using pHrodo succinimidyl ester', *Journal of Immunological Methods*. Elsevier B.V., 342(1–2), pp. 71–77. doi: 10.1016/j.jim.2008.11.019.

Mitrophanov, A. Y. and Groisman, E. A. (2008) 'Signal integration in bacterial two-component regulatory systems.', *Genes & development*, 22(19), pp. 2601–11. doi: 10.1101/gad.1700308.

Mizerska-Dudka, M. and Andrejko, M. (2014) 'Galleria mellonella hemocytes

destruction after infection with Pseudomonas aeruginosa', *Journal of Basic Microbiology*, 54(3), pp. 232–246. doi: 10.1002/jobm.201200273.

Mizrahi, I., Biran, D. and Ron, E. Z. (2006) 'Requirement for the acetyl phosphate pathway in Escherichia coli ATP-dependent proteolysis', *Molecular Microbiology*, 62(1), pp. 201–211. doi: 10.1111/j.1365-2958.2006.05360.x.

Mizrahi, I., Biran, D. and Ron, E. Z. (2009) 'Involvement of the Pta-AckA pathway in protein folding and aggregation', *Research in Microbiology*. Elsevier Masson SAS, 160(2009), pp. 80–84. doi: 10.1016/j.resmic.2008.10.007.

Mizuno, Y. *et al.* (2016) 'Altered acetylation and succinylation profiles in Corynebacterium glutamicum in response to conditions inducing glutamate overproduction', *MicrobiologyOpen*, 5(1), pp. 152–173. doi: 10.1002/mbo3.320.

Morgan, M. K. and Decker, C. F. (2016) 'Gonorrhea', *Disease-a-Month*, 62(8), pp. 260–268. doi: 10.1016/j.disamonth.2016.03.009.

Morse, Stephen A., Stein, S. and Hines, J. (1974) 'Glucose Metabolism in Neisseria gonorrhoeae', *Journal of Bacteriology*, 120(2), pp. 702–714. doi: 10.1128/JB.120.2.702-714.1974.

Müller, A. *et al.* (2000) 'Targeting of the pro-apoptotic VDAC-like porin (PorB) of Neisseria gonorrhoeae to mitochondria of infected cells.', *The EMBO journal*, 19(20), pp. 5332–5343. doi: 10.1093/emboj/19.20.5332.

Müller, T. and Winter, D. (2017) 'Systematic Evaluation of Protein Reduction and Alkylation Reveals Massive Unspecific Side Effects by Iodine-containing Reagents', *Molecular & Cellular Proteomics*, 16(7), pp. 1173–1187. doi: 10.1074/mcp.M116.064048.

Munoz-Elias, E. J. and McKinney, J. D. (2006) 'Carbon metabolism of intracellular bacteria', *Cellular Microbiology*, 8(1), pp. 10–22. doi: 10.1111/j.1462-5822.2005.00648.x.

Nakayasu, E. S. *et al.* (2017) 'Ancient Regulatory Role of Lysine Acetylation in Central Metabolism', *mBio*. Edited by T. Msadek, 8(6), pp. 1–12. doi: 10.1128/mBio.01894-17.

Narita, T., Weinert, B. T. and Choudhary, C. (2019) 'Functions and mechanisms of non-histone protein acetylation', *Nature Reviews Molecular Cell Biology*. Springer US, 20(3), pp. 156–174. doi: 10.1038/s41580-018-0081-3.

Niu, D. *et al.* (2014) 'Highly efficient L-lactate production using engineered Escherichia coli with dissimilar temperature optima for L-lactate formation and cell growth', *Microbial Cell Factories*, 13(1), p. 78. doi: 10.1186/1475-2859-13-78.

O'Hanlon, D. E. *et al.* (2010) 'Cervicovaginal fluid and semen block the microbicidal activity of hydrogen peroxide produced by vaginal lactobacilli', *BMC Infectious Diseases*, 10(1), p. 120. doi: 10.1186/1471-2334-10-120.

O'Neill, J. (2016) *TACKLING DRUG-RESISTANT INFECTIONS GLOBALLY: FINAL REPORT AND RECOMMENDATIONS*, *THE REVIEW ON ANTIMICROBIAL RESISTANCE*. Available at: https://amr-review.org/sites/default/files/160518_Final paper_with cover.pdf.

Obergfell, K. P. and Seifert, H. S. (2016) 'The Pilin N-terminal Domain Maintains Neisseria gonorrhoeae Transformation Competence during Pilus Phase Variation', *PLoS Genetics*, 12(5), pp. 1–20. doi: 10.1371/journal.pgen.1006069.

Ogasawara, H. *et al.* (2007) 'PdhR (Pyruvate Dehydrogenase Complex Regulator) Controls the Respiratory Electron Transport System in Escherichia coli', *Journal of*

*Bacteriology*, 189(15), pp. 5534–5541. doi: 10.1128/JB.00229-07.

Ortiz, M. C. *et al.* (2015) 'Neisseria gonorrhoeae Modulates Immunity by Polarizing Human Macrophages to a M2 Profile', *PLOS ONE*. Edited by M. A. Olszewski, 10(6), p. e0130713. doi: 10.1371/journal.pone.0130713.

Ouidir, T., Kentache, T. and Hardouin, J. (2016) 'Protein lysine acetylation in bacteria: Current state of the art', *Proteomics*, 16(2), pp. 301–309. doi: 10.1002/pmic.201500258.

Overton, T. W. *et al.* (2006) 'Coordinated Regulation of the Neisseria gonorrhoeae - truncated Denitrification Pathway by the Nitric Oxide-sensitive Repressor, NsrR, and Nitrite-insensitive NarQ-NarP', *Journal of Biological Chemistry*, 281(44), pp. 33115–33126. doi: 10.1074/jbc.M607056200.

Pang, H. *et al.* (2020) 'Acetylome profiling of Vibrio alginolyticus reveals its role in bacterial virulence', *Journal of Proteomics*. Elsevier, 211(October 2019), p. 103543. doi: 10.1016/j.jprot.2019.103543.

Parks, A. R. and Escalante-Semerena, J. C. (2020) 'Modulation of the bacterial CobB sirtuin deacylase activity by N-terminal acetylation', *Proceedings of the National Academy of Sciences*, 117(27), pp. 15895–15901. doi: 10.1073/pnas.2005296117.

Parsons, N. J. *et al.* (1996) 'Lactic acid is the factor in blood cell extracts which enhances the ability of CMP-NANA to sialylate gonococcal lipopolysaccharide and induce serum resistance', *Microbial Pathogenesis*. Academic Press, pp. 87–100. doi: 10.1006/mpat.1996.0008.

Patel, M. S. *et al.* (2014) 'The Pyruvate Dehydrogenase Complexes: Structure-based Function and Regulation', *Journal of Biological Chemistry*, 289(24), pp. 16615–16623. doi: 10.1074/jbc.R114.563148.

Pegan, S. D. *et al.* (2013) 'Active Site Loop Dynamics of a Class IIa Fructose 1,6-Bisphosphate Aldolase from Mycobacterium tuberculosis', *Biochemistry*, 52(5), pp. 912–925. doi: 10.1021/bi300928u.

Pisithkul, T., Patel, N. M. and Amador-Noguez, D. (2015) 'Post-translational modifications as key regulators of bacterial metabolic fluxes', *Current Opinion in Microbiology*, 24, pp. 29–37. doi: 10.1016/j.mib.2014.12.006.

Plant, L. J. and Jonsson, A.-B. (2006) 'Type IV Pili of Neisseria gonorrhoeae Influence the Activation of Human CD4+ T Cells', *Infection and Immunity*, 74(1), pp. 442–448. doi: 10.1128/IAI.74.1.442-448.2006.

Post, D. M. B. *et al.* (2017) 'Identification and characterization of AckA-dependent protein acetylation in Neisseria gonorrhoeae', *PLOS ONE*. Edited by M. J. Edelmann, 12(6), p. e0179621. doi: 10.1371/journal.pone.0179621.

Puri, P. *et al.* (2014) 'Regulation of acetate kinase isozymes and its importance for mixed-acid fermentation in Lactococcus lactis', *Journal of Bacteriology*, 196(7), pp. 1386–1393. doi: 10.1128/JB.01277-13.

Quillin, S. J. and Seifert, H. S. (2018) 'Neisseria gonorrhoeae host adaptation and pathogenesis', *Nature Reviews Microbiology*. Nature Publishing Group, 16(4), pp. 226–240. doi: 10.1038/nrmicro.2017.169.

Ramos-Montañez, S. *et al.* (2010) 'Instability of ackA (acetate kinase) mutations and their effects on acetyl phosphate and ATP amounts in Streptococcus pneumoniae D39', *Journal of Bacteriology*, 192(24), pp. 6390–6400. doi: 10.1128/JB.00995-10.

Ramsey, M. E., Woodhams, K. L. and Dillard, J. P. (2011) 'The gonococcal genetic island and type IV secretion in the pathogenic Neisseria', *Frontiers in Microbiology*, 2(APR).

doi: 10.3389/fmicb.2011.00061.

Ray, K. *et al.* (2009) 'Life on the inside: the intracellular lifestyle of cytosolic bacteria', *Nature Reviews Microbiology*, 7(5), pp. 333–340. doi: 10.1038/nrmicro2112.

Ree, R., Varland, S. and Arnesen, T. (2018) 'Spotlight on protein N-terminal acetylation', *Experimental & Molecular Medicine*. Springer US, 50(7), pp. 1–13. doi: 10.1038/s12276-018-0116-z.

Regan, T. *et al.* (1999) 'Regulation of the lipopolysaccharide-specific sialyltransferase activity of gonococci by the growth state of the bacteria, but not by carbon source, catabolite repression or oxygen supply', *Antonie van Leeuwenhoek, International Journal of General and Molecular Microbiology*, 75(4), pp. 369–379. doi: 10.1023/A:1002019420453.

Ren, J. *et al.* (2016) 'Acetylation of Lysine 201 Inhibits the DNA-Binding Ability of PhoP to Regulate Salmonella Virulence', *PLOS Pathogens*. Edited by E. A. Groisman, 12(3), p. e1005458. doi: 10.1371/journal.ppat.1005458.

Ren, J. *et al.* (2017) 'Protein Acetylation and Its Role in Bacterial Virulence', *Trends in Microbiology*. Elsevier Ltd, 25(9), pp. 768–779. doi: 10.1016/j.tim.2017.04.001.

Ren, J. *et al.* (2019) 'Metabolic intermediate acetyl phosphate modulates bacterial virulence via acetylation', *Emerging Microbes & Infections*, 8(1), pp. 55–69. doi: 10.1080/22221751.2018.1558963.

Reverdy, A. *et al.* (2018) 'Protein lysine acetylation plays a regulatory role in bacillus subtilis multicellularity', *PLoS ONE*, 13(9), pp. 1–25. doi: 10.1371/journal.pone.0204687.

Ritter, J. L. and Genco, C. A. (2018) 'Neisseria gonorrhoeae –Induced Inflammatory

Pyroptosis in Human Macrophages is Dependent on Intracellular Gonococci and Lipooligosaccharide', *Journal of Cell Death*, 11. doi: 10.1177/1179066017750902.

Romano, A. H. and Conway, T. (1996) 'Evolution of carbohydrate metabolic pathways', *Research in Microbiology*, 147(6–7), pp. 448–455. doi: 10.1016/0923-2508(96)83998-2.

Rouquette-Loughlin, C. E. *et al.* (2017a) 'Control of gdhR Expression in Neisseria gonorrhoeae via Autoregulation and a Master Repressor (MtrR) of a Drug Efflux Pump Operon', *mBio*. Edited by M. S. Gilmore, 8(2), pp. e00449-17. doi: 10.1128/mBio.00449-17.

Rouquette-Loughlin, C. E. *et al.* (2017b) 'Control of gdhR Expression in Neisseria gonorrhoeae via Autoregulation and a Master Repressor (MtrR) of a Drug Efflux Pump Operon', *mBio*. Edited by M. S. Gilmore, 8(2), pp. 1–12. doi: 10.1128/mBio.00449-17.

Rowley, J. *et al.* (2019) 'Chlamydia, gonorrhoea, trichomoniasis and syphilis: global prevalence and incidence estimates, 2016.', *Bulletin of the World Health Organization*, 97(8), pp. 548-562P. doi: 10.2471/BLT.18.228486.

Rudel, T. *et al.* (1992) 'Interaction of two variable proteins (PilE and PilC) required for pilus-mediated adherence of Neisseria gonorrhoeae to human epithelial cells', *Molecular Microbiology*, 6(22), pp. 3439–3450. doi: 10.1111/j.1365-2958.1992.tb02211.x.

Sadykov, M. R. *et al.* (2013) 'Inactivation of the Pta-AckA Pathway Causes Cell Death in Staphylococcus aureus', *Journal of Bacteriology*, 195(13), pp. 3035–3044. doi: 10.1128/JB.00042-13.

Samland, A. K. and Sprenger, G. A. (2009) 'Transaldolase: From biochemistry to human disease', *The International Journal of Biochemistry & Cell Biology*, 41(7), pp. 1482–1494. doi: 10.1016/j.biocel.2009.02.001.

Sang, Y. *et al.* (2017) 'Acetylation Regulating Protein Stability and DNA-Binding Ability of HilD, thus Modulating Salmonella Typhimurium Virulence', *The Journal of Infectious Diseases*, 216(8), pp. 1018–1026. doi: 10.1093/infdis/jix102.

Sauer, U. and Eikmanns, B. J. (2005) 'The PEP-pyruvate-oxaloacetate node as the switch point for carbon flux distribution in bacteria.', *FEMS microbiology reviews*, 29(4), pp. 765–94. doi: 10.1016/j.femsre.2004.11.002.

Schilling, B. *et al.* (2015) 'Protein acetylation dynamics in response to carbon overflow in Escherichia coli', *Molecular Microbiology*, 98(5), pp. 847–863. doi: 10.1111/mmi.13161.

Schilling, B. *et al.* (2019) ' Global Lysine Acetylation in Escherichia coli Results from Growth Conditions That Favor Acetate Fermentation ', *Journal of Bacteriology*, 201(9), pp. 1–9. doi: 10.1128/jb.00768-18.

Schütze, A. *et al.* (2020) 'The Impact of ackA, pta, and ackA-pta Mutations on Growth, Gene Expression and Protein Acetylation in Escherichia coli K-12', *Frontiers in Microbiology*, 11(February), pp. 1–13. doi: 10.3389/fmicb.2020.00233.

Schwartz, E. R. and Reed, L. J. (1970) 'α-Keto acid dehydrogenase complexes. XIV. Regulation of the activity of the pyruvate dehydrogenase complex of Escherichia coli', *Biochemistry*, 9(6), pp. 1434–1439. doi: 10.1021/bi00808a019.

Sgrignani, J. *et al.* (2018) 'How phosphorylation influences E1 subunit pyruvate dehydrogenase: A computational study', *Scientific Reports*. Springer US, 8(1), pp. 1–11. doi: 10.1038/s41598-018-33048-z.

Shafer, W. M. *et al.* (1990) 'Molecular mechanism for the antigonococcal action of lysosomal cathepsin G', *Molecular Microbiology*, 4(8), pp. 1269–1277. doi:

10.1111/j.1365-2958.1990.tb00706.x.

Shestov, A. A. *et al.* (2014) 'Quantitative determinants of aerobic glycolysis identify flux through the enzyme GAPDH as a limiting step', *eLife*, 3(July2014), pp. 1–18. doi: 10.7554/eLife.03342.

Shi, L. *et al.* (2015) 'Infection with Mycobacterium tuberculosis induces the Warburg effect in mouse lungs', *Scientific Reports*. Nature Publishing Group, 5(November), pp. 1–13. doi: 10.1038/srep18176.

Shibutani, S. T. and Yoshimori, T. (2014) 'Autophagosome formation in response to intracellular bacterial invasion', *Cellular Microbiology*, 16(11), pp. 1619–1626. doi: 10.1111/cmi.12357.

Sigurlásdóttir, S. *et al.* (2017) 'Host cell-derived lactate functions as an effector molecule in Neisseria meningitidis microcolony dispersal', *PLOS Pathogens*. Edited by C. Tang, 13(4), p. e1006251. doi: 10.1371/journal.ppat.1006251.

Sintsova, A. *et al.* (2014) 'Global Analysis of Neutrophil Responses to Neisseria gonorrhoeae Reveals a Self-Propagating Inflammatory Program', *PLoS Pathogens*. Edited by R. M. Tsolis, 10(9), p. e1004341. doi: 10.1371/journal.ppat.1004341.

Sintsova, A. *et al.* (2015) 'Selection for a CEACAM Receptor-Specific Binding Phenotype during Neisseria gonorrhoeae Infection of the Human Genital Tract', *Infection and Immunity*. Edited by R. P. Morrison, 83(4), pp. 1372–1383. doi: 10.1128/IAI.03123-14.

Smith, H. *et al.* (2001) 'Lactate stimulation of gonococcal metabolism in media containing glucose: Mechanism, impact on pathogenicity, and wider implications for other pathogens', *Infection and Immunity*, 69(11), pp. 6565–6572. doi:

10.1128/IAI.69.11.6565-6572.2001.

Smith, H., Tang, C. M. and Exley, R. M. (2007) ‘Effect of host lactate on gonococci and meningococci: New concepts on the role of metabolites in pathogenicity’, *Infection and Immunity*, 75(9), pp. 4190–4198. doi: 10.1128/IAI.00117-07.

Somerville, G. A. *et al.* (2003) ‘Correlation of Acetate Catabolism and Growth Yield in Staphylococcus aureus: Implications for Host-Pathogen Interactions’, *Infection and Immunity*, 71(8), pp. 4724–4732. doi: 10.1128/IAI.71.8.4724-4732.2003.

Šoštarić, N. *et al.* (2018) ‘Effects of Acetylation and Phosphorylation on Subunit Interactions in Three Large Eukaryotic Complexes’, *Molecular & Cellular Proteomics*, 17(12), pp. 2387–2401. doi: 10.1074/mcp.RA118.000892.

Spencer-Smith, R. *et al.* (2016) ‘DNA uptake sequences in Neisseria gonorrhoeae as intrinsic transcriptional terminators and markers of horizontal gene transfer’, *Microbial Genomics*, 2(8), p. e000069. doi: 10.1099/mgen.0.000069.

Starai, V. J. *et al.* (2002) ‘Sir2-dependent activation of Acetyl-CoA Synthetase by deacetylation of active lysine.’, *Science.*, 298(5602), pp. 2390–2392. doi: 10.1126/science.1077650.

Starai, V. J. and Escalante-Semerena, J. C. (2004) ‘Identification of the protein acetyltransferase (Pat) enzyme that acetylates acetyl-CoA synthetase in Salmonella enterica’, *Journal of Molecular Biology*, 340(5), pp. 1005–1012. doi: 10.1016/j.jmb.2004.05.010.

Stein, D. C. *et al.* (2015) ‘Expression of Opacity Proteins Interferes with the Transmigration of Neisseria gonorrhoeae across Polarized Epithelial Cells’, *PLOS ONE*. Edited by J.-P. Gorvel, 10(8), p. e0134342. doi: 10.1371/journal.pone.0134342.

Stern, A. *et al.* (1986) 'Opacity genes in Neisseria gonorrhoeae: Control of phase and antigenic variation', *Cell*, 47(1), pp. 61–71. doi: 10.1016/0092-8674(86)90366-1.

Stincone, A. *et al.* (2015) 'The return of metabolism: biochemistry and physiology of the pentose phosphate pathway', *Biological Reviews*, 90(3), pp. 927–963. doi: 10.1111/brv.12140.

Strickler, S. S. *et al.* (2006) 'Protein stability and surface electrostatics: A charged relationship', *Biochemistry*, 45(9), pp. 2761–2766. doi: 10.1021/bi0600143.

Studier, F. W. and Moffatt, B. A. (1986) 'Use of bacteriophage T7 RNA polymerase to direct selective high-level expression of cloned genes', *Journal of Molecular Biology*, 189(1), pp. 113–130. doi: 10.1016/0022-2836(86)90385-2.

Tacconelli, E. and Magrini, N. (2017) *Global Priority List Of Antibiotic-Resistant Bacteria To Guide Research, Discovery, And Development Of New Antibiotics*, *WHO*. Available at: http://www.who.int/medicines/publications/WHO-PPL-Short_Summary_25Feb-ET_NM_WHO.pdf?ua=1 (Accessed: 7 July 2017).

Tait, S. W. G. and Green, D. R. (2010) 'Mitochondria and cell death: outer membrane permeabilization and beyond', *Nature Reviews Molecular Cell Biology*. Nature Publishing Group, 11(9), pp. 621–632. doi: 10.1038/nrm2952.

Tammam, S. *et al.* (2011) 'Characterization of the PilN, PilO and PilP type IVa pilus subcomplex', *Molecular Microbiology*, 82(6), pp. 1496–1514. doi: 10.1111/j.1365-2958.2011.07903.x.

Thao, S. *et al.* (2010) 'Nε−Lysine Acetylation of a Bacterial Transcription Factor Inhibits Its DNA-Binding Activity', *PLoS ONE*. Edited by C. Herman, 5(12), p. e15123. doi: 10.1371/journal.pone.0015123.

Thao, S. and Escalante-Semerena, J. C. (2011) 'Biochemical and Thermodynamic Analyses of Salmonella enterica Pat, a Multidomain, Multimeric Nε-Lysine Acetyltransferase Involved in Carbon and Energy Metabolism', *mBio*. Edited by S. Adhya, 2(5). doi: 10.1128/mBio.00216-11.

Todd, J. J. (2014) 'Lactate: valuable for physical performance and maintenance of brain function during exercise', *Bioscience Horizons*, 7, pp. 1–7. doi: 10.1093/biohorizons/hzu001.

Tsai, C. J.-Y., Loh, J. M. S. and Proft, T. (2016) 'Galleria mellonella infection models for the study of bacterial diseases and for antimicrobial drug testing', *Virulence*. Taylor & Francis, 7(3), pp. 214–229. doi: 10.1080/21505594.2015.1135289.

Tsai, M.-Y. *et al.* (2016) 'Electrostatics, structure prediction, and the energy landscapes for protein folding and binding', *Protein Science*, 25(1), pp. 255–269. doi: 10.1002/pro.2751.

Tyanova, S., Temu, T. and Cox, J. (2016) 'The MaxQuant computational platform for mass spectrometry-based shotgun proteomics', *Nature Protocols*. Nature Publishing Group, 11(12), pp. 2301–2319. doi: 10.1038/nprot.2016.136.

Tzeng, Y.-L. *et al.* (2004) 'The MisR/MisS Two-component Regulatory System Influences Inner Core Structure and Immunotype of Lipooligosaccharide in Neisseria meningitidis', *Journal of Biological Chemistry*, 279(33), pp. 35053–35062. doi: 10.1074/jbc.M401433200.

Unemo, M. and Jensen, J. S. (2017) 'Antimicrobial-resistant sexually transmitted infections: gonorrhoea and Mycoplasma genitalium', *Nature Reviews Urology*, 14(3), pp. 139–152. doi: 10.1038/nrurol.2016.268.

Valgepea, K. *et al.* (2010) ‘Systems biology approach reveals that overflow metabolism of acetate in Escherichia coli is triggered by carbon catabolite repression of acetyl-CoA synthetase.’, *BMC systems biology*, 4(166), pp. 1–13. doi: 10.1186/1752-0509-4-166.

VanCleave, T. T. *et al.* (2017) ‘Impact of Gentamicin Concentration and Exposure Time on Intracellular Yersinia pestis’, *Frontiers in Cellular and Infection Microbiology*, 7(December), pp. 1–11. doi: 10.3389/fcimb.2017.00505.

VanDrisse, C. M. and Escalante-Semerena, J. C. (2019) ‘Protein Acetylation in Bacteria’, *Annual Review of Microbiology*, 73(1), pp. 1–22. doi: 10.1146/annurev-micro-020518-115526.

Vascon, F. *et al.* (2020) ‘Protein electrostatics: From computational and structural analysis to discovery of functional fingerprints and biotechnological design’, *Computational and Structural Biotechnology Journal*. The Author(s), 18, pp. 1774–1789. doi: 10.1016/j.csbj.2020.06.029.

Velmurugan, K. *et al.* (2007) ‘Mycobacterium tuberculosis nuoG Is a virulence gene that inhibits apoptosis of infected host cells’, *PLoS Pathogens*, 3(7), pp. 0972–0980. doi: 10.1371/journal.ppat.0030110.

Venkat, S., Gregory, C., Gan, Q., *et al.* (2017) ‘Biochemical Characterization of the Lysine Acetylation of Tyrosyl-tRNA Synthetase in Escherichia coli’, *ChemBioChem*, 18(19), pp. 1928–1934. doi: 10.1002/cbic.201700343.

Venkat, S., Gregory, C., Sturges, J., *et al.* (2017) ‘Studying the Lysine Acetylation of Malate Dehydrogenase’, *Journal of Molecular Biology*. Elsevier Ltd, 429(9), pp. 1396–1405. doi: 10.1016/j.jmb.2017.03.027.

Venkat, S. *et al.* (2018) ‘Characterizing Lysine Acetylation of Isocitrate Dehydrogenase

in Escherichia coli', *Journal of Molecular Biology*. Elsevier Ltd, 430(13), pp. 1901–1911. doi: 10.1016/j.jmb.2018.04.031.

Verdin, E. and Ott, M. (2013) 'Acetylphosphate: A novel link between Lysine Acetylation and intermediary metabolism in bacteria', *Molecular Cell*. Elsevier Inc., 51(2), pp. 132–134. doi: 10.1016/j.molcel.2013.07.006.

Verdin, E. and Ott, M. (2015) '50 years of protein acetylation: from gene regulation to epigenetics, metabolism and beyond', *Nature Reviews Molecular Cell Biology*. Nature Publishing Group, 16(4), pp. 258–264. doi: 10.1038/nrm3931.

Vetting, M. W. *et al.* (2005) 'Structure and functions of the GNAT superfamily of acetyltransferases', *Archives of Biochemistry and Biophysics*, 433(1), pp. 212–226. doi: 10.1016/j.abb.2004.09.003.

Virji, M. (2009) 'Pathogenic neisseriae: surface modulation, pathogenesis and infection control', *Nature Reviews Microbiology*, 7(4), pp. 274–286. doi: 10.1038/nrmicro2097.

Vogel, H. *et al.* (2011) 'A comprehensive transcriptome and immune-gene repertoire of the lepidopteran model host Galleria mellonella', *BMC Genomics*, 12(1), p. 308. doi: 10.1186/1471-2164-12-308.

Vogelauer, M. *et al.* (2012) 'Stimulation of Histone Deacetylase Activity by Metabolites of Intermediary Metabolism', *Journal of Biological Chemistry*. Â© 2012 ASBMB. Currently published by Elsevier Inc; originally published by American Society for Biochemistry and Molecular Biology., 287(38), pp. 32006–32016. doi: 10.1074/jbc.M112.362467.

Wagner, G. R. and Payne, R. M. (2013) 'Widespread and enzyme-independent NE-acetylation and NE-succinylation of proteins in the chemical conditions of the

mitochondrial matrix', *Journal of Biological Chemistry*, 288(40), pp. 29036–29045. doi: 10.1074/jbc.M113.486753.

Waligora, E. A. *et al.* (2014) 'Role of intracellular carbon metabolism pathways in Shigella flexneri virulence', *Infection and Immunity*, 82(7), pp. 2746–2755. doi: 10.1128/IAI.01575-13.

Wang, G. *et al.* (2020) 'Proteomics analysis reveals the effect of Aeromonas hydrophila sirtuin CobB on biological functions', *Journal of Proteomics*. Elsevier, 225(May), p. 103848. doi: 10.1016/j.jprot.2020.103848.

Wang, Q. *et al.* (2010) 'Acetylation of Metabolic Enzymes Coordinates Carbon Source Utilization and Metabolic Flux', *Science*, 327(5968), pp. 1004–1007. doi: 10.1126/science.1179687.

Wanner, B. L. and Wilmes-Riesenberg, M. R. (1992) 'Involvement of phosphotransacetylase, acetate kinase, and acetyl phosphate synthesis in control of the phosphate regulon in Escherichia coli', *Journal of Bacteriology*, 174(7), pp. 2124–2130. Available at: https://www.ncbi.nlm.nih.gov/pmc/articles/PMC205829/pdf/jbacter00073-0082.pdf (Accessed: 24 July 2017).

Weiss, G. and Schaible, U. E. (2015) 'Macrophage defense mechanisms against intracellular bacteria', *Immunological Reviews*, 264(1), pp. 182–203. doi: 10.1111/imr.12266.

Whiteley, H. R. and Pelroy, R. A. (1972) 'Purification and Properties of Phosphotransacetylase from Vellionella alcalescens', *The Journal of biological chemistry*, 247(6), pp. 1911–1917.

WHO (2016) *Global Health Sector Strategy on Sexually Transmitted Infections 2016-*

*2021*, *World Health Organization*. doi: 10.1055/s-2007-970201.

WHO (2019a) 'Progress report on HIV, viral hepatitis and sexually transmitted infections 2019. Accountability for the global health sector strategies, 2016–2021', *World Health Organization*, pp. 1–48.

WHO (2019b) *Sexually Transmitted Infections*, *WHO*.

Winther-Larsen, H. C. *et al.* (2001) 'Neisseria gonorrhoeae PilV, a type IV pilus-associated protein essential to human epithelial cell adherence', *Proceedings of the National Academy of Sciences*, 98(26), pp. 15276–15281. doi: 10.1073/pnas.261574998.

Wise, J. (2020) 'Gonorrhoea cases in England hit highest level since records began', *BMJ*, 370, p. m3425. doi: 10.1136/bmj.m3425.

Wolfe, A. J. (2005) 'The Acetate Switch', *Microbiology and Molecular Biology Reviews*, 69(1), pp. 12–50. doi: 10.1128/MMBR.69.1.12-50.2005.

Wolfe, A. J. (2016) 'Bacterial protein acetylation: new discoveries unanswered questions', *Current Genetics*. Springer Berlin Heidelberg, 62(2), pp. 335–341. doi: 10.1007/s00294-015-0552-4.

Won, H. I. *et al.* (2021) 'Inactivation of the Pta-AckA Pathway Impairs Fitness of Bacillus anthracis during Overflow Metabolism', *Journal of Bacteriology*. Edited by M. Y. Galperin, 203(9), pp. 1–12. doi: 10.1128/JB.00660-20.

Xiong, Y. and Guan, K.-L. (2012) 'Mechanistic insights into the regulation of metabolic enzymes by acetylation', *Journal of Cell Biology*, 198(2), pp. 155–164. doi: 10.1083/jcb.201202056.

Xu, J.-Y. *et al.* (2018) 'Protein Acetylation and Butyrylation Regulate the Phenotype and Metabolic Shifts of the Endospore-forming Clostridium acetobutylicum', *Molecular &*

*Cellular Proteomics*, 17(6), pp. 1156–1169. doi: 10.1074/mcp.RA117.000372.

Xu, Y. *et al.* (2014) 'Oxidative Stress Activates SIRT2 to Deacetylate and Stimulate Phosphoglycerate Mutase', *Cancer Research*, 74(13), pp. 3630–3642. doi: 10.1158/0008-5472.CAN-13-3615.

Yahara, K. *et al.* (2018) 'Genomic surveillance of Neisseria gonorrhoeae to investigate the distribution and evolution of antimicrobial-resistance determinants and lineages', *Microbial Genomics*, 4(8). doi: 10.1099/mgen.0.000205.

Yang, X.-J. and Seto, E. (2008) 'Lysine Acetylation: Codified Crosstalk with Other Posttranslational Modifications', *Molecular Cell*, 31(4), pp. 449–461. doi: 10.1016/j.molcel.2008.07.002.

Yang, Y.-T., Bennett, G. N. and San, K.-Y. (1999) 'Effect of inactivation of nuo and ackA-pta on redistribution of metabolic fluxes inEscherichia coli', *Biotechnology and Bioengineering*, 65(3), pp. 291–297. doi: 10.1002/(SICI)1097-0290(19991105)65:3<291::AID-BIT6>3.0.CO;2-F.

Yates, E. *et al.* (2000) 'In a medium containing glucose, lactate carbon is incorporated by gonococci predominantly into fatty acids and glucose carbon incorporation is increased: implications regarding lactate stimulation of metabolism', *International Journal of Medical Microbiology*, 290(7), pp. 627–639. doi: http://dx.doi.org/10.1016/S1438-4221(00)80012-0.

Ye, Q. *et al.* (2017) 'Acetylation of lysine ϵ-amino groups regulates aminoacyl-tRNA synthetase activity in Escherichia coli', *Journal of Biological Chemistry*, 292(25), pp. 10709–10722. doi: 10.1074/jbc.M116.770826.

Yoshida, Y. *et al.* (2019) 'Characterization of the phosphotransacetylase-acetate kinase

pathway for ATP production in Porphyromonas gingivalis', *Journal of Oral Microbiology*. Taylor & Francis, 11(1), p. 1588086. doi: 10.1080/20002297.2019.1588086.

Yu, B. J. *et al.* (2008) 'The diversity of lysine-acetylated proteins in Escherichia coli', *Journal of Microbiology and Biotechnology*, 18(9), pp. 1529–1536. doi: 7509 [pii].

Zalucki, Y. M., Dhulipala, V. and Shafer, W. M. (2012) 'Dueling regulatory properties of a transcriptional activator (MtrA) and repressor (MtrR) that control efflux pump gene expression in Neisseria gonorrhoeae.', *mBio*, 3(6), pp. 1–7. doi: 10.1128/mBio.00446-12.

Zhang, J. *et al.* (2008) 'Lysine Acetylation Is a Highly Abundant and Evolutionarily Conserved Modification in Escherichia Coli', *Molecular & Cellular Proteomics*, 8(2), pp. 215–225. doi: 10.1074/mcp.M800187-MCP200.

Zhang, K. *et al.* (2013) 'Comprehensive profiling of protein lysine acetylation in Escherichia coli', *Journal of Proteome Research*, 12(2), pp. 844–851. doi: 10.1021/pr300912q.

Zhao, S. *et al.* (2010) 'Regulatory Role of the MisR/S Two-Component System in Hemoglobin Utilization in Neisseria meningitidis', *Infection and Immunity*, 78(3), pp. 1109–1122. doi: 10.1128/IAI.00363-09.

Zhou, Q. *et al.* (2018) 'Biochemical Basis of E. coli Topoisomerase I Relaxation Activity Reduction by Nonenzymatic Lysine Acetylation', *International Journal of Molecular Sciences*, 19(5), p. 1439. doi: 10.3390/ijms19051439.

Zhu, W. *et al.* (2012) 'Neisseria gonorrhoeae Suppresses Dendritic Cell-Induced, Antigen-Dependent CD4 T Cell Proliferation', *PLoS ONE*. Edited by D. Chakravortty, 7(7), p. e41260. doi: 10.1371/journal.pone.0041260.

Ziveri, J. *et al.* (2017) 'The metabolic enzyme fructose-1,6-bisphosphate aldolase acts as a transcriptional regulator in pathogenic Francisella', *Nature Communications*. Springer US, 8(1), p. 853. doi: 10.1038/s41467-017-00889-7.

Zughaier, S. M., Kandler, J. L. and Shafer, W. M. (2014) 'Neisseria gonorrhoeae Modulates Iron-Limiting Innate Immune Defenses in Macrophages', *PLoS ONE*. Edited by B. Adler, 9(1), p. e87688. doi: 10.1371/journal.pone.0087688.

Zughaier, S. M., Rouquette-Loughlin, C. E. and Shafer, W. M. (2020) 'Identification of a neisseria gonorrhoeae histone deacetylase: Epigenetic impact on host gene expression', *Pathogens*, 9(2). doi: 10.3390/pathogens9020132.

# Supplements

# 8 Supplements

**Table 8.1 Genes of proteins with five or more acetylation sites identified in the KEGG pathway sin *N. gonorrhoeae* MS11**

| KEGG.name | Count | Genes |
|---|---|---|
| **ABC transporters** | 15 | macB, fbpC, NGO_2139, NGO_2056, potA, NGO_0269, lolD, NGO_1605, NGO_2137, msbA, NGO_0196, NGO_0217, NGO_1253, NGO_0195, NGO_1922 |
| **Alanine, aspartate and glutamate metabolism** | 17 | carA, pyrB, NGO_1358, pyrI, NGO_1600, carB, purF, NGO_1452, argH, NGO_1711, gabD, NGO_1568, glmS, aspA, NGO_1047, purA, argG |
| **Amino sugar and nucleotide sugar metabolism** | 11 | pgi1, NGO_0375, glmS, glmU, murA, glmM, murB, glk, NGO_0220, NGO_1896, pgi2 |
| **Aminoacyl-tRNA biosynthesis** | 23 | ileS, leuS, proS, glyQ, cysS, gltX, metG, glnS, glyS, lysS, alaS, argS, fmt, valS, gatB, gatA, trpS, pheT, thrS, pheS, tyrS, hisS, gatC |
| **Arginine and proline metabolism** | 17 | argB, NGO_1358, NGO_0949, argD, NGO_1600, NGO_1487, NGO_1452, argH, NGO_0435, NGO_0713, proC, proA, argG, speB, argC, argJ, argF |
| **Bacterial secretion system** | 9 | ffh, NGO_0188, secA, ftsY, yidC, secY, secE, secD, tatA |
| **Base excision repair** | 7 | NGO_0414, polA, ligA, NGO_1994, nth, NGO_0710, NGO_1561 |
| **Butanoate metabolism** | 7 | aceE, NGO_0186, NGO_0921, gabD, NGO_1235, NGO_1236, NGO_0923 |
| **C5-Branched dibasic acid metabolism** | 6 | sucD, leuD, NGO_1235, NGO_1236, leuC, sucC |
| **Carbon fixation pathways in prokaryotes** | 17 | NGO_1231, ackA, NGO_0929, NGO_0921, NGO_0214, ppc, accA, NGO_0200, sucD, fhs, NGO_0044, accD, sucC, NGO_1082, NGO_0923, fumC, folD |
| **TCA cycle (TCA cycle)** | 15 | NGO_0562, gltA, aceE, NGO_0916, NGO_1231, NGO_0921, sucA, sucD, NGO_0925, NGO_0915, NGO_0564, sucC, NGO_1082, NGO_0923, fumC |
| **Cysteine and methionine metabolism** | 20 | NGO_0386, NGO_1209, NGO_1149, metXS, NGO_1773, NGO_0956, NGO_0340, NGO_0676, NGO_1452, metE, NGO_0435, NGO_0779, asd, metK, mtnN, NGO_1795, NGO_0873, NGO_1329, NGO_1991, luxS |
| **DNA replication** | 11 | dnaG, NGO_1031, NGO_0283, dnaQ, NGO_0078, polA, NGO_0002, ligA, NGO_0347, dnaX, NGO_0451 |
| **Fatty acid biosynthesis** | 10 | NGO_1763, fabH, accA, fabZ, NGO_0044, NGO_1666, NGO_2166, NGO_0045, accD, fabG |
| **Folate biosynthesis** | 5 | NGO_1342, NGO_0131, NGO_0266, NGO_2112, NGO_0323 |
| **Glutathione metabolism** | 8 | gshB, pepN, zwf, pepA, NGO_1914, NGO_0680, NGO_0435, NGO_1082 |
| **Glycerophospholipid metabolism** | 6 | NGO_1216, gpsA, plsX, psd, NGO_1492, NGO_2069 |
| **Glycine, serine and threonine metabolism** | 18 | NGO_0562, NGO_0386, gcvT, trpA, thrB, NGO_1468, NGO_1773, glyA, NGO_0956, NGO_0925, NGO_0915, NGO_0689, NGO_0779, trpB, serC, gcvP, ilvA, asd |
| **Glycolysis / Gluconeogenesis** | 18 | NGO_0562, aceE, gapA, gpmA, NGO_1931, eno, pgi1, NGO_0375, NGO_0925, NGO_1881, NGO_0915, tpiA, NGO_0564, pgk, NGO_0034, glk, fbp, pgi2 |

| | | |
|---|---|---|
| **Glyoxylate and dicarboxylate metabolism** | 5 | gltA, NGO_1231, NGO1052, NGO_0713, NGO_0203 |
| **Histidine metabolism** | 11 | hisG, NGO_1860, hisI, hisA, hisH, hisB, hisF, hisD, hisC, hisZ, hisE |
| **Homologous recombination** | 17 | NGO_0414, NGO_1031, NGO_0283, recB, dnaQ, NGO_0078, polA, recA, NGO_0002, recD, recR, ruvC, NGO_0347, ruvA, dnaX, recC, ruvB |
| **Lipopolysaccharide biosynthesis** | 12 | hldD, lpxD, NGO_0987, NGO_0105, NGO_1915, kdsA, lpxA, NGO_1608, lpxK, gmhA, kdsB, lpxB |
| **Lysine biosynthesis** | 15 | argB, NGO_0460, dapB, NGO_0956, argD, dapE, dapD, NGO_0779, asd, dapA, argC, murE, dapF, murF, lysA |
| **Methane metabolism** | 13 | NGO_1767, gpmA, ackA, NGO_1468, NGO_0929, eno, glyA, NGO_0214, ppc, NGO_0200, NGO_0034, serC, fbp |
| **Mismatch repair** | 14 | NGO_0414, mutL, NGO_1031, xseA, NGO_0283, dnaQ, NGO_0078, mutS, NGO_1757, NGO_0002, xseB, ligA, NGO_0347, dnaX |
| **Nicotinate and nicotinamide metabolism** | 7 | NGO_1565, nadA, NGO_1568, pncB, NGO_1933, nadK, pntB |
| **Nitrogen metabolism** | 10 | NGO_0386, gcvT, NGO_1024, NGO_1358, NGO_1600, NGO_2079, NGO_0574, aspA, NGO_1276, NGO_1514 |
| **Nucleotide excision repair** | 7 | uvrB, uvrA, polA, NGO_1757, mfd, ligA, uvrC |
| **One carbon pool by folate** | 9 | gcvT, NGO_0929, glyA, fmt, fhs, purH, thyA, folD, purN |
| **Oxidative phosphorylation** | 21 | atpG, atpH, ppa, atpC, NGO_0921, NGO_1373, atpA, NGO_1746, nuoI, nuoB, atpF, NGO_2029, nuoD, atpD, NGO_1745, NGO_1747, NGO_0923, ppk, NGO_2031, nuoC, NGO_1372 |
| **Pantothenate and CoA biosynthesis** | 13 | NGO_1307, acpS, ilvC, birA/coaX, ilvD, NGO_1235, NGO_1236, panB, NGO_1665, panC, coaD, coaE, panD |
| **Pentose phosphate pathway** | 14 | NGO_0714, pgl, rpiA, pgi1, NGO_0375, zwf, NGO_1914, prs, NGO_0034, NGO_1028, NGO_0713, tal, fbp, pgi2 |
| **Peptidoglycan biosynthesis** | 12 | ddl, NGO_0107, NGO_0443, murA, murB, murG, mraY, murD, murJ, murC, murE, murF |
| **Phenylalanine, tyrosine and tryptophan biosynthesis** | 17 | trpD, trpC, trpA, NGO_1695, hisC, NGO_1452, aroC, aroK, trpF, trpB, trpE, aroA, aroD, pheA, NGO_1204, NGO_1329, aroB |
| **Porphyrin and chlorophyll metabolism** | 9 | gltX, hemH, hemA, hemL, hemE, NGO_0385, NGO_1580, NGO_0234, NGO_0360 |
| **Propanoate metabolism** | 8 | ackA, NGO_0214, accA, sucD, NGO_0044, NGO_0045, accD, sucC |
| **Protein export** | 10 | ffh, NGO_0188, NGO_0343, secA, ftsY, yidC, secY, secE, secD, tatA |
| **Purine metabolism** | 36 | NGO_0221, NGO_1041, pnp, rpoC, NGO_0614, NGO_1382, guaB, NGO_0283, dnaQ, rpoA, purD, NGO_0375, rpoB, NGO_0078, polA, prs, purF, apaH, purC, NGO_1711, purH, NGO_1881, NGO_0002, guaA, purM, adk, purL, NGO_1308, NGO_2035, NGO_0347, purE, dnaX, purA, purK, apt, purN |
| **Pyrimidine metabolism** | 29 | carA, cmk, pnp, rpoC, NGO_0614, pyrB, pyrI, NGO_0283, dnaQ, NGO_0580, rpoA, rpoB, pyrD, NGO_0078, carB, polA, pyrG, NGO_0002, tmk, pyrE, upp, pyrC, thyA, NGO_0347, dnaX, pyrF, pyrH, dut, dcd |
| **Pyruvate metabolism** | 19 | NGO_0562, aceE, leuA, ackA, NGO_0214, NGO_1336, ppc, accA, NGO_0200, lldD, NGO_0925, NGO_1881, NGO_0915, NGO_0564, dld, NGO_0044, NGO_0045, accD, mqo |
| **Riboflavin metabolism** | 5 | ribA, NGO_0089, ribH, NGO_0068, ribB |
| **Ribosome** | 52 | rplW, rplX, rplC, rplA, rplE, rpsB, rpsT, rplB, rplF, rplV, rpsE, rpsC, rpsA, rplO, rplP, rplL, rplN, rpsR, rplD, rplY, rpsJ, rpmE, rpmJ, rplJ, rpsM, rplU, rpsH, rpsG, rpsP, rpsS, rplI, rplS, rplR, |

| | | |
|---|---|---|
| | | rpsL, rplT, rpmH, rplQ, rplK, rpsO, rpmA, rpsQ, rplM, rpsK, rpsN, rpmG, rpmD, rpsI, rpsF, rpsU, rpsD, rpmC, rpmI |
| **RNA degradation** | 12 | groL, pnp, eno, rho, dnaK, rnr, pcnB, rne, rppH, NGO_1722, ppk, hfq |
| **RNA polymerase** | 5 | rpoC, NGO_1944, rpoD, rpoA, rpoB |
| **Starch and sucrose metabolism** | 5 | pgi1, NGO_0375, glk, NGO_0220, pgi2 |
| **Streptomycin biosynthesis** | 5 | NGO_0375, NGO_0671, NGO_0332, NGO_2161, glk |
| **Terpenoid backbone biosynthesis** | 9 | dxs, NGO_1675, ispG, ispD, dxr, NGO_1735, ispH, ispE, ispF |
| **Thiamine metabolism** | 6 | NGO_0221, thiG, iscS, thiL, NGO_1160, thiE |
| **Two-component system** | 5 | NGO_0752, dnaA, NGO_1600, glnD, NGO_1182 |
| **Tyrosine metabolism** | 5 | NGO_1860, hisC, NGO_1452, gabD, NGO_1329 |
| **Ubiquinone and other terpenoid-quinone biosynthesis** | 6 | ubiB, ubiG, ubiD, ubiE, ubiX, ubiA |
| **Valine, leucine and isoleucine biosynthesis** | 15 | ileS, aceE, leuS, leuA, ilvC, leuD, valS, ilvD, NGO_1235, NGO_1236, leuC, NGO_1047, ilvA, NGO_1665, leuB |
| **Valine, leucine and isoleucine degradation** | 5 | NGO_0562, NGO_0925, NGO_0915, NGO_1665, NGO_1243 |

**Table 8.2 Acetylome of isogenic mutant strains.** The proteins with more than 2 significant acetylation sites were selected in the three isogenic mutant strains. The sites were classified according to the fold change difference and the position of the acetylated lysines are indicated in the last three columns for each strain.

| Protein name | UniProt entry | Gene name | Fold change | Δ*ackA* | Δ*pta* | Δ*hdac* |
|---|---|---|---|---|---|---|
| **10 kDa chaperonin** | Q5F542 | groS | Increased | 20, 34, 47, 76, 69, 64, 60 | 34, 47, 64, 76 | 20, 34, 47 |
| **10 kDa chaperonin** | Q5F542 | groS | Decreased | - | 69, 64 | - |
| **16S rRNA methyltransferase** | Q5F5P8 | NGO_1869 | Increased | 191, 107 | - | - |
| **2-C-methyl-D-erythritol 2,4-cyclodiphosphate synthase** | Q5F830 | ispF | Increased | 135, 139 | - | - |
| **2-C-methyl-D-erythritol 4-phosphate cytidylyltransferase** | Q5F829 | ispD | Increased | 212, 145 | - | - |
| **2-isopropylmalate synthase** | Q5F8D4 | leuA | Decreased | 69, 400 | - | - |
| **2-oxoglutarate dehydrogenase** | Q5F874 | sucA | Increased | 46, 69, 563, 517 | 46, 867, 517, 86 | 46, 877 |
| **2-oxoglutarate dehydrogenase** | Q5F874 | sucA | Decreased | - | 477, 872, 563 | - |
| **2,3-bisphosphoglycerate-dependent phosphoglycerate mutase** | Q5F7C0 | gpmA | Increased | 103, 97, 152, 174, 103, 40, 26, 98, 97 | - | - |
| **2,3-bisphosphoglycerate-dependent phosphoglycerate mutase** | Q5F7C0 | gpmA | Decreased | - | 98, 97 | - |
| **23S rRNA pseudouridine synthase RluD** | Q5F9V9 | NGO_0278 | Increased | 47, 228 | - | - |
| **3'-5' exonuclease** | Q5FA73 | NGO_0156 | Increased | 240, 253 | - | - |
| **3-deoxy-D-manno-octulosonic acid transferase** | Q5F5K9 | NGO_1915 | Decreased | - | 157, 223 | - |
| **3-hydroxyacyl-[acyl-carrier-protein] dehydratase FabZ** | Q5F5W5 | fabZ | Increased | 14, 125 | - | - |
| **3-isopropylmalate dehydratase large subunit** | Q5F8T1 | leuC | Increased | 277, 81 | - | - |
| **3-oxoacyl-acyl-carrier-protein synthase 2** | Q5F603 | NGO_1763 | Increased | 316, 66 | - | - |
| **3-oxoacyl-acyl-carrier-protein synthase 3** | Q5F4X5 | fabH | Increased | 189, 26, 217 | 173, 189, 26 | 189, 26 |
| **3,4-dihydroxy-2-butanone 4-phosphate synthase** | Q5F8Q9 | ribB | Increased | 263, 397 | - | - |
| **3,4-dihydroxy-2-butanone 4-phosphate synthase** | Q5F8Q9 | ribB | Decreased | - | 263, 397 | - |
| **30S ribosomal protein S1** | Q5F905 | rpsA | Increased | 156, 517, 248, 253, 553, 156, 517, 245 | 197, 451, 245 | - |
| **30S ribosomal protein S10** | Q5F5S5 | rpsJ | Increased | 82, 45, 37 | - | - |
| **30S ribosomal protein S12** | Q5F5S1 | rpsL | Decreased | 30, 20 | - | - |
| **30S ribosomal protein S17** | Q5F5T6 | rpsQ | Increased | 83, 45 | 71, 45 | - |

| | | | | | | |
|---|---|---|---|---|---|---|
| **30S ribosomal protein S2** | Q5F5F3 | rpsB | Increased | 45, 117, 131, 117 | - | - |
| **30S ribosomal protein S3** | Q5F5T3 | rpsC | Increased | 126, 88, 34, 88, 80 | - | 209, 34 |
| **30S ribosomal protein S7** | Q5F5S2 | rpsG | Increased | 76, 52, 53 | - | - |
| **4-hydroxy-3-methylbut-2-en-1-yl diphosphate synthase** | Q5F913 | ispG | Increased | 205, 156 | - | - |
| **50S ribosomal protein L1** | Q5F5R2 | rplA | Increased | 31, 154, 141 | - | 198, 141 |
| **50S ribosomal protein L11** | Q5F5R1 | rplK | Increased | 97, 81, 72, 82, 81 | 97, 72 | - |
| **50S ribosomal protein L14** | Q5F5T7 | rplN | Increased | 78, 90 | - | - |
| **50S ribosomal protein L17** | Q5F5V3 | rplQ | Increased | 78, 118 | - | - |
| **50S ribosomal protein L18** | Q5F5U3 | rplR | Increased | 63, 76 | - | - |
| **50S ribosomal protein L20** | Q5F9U1 | rplT | Decreased | - | 112, 78 | - |
| **50S ribosomal protein L22** | Q5F5T2 | rplV | Decreased | 78, 98 | - | - |
| **50S ribosomal protein L24** | Q5F5T8 | rplX | Increased | 91, 84 | - | - |
| **50S ribosomal protein L25** | Q5F9F4 | rplY | Increased | 54, 63, 175, 188, 189 | - | - |
| **50S ribosomal protein L3** | Q5F5S7 | rplC | Decreased | 71, 172 | - | - |
| **50S ribosomal protein L31** | Q5F513 | rpmE | Increased | 64, 64, 60, 70 | - | - |
| **50S ribosomal protein L33** | Q5F683 | rpmG | Increased | 46, 49 | - | - |
| **50S ribosomal protein L5** | Q5F5T9 | rplE | Increased | - | 18, 167, 33 | - |
| **50S ribosomal protein L6** | Q5F5U2 | rplF | Increased | 77, 85 | - | - |
| **50S ribosomal protein L7/L12** | Q5F5R4 | rplL | Increased | 68, 84, 87 | 68, 103 | - |
| **50S ribosomal protein L9** | Q5F922 | rplI | Increased | 82, 45, 71, 82, 22 | - | - |
| **50S ribosomal protein L9** | Q5F922 | rplI | Decreased | 35, 122 | - | - |
| **6-phosphogluconolactonase** | Q5F8Q1 | pgl | Increased | 197, 125 | - | - |
| **60 kDa chaperonin** | Q5F541 | groL | Increased | 132, 390, 242, 468, 122, 362, 364, 225, 277, 272 | 132, 65, 468, 122 | 132, 242, 122, 225 |
| **ABC transporte Energy-dependent translational throttle protein EttA?** | Q5F6I5 | NGO_1573 | Increased | 390, 370, 405 | - | 538, 405 |
| **ABC transporte Energy-dependent translational throttle protein EttA** | Q5F6I5 | NGO_1573 | Decreased | - | 390, 370 | - |
| **ABC transporter sulfate-transporting ATPase** | Q5F8B6 | NGO_0870 | Increased | 308, 47 | - | - |
| **Acetate kinase** | Q5F824 | ackA | Decreased | 169, 195 | - | - |
| **Acetolactate synthase** | Q5F7E2 | NGO_1236 | Decreased | 291, 195, 205 | 291, 195, 205 | - |
| **Acetyl-coenzyme A carboxylase carboxyl transferase subunit alpha** | Q5F8F5 | accA | Increased | 54, 289, 257, 266, 257, 266 | - | - |

| | | | | | | |
|---|---|---|---|---|---|---|
| **Acetyl-coenzyme A carboxylase carboxyl transferase subunit beta** | Q5F9Y5 | accD | Increased | 258, 88 | - | - |
| **Acetylornithine aminotransferase** | Q5F8W4 | argD | Increased | 305, 105 | - | - |
| **Acetyltransferase component of pyruvate dehydrogenase complex** | Q5F940 | NGO_0564 | Increased | 357, 419, 430, 431, 299 | - | - |
| **Acetyltransferase component of pyruvate dehydrogenase complex** | Q5F940 | NGO_0564 | Decreased | 226, 266, 430 | - | - |
| **Aconitate hydratase B** | Q5F7E7 | NGO_1231 | Increased | 221, 62, 213, 622, 651 | 221, 377, 267 | 221, 622, 651 |
| **Aconitate hydratase B** | Q5F7E7 | NGO_1231 | Decreased | 385, 742 | - | - |
| **Acyl-CoA thioester hydrolase** | Q5F7U2 | NGO_1078 | Increased | - | 72, 140 | - |
| **Adenylate kinase** | Q5F9J3 | adk | Increased | 40, 50 | - | - |
| **Adenylosuccinate lyase** | Q5F655 | NGO_1711 | Increased | - | 145, 93 | - |
| **ADP-L-glycero-D-manno-heptose-6-epimerase** | Q5F9J0 | hldD | Increased | 319, 312, 294, 305, 305 | - | - |
| **Agmatinase** | Q5F6R3 | speB | Increased | 194, 195 | - | - |
| **Alanine--tRNA ligase** | Q5F7C4 | alaS | Increased | 703, 831, 646, 456, 831, 825, 360, 351 | 703, 281, 456 | 703, 441 |
| **Alkyl hydroperoxide reductase AhpD** | Q5F7C9 | NGO_1249 | Increased | 13, 13, 14, 6 | - | - |
| **Amino acid ABC transporter substrate-binding protein** | Q5F9M1 | NGO_0372 | Increased | 193, 66, 92, 104, 210 | - | - |
| **Aminopeptidase N** | Q5FA72 | pepN | Increased | 771, 56, 206, 498, 270 | - | - |
| **Aminotransferase** | Q5F6U3 | NGO_1452 | Increased | - | - | 38, 22 |
| **Aminotransferase** | Q5F758 | NGO_1329 | Increased | 343, 38, 22 | - | - |
| **Arginine--tRNA ligase** | Q5F835 | argS | Increased | 259, 126 | 407, 259 | - |
| **Arginine--tRNA ligase** | Q5F835 | argS | Decreased | 418, 537 | 292, 418 | - |
| **Argininosuccinate lyase** | Q5FA15 | argH | Decreased | 284, 96 | - | - |
| **Aspartate carbamoyltransferase** | Q5F5P0 | pyrB | Increased | 244, 240 | - | - |
| **Aspartate carbamoyltransferase** | Q5F5P0 | pyrB | Decreased | 176, 83 | - | - |
| **Aspartate carbamoyltransferase regulatory chain** | Q5F5P1 | pyrI | Increased | 5, 13 | 68, 13 | - |
| **Aspartokinase** | Q5F842 | NGO_0956 | Increased | 221, 317, 103 | - | - |
| **Aspartokinase** | Q5F842 | NGO_0956 | Decreased | - | 7, 103 | - |
| **Aspartyl/glutamyl-tRNA** | Q5F8V0 | gatB | Increased | 61, 456, 445 | - | - |
| **Aspartyl/glutamyl-tRNA** | Q5F8V0 | gatB | Decreased | 386, 24 | 58, 472 | - |

| | | | | | | |
|---|---|---|---|---|---|---|
| **ATP-dependent DNA helicase Rep** | Q5F8N1 | rep | Increased | 331, 501 | - | - |
| **ATP-dependent helicase** | Q5F7H8 | NGO_1199 | Decreased | 53, 674 | - | - |
| **ATP phosphoribosyltransferase** | Q5F7E0 | hisG | Increased | 215, 36, 96 | - | - |
| **ATP phosphoribosyltransferase regulatory subunit** | Q5F9J6 | hisZ | Increased | 201, 382 | - | - |
| **ATP synthase epsilon chain** | Q5F4Y9 | atpC | Increased | 120, 130 | - | - |
| **ATP synthase gamma chain** | Q5F4Z1 | atpG | Decreased | 252, 31 | 263, 31, 98 | - |
| **ATP synthase subunit alpha** | Q5F4Z2 | atpA | Increased | 384, 13, 498, 387, 384, 131, 387 | - | - |
| **ATP synthase subunit alpha** | Q5F4Z2 | atpA | Decreased | - | 387, 384 | - |
| **ATP synthase subunit beta** | Q5F4Z0 | atpD | Increased | 193, 114, 233 | - | - |
| **ATP synthase subunit delta** | Q5F4Z3 | atpH | Increased | 74, 69 | - | 74, 69 |
| **Beta sliding clamp** | Q5FAJ1 | NGO_0002 | Increased | 222, 255 | 222, 255 | - |
| **Bifunctional protein GlmU [Includes: UDP-N-acetylglucosamine pyrophosphorylase** | Q5F577 | glmU | Increased | - | - | 155, 248 |
| **Bifunctional protein PutA [Includes: Proline dehydrogenase** | A0A0H4IVH0 | NGO_08225 | Increased | 1028, 1036, 1044, 246 | - | - |
| **Bifunctional protein PutA [Includes: Proline dehydrogenase** | A0A0H4IVH0 | NGO_08225 | Decreased | 106, 143, 558 | - | - |
| **Biotin carboxylase** | Q5FAH6 | NGO_0044 | Increased | 415, 324, 326 | - | - |
| **Bis** | Q5FA03 | apaH | Decreased | - | 148, 195 | - |
| **Branched-chain amino acid aminotransferase** | Q5F697 | NGO_1665 | Increased | - | 161, 250 | - |
| **Butanediol dehydrogenase** | Q5FA46 | NGO_0186 | Increased | 199, 308, 347, 314, 147, 235, 329, 199, 207, 326 | - | - |
| **Carbamoyl-phosphate synthase large chain** | Q5FAH2 | carB | Increased | 358, 469 | - | - |
| **Catalase** | Q5F601 | NGO_1767 | Increased | 77, 227 | - | - |
| **Cell division protein FtsA** | Q5F6M2 | ftsA | Decreased | - | 243, 96 | - |
| **Cell division protein FtsK** | Q5F8D2 | NGO_0851 | Decreased | - | 564, 176 | - |
| **Cell division protein FtsN** | Q5F9X1 | NGO_0265 | Decreased | - | 284, 17 | - |
| **Cell division protein FtsZ** | Q5F6M3 | ftsZ | Increased | 298, 324 | - | - |
| **Cell division protein ZapE** | Q5F909 | NGO_0598 | Increased | 236, 55 | - | - |
| **Cell division protein ZipA** | Q5F9Z8 | NGO_0236 | Increased | 413, 398, 140, 92 | - | - |
| **Cell division protein ZipA** | Q5F9Z8 | NGO_0236 | Decreased | - | 398, 156 | - |

| | | | | | | |
|---|---|---|---|---|---|---|
| **Chaperone protein ClpB** | Q5F7W9 | clpB | Increased | 61, 96, 463, 779, 783, 562, 565 | 615, 749 | 61, 96 |
| **Chaperone protein ClpB** | Q5F7W9 | clpB | Decreased | - | 779, 529 | - |
| **Chaperone protein DnaJ** | Q5F5M1 | dnaJ | Increased | 31, 46, 48, 31 | - | - |
| **Chaperone protein DnaK** | Q5F6W5 | dnaK | Increased | 305, 246, 571, 80, 641, 76, 638 | 183, 588 | - |
| **Chaperone protein DnaK** | Q5F6W5 | dnaK | Decreased | - | 415, 104 | - |
| **Chaperone protein HscA homolog** | Q5F8E8 | hscA | Increased | 135, 431 | 135, 431 | - |
| **Chromosomal replication initiator protein DnaA** | Q5FAJ2 | dnaA | Increased | 311, 497, 273 | - | - |
| **Chromosomal replication initiator protein DnaA** | Q5FAJ2 | dnaA | Decreased | - | 262, 273 | - |
| **Chromosome partitioning protein ParB** | Q5F4Z9 | NGO_2141 | Increased | 134, 202 | 134, 202 | - |
| **Clp protease ClpX** | Q5F9I6 | clpA | Increased | 750, 729 | - | - |
| **Clp protease ClpX** | Q5F9I6 | clpA | Decreased | - | 750, 716, 698 | - |
| **CMP-N-acetylneuraminate-beta-galactosamide-alpha-2, 3-sialyltransferase** | Q5F7T9 | NGO_1081 | Decreased | - | 216, 259 | - |
| **Cobalamin-independent methionine synthase** | Q5F863 | metE | Increased | 222, 40 | 596, 136, 222, 40 | - |
| **Cobalamin biosynthesis protein CobW** | Q5F960 | NGO_0543 | Increased | 302, 25, 176 | - | - |
| **Copper-containing nitrite reductase** | Q5F7A4 | NGO_1276 | Decreased | - | 91, 88 | - |
| **Cro/Cl family transcriptional regulator** | Q5F9C0 | NGO_0479 | Increased | 34, 59 | - | - |
| **CTP synthase** | Q5F7G6 | pyrG | Increased | 536, 101, 343 | - | - |
| **Cysteine--tRNA ligase** | Q5F5D6 | cysS | Decreased | 175, 73 | - | - |
| **Cysteine desulfurase IscS** | Q5F8X4 | iscS | Increased | 196, 272 | - | - |
| **Cysteine desulfurase IscS** | Q5F8X4 | iscS | Decreased | - | 19, 4 | - |
| **Cysteine synthase** | Q5F9Q2 | NGO_0340 | Increased | 89, 236, 18, 57, 243, 89, 24, 57, 60 | 89, 18, 192, 57, 243 | 18, 57 |
| **Cytochrome** | Q5F759 | NGO_1328 | Increased | - | 189, 201 | - |
| **Cytochrome** | Q5F759 | NGO_1328 | Decreased | 241, 278 | - | - |
| **Cytosine-specific methyltransferase II** | Q5F8B3 | NGO_0873 | Increased | 134, 280 | - | - |
| **Cytosine-specific methyltransferase III** | Q5F7G9 | NGO_1209 | Decreased | - | 236, 248 | - |
| **Damage-inducible protein D** | Q5F9I8 | dinD | Increased | 66, 158, 262, 270, 259 | - | - |
| **Delta-aminolevulinic acid dehydratase** | Q5F9K8 | NGO_0385 | Increased | 223, 226 | - | - |

| | | | | | | |
|---|---|---|---|---|---|---|
| **Diaminopimelate decarboxylase** | Q5F538 | lysA | Decreased | - | 253, 159 | - |
| **Dihydrolipoamide dehydrogenase** | Q5F866 | NGO_0925 | Increased | 112, 119 | 286, 52 | - |
| **Dihydrolipoyl dehydrogenase I** | Q5F942 | NGO_0562 | Increased | 293, 341, 345 | 359, 341, 498 | - |
| **Dihydrolipoyl dehydrogenase I** | Q5F942 | NGO_0562 | Decreased | 421, 261 | - | - |
| **Dihydrolipoyl dehydrogenase II** | Q5F876 | NGO_0915 | Decreased | 300, 112, 233 | - | - |
| **Dihydrolipoyllysine-residue succinyltransferase component of 2-oxoglutarate dehydrogenase complex** | Q5F875 | NGO_0916 | Increased | 214, 219 | - | - |
| **Dihydroxy-acid dehydratase** | Q5F8G6 | ilvD | Increased | 401, 503, 366 | - | - |
| **Dihydroxy-acid dehydratase** | Q5F8G6 | ilvD | Decreased | - | 366, 608, 247 | - |
| **DNA-directed RNA polymerase subunit alpha** | Q5F5V2 | rpoA | Increased | 103, 270 | - | - |
| **DNA-directed RNA polymerase subunit beta'** | Q5F5R6 | rpoC | Increased | 791, 389, 397 | - | - |
| **DNA-directed RNA polymerase subunit beta'** | Q5F5R6 | rpoC | Decreased | - | 98, 397, 1076, 389, 41 | - |
| **DNA-directed RNA polymerase subunit beta** | Q5F5R5 | rpoB | Increased | 1056, 262, 871, 418 | - | - |
| **DNA-directed RNA polymerase subunit beta** | Q5F5R5 | rpoB | Decreased | 799, 165, 666, 936, 724, 1188, 9, 927 | - | - |
| **DNA gyrase subunit A** | Q5F8Y0 | gyrA | Increased | 404, 505 | - | - |
| **DNA gyrase subunit A** | Q5F8Y0 | gyrA | Decreased | 285, 490 | - | - |
| **DNA gyrase subunit B** | Q5F5Z6 | gyrB | Increased | 592, 107, 638 | - | - |
| **DNA helicase** | Q5F609 | NGO_1757 | Decreased | - | 695, 728 | - |
| **DNA methylase** | Q5F6P5 | NGO_1504 | Increased | 77, 329 | 135, 106 | - |
| **DNA polymerase I** | Q5F533 | polA | Increased | 194, 267 | - | - |
| **DNA polymerase III subunit epsilon II** | Q5F828 | dnaQ | Increased | 199, 69 | - | - |
| **DNA primase** | Q5F806 | dnaG | Increased | 27, 588 | - | - |
| **DNA repair protein RadA** | Q5F9M6 | radA | Increased | 416, 113 | - | - |
| **DNA topoisomerase 1** | Q5F5Q4 | topA | Increased | 53, 505, 453, 394, 211, 207, 568 | - | - |
| **DNA topoisomerase 1** | Q5F5Q4 | topA | Decreased | - | 575, 505, 211 | - |
| **DNA topoisomerase 4 subunit A** | Q5F7B9 | parC | Increased | 746, 552, 692 | - | - |
| **DNA topoisomerase 4 subunit A** | Q5F7B9 | parC | Decreased | - | 255, 746, 552 | - |

| | | | | | | |
|---|---|---|---|---|---|---|
| **Dual-specificity RNA methyltransferase RlmN** | Q5F911 | rlmN | Increased | 354, 50 | - | - |
| **DUF1853 family protein** | Q5F8U1 | NGO_0669 | Increased | 158, 152 | - | - |
| **DUF4043 family protein?** | Q5F7T0 | NGO_1090 | Increased | 327, 344, 336, 243 | - | - |
| **Elongation factor 4** | Q5F9P9 | lepA | Increased | 55, 316 | - | - |
| **Elongation factor G** | Q5F5S3 | fusA | Decreased | 143, 551, 315, 353 | - | - |
| **Elongation factor P** | Q5F856 | efp | Increased | 24, 55 | - | 59, 24 |
| **Elongation factor Ts** | Q5F5F4 | tsf | Increased | 98, 216, 209, 36 | 209, 36 | - |
| **Elongation factor Tu** | Q5F5Q8 | tuf1 | Increased | 249, 57, 38, 57, 45, 5, 304, 295 | - | - |
| **Endonuclease** | Q5F7D9 | NGO_1239 | Increased | 6, 7 | - | - |
| **Enolase** | Q5F8Z2 | eno | Increased | 62, 328, 190, 191, 349 | 196, 253, 349 | - |
| **Enoyl-acyl-carrier-protein reductase NADH** | Q5F696 | NGO_1666 | Increased | 129, 194 | 129, 194 | - |
| **EtfB protein** | Q5F5I9 | NGO_1935 | Increased | 66, 243, 241, 216, 219 | - | - |
| **Ethanol-active dehydrogenase/acetaldehyde -active reductase** | Q5F6V3 | adhP | Increased | 227, 74 | - | - |
| **Exopolyphosphatase** | Q5F7X4 | NGO_1041 | Decreased | - | 255, 38 | - |
| **Fe-S binding protein** | Q5F885 | NGO_0904 | Decreased | 115, 145 | - | - |
| **Fe-S cluster binding protein** | Q5F883 | NGO_0906 | Increased | 154, 252, 7 | - | - |
| **Fe-S cluster binding protein** | Q5F883 | NGO_0906 | Decreased | - | 26, 7, 477 | - |
| **Ferredoxin-NADP reductase** | Q5F8S3 | NGO_0687 | Increased | 93, 84 | - | - |
| **Ferric uptake regulation protein** | Q5F5Y9 | fur | Increased | 30, 97, 16, 3, 11, 16 | - | - |
| **Ferrochelatase** | Q5F9U6 | hemH | Increased | - | - | 83, 265 |
| **Formate--tetrahydrofolate ligase** | Q5FAG1 | fhs | Increased | 369, 545, 49, 500, 4 | 369, 500, 4 | 545, 500, 4 |
| **Formate--tetrahydrofolate ligase** | Q5FAG1 | fhs | Decreased | 483, 490 | - | - |
| **Fructose-1,6-bisphosphate aldolase** | Q5FAI4 | NGO_0034 | Increased | 333, 339 | - | - |
| **Fructose-1,6-bisphosphate aldolase** | Q5FAI4 | NGO_0034 | Decreased | - | 331, 339 | - |
| **Glucokinase** | Q5F8Q0 | glk | Increased | 36, 229 | - | - |
| **Glucose-6-phosphate 1-dehydrogenase** | Q5F8Q2 | zwf | Increased | 104, 146, 180, 58 | 104, 146 | 104, 58 |
| **Glucose-6-phosphate isomerase 1** | Q5F8P8 | pgi1 | Increased | 345, 12, 193 | 530, 516, 193 | 516, 12 |
| **Glutamate--cysteine ligase** | Q5F8T0 | NGO_0680 | Increased | 277, 268 | - | - |
| **Glutamate--tRNA ligase** | Q5F5J8 | gltX | Increased | 425, 156, 241, 425, 416 | 416, 383 | 156, 343 |
| **Glutamate--tRNA ligase** | Q5F5J8 | gltX | Decreased | - | 425, 428 | - |

| | | | | | | |
|---|---|---|---|---|---|---|
| **Glutamate dehydrogenase** | Q5F731 | NGO_1358 | Increased | 12, 41, 416 | - | - |
| **Glutamine--fructose-6-phosphate aminotransferase [isomerizing]** | Q5F584 | glmS | Decreased | - | 62, 23 | - |
| **Glutamine--tRNA ligase** | Q5F7G0 | glnS | Decreased | 364, 556 | - | - |
| **Glutamine synthetase** | Q5F6F9 | NGO_1600 | Increased | 243, 356 | - | - |
| **Glutamyl-tRNA amidotransferase** | Q5F507 | NGO_2133 | Increased | 55, 58, 12 | 12, 78 | - |
| **Glutathione peroxidase** | Q5F865 | NGO_0926 | Increased | 195, 34, 244, 153, 162, 187, 25, 25, 34, 36 | 195, 153, 179 | 195, 162, 187 |
| **Glutathione synthetase** | Q5F7G1 | gshB | Increased | 128, 14, 266, 179, 71 | 128, 179 | - |
| **Glutathione synthetase** | Q5F7G1 | gshB | Decreased | - | 266, 71 | - |
| **Glyceraldehyde-3-phosphate dehydrogenase** | Q5F5Z2 | gapA | Decreased | 212, 227 | - | - |
| **Glycine--tRNA ligase beta subunit** | Q5F4Y7 | glyS | Increased | 569, 378 | - | - |
| **Glycine--tRNA ligase beta subunit** | Q5F4Y7 | glyS | Decreased | - | 358, 443 | - |
| **Glycine dehydrogenase** | Q5F761 | gcvP | Decreased | - | 183, 784 | - |
| **GMP synthase [glutamine-hydrolyzing]** | Q5F4X9 | guaA | Increased | 320, 371 | - | - |
| **GTP-binding protein** | Q5F8H0 | NGO_0803 | Increased | 537, 539 | - | - |
| **GTP cyclohydrolase-2** | Q5F7N6 | ribA | Increased | 147, 190, 155, 147 | - | - |
| **GTP pyrophosphokinase II** | Q5F707 | NGO_1382 | Increased | 490, 524, 582, 562, 230 | - | - |
| **GTP pyrophosphokinase II** | Q5F707 | NGO_1382 | Decreased | - | 160, 689 | - |
| **GTPase Der** | O87407 | der | Increased | 245, 199 | - | - |
| **GTPase Der** | O87407 | der | Decreased | - | 330, 443, 199 | - |
| **Guanine permease** | Q5F6M4 | NGO_1527 | Decreased | 280, 16 | 280, 16 | - |
| **Guanosine-3',5'-bis** | Q5F777 | NGO_1308 | Decreased | 149, 228 | 149, 120 | - |
| **HAD family hydrolase** | Q5F8E0 | NGO_0842 | Increased | 43, 155, 209 | - | - |
| **Helix-turn-helix transcriptional regulator NGO_1427** | Q5F6W7 | NGO_1427 | Increased | 43, 48, 182 | - | - |
| **Heme ABC transporter ATP-binding protein** | Q5F8K8 | NGO_0764 | Increased | 23, 538 | - | - |
| **Heme biosynthesis protein HemY** | Q5F9N2 | NGO_0361 | Increased | 382, 372 | - | - |
| **Heme biosynthesis protein HemY** | Q5F9N2 | NGO_0361 | Decreased | - | 102, 382 | - |
| **Heme transporter CcmA** | Q5F768 | NGO_1318 | Increased | 44, 86 | - | - |
| **Heme transporter CcmA** | Q5F768 | NGO_1318 | Decreased | - | 44, 13 | - |

| | | | | | | |
|---|---|---|---|---|---|---|
| **Histidinol-phosphate aminotransferase** | Q5F7D7 | hisC | Increased | 317, 276 | - | - |
| **Holo-ACP synthase** | Q5F6P2 | acpS | Increased | 51, 21, 20 | - | - |
| **Hypoxanthine phosphoribosyltransferase** | Q5F594 | NGO_2035 | Increased | 93, 84 | - | - |
| **Indole-3-glycerol phosphate synthase** | Q5F645 | trpC | Increased | 61, 258 | - | - |
| **Inorganic pyrophosphatase** | Q5FA11 | ppa | Increased | 122, 96, 143, 146, 146 | - | - |
| **Inorganic pyrophosphatase** | Q5FA11 | ppa | Decreased | - | 143, 146, 143 | - |
| **Inosine-5'-monophosphate dehydrogenase** | Q5F8H4 | guaB | Increased | 6, 32 | 412, 203 | - |
| **Inositol-1-monophosphatase** | Q5F8T9 | NGO_0671 | Increased | - | 63, 56 | - |
| **Integrase/recombinase, phage associated protein** | Q5F6E6 | NGO_1613 | Increased | 317, 62 | - | - |
| **Isocitrate dehydrogenase [NADP]** | Q5F7T8 | NGO_1082 | Increased | 527, 640, 39, 121, 242, 723 | 121, 242 | 121, 242 |
| **Isoleucine--tRNA ligase** | Q5FAF5 | ileS | Decreased | - | 424, 913, 280 | - |
| **Lacto-N-neotetraose biosynthesis glycosyl transferase** | Q5F4Y4 | NGO_2159 | Increased | 127, 99 | - | - |
| **Lacto-N-neotetraose biosynthesis glycosyl transferase** | Q5F4Y4 | NGO_2159 | Decreased | 270, 134 | - | - |
| **Large pilS cassette protein** | A0A0H4ISA9 | NGO_10975 | Increased | 147, 85, 185 | 147, 85, 185 | - |
| **LD-carboxypeptidase** | Q5F7A6 | NGO_1274 | Increased | 320, 313 | - | - |
| **LdhA, NAD-linked D-LDH** | Q5F751 | NGO_1336 | Increased | 248, 40 | - | 248, 40 |
| **LdhA, NAD-linked D-LDH** | Q5F751 | NGO_1336 | Decreased | 93, 154 | 93, 63 | - |
| **Leucine--tRNA ligase** | Q5FAJ3 | leuS | Increased | 854, 621, 521 | - | - |
| **Leucine--tRNA ligase** | Q5FAJ3 | leuS | Decreased | 309, 32 | 634, 521 | - |
| **Lipoyl synthase** | Q5F8I0 | lipA | Increased | 217, 283, 34, 27 | - | - |
| **Lon protease** | Q5F8J8 | lon | Increased | 678, 147, 215 | - | - |
| **Lon protease** | Q5F8J8 | lon | Decreased | 568, 374, 590 | 332, 678, 345, 215 | - |
| **Long-chain fatty acid--CoA ligase II** | Q5F7G5 | NGO_1213 | Decreased | - | 35, 296 | - |
| **LysM peptidoglycan-binding domain-containing protein** | Q5F901 | NGO_0608 | Increased | 353, 572 | - | - |
| **LysR family transcriptional regulator II** | Q5F5V6 | NGO_1813 | Increased | 37, 137 | - | - |
| **MacA family efflux pump subunit** | Q5F6V5 | NGO_1440 | Decreased | 161, 75 | 161, 75, 124 | - |
| **Membrane protein insertase YidC** | Q5F4W6 | yidC | Increased | 389, 413 | - | - |

| | | | | | | |
|---|---|---|---|---|---|---|
| **Methionine--tRNA ligase** | Q5F585 | metG | Increased | 130, 650 | 130, 647 | - |
| **Methionine biosynthesis protein MetW** | Q5F857 | NGO_0934 | Increased | - | 160, 38 | - |
| **Methylenetetrahydrofolate reductase** | Q5F862 | NGO_0929 | Increased | 52, 135, 231 | - | 135, 231 |
| **Molecular chaperone DnaJ** | Q5F952 | NGO_0551 | Increased | 30, 21 | - | - |
| **N-acetylmuramoyl-L-alanine amidase** | Q5F6P7 | amiC | Increased | 29, 59 | 29, 338 | - |
| **Na-translocating NADH-quinone reductase subunit A** | Q5F6Y0 | nqrA | Increased | 112, 117 | - | - |
| **Na-translocating NADH-quinone reductase subunit A** | Q5F6Y0 | nqrA | Decreased | 445, 272 | 445, 61, 272 | - |
| **Nicotinate-nucleotide pyrophosphorylase** | Q5F6I9 | NGO_1565 | Increased | 152, 233 | - | - |
| **Nitrogen regulatory protein P-II 1** | Q5F7J5 | NGO_1182 | Increased | - | 12, 90 | - |
| **Nitroreductase** | Q5F7A2 | NGO_1279 | Increased | 78, 78, 79 | - | - |
| **Nucleoid-associated protein NGO0742** | Q5F8M8 | NGO0742 | Increased | 27, 12 | 27, 12 | - |
| **Oligopeptidase A** | Q5F5Z8 | NGO_1770 | Increased | 339, 19 | 114, 339, 24, 344 | - |
| **Oligopeptidase A** | Q5F5Z8 | NGO_1770 | Decreased | - | 19, 424, 387, 353 | - |
| **Oligoribonuclease** | Q5FAH8 | orn | Increased | 137, 141 | - | - |
| **Orotate phosphoribosyltransferase** | Q5FAK5 | pyrE | Increased | 19, 10, 19 | - | - |
| **Osmoprotectant transport activator ProQ** | Q5F755 | NGO_1332 | Increased | 12, 34 | 12, 34 | - |
| **Peptidase M24** | Q5F6U0 | NGO_1456 | Increased | 297, 77 | - | - |
| **Peptidase_M14 domain-containing protein** | Q5F8D7 | NGO_0845 | Increased | 237, 309 | 237, 309 | 237, 309 |
| **Peptide chain release factor 3** | Q5FA25 | prfC | Increased | 52, 63, 49 | - | - |
| **Peptide chain release factor 3** | Q5FA25 | prfC | Decreased | - | 52, 49 | - |
| **Peptidoglycan-binding outer membrane protein RmpM** | Q5F6I1 | NGO_1577 | Decreased | 55, 103 | - | - |
| **Peptidoglycan DD-metalloendopeptidase family protein** | Q5F933 | NGO_0571 | Decreased | - | 360, 340 | - |
| **Peptidyl-prolyl cis-trans isomerase** | Q5F9L7 | NGO_0376 | Increased | 148, 32, 118 | 148, 118 | - |
| **Peptidyl-prolyl cis-trans isomerase** | Q5F9L7 | NGO_0376 | Decreased | 19, 115 | - | - |
| **Peptidyl-tRNA hydrolase** | Q5F9L4 | pth | Increased | 120, 125 | - | - |
| **Peptidylprolyl isomerase NGO_1656** | Q5F6A4 | NGO_1656 | Increased | 75, 221, 129, 86 | 129, 164 | 75, 221, 129 |
| **Phenylalanine--tRNA ligase beta subunit** | Q5F9T6 | pheT | Increased | 605, 202, 104 | - | - |

| | | | | | | |
|---|---|---|---|---|---|---|
| **Phenylalanine--tRNA ligase beta subunit** | Q5F9T6 | pheT | Decreased | 631, 623 | 236, 631, 661, 695, 623 | - |
| **Phosphate acetyltransferase** | Q5FA20 | NGO_0214 | Increased | 450, 400 | - | - |
| **Phosphate acetyltransferase** | Q5FA20 | NGO_0214 | Decreased | - | 212, 231, 222, 400, 422 | - |
| **Phosphate acyltransferase** | Q5F4X3 | plsX | Increased | 244, 79 | - | - |
| **Phospho-2-dehydro-3-deoxyheptonate aldolase** | Q5F668 | NGO_1695 | Decreased | - | 263, 99, 188 | - |
| **Phosphocarrier protein HPr** | Q5F592 | NGO_2037 | Increased | 30, 21, 30, 11 | - | - |
| **Phosphoenolpyruvate-protein phosphotransferase** | Q5F591 | NGO_2038 | Increased | 327, 491, 108 | - | - |
| **Phosphoenolpyruvate carboxylase** | Q5F5A9 | ppc | Increased | 243, 642, 812, 346 | 812, 346 | 243, 812, 346 |
| **Phosphoenolpyruvate synthase** | Q5FA34 | NGO_0200 | Increased | 71, 37, 628, 631 | - | 71, 37 |
| **Phosphoenolpyruvate synthase** | Q5FA34 | NGO_0200 | Decreased | 270, 747, 357 | 628, 747 | - |
| **Phosphoglucomutase** | Q5F9L8 | NGO_0375 | Increased | 10, 165, 187, 330, 20 | 10, 20 | - |
| **Phosphogluconate dehydratase** | Q5F8Q3 | NGO_0714 | Increased | 542, 346, 494 | 508, 388, 346, 60, 494 | - |
| **Phosphoglucosamine mutase** | Q5F746 | glmM | Increased | 386, 383 | - | - |
| **Phosphoribosyl-ATP pyrophosphatase** | Q5FA47 | hisE | Increased | 36, 39 | - | - |
| **Phosphoribosylamine--glycine ligase** | Q5F5I6 | purD | Increased | 404, 88 | 221, 143 | - |
| **Phosphoribosylaminoimidazole-succinocarboxamide synthase** | Q5F9Q8 | purC | Increased | 60, 8, 116, 116, 276 | - | - |
| **Phosphoribosylformylglycinamidine cyclo-ligase** | Q5F973 | purM | Increased | 237, 23 | 237, 23 | - |
| **Phosphoribosylformylglycinamidine synthase** | Q5F7J4 | purL | Decreased | - | 786, 395 | - |
| **Phosphoribosyltransferase** | Q5F4X2 | NGO_2172 | Increased | 129, 115 | - | - |
| **Pilus assembly/adherence protein PilC NGO_0055** | Q5FAG7 | NGO_10270 | Decreased | 927, 285 | 927, 445, 285 | - |
| **pilus assembly/adherence protein PilC?NGO_10270** | A0A0H4IWH7 | NGO_10270 | Decreased | - | 957, 550 | - |
| **Polyribonucleotide nucleotidyltransferase** | Q5F9Q7 | pnp | Increased | 693, 540, 246 | 693, 80 | - |
| **Probable Fe 2-trafficking protein** | Q5F553 | NGO2083 | Increased | 18, 28 | - | - |
| **Probable GTP-binding protein EngB** | Q5FAC6 | engB | Increased | 8, 181, 154 | - | - |
| **Probable GTP-binding protein EngB** | Q5FAC6 | engB | Decreased | 54, 143 | 54, 143 | - |
| **Probable malate:quinone oxidoreductase** | Q5F5E9 | mqo | Increased | 467, 218 | - | - |

| | | | | | | |
|---|---|---|---|---|---|---|
| **Probable septum site-determining protein MinC** | Q5F5V4 | minC | Increased | 118, 217 | - | - |
| **Probable transcriptional regulatory protein NGO1291** | Q5F792 | NGO1291 | Increased | 106, 72, 216 | - | - |
| **Proline--tRNA ligase** | Q5F938 | proS | Increased | 418, 12, 461 | 12, 461 | 418, 12 |
| **Protease** | Q5F771 | NGO_1314 | Increased | 290, 297, 287, 45 | - | - |
| **Protein GrpE** | Q5F6X1 | grpE | Increased | 83, 170, 135, 57, 88 | - | - |
| **Protein GrpE** | Q5F6X1 | grpE | Decreased | - | 83, 135 | - |
| **Protein translocase subunit SecY** | Q5F5U7 | secY | Decreased | - | 423, 12 | - |
| **Putative DNA mimic protein DMP12?** | Q5F5G1 | NGO_1966 | Increased | - | 109, 85 | - |
| **Putative phage associated protein** | Q5F6D9 | NGO_1620 | Increased | - | 180, 184 | - |
| **Pyridoxal phosphate homeostasis protein** | Q5F5L6 | NGO_1907 | Increased | 17, 175 | - | - |
| **Pyridoxine 5'-phosphate synthase** | Q5F6P1 | pdxJ | Increased | - | 118, 59 | - |
| **Pyrroline-5-carboxylate reductase** | Q5F5L8 | proC | Increased | 216, 219 | - | 216, 219 |
| **Pyruvate dehydrogenase E1 component** | Q5F939 | aceE | Increased | 878, 409, 41, 486, 717, 68, 874, 305, 886, 878, 717, 508, 510, 721 | 878, 325, 486, 68, 551, 388, 388 | - |
| **Pyruvate dehydrogenase E1 component** | Q5F939 | aceE | Decreased | 417, 409, 388 | 410, 508, 510, 409 | - |
| **Pyruvate kinase** | Q5F5N5 | NGO_1881 | Increased | 223, 276 | - | - |
| **Quinone-dependent D-lactate dehydrogenase** | Q5F898 | dld | Increased | 389, 365, 466, 324 | - | 389, 466 |
| **RecBCD enzyme subunit RecB** | Q5F9M3 | recB | Increased | 723, 277 | - | - |
| **Respiratory L-Lactate dehydrogenase** | Q5F8X1 | lldD | Decreased | - | 266, 147 | - |
| **Restriction endonuclease EcoprrI subunit S** | A0A0H4IW12 | NGO_02155 | Increased | - | 52, 160 | - |
| **Restriction endonuclease HaeII** | Q5F5D7 | NGO_1992 | Decreased | - | 75, 83 | - |
| **Restriction endonuclease subunit M** | Q5F8W9 | NGO_0641 | Increased | 437, 381 | 437, 381, 499, 447 | - |
| **Restriction endonuclease, M subunit** | Q5F9I9 | NGO_0404 | Increased | 206, 422, 497 | - | - |
| **Ribonuclease E** | Q5F5Y3 | rne | Increased | 575, 318, 452 | - | - |
| **Ribonuclease E** | Q5F5Y3 | rne | Decreased | - | 517, 575 | - |
| **Ribonuclease II** | Q5F653 | NGO_1713 | Increased | 596, 119, 151 | - | - |
| **Ribonuclease II** | Q5F653 | NGO_1713 | Decreased | 178, 172 | 613, 119, 178 | - |

| | | | | | | |
|---|---|---|---|---|---|---|
| **Ribonuclease R** | Q5F8H2 | rnr | Decreased | 500, 95, 6, 13 | - | - |
| **Ribonucleoside-diphosphate reductase** | Q5F8Z6 | NGO_0614 | Decreased | 714, 725 | 714, 156, 23 | - |
| **Ribose-phosphate pyrophosphokinase** | Q5F9F5 | prs | Increased | 185, 196 | - | - |
| **Ribosomal large subunit pseudouridine synthase B** | Q5F8V3 | NGO_0657 | Increased | 150, 76 | - | - |
| **Ribosomal RNA large subunit methyltransferase H** | Q5F554 | rlmH | Increased | 58, 90 | - | - |
| **Ribosomal RNA large subunit methyltransferase J** | Q5F8C6 | rlmJ | Decreased | - | 171, 182 | - |
| **Ribosomal RNA small subunit methyltransferase H** | Q5F6K7 | rsmH | Increased | 253, 257 | - | - |
| **Ribosomal RNA small subunit methyltransferase J** | Q5F7B7 | rsmJ | Increased | 77, 51, 235 | 77, 235 | - |
| **Ribosomal small subunit pseudouridine synthase A** | Q5F902 | NGO_0607 | Increased | 141, 141, 131 | - | - |
| **Ribosome-recycling factor** | Q5F5X3 | frr | Increased | 140, 141 | - | - |
| **Ribosome maturation factor RimP** | Q5F799 | rimP | Increased | 97, 99 | - | - |
| **Ribosome maturation factor RimP** | Q5F799 | rimP | Decreased | - | 97, 99 | - |
| **RluA family pseudouridine synthase** | Q5F5Y5 | NGO_1783 | Decreased | 193, 206 | - | - |
| **RNA polymerase sigma factor RpoD** | Q5F805 | rpoD | Increased | - | 279, 383, 394 | - |
| **RNA polymerase sigma factor RpoD** | Q5F805 | rpoD | Decreased | 617, 364, 517 | 442, 373, 486, 250, 140 | - |
| **SAM-dependent methyltransferase** | Q5F8U2 | NGO_0668 | Increased | 367, 328 | - | 367, 328 |
| **Serine hydroxymethyltransferase** | Q5F8C0 | glyA | Increased | 275, 283, 302 | - | - |
| **Serine hydroxymethyltransferase** | Q5F8C0 | glyA | Decreased | - | 275, 353 | - |
| **Shikimate kinase** | Q5FAD3 | aroK | Increased | 166, 132 | - | - |
| **Signal recognition particle protein** | Q5F666 | ffh | Increased | 416, 21, 278 | - | - |
| **Signal recognition particle protein** | Q5F666 | ffh | Decreased | - | 14, 372 | - |
| **Site-determining protein** | A0A0H4IVK1 | NGO_09675 | Increased | 104, 112 | - | - |
| **Sodium/glutamate symporter** | Q5F5N0 | gltS | Increased | 212, 212 | - | - |
| **Sodium:alanine symporter** | Q5F5Y1 | NGO_1787 | Increased | 459, 467 | - | - |
| **Stringent starvation protein A** | Q5F510 | NGO_2130 | Increased | 116, 99, 120, 170, 177 | - | - |
| **Succinate dehydrogenase flavoprotein subunit** | Q5F870 | NGO_0921 | Decreased | - | 28, 584 | - |
| **Succinyl-CoA synthetase subunit alpha** | Q5F879 | sucD | Increased | 291, 19 | - | - |

| | | | | | | |
|---|---|---|---|---|---|---|
| **Succinyl-CoA synthetase subunit beta** | Q5F878 | sucC | Increased | 368, 41, 46 | - | - |
| **Succinyl-diaminopimelate desuccinylase** | Q5F812 | dapE | Decreased | - | 151, 379 | - |
| **Thiamine ABC transporter substrate-binding protein** | Q5F574 | NGO_2056 | Increased | 230, 242 | 86, 242 | - |
| **Thioredoxin TrxA** | Q5F8V8 | NGO_0652 | Increased | - | 59, 92 | - |
| **Threonine--tRNA ligase** | Q5F9U4 | thrS | Decreased | 300, 560 | - | - |
| **Threonine synthase** | Q5F8S1 | NGO_0689 | Increased | 212, 45 | - | - |
| **Transaldolase** | Q5F6E9 | tal | Increased | 337, 65 | - | - |
| **Transcriptional regulator HU subunit alpha** | Q5F8J6 | NGO_0777 | Increased | 18, 75, 78, 64 | 75, 18, 75 | - |
| **Transketolase** | Q5F7Y3 | NGO_1028 | Decreased | - | 50, 534 | - |
| **Translation initiation factor IF-2** | Q5F797 | infB | Increased | 22, 143, 141, 907 | - | - |
| **Translation initiation factor IF-2** | Q5F797 | infB | Decreased | - | 22, 659, 877, 763, 277 | - |
| **Translation initiation factor IF-3** | Q5F9U3 | infC | Decreased | 17, 89, 118 | 89, 92 | - |
| **Trigger factor** | Q5F915 | tig | Increased | 86, 303, 31 | - | 303, 31 |
| **tRNA uridine 5-carboxymethylaminomethyl modification enzyme MnmG** | Q5F5Y0 | mnmG | Increased | 570, 489, 621 | - | 570, 489 |
| **tRNA uridine 5-carboxymethylaminomethyl modification enzyme MnmG** | Q5F5Y0 | mnmG | Decreased | 283, 191, 105 | 191, 105 | - |
| **Tryptophan--tRNA ligase** | Q5F7X0 | trpS | Increased | 219, 220 | - | - |
| **Two-component system response regulator MisR** | Q5FA55 | NGO_0177 | Increased | 143, 205 | - | - |
| **Type IV pilus twitching motility protein PilT NGO_0346** | Q5F9P7 | NGO_0346 | Increased | 347, 115, 126, 39, 131, 115, 126, 112 | 347, 126, 39 | 347, 126 |
| **Type IV pilus twitching motility protein PilT NGO_1909** | Q5F5L4 | NGO_1909 | Increased | 203, 20 | - | - |
| **Tyrosine--tRNA ligase** | Q5FAF7 | tyrS | Increased | 82, 245, 234 | - | - |
| **Tyrosine--tRNA ligase** | Q5FAF7 | tyrS | Decreased | - | 266, 245 | - |
| **Ubiquinone biosynthesis O-methyltransferase** | Q5F562 | ubiG | Increased | 19, 35 | - | - |
| **UDP-N-acetylglucosamine 1-carboxyvinyltransferase** | Q5F5K6 | murA | Increased | - | 55, 146 | - |
| **UDP-N-acetylmuramate--L-alanyl-gamma-D-glutamyl-meso-2,6-diaminoheptandioate ligase** | Q5F8G0 | mpl | Increased | 319, 430, 375, 27 | 319, 430 | - |
| **Uncharacterized protein NGO_0163** | Q5FA68 | NGO_0163 | Increased | 97, 18 | - | - |
| **Uncharacterized protein NGO_0701** | Q5F8R2 | NGO_0701 | Increased | 62, 145 | 62, 87 | - |

| | | | | | | |
|---|---|---|---|---|---|---|
| **Uncharacterized protein NGO_0863** | Q5F8C2 | NGO_0863 | Increased | 68, 52, 52, 53, 11, 13 | - | 68, 52, 57 |
| **Uncharacterized protein NGO_1097** | Q5F7S3 | NGO_1097 | Increased | 112, 352 | - | - |
| **Uncharacterized protein NGO_1150** | Q5F7M0 | NGO_1150 | Increased | 14, 59 | - | - |
| **Uncharacterized protein NGO_1215** | Q5F7G3 | NGO_1215 | Increased | - | 129, 98 | - |
| **Uncharacterized protein NGO_1588** | Q5F6H1 | NGO_1588 | Increased | 92, 44 | - | - |
| **UPF0210 protein NGO1297** | Q5F786 | NGO1297 | Decreased | 248, 62 | 248, 62, 450 | - |
| **UPF0246 protein NGO0461** | Q5F9D8 | NGO0461 | Increased | 182, 183, 194 | - | - |
| **Uridylate kinase** | Q5F5F5 | pyrH | Increased | 196, 193 | - | - |
| **UvrABC system protein A** | Q5F7H1 | uvrA | Increased | 351, 321, 665 | - | - |
| **UvrABC system protein A** | Q5F7H1 | uvrA | Decreased | - | 321, 625, 467, 789 | - |
| **UvrABC system protein B** | Q5F931 | uvrB | Increased | 384, 195, 582 | - | - |
| **Valine--tRNA ligase** | Q5F5W0 | valS | Increased | 323, 537, 875 | - | - |
| **Valine--tRNA ligase** | Q5F5W0 | valS | Decreased | 4, 932 | 942, 285, 4 | - |

**Table 8.3 Proteins with acetyl-phosphate-dependent acetylation sites.** The terms with more than two proteins were classified in four different ontologies (KEGG pathway, biological process, molecular function and family).

| Ontology | Term | Count | Gene name | Protein name |
|---|---|---|---|---|
| **KEGG** | Aminoacyl-tRNA biosynthesis | 6 | gltX | Glutamate--tRNA ligase |
| | | | ileS | Isoleucine--tRNA ligase |
| | | | cysS | Cysteine--tRNA ligase |
| | | | tyrS | Tyrosine--tRNA ligase |
| | | | thrS | Threonine--tRNA ligase |
| | | | leuS | Leucine--tRNA ligase |
| **KEGG** | Methane metabolism | 6 | gpmA | 2,3-bisphosphoglycerate-dependent phosphoglycerate mutase |
| | | | NGO_1468 | Phosphoserine phosphatase SerB |
| | | | glyA | Serine hydroxymethyltransferase |
| | | | NGO_0214 | Phosphate acetyltransferase |
| | | | NGO_0200 | Phosphoenolpyruvate synthase |
| | | | NGO_0034 | Fructose-1,6-bisphosphate aldolase |
| **KEGG** | Pyruvate metabolism | 6 | accD | Acetyl-coenzyme A carboxylase carboxyl transferase subunit beta |
| | | | NGO_0214 | Phosphate acetyltransferase |
| | | | lldD | Respiratory L-Lactate dehydrogenase |
| | | | mqo | Probable malate:quinone oxidoreductase |
| | | | NGO_0200 | Phosphoenolpyruvate synthase |
| | | | aceE | Pyruvate dehydrogenase E1 component |
| **KEGG** | Purine metabolism | 5 | dnaQ | DNA polymerase III subunit epsilon II |
| | | | apaH | Bis(5'-nucleosyl)-tetraphosphatase, symmetrical |
| | | | purC | Phosphoribosylaminoimidazole-succinocarboxamide synthase |
| | | | rpoC | DNA-directed RNA polymerase subunit beta' |
| | | | NGO_2035 | Hypoxanthine phosphoribosyltransferase |
| **KEGG** | Ribosome | 5 | rpsM | 30S ribosomal protein S13 |
| | | | rpsC | 30S ribosomal protein S3 |
| | | | rplY | 50S ribosomal protein L25 |
| | | | rpsG | 30S ribosomal protein S7 |
| | | | rpsF | 30S ribosomal protein S6 |

| | | | | |
|---|---|---|---|---|
| **KEGG** | Glycine, serine and threonine metabolism | 4 | NGO_1468 | Phosphoserine phosphatase SerB |
| | | | glyA | Serine hydroxymethyltransferase |
| | | | NGO_0689 | Threonine synthase |
| | | | NGO_0956 | Aspartokinase |
| **KEGG** | Nucleotide excision repair | 4 | mfd | Transcription-repair-coupling factor |
| | | | uvrA | UvrABC system protein A |
| | | | NGO_1757 | DNA helicase |
| | | | uvrB | UvrABC system protein B |
| **KEGG** | Valine, leucine and isoleucine biosynthesis | 4 | ilvD | Dihydroxy-acid dehydratase |
| | | | ileS | Isoleucine--tRNA ligase |
| | | | aceE | Pyruvate dehydrogenase E1 component |
| | | | leuS | Leucine--tRNA ligase |
| **KEGG** | Oxidative phosphorylation | 3 | atpG | ATP synthase gamma chain |
| | | | atpA | ATP synthase subunit alpha |
| | | | ppa | Inorganic pyrophosphatase |
| **KEGG** | Glycolysis / Gluconeogenesis | 3 | gpmA | 2,3-bisphosphoglycerate-dependent phosphoglycerate mutase |
| | | | NGO_0034 | Fructose-1,6-bisphosphate aldolase |
| | | | aceE | Pyruvate dehydrogenase E1 component |
| **KEGG** | Mismatch repair | 3 | dnaQ | DNA polymerase III subunit epsilon II |
| | | | xseB | Exodeoxyribonuclease 7 small subunit |
| | | | NGO_1757 | DNA helicase |
| **KEGG** | Carbon fixation pathways in prokaryotes | 3 | accD | Acetyl-coenzyme A carboxylase carboxyl transferase subunit beta |
| | | | NGO_0214 | Phosphate acetyltransferase |
| | | | NGO_0200 | Phosphoenolpyruvate synthase |
| **Biological process** | translation [GO:0006412] | 5 | rpsM | 30S ribosomal protein S13 |
| | | | rpsC | 30S ribosomal protein S3 |
| | | | rplY | 50S ribosomal protein L25 |
| | | | rpsG | 30S ribosomal protein S7 |
| | | | rpsF | 30S ribosomal protein S6 |
| **Biological process** | protein folding [GO:0006457] | 3 | grpE | Protein GrpE |
| | | | dnaJ | Chaperone protein DnaJ |
| | | | groS | 10 kDa chaperonin |

| | | | | |
|---|---|---|---|---|
| **Biological process** | tricarboxylic acid cycle [GO:0006099] | 3 | aspA | Aspartate ammonia-lyase |
| | | | sucA | 2-oxoglutarate dehydrogenase |
| | | | mqo | Probable malate:quinone oxidoreductase |
| **Molecular function** | ATP binding [GO:0005524] | 38 | NGO_1573 | ABC transporte Energy-dependent translational throttle protein EttA |
| | | | atpG | ATP synthase gamma chain |
| | | | gltX | Glutamate--tRNA ligase |
| | | | atpA | ATP synthase subunit alpha |
| | | | clpA | Clp protease ClpX |
| | | | mfd | Transcription-repair-coupling factor |
| | | | parC | DNA topoisomerase 4 subunit A |
| | | | aroK | Shikimate kinase |
| | | | lon | Lon protease |
| | | | ileS | Isoleucine--tRNA ligase |
| | | | macB | Macrolide export ATP-binding/permease protein MacB |
| | | | uvrA | UvrABC system protein A |
| | | | accD | Acetyl-coenzyme A carboxylase carboxyl transferase subunit beta |
| | | | NGO_0851 | Cell division protein FtsK |
| | | | cysS | Cysteine--tRNA ligase |
| | | | gshB | Glutathione synthetase |
| | | | argG | Argininosuccinate synthase |
| | | | coaD | Phosphopantetheine adenylyltransferase |
| | | | dnaA | Chromosomal replication initiator protein DnaA |
| | | | NGO_1757 | DNA helicase |
| | | | recD | RecBCD enzyme subunit RecD |
| | | | dnaJ | Chaperone protein DnaJ |
| | | | purC | Phosphoribosylaminoimidazole-succinocarboxamide synthase |
| | | | NGO_0650 | DEAD/DEAH box helicase NGO_0650 |
| | | | NGO_1732 | Multidrug ABC transporter ATP-binding protein |
| | | | tyrS | Tyrosine--tRNA ligase |

| | |
|---|---|
| NGO_0956 | Aspartokinase |
| uvrB | UvrABC system protein B |
| NGO_0200 | Phosphoenolpyruvate synthase |
| clpB | Chaperone protein ClpB |
| groS | 10 kDa chaperonin |
| thrS | Threonine--tRNA ligase |
| leuS | Leucine--tRNA ligase |

| | | | | |
|---|---|---|---|---|
| **Molecular function** | cytoplasm [GO:0005737] | 34 | gltX | Glutamate--tRNA ligase |
| | | | grpE | Protein GrpE |
| | | | mfd | Transcription-repair-coupling factor |
| | | | aroK | Shikimate kinase |
| | | | lon | Lon protease |
| | | | pepA | Probable cytosol aminopeptidase |
| | | | glyA | Serine hydroxymethyltransferase |
| | | | infB | Translation initiation factor IF-2 |
| | | | ileS | Isoleucine--tRNA ligase |
| | | | xseB | Exodeoxyribonuclease 7 small subunit |
| | | | prfC | Peptide chain release factor 3 |
| | | | uvrA | UvrABC system protein A |
| | | | cysS | Cysteine--tRNA ligase |
| | | | argG | Argininosuccinate synthase |
| | | | coaD | Phosphopantetheine adenylyltransferase |
| | | | dnaA | Chromosomal replication initiator protein DnaA |
| | | | hisZ | ATP phosphoribosyltransferase regulatory subunit |
| | | | NGO_1757 | DNA helicase |
| | | | dnaJ | Chaperone protein DnaJ |
| | | | rne | Ribonuclease E |
| | | | ppa | Inorganic pyrophosphatase |
| | | | fur | Ferric uptake regulation protein |
| | | | rimP | Ribosome maturation factor RimP |
| | | | tyrS | Tyrosine--tRNA ligase |
| | | | uvrB | UvrABC system protein B |
| | | | clpB | Chaperone protein ClpB |
| | | | groS | 10 kDa chaperonin |
| | | | thrS | Threonine--tRNA ligase |
| | | | leuS | Leucine--tRNA ligase |

| | | | | |
|---|---|---|---|---|
| **Molecular function** | integral component of membrane [GO:0016021] | 11 | NGO_0551 | Molecular chaperone DnaJ |
| | | | NGO_0236 | Cell division protein ZipA |
| | | | NGO_1771 | Mechanosensitive ion channel family protein NGO_1771 |
| | | | macB | Macrolide export ATP-binding/permease protein MacB |
| | | | NGO_0265 | Cell division protein FtsN |
| | | | NGO_0291 | Potassium transporter |
| | | | secE | Protein translocase subunit SecE |
| | | | NGO_0361 | Heme biosynthesis protein HemY |
| | | | NGO_1732 | Multidrug ABC transporter ATP-binding protein |
| | | | NGO_1998 | RDD family protein |
| | | | secY | Protein translocase subunit SecY |
| **Molecular function** | zinc ion binding [GO:0008270] | 9 | gltX | Glutamate--tRNA ligase |
| | | | ileS | Isoleucine--tRNA ligase |
| | | | uvrA | UvrABC system protein A |
| | | | accD | Acetyl-coenzyme A carboxylase carboxyl transferase subunit beta |
| | | | cysS | Cysteine--tRNA ligase |
| | | | dnaJ | Chaperone protein DnaJ |
| | | | rne | Ribonuclease E |
| | | | ribA | GTP cyclohydrolase-2 |
| | | | NGO_0034 | Fructose-1,6-bisphosphate aldolase |
| **Molecular function** | DNA binding [GO:0003677] | 9 | dnaQ | DNA polymerase III subunit epsilon II |
| | | | parC | DNA topoisomerase 4 subunit A |
| | | | uvrA | UvrABC system protein A |
| | | | NGO_0851 | Cell division protein FtsK |
| | | | NGO_1757 | DNA helicase |
| | | | topA | DNA topoisomerase 1 |
| | | | recD | RecBCD enzyme subunit RecD |
| | | | rpoC | DNA-directed RNA polymerase subunit beta' |
| | | | uvrB | UvrABC system protein B |

| | | | | |
|---|---|---|---|---|
| **Molecular function** | metal ion binding [GO:0046872] | 9 | dnaQ | DNA polymerase III subunit epsilon II |
| | | | ilvD | Dihydroxy-acid dehydratase |
| | | | gshB | Glutathione synthetase |
| | | | NGO_1770 | Oligopeptidase A |
| | | | topA | DNA topoisomerase 1 |
| | | | fur | Ferric uptake regulation protein |
| | | | NGO_0200 | Phosphoenolpyruvate synthase |
| | | | aceE | Pyruvate dehydrogenase E1 component |
| | | | thrS | Threonine--tRNA ligase |
| **Molecular function** | RNA binding [GO:0003723] | 6 | rlmJ | Ribosomal RNA large subunit methyltransferase J |
| | | | NGO_1713 | Ribonuclease II |
| | | | NGO_1504 | DNA methylase |
| | | | rne | Ribonuclease E |
| | | | tyrS | Tyrosine--tRNA ligase |
| | | | NGO_1783 | RluA family pseudouridine synthase |
| **Molecular function** | plasma membrane [GO:0005886] | 6 | atpG | ATP synthase gamma chain |
| | | | atpA | ATP synthase subunit alpha |
| | | | NGO_0236 | Cell division protein ZipA |
| | | | macB | Macrolide export ATP-binding/permease protein MacB |
| | | | secE | Protein translocase subunit SecE |
| | | | secY | Protein translocase subunit SecY |
| **Molecular function** | ATPase activity [GO:0016887] | 5 | NGO_1573 | ABC transporte Energy-dependent translational throttle protein EttA? |
| | | | clpA | Clp protease ClpX |
| | | | macB | Macrolide export ATP-binding/permease protein MacB |
| | | | uvrA | UvrABC system protein A |
| | | | uvrB | UvrABC system protein B |
| **Molecular function** | tRNA binding [GO:0000049] | 5 | gltX | Glutamate--tRNA ligase |
| | | | rpsM | 30S ribosomal protein S13 |
| | | | ileS | Isoleucine--tRNA ligase |
| | | | rpsG | 30S ribosomal protein S7 |
| | | | thrS | Threonine--tRNA ligase |

| | | | | |
|---|---|---|---|---|
| **Molecular function** | structural constituent of ribosome [GO:0003735] | 5 | rpsM | 30S ribosomal protein S13 |
| | | | rpsC | 30S ribosomal protein S3 |
| | | | rplY | 50S ribosomal protein L25 |
| | | | rpsG | 30S ribosomal protein S7 |
| | | | rpsF | 30S ribosomal protein S6 |
| **Molecular function** | translation [GO:0006412] | 5 | rpsM | 30S ribosomal protein S13 |
| | | | rpsC | 30S ribosomal protein S3 |
| | | | rplY | 50S ribosomal protein L25 |
| | | | rpsG | 30S ribosomal protein S7 |
| | | | rpsF | 30S ribosomal protein S6 |
| **Molecular function** | rRNA binding [GO:0019843] | 4 | rpsM | 30S ribosomal protein S13 |
| | | | rpsC | 30S ribosomal protein S3 |
| | | | rpsG | 30S ribosomal protein S7 |
| | | | rpsF | 30S ribosomal protein S6 |
| **Molecular function** | magnesium ion binding [GO:0000287] | 4 | aroK | Shikimate kinase |
| | | | ribB | 3,4-dihydroxy-2-butanone 4-phosphate synthase |
| | | | rne | Ribonuclease E |
| | | | ppa | Inorganic pyrophosphatase |
| **Molecular function** | GTP binding [GO:0005525] | 4 | infB | Translation initiation factor IF-2 |
| | | | prfC | Peptide chain release factor 3 |
| | | | ribA | GTP cyclohydrolase-2 |
| | | | der | GTPase Der |
| **Molecular function** | protein folding [GO:0006457] | 3 | grpE | Protein GrpE |
| | | | dnaJ | Chaperone protein DnaJ |
| | | | groS | 10 kDa chaperonin |
| **Molecular function** | ribosome [GO:0005840] | 3 | rpsM | 30S ribosomal protein S13 |
| | | | rplY | 50S ribosomal protein L25 |
| | | | rpsF | 30S ribosomal protein S6 |
| **Molecular function** | tricarboxylic acid cycle [GO:0006099] | 3 | aspA | Aspartate ammonia-lyase |
| | | | sucA | 2-oxoglutarate dehydrogenase |
| | | | mqo | Probable malate:quinone oxidoreductase |

| | | | | |
|---|---|---|---|---|
| **Family** | DNA repairs and recombination proteins | 6 | dnaQ | DNA polymerase III subunit epsilon II |
| | | | mfd | Transcription-repair-coupling factor |
| | | | uvrA | UvrABC system protein A |
| | | | NGO_1757 | DNA helicase |
| | | | topA | DNA topoisomerase 1 |
| | | | recD | RecBCD enzyme subunit RecD |
| **Family** | Pyruvate metabolism | 5 | accD | Acetyl-coenzyme A carboxylase carboxyl transferase subunit beta |
| | | | NGO_0214 | Phosphate acetyltransferase |
| | | | lldD | Respiratory L-Lactate dehydrogenase |
| | | | NGO_0200 | Phosphoenolpyruvate synthase |
| | | | aceE | Pyruvate dehydrogenase E1 component |
| **Family** | Methane metabolism | 4 | NGO_1468 | Phosphoserine phosphatase SerB |
| | | | NGO_0214 | Phosphate acetyltransferase |
| | | | NGO_0200 | Phosphoenolpyruvate synthase |
| | | | NGO_0034 | Fructose-1,6-bisphosphate aldolase |
| **Family** | Secretion system | 4 | NGO_0098 | Pilus assembly protein PilM |
| | | | NGO_0055 | Pilus assembly/adherence protein PilC NGO_0055 |
| | | | secE | Protein translocase subunit SecE |
| | | | secY | Protein translocase subunit SecY |
| **Family** | Ribosome biogenesis | 3 | rlmJ | Ribosomal RNA large subunit methyltransferase J |
| | | | rne | Ribonuclease E |
| | | | NGO_1783 | RluA family pseudouridine synthase |
| **Family** | Glycin, serine and threonine metabolism | 3 | NGO_1468 | Phosphoserine phosphatase SerB |
| | | | NGO_0689 | Threonine synthase |
| | | | NGO_0956 | Aspartokinase |
| **Family** | DNA replication proteins | 3 | dnaQ | DNA polymerase III subunit epsilon II |
| | | | parC | DNA topoisomerase 4 subunit A |
| | | | topA | DNA topoisomerase 1 |
| **Family** | Nucleotide excision repair | 3 | mfd | Transcription-repair-coupling factor |
| | | | uvrA | UvrABC system protein A |
| | | | NGO_1757 | DNA helicase |
| **Family** | Peptidases and inhibitors | 3 | lon | Lon protease |
| | | | pepA | Probable cytosol aminopeptidase |

| | | | | |
|---|---|---|---|---|
| | | | NGO_1770 | Oligopeptidase A |
| **Family** | Transporters | 3 | NGO_0291 | Potassium transporter |
| | | | NGO_1732 | Multidrug ABC transporter ATP-binding protein |
| | | | NGO_2130 | Stringent starvation protein A |
| **Family** | Quorum sensing | 3 | secE | Protein translocase subunit SecE |
| | | | NGO_1695 | Phospho-2-dehydro-3-deoxyheptonate aldolase |
| | | | secY | Protein translocase subunit SecY |

**Table 8.4 Acetylation sites of tRNA proteins in the three isogenic mutants of *N. gonorrhoeae* MS11**

| Protein name | Protein entry | Δ*ackA* | Δ*pta* | Δ*hdac* |
|---|---|---|---|---|
| **Alanine--tRNA ligase** | Q5F7C4 | K703, K831, K646, K456, K831, K825, K360, K351 | K703, K743, K281, K456 | K703, K441 |
| **Arginine--tRNA ligase** | Q5F835 | K259, K418, K537, K126 | K407, K259, K292, K418 | - |
| **Aspartyl/glutamyl-tRNA** | Q5F8V0 | K61, K386, K24, K456, K445 | K58, K472 | K58 |
| **Cysteine--tRNA ligase** | Q5F5D6 | K175, K185, K73 | K298, K185 | - |
| **D-aminoacyl-tRNA deacylase** | Q5F6A6 | K52 | - | - |
| **Glutamate--tRNA ligase** | Q5F5J8 | K425, K156, K428, K241, K425, K416 | K425, K416, K428, K383 | K156, K343 |
| **Glutamine--tRNA ligase** | Q5F7G0 | K364, K556 | K276 | - |
| **Glutamyl-tRNA amidotransferase** | Q5F507 | K55, K58, K12 | K12, K78 | - |
| **Glutamyl-tRNA reductase** | Q9ZHD6 | - | K145 | - |
| **Glycine--tRNA ligase alpha subunit** | Q5F4Y8 | K290 | - | - |
| **Glycine--tRNA ligase beta subunit** | Q5F4Y7 | K569, K378 | K358, K569, K443 | - |
| **Isoleucine--tRNA ligase** | Q5FAF5 | K913 | K424, K913, K280 | - |
| **Leucine--tRNA ligase** | Q5FAJ3 | K309, K854, K621, K32, K521 | K634, K621, K521 | - |
| **Lysine--tRNA ligase** | Q5F6U2 | K351 | K165 | - |
| **Methionine--tRNA ligase** | Q5F585 | K569, K130, K650 | K130, K647 | - |
| **Methionyl-tRNA formyltransferase** | Q5F5P7 | - | K205 | - |
| **Peptidyl-tRNA hydrolase** | Q5F9L4 | K120, K108, K125 | K125 | - |

| | | | | |
|---|---|---|---|---|
| **Phenylalanine--tRNA ligase alpha subunit** | Q5F9U0 | K43 | K43, K82 | - |
| **Phenylalanine--tRNA ligase beta subunit** | Q5F9T6 | K605, K202, K631, K623, K104 | K236, K631, K661, K695, K623 | K202 |
| **Proline--tRNA ligase** | Q5F938 | K126, K418, K12, K461 | K24, K12, K461 | K418, K12 |
| **Queuine tRNA-ribosyltransferase** | Q5F9U5 | K120 | - | - |
| **Threonine--tRNA ligase** | Q5F9U4 | K300, K323, K560 | K323 | - |
| **tRNA-2-methylthio-N** | Q5FAI1 | K58 | K58, K323 | - |
| **tRNA-specific 2-thiouridylase MnmA** | Q5F7G4 | K109 | K176 | - |
| **tRNA pseudouridine synthase B** | Q5F8W8 | K73 | - | - |
| **tRNA synthetase RNA-binding protein** | Q5F8F4 | - | K14 | - |
| **tRNA uridine 5-carboxymethylaminomethyl modification enzyme MnmG** | Q5F5Y0 | K283, K570, K191, K489, K621, K105 | K191, K105 | K570, K489 |
| **Tryptophan--tRNA ligase** | Q5F7X0 | K227, K219, K220 | K227 | - |
| **Tyrosine--tRNA ligase** | Q5FAF7 | K82, K245, K234 | K266, K245 | - |
| **Valine--tRNA ligase** | Q5F5W0 | K323, K537, K875, K4, K932 | K942, K285, K4 | K263 |

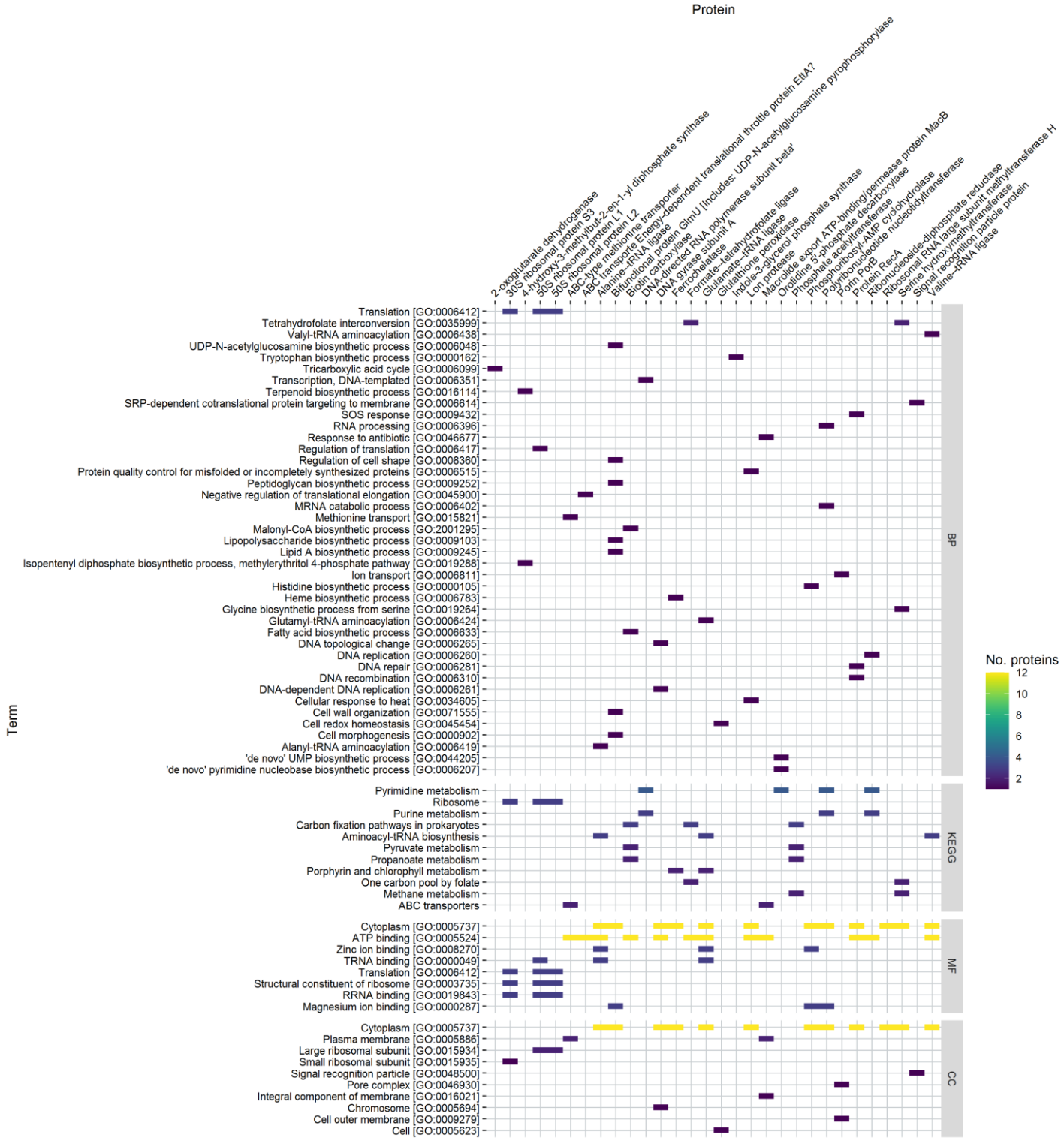


**Figure 8.1 Ontologies of the possible target of HDAC.** Heat map of gene ontologies and the enzymes classified as possible targets of HDAC. The terms correspond to the gene ontologies of biological process (BP), KEGG pathways (KEGG), molecular function (MF) and cellular component (CC).

**Table 8.5 T-test analysis of growth in different carbon sources.** The growth of the isogenic mutant strains in glucose, lactate, and pyruvate was compared for each hour of growth.

| Time (h) | Strain | Glucose | | Lactate | | Pyruvate | |
|---|---|---|---|---|---|---|---|
| | | *p* value | Significance | *p* value | Significance | *p* value | Significance |
| 0 | Δ*ackA* | 0.0078 | ** | 0.0131 | * | 0.72915 | ns |
| | Δ*pta* | 0.01244 | * | 0.0032 | ** | 0.57992 | ns |
| | Δ*hdac* | 0.83495 | ns | 0.0754 | ns | 0.47679 | ns |
| 1 | Δ*ackA* | 0.02549 | * | 9.40E-06 | **** | 0.02522 | * |
| | Δ*pta* | 0.35928 | ns | 3.90E-06 | **** | 0.06052 | ns |
| | Δ*hdac* | 0.90723 | ns | 0.6161 | ns | 0.52659 | ns |
| 2 | Δ*ackA* | 0.0059 | ** | 0.0071 | ** | 0.00391 | ** |
| | Δ*pta* | 0.01818 | * | 0.0068 | ** | 0.00481 | ** |
| | Δ*hdac* | 0.01021 | * | 0.6311 | ns | 0.26542 | ns |
| 3 | Δ*ackA* | 0.00031 | *** | 0.0438 | * | 0.00211 | ** |
| | Δ*pta* | 0.00133 | ** | 0.0442 | * | 0.00068 | *** |
| | Δ*hdac* | 0.03373 | * | 0.5802 | ns | 0.1378 | ns |
| 4 | Δ*ackA* | 0.05263 | ns | 0.0624 | ns | 0.00112 | ** |
| | Δ*pta* | 0.04246 | * | 0.0633 | ns | 0.00087 | *** |
| | Δ*hdac* | 0.06692 | ns | 0.559 | ns | 0.16023 | ns |
| 5 | Δ*ackA* | 0.14309 | ns | 0.044 | * | 0.00127 | ** |
| | Δ*pta* | 0.06468 | ns | 0.0458 | * | 0.00148 | ** |
| | Δ*hdac* | 0.07093 | ns | 0.3209 | ns | 0.18022 | ns |
| 6 | Δ*ackA* | 0.34847 | ns | 0.0164 | * | 5.80E-05 | **** |
| | Δ*pta* | 0.10656 | ns | 0.0175 | * | 4.30E-05 | **** |
| | Δ*hdac* | 0.07813 | ns | 0.4604 | ns | 0.75285 | ns |
| 7 | Δ*ackA* | 0.68511 | ns | 0.013 | * | 0.0002 | *** |
| | Δ*pta* | 0.15478 | ns | 0.0145 | * | 0.0002 | *** |
| | Δ*hdac* | 0.10733 | ns | 0.4645 | ns | 0.3038 | ns |
| 8 | Δ*ackA* | 0.25729 | ns | 0.0228 | * | 0.00062 | *** |
| | Δ*pta* | 0.04898 | * | 0.0312 | * | 0.00092 | *** |
| | Δ*hdac* | 0.11266 | ns | 0.5298 | ns | 0.13682 | ns |
| 9 | Δ*ackA* | 0.32928 | ns | 0.0368 | * | 0.0009 | *** |
| | Δ*pta* | 0.1511 | ns | 0.0703 | ns | 0.00124 | ** |
| | Δ*hdac* | 0.1535 | ns | 0.4857 | ns | 0.09689 | ns |
| 10 | Δ*ackA* | 0.14549 | ns | 0.0431 | * | 0.00288 | ** |
| | Δ*pta* | 0.07112 | ns | 0.0893 | ns | 0.00393 | ** |
| | Δ*hdac* | 0.12211 | ns | 0.3302 | ns | 0.14726 | ns |

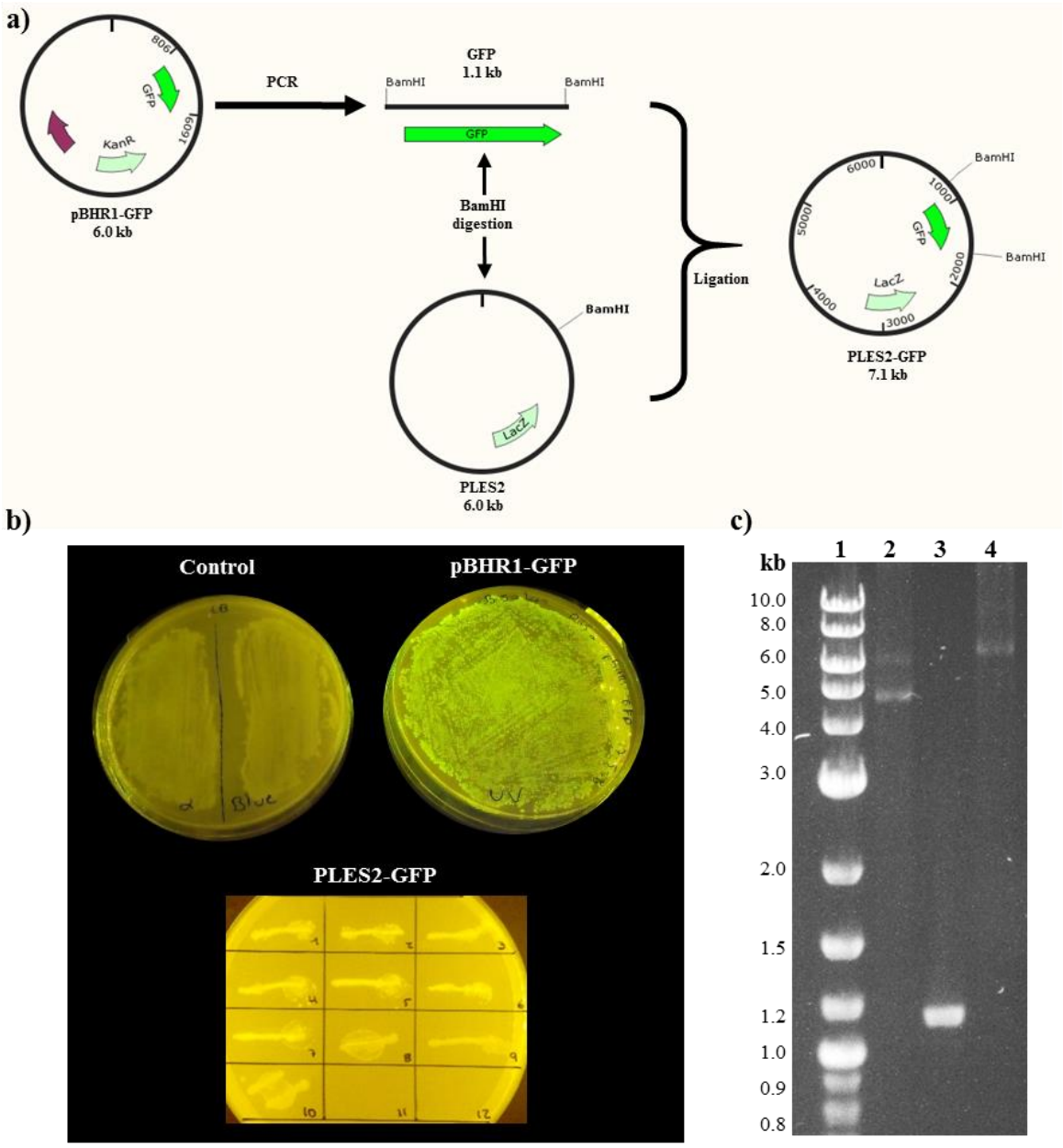


**Figure 8.2 Construction of pLES2-GFP. a)** Procedure for the construction of pLES2-GFP. gfp was amplified from pBHR1 by PCR, with primers containing the restriction sequence for BamHI. pLES2 and the PCR GFP product were digested with BamHI and then both were ligated. **b)** For the selection of the colonies with the plasmid, agar plates were located onto a UV transilluminator to prove the synthesis of GFP. At the top left corner is *E. coli* DH5α and *E. coli* XL1-Blue with any plasmid as controls; on the top right corner is *E. coli* DH5α with pBHR1-GFP showing fluorescence; and at the bottom are the 9 selected colonies after pLES2-GFP transformation, and the control (10). Colonies from 1-7 showed fluorescence and the colonies 2 and 7 were selected for PCR amplification and sequencing. **c)** Agarose electrophoresis gel. The pLES2 plasmid of 6.0 kb (2) and the *gfp* PCR product (3), 1.1 kb, were ligated to form pLES2-GFP (4) of ≈7.1 kb. A two log DNA ladder was used (1).


**Figure 8.3 Relative mRNA expression of genes involved in the virulence and metabolism of *N. gonorrhoeae* MS11.** RNA was extracted from the neisserial strains and the relative mRNA expression was determined by RT-qPCR. The relative expression was calculated from the housekeeping gene 16S rRNA and the expression of the WT. Replicates were performed between 3-5 times for each gene. The significance and *p* value are shown on top of the graphs. ns, no significance;*, *p* value <0.05; **, *p* value <0.01.

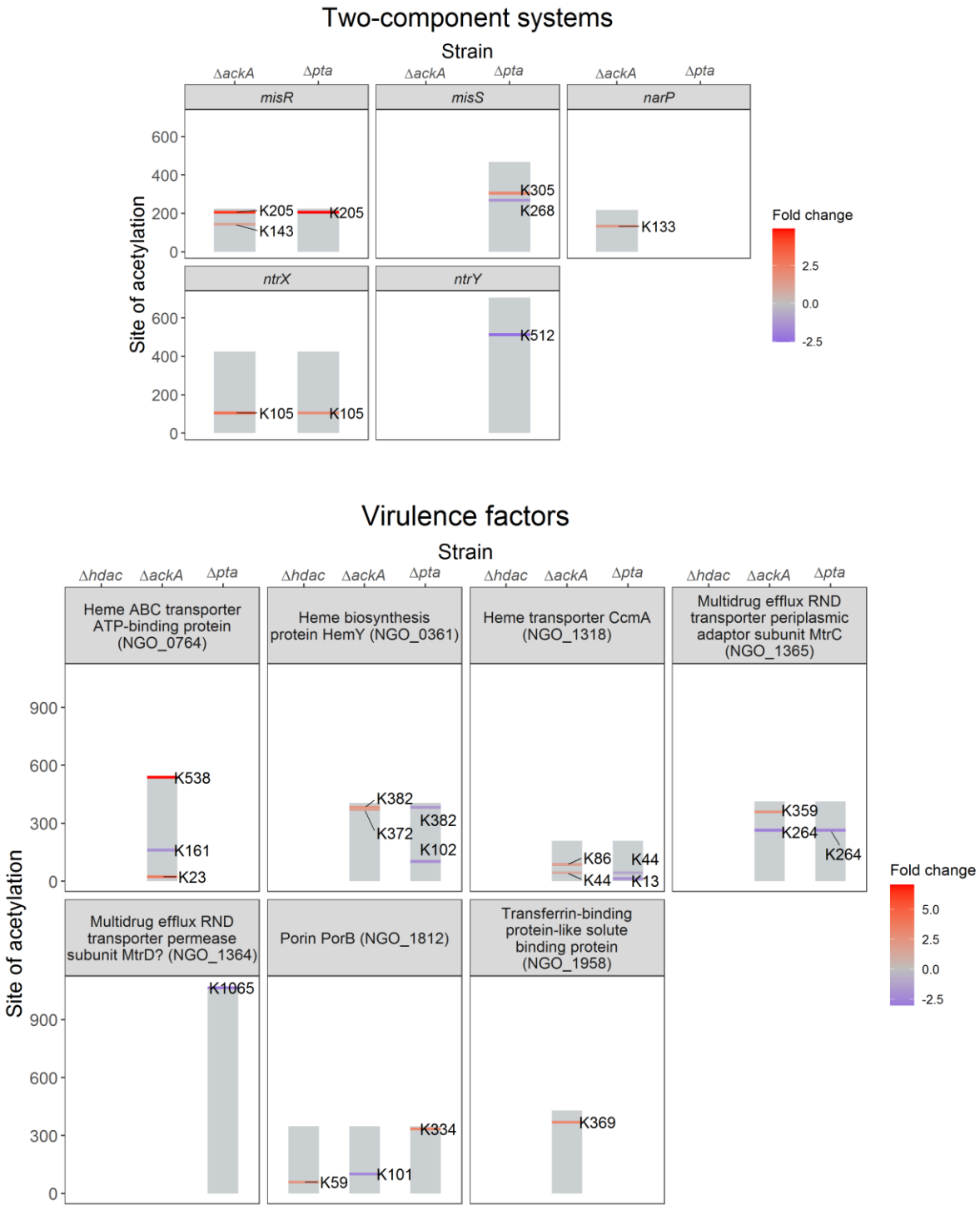


**Figure 8.4 Acetylation sites of two-component system proteins and virulence factors.** The significant different lysine acetylation sites were identified. Each plot shows the protein name and locus. The tiles are fill with a gradient according to the fold change in acetylation. The bar at the background shows the length of the protein.

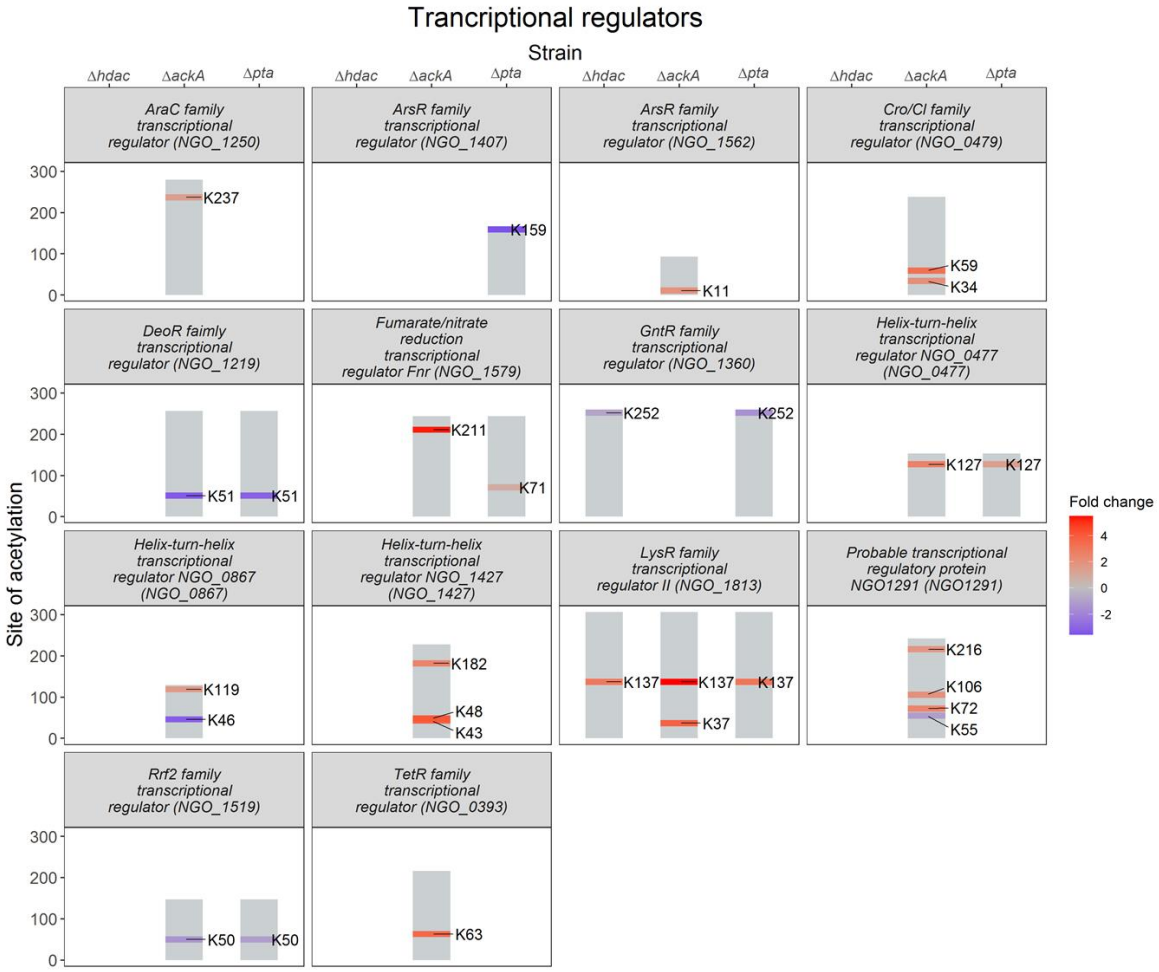


**Figure 8.5 Acetylation sites of transcriptional regulators.** The significant different lysine acetylation sites were identified. Each plot shows the protein name and locus. The tiles are fill with a gradient according to the fold change in acetylation. The bar at the background shows the length of the protein.

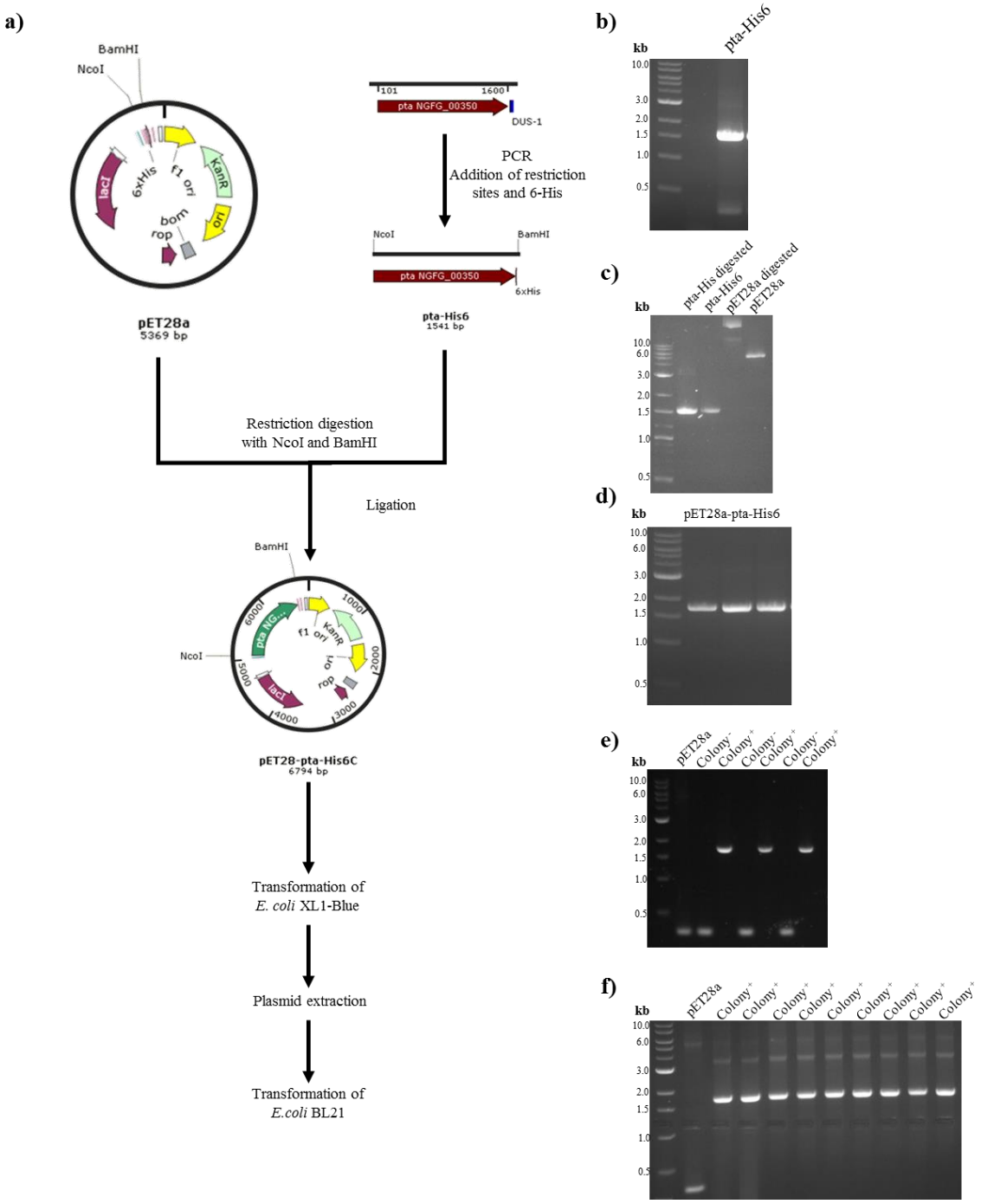


**Figure 8.6 Construction of *E. coli* BL21 pET28a-pta-His6 for the overexpression of the phosphotransacetylase of *N. gonorrhoeae*. a)** Workflow for the construction of *E. coli* BL21 pET28a-pta-6His. **b)** The gene *pta* was amplified by PCR adding the restriction sites for NcoI and BamHI, and the 6 His tag (pta-His6) for the purification of the protein. **c)** The plasmid pET28a and pta-His6 were digested with NcoI and BamHI and **d)** then ligated, **e)** for the transformation of *E. coli* XL1-Blue, used for the production of the plasmid. The plasmid was extracted and **f)** then the strain of *E. coli* BL21 was transformed with the plasmid for the expression of the protein. 1.5% agarose gels. The insert was amplified for validation using T7 primers.